An Investigation into

Bicycle Performance and Design

Thesis submitted in fulfilment of a PhD

Auckland University of Technology

Te Wānanga Aronui o Tamaki Makau Rau

Auckland

New Zealand

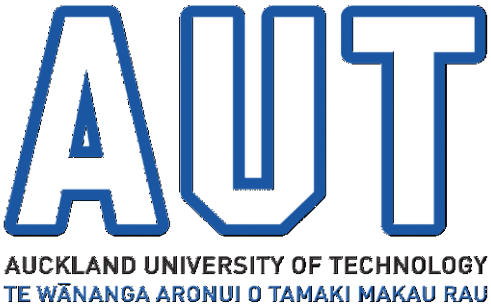

By John Prince

Prof Ahmed Al-Jumaily, Primary Supervisor

July 2014

ABSTRACT

Research into bicycle dynamics has been evolving for many years, yet many questions still need to be resolved. This field has proved to be a fertile area for scientific discovery encompassing the disciplines of: design, control, rigid body dynamics, computer simulation and practical experimentation. In this thesis, first the literature in the field of bicycle rigid body dynamics, control and design was examined in detail to find out what was known and what was yet to be discovered.

The main hypothesis of this thesis was to determine to what extent mathematical modelling could influence the dynamics of the bicycle and improve handling performance. Hence a main objective was to develop valid and effective design tools that bicycle manufacturers could use to optimise their designs.

To do this equations of motion for a bicycle were developed and solved using Simulink in a Matlab environment and appropriate physical parameters were used to find the dynamic response of the bicycle in terms of yaw and roll. Using this model it was possible to investigate and understand the following issues:

- the dynamic responses of the bicycle and how they relate to the rider
- which terms in the equations are critical to the design process
- the effectiveness of the model in determining bicycle performance
- how the bicycle can be optimised in terms of specific performance criteria?

A design methodology was developed that designers could use to guide their bicycle design decisions. The proposed design methodology consists of four Design Charts covering:

1. Steering geometry (head tube angle, rake and trail)
2. Wheel properties (diameter and moment of inertia)
3. Frame geometry (vertical and longitudinal position of the mass and wheelbase)
4. Mass and roil inertia (bicycle mass and moment of inertia of the rear assembly)

The validity of these Design Charts was confirmed by comparing them to historical design practice and then to elite riders and bicycles from the 2013 Tour de France bicycle race. This comparison showed that these bicycle designs conformed to the Charts, indicating the Charts' relevance and usefulness. The Charts also display appropriate design envelopes for designers' guidance.

ATTESTATION OF AUTHORSHIP

I state that this submission is my own work and contains no material previously published or written by another person, except where defined in the acknowledgements, nor any material which to a substantial extent has been submitted for any other degree or qualification from a University or Institution of higher learning.

John Prince, July 2014

ACKNOWLEDGEMENTS

In completing this investigation I received help from many different people. I must thank Auckland University of Technology (AUT) and its Engineering School for a wide range of assistance. The University gave me significant support for my studies by awarding me a Vice Chancellor's Doctoral Scholarship. This enabled me to write my thesis with a degree of calm and reflection. My colleagues in the Engineering School also gave generously in time and in discussions about my work.

Special thanks go to my supervisor, Professor Ahmed Al-Jumaily, who strongly encouraged me during this research. During the course of my investigation, Ahmed maintained his enthusiasm for my work despite the usual (and predictable) setbacks that most PhD students encounter. He provided sound advice on how to proceed and on how I could successfully complete this investigation.

Associate Professor Loulin Huang as one of my two secondary supervisors was of great help in providing feedback and advice as this work progressed.

I must also thank the Head of AUT's Engineering School, Professor John Raine, for the School's generous support during the course of my studies. Professor Raine, who was my other secondary supervisor, has been very understanding about the demands my studies have had on my time.

Another colleague and friend Julie Douglas kindly agreed to step into my professional role at the University for six months while I focussed solely on this thesis. Thank you Julie and I hope I can return the favour one day.

Bachelor of Engineering Technology student, Karan Grewal gave me permission to study the bicycle database that he completed as part of his Third Year Project. His work helped with my Tour de France bicycle database.

Finally a thanks to all my cycling friends over many years, Stan, Richard, Perry, Tim, Bridget, Bugsy, Adrian, Ross, Peter and many others, who helped to spark my initial interest in this fascinating field.

John Prince, July 2014

TABLE OF CONTENTS

TABLE OF FIGURES

LIST OF TABLES

NOMENCLATURE

This nomenclature section defines all the variables, notations and terms used in this thesis

Table 1 List of variables

Symbol	Meaning	Units
a	linear acceleration	m/s^2
a	horizontal distance from centre of front wheel to centre of mass	m
b	horizontal distance from centre of rear wheel to centre of mass	m
c	clearance distance between seat tube centreline and outside of rear wheel	mm
d_1	crank sideways offset	mm
d_2	crank length	mm
d_3	shoe extension	mm
D	wheel diameter	m (or mm)
F	force	N
FS	frame size	cm or mm
g	acceleration due to gravity = $9.81 m/s^2$	m/s^2
G	linear momentum	kgm/s
$\dot{G}$	change in linear momentum	kgm/s^2
h	vertical distance from ground to centre of mass	m
h_1	distance vertically from rear wheel hub to *B*	mm
h_2	distance vertically from ground level to *B*	mm
h_3	distance vertically from ground level to *C*	mm
h_4	distance vertically from wheel hubs to *C* (bottom bracket drop)	mm
H	angular momentum	kgm^2/s
$\dot{H}$	change in angular momentum	kgm^2/s^2
H	vertical distance from ground to centre of front wheel hub	m
i	distance from *A* to *D*	mm
I	mass moment of inertia (also MOI)	kgm^2
IS	inseam leg measurement of the rider	mm

I_{XA}	moment of inertia of assembly A about X axis (roll)	kgm^2
I_{ZA}	moment of inertia of assembly A about Z axis (yaw)	kgm^2
I_{XB}	moment of inertia of assembly B about X axis (roll)	kgm^2
I_{XF}	moment of inertia of front wheel about X axis (roll)	kgm^2
I_{YF}	moment of inertia of front wheel about Y axis (rotational)	kgm^2
I_{ZF}	moment of inertia of front wheel about Z axis (yaw)	kgm^2
I_{XR}	moment of inertia of rear wheel about X axis (roll)	kgm^2
I_{YR}	moment of inertia of rear wheel about Y axis (rotational)	kgm^2
I_{ZR}	moment of inertia of rear wheel about Z axis (yaw)	kgm^2
I_{XW}	moment of inertia of wheel about X axis (roll)	kgm^2
I_{YW}	moment of inertia of wheel about Y axis (rotational)	kgm^2
I_{ZW}	moment of inertia of wheel about Z axis (yaw)	kgm^2
j	distance from *J* to *K* measured parallel to seat tube	mm
k	radius of gyration	mm
k	distance from *K* to centre of mass measured perpendicular to seat tube	mm
L	bicycle wheelbase	m
L_1	distance horizontally from rear wheel hub to *A*	mm
L_2	distance horizontally from *A* to centre of mass	mm
L_3	distance horizontally from rear wheel hub to *C*	mm
L_4	distance horizontally from rear wheel hub to *D*	mm
L_5	distance horizontally from *C* to *D*	mm
m	mass	kg
M	mass of the bicycle and rider	kg
MOI	mass moment of inertia (also I)	kgm^2
O	distance from *A* to bottom bracket spindle centreline measured parallel to seat tube	mm
P	depth of wheel rim	m (or mm)
r	radius of the bicycle wheel	m (or mm)
r_1	clearance radius of rear wheel	mm

r_2	adjusted radius of front wheel allowing for bottom bracket drop (h_4)	mm
r_3	reduced radius of front wheel allowing for crank sideways offset (d_1)	mm
R	radius of the corner	m
STA	seat tube angle also called γ (gamma)	degrees
t	wall thickness of wheel rim	m
t	period of oscillation	sec/cycle
T	torque	Nm
v	linear speed of the bicycle (velocity)	m/s
T_{Frame}	or T_f the torque one assembly exerts on the other assembly corrected for the head tube angle i.e. the torque assembly A exerts on assembly B is equal in magnitude but opposite in direction to the torque assembly B exerts on A	Nm
T_{Steer}	or T_S the steering torque input by rider, corrected for the head tube angle	Nm
$\dot{v}$	change in velocity	m/s^2
w	width of wheel rim	m (or mm)

Table 2 List of variables (Greek symbols)

Greek Symbol	Meaning	Units
β (beta)	rake of front forks, also called offset	m
γ (gamma)	seat tube angle (also abbreviated as STA)	degrees
Γ (GAMMA)	torsional damping constant	Js
Δ (DELTA)	front wheel trail also called projected or conventional trail	m
Δ_e (DELTA e)	front wheel effective trail also called mechanical or normal trail	m
λ (lamda)	roll angle of bicycle (also called lean angle)	radians
P (rho)	material density	kg/m^3
σ (sigma)	yaw angle of bicycle front wheel (also called steer angle)	radians
Σ (SIGMA)	angle between seat tube centreline and line AD	degrees
Φ (PHI)	head tube angle of front wheel (also abbreviated as HTA), also called steering tube angle, steering head angle or rake angle	radians
ω_X (omega X)	angular speed about X (roll)	rads/s
ω_Y (omega Y)	angular speed about Y (pitch of the bicycle or rotation in the case of wheels)	rads/s
ω_Z (omega Z)	angular speed of the wheels about Z (yaw)	rads/s

Table 3 Notation used

Symbol	Meaning	Units
A	the front wheel, front forks, handlebars assembly	
A	Intersection of seat tube centreline with ground	
B	the frame, seat and seat post, rear wheel, transmission, rider assembly	
B	intersection of seat tube centreline with vertical line passing through rear wheel hub centreline	
BM	refers to the benchmark bicycle with all parameters defined	
C	the % change in impulse response settling time for each 1% change in a parameter	
C	bottom bracket spindle centreline position	
COG	centre of gravity position	
COM	centre of mass position	
D	Intersection of ground and a vertical line tangential to rear of front wheel	
K	position located along the seat post between the bottom bracket and the top of the seat post, used to define the centre of mass position	
R^2	coefficient of determination, which describes the strength of the linear relationship between two variables	ratio
S	the 2% settling time of the impulse response	second
u	the Jones stability criterion, used to define the steering stability of individual bicycles	ratio
X	horizontal longitudinal axis as defined by the International Standard ISO 8855 (1) [1]	
Y	horizontal transverse axis as defined by ISO 8855	
Z	vertical axis as defined by ISO 8855	

[1] See corresponding reference number in the Bibliography Section

GLOSSARY

This glossary section defines important terms used in this thesis

Table 4 Definitions of terms

Item	Meaning
accuracy	this is how close the recorded value of a sensor is to the true value
asymptotically stable	the output approaches desired value in an asymptotic manner
asymptotically unstable	the output departs from desired value in an asymptotic manner
benchmark bicycle	the benchmark bicycle has specific parameters defined and is used as a point to compare other bicycles to
bifilar pendulum	a special type of pendulum with two suspension cords, used to find moments of inertia of bodies
bounce	linear motion along axis Z
capsize	loss of stability due to excessive roll, resulting in the bicycle falling over sideways
castor action	the self-centring ability of a front wheel that gives fore and aft stability, due to the trail of the front wheel
castor torque	the torque that causes a front steering wheel to self-centre due to geometry of its steering axis, see castor action
centre of gravity	the point about which gravity can be said to act on a body
centre of mass	the point about which mass can be said to concentrated in a body
centrifugal effect	the effect on a body moving in a circular path which causes it to deviate in a radial outward direction, acting in manner opposite but equal to the centripetal effect
centripetal force	a force acting on a body which causes it to move along a curved path
chain stays	two identical tubes which connect the bottom bracket to the rear dropouts (which support the rear wheel)
compound pendulum	a type of pendulum about which the mass cannot be said to be concentrated at a single point (unlike the point mass of a simple pendulum)

Coriolis effect	the Coriolis effect on a moving body in a rotating reference frame causes it to deviate perpendicular to its velocity vector
counter-steer	the bicycle turning manoeuvre where the bike initially turns slightly away from the intended turn direction before coming back and following the correct path
damping	the ability of a system to suppress vibrations by dissipating energy
design chart	a chart indicating the relationships between important design parameters and bicycling handling performance (defined by the 2% settling time)
directional stability	the degree with which a vehicle proceeds along a straight course despite external disturbing forces
down tube	the bicycle frame tube that connects the head tube to the bottom bracket
effective trail	the distance between the vertical projection of the front wheel centre and the projection of the front fork steering axis, measured perpendicular to the steering axis
Euler equations	the general momentum equations of rigid body motion can be simplified to the Euler equations when the reference axes X-Y-Z coincide with the principal axes
ETRTO	European Tyre and Rim Technical Organisation, responsible for defining bicycle tyre sizes in Europe, also widely used internationally
frequency response	an analysis of the output responses of a system measured across a range of inputs with different frequencies
frame size	traditionally measured parallel to the seat tube being the distance from the centre of the bottom bracket to centre of top tube (assuming the top tube is horizontal and not inclined)
front fork	the curved tubular assembly that the bicycle front wheel is directly fitted to, attached to a steerer tube and handle bars, it is free to rotate
gravitational torque	torque due to the pull of earth's gravity
gyroscopic effect	the effect that occurs when the axis about which a body is rotating is itself rotated about another axis
gyroscopic torque	torque due to the gyroscopic effect
head tube	the part of the bicycle frame that the steering tube fits within
head tube angle	the angle the bicycle head tube makes with the horizontal plane, generally for bicycles it lies between 70 and 75 degrees, also see rake angle

heave	linear motion about the Z axis
hip steer	a bicycle turning manoeuvre made by a rider, riding without using their hands where the bike turns in the same direction that the rider's hips are moved in
holonomic systems	systems whose equations of constraint contain only co-ordinates, or co-ordinates and time
hub	a rotating assembly at the centre of each wheel, it contains a wheel axle and bearings and the hub flanges that the wheel spokes fit into
impulse input	an input that has infinite magnitude over zero time (mathematically possible, but not physically achievable) in practice an impulse of sufficiently large magnitude and of a very short time duration is considered to be an impulse response, also see unit impulse
inseam	the inside length of a person's leg measured when standing, used to determine the correct size of bicycle
iso-handling lines	lines of constant 2% settling time displayed on the design charts
ISO	International Organization for Standardization, the body responsible for the international system of measurements and standards
Jones torque	the torque that causes a front steering wheel turn into a leaned corner, named after Jones the first researcher to describe it, see also trail steer (2)
Jones stability criterion	the term used by Jones to define the steering stability of individual bicycles, also called the Jones stability parameter (with the symbol u)
kink torque	a torque that causes the bike to roll and is due a Coriolis effect caused by to the difference in paths followed by different parts of the bike according to their longitudinal position i.e. the difference between the circular paths of the front wheel, the centre of mass and the rear wheel
lean angle	see roll angle
linearity error	also called an angularity error, there should be a linear relationship between a set of true readings and the corresponding sensor readings, if there isn't, then a linearity error exists
mass	the quantity of matter in a body
moments of inertia	also called products of inertia and equal to the sum of Σmr^2 taken over all particles of a body, where 'm' is mass and 'r' is the radius from a specified centre

nonholonomic systems	systems whose equations of constraint contain velocities
offset	a term only used in motorcycling terminology, the perpendicular distance from front wheel hub centre to front fork's steering axis, see also rake
period	the time an oscillating body takes to complete one cycle of oscillation (periodic motion)
perturbation	a small disturbance external to the studied system
pitch	angular motion about Y
precision	this is the agreement amongst a set of sensor readings
principal axes	the axes of a body about which the principal moments of inertia occur, see the Euler equations
principal moments of inertia	the maximum, minimum and intermediate values for the moments of inertia for the particular origin chosen
projected trail	see trail
radius of gyration	the position about which the mass of a rotating body can be thought of as being concentrated
rake	a term only used in motorcycling terminology, the perpendicular distance from front wheel hub centre to front fork's steering axis, see also offset
rake angle	the angle the head tube makes with the vertical plane, only used in motorcycling terminology, see also head tube angle
ramp input	an input that increases at a constant rate with respect to time
reach	horizontal distance from centre of bottom bracket to centre of head tube (measured at its top end)
roll	angular motion about X axis
seat stays	two identical tubes which connect the seat tube to the rear dropouts (which support the rear wheel)
seat tube	the near vertical bicycle frame tube directly beneath the bicycle's seat
self-stability	the ability of a system to maintain a stable state without active control action
sensitivity	this is the smallest input value to which a sensor can respond, or the ratio between a change in a parameter's value and the resulting change in a system's output

settling time	the time taken for a system to reach a certain percentage (usually 5% or 2%) of a desired value after a defined step or impulse input
side slip	linear motion about Z axis
six degrees of freedom	the three linear degrees of freedom about axes X, Y & Z and the three rotational degrees of freedom in the a, b & c directions
stack	vertical distance from centre of bottom bracket to centre of head tube (measured at its top end)
span error	occurs when the sensor doesn't change value at the correct rate, i.e. a one degree change in true temperature value should show as a one degree change in sensor reading, also called a range error
speed wobble	oscillations of a vehicle front wheel about the steering axis
steering angle	the angle the bicycle front steering wheel makes with the longitudinal centreline of the frame and rear wheel, it is measured in the vertical plane, see also yaw angle
steering geometry	relevant dimensions and angles of the front steering wheel assembly namely, the steering tube angle, rake, trail and wheel diameter
steering response	the nature of the dynamic output of a bicycle in response to a steering input
steering torque	the input torque provided by the rider to control and steer a bicycle
steerer tube	the tube attached to the top of the bicycle front forks which is aligned by headset bearings and mated within the head tube, also called steering tube
step input	an input that increases instantaneously from a constant value to another constant value
stiffness	the ability of a system to resist deflection or displacement
surge	linear motion about X axis
sway	linear motion about Y axis, see also side slip
TdF	the Tour de France race which is the pre-eminent international bicycle race and one of the three grand tours of road racing
trail	the distance between the vertical projection of the front wheel centre and the projection of the front fork steering axis measured horizontally along the road, see also projected trail

trail steer	the torque that causes a front steering wheel turn into a leaned corner, see also Jones torque (2)
top tube	the near horizontal bicycle frame tube at the top of the frame and below the rider
UCI	Union Cycliste International is the international body authorised to regulate, control and run the majority of cycle sports (3)
unit impulse	an impulse where the area A under the graph is equal to 1 is called the unit impulse function and is written as $\delta(t)$
weave	yaw oscillations of the rider and rear frame of the bicycle (assembly B)
wheel base	horizontal distance between the centres of the bicycle's front and rear wheels
wobble	oscillations of a vehicle front wheel about the steering axis
yaw	angular motion about Z axis
yaw angle	the angle the bicycle front steering wheel makes with the longitudinal centreline of the frame and rear wheel, see also steering angle
zero error	sensor's reading should return to zero when the input is zero, if it doesn't a zero error is present

1. RATIONALE AND SIGNIFICANCE OF THE STUDY

This Chapter outlines the main hypothesis of this investigation and summarises the methods used and the results achieved.

1.1. HYPOTHESIS

The main hypothesis of this thesis is to determine to what extent mathematical modelling can influence the dynamics of bicycle design characteristics and also improve handling performance for the rider. The objective is to develop effective and valid design tools that bicycle manufacturers can make use of to optimise their designs. At the moment manufactures rely heavily on past experience and empirical techniques and as far as is known there are no scientifically rigorous design methodologies. Existing literature does contain some techniques and advice, but their use would be problematic in many respects.

Of particular interest is the question of how and why a bicycle's steering remains stable. This needs further understanding and analysis (4, 5)[2]. This investigation examines the effects of different steering geometries, on steering response, system stability and frequency response of bicycles.

Research into bicycle dynamics has been evolving for many years, but even so many questions still need to be resolved (5-9). *"The bicycle has been in existence for over a century but yet many mysteries surround the bicycle. Upon reflection, the bicycle is a deceptive object as it looks simple and yet it isn't* (5)."

"While 150 years of evolution have turned the standard, two wheeled velocipede into a thing of beauty, we still don't understand exactly how it works. We have the equations, it's just we don't know what they mean. Why does the bicycle steer the proper amounts at the proper times to assure self-stability? We have found no simple physical explanation (9)."

Some key questions on quantifying bicycle performance are still unanswered. What effect and importance do the different design parameters such as head tube angle, trial, and wheelbase have? How can a designer systematically assess bicycle performance and base design decisions on scientific theories as opposed to the empirical methods currently used?

Wilson says *"unfortunately the equations purporting to describe bicycle motion and self-stability are difficult and have not been validated experimentally, so design guidance remains highly empirical"* (10).

"You can't possibly get a good technology going without an enormous number of failures. It's a universal rule. If you look at bicycles, there were thousands of weird models built and tried before they found the one that really worked. You could never design a bicycle theoretically. Even now, after we've been building them for 100 years, it's very difficult to understand just why a bicycle works - it's even difficult to formulate it as a mathematical problem. But just by trial and error, we found out

[2] See corresponding reference number in the Bibliography Section

how to do it, and the error was essential. The same is true of airplanes." Freeman Dyson, British Physicist and author (11)

How can we assess various bicycles and understand how and why they are different from each other? This research develops general design principles and methodologies that will show how the handling performance of bicycles can be described and optimised.

An important issue is to determine what sort of handling performance is desirable. Too much directional stability in a bicycle is as much a problem as too little and while the beginner wants a stable, insensitive bicycle, the more expert rider wants a sensitive bicycle that can respond quickly when taking rapid evasive action to avoid a hazard.

While it is clear that certain myths about bicycle motion still persist and more work needs to be done at least some key questions about bicycle dynamics and control have been answered and valid equations to describe bicycle motion have been independently formulated by several researchers (12-15).

One surprising myth is that many people suppose that bicycles are inherently unstable and must have active rider control to remain upright. In fact it can be shown that riderless bicycles moving above a critical speed have a large amount of self-stability. They can remain upright and will travel in an approximately straight line for a considerable distance before their speed drops below a critical value and they capsize. They can even recover from large yaw and roll disturbances and make corrective actions and still continue upright (16).

Another myth is that it is commonly assumed that a front wheel castor is essential for bicycle stability. In fact bicycles with zero trail and even 90 degree head angles though not ideal, are quite rideable and the very first bicycle, the Hobbyhorse of 1817 was one such bicycle (6).

The incorrect notion that bicycles depend on gyroscopic effects in order to be rideable still persists (17). This is despite numerous researchers showing both experimentally and mathematically that gyroscopic action, while it exists, is completely unnecessary for stability and the best known demonstration of this was Jones' zero-gyroscopic bicycle (2). Despite the bicycle's self-stability they are challenging for beginners to learn to ride. The often heard advice from parents to children "to ride faster" (in order to reach a critical velocity) is correct in one sense but also unhelpful as novices don't understand counter-steering. The necessary counter-steering action is counter intuitive and not is immediately mastered. Riding a bicycle is a complex task *"all in all 'as easy as riding a bike' is turning out to be a rather misleading saying. "I have a colleague who studies how pilots control aircraft and he says riding a bike is much more complex" says Mont Hubbard. "We're trying to answer an important question, how complicated a system can a human deal with* (18)?" What can a thorough review of the literature tell us about such issues?

1.2. REVIEW OF LITERATURE

A review was made of the current state of knowledge including the development of equations of motion for bicycles, stability and sensitivity analysis and the current design tools. The field happily

remains a rich area for scientific discovery encompassing the disciplines of: design, control theory, rigid body dynamics and practical experimentation. Over 70 major papers about bicycle motion have been written and it has attracted some famous names: Rankine, Whipple, Timoshenko and F. Klein to name a few and it remains a challenging problem to study. At the undergraduate level it is perhaps too challenging, unless many simplifying assumptions are used which may compromise the validity of the analysis. This thesis makes suggestions as to what sorts of assumptions are sensible for different applications. Chapter Two examines in more detail the literature in this field and identifies what has been done and what remains to be done.

1.3. MATHEMATICAL MODELLING

In this investigation the physical laws of nature were applied to a bicycle to obtain a mathematical formulation for the complete dynamic model. Simulink computer software was then used to solve the resulting multibody dynamic equations of motion and this is described in Chapters Three and Four. The Simulink model ran many simulations using different combinations of system parameters and physical scenarios to investigate the dynamic responses. This model can simulate different bicycle designs, allowing different steering geometries (and other terms) to be quantified in terms of performance. This model was validated in Chapter Four from data available in the literature and from an experimental investigation conducted using a specially adapted bicycle fitted with measurement sensors to record yaw and roll angles.

Design parameters were examined in detail in Chapters Five where their actual importance was determined by systematically changing each parameter one at a time while keeping all others constant. Large variations in roll and yaw responses showed how sensitive bicycles are to small changes of key parameters such as the head tube angles and rake dimensions. At higher speeds the observed steering responses support the common observation that bicycles are more stable and easier to ride at higher velocities. These simulations showed the importance of correctly selecting the bicycle's parameters in order to optimise handling performance.

1.4. DESIGN METHODLOGY

Designers need to be able to use a design methodology based on scientific theories as opposed to the current empirical methods. This is so their design decisions can be based on a clear understanding of how sensitive the bicycle is to changes key parameters. According to Meijaard et al "*Through trial and error, bicycles had evolved by 1890 to be stable enough to survive to the present day with essentially no modification. Because bicycle design has been based on tinkering rather than equations, there has been little scrutiny of bicycle analyses"* (14).

This research was used to develop in Chapter Six, several design methodologies that indicate how the handling performance of bicycles can be optimised. The design methodologies considered included: design criteria, design tables, handling equation (from simplified equations of motion) and design charts. After consideration of a range of requirements this thesis recommends the use of four Design Charts associated with: the steering geometry, wheel properties, frame geometry and

the mass/roll inertia. Used together these four Design Charts provide a designer with a robust methodology to select the best combinations of parameters for a desired purpose.

The Design Charts were validated in Chapter Seven by comparing them to bicycles designed according to historical design practice and secondly to riders and bicycles from the 2013 Tour de France bicycle race. These comparisons showed that the Charts' are relevant and useful and can offer designers valuable guidance.

2. LITERATURE SURVEY

2.1. INTRODUCTION

This Chapter examines in detail the literature in the field of bicycle dynamic motion, it reviews what is known and what is yet to be discovered. Many papers about bicycle dynamics have been written and the topic has interested some famous names such as: Rankine, Whipple, F. Klein, and Timoshenko, but it still remains challenging. Why does such a supposedly simple object as a bicycle remain a puzzle in terms of its dynamics and stability?

Richard E. Klein when discussing the complexity of bicycle dynamics wrote *"issues complicating the bicycle include the nonholomonic (or velocity) constraints, the algebraically coupled higher derivative terms, the vague nature of the lateral tyre road forces which are so hard to quantify and the often misunderstood role of gyroscopic effects* (5)."

Later Moon wrote in his text on multibody dynamics: *"in spite of the ubiquitous nature of the bicycle and the recent improvements in the so called mountain bicycle, very little hard dynamic knowledge is known about this system apart from empirical trials and observations* (19)."

This agrees with the author's view that little qualitative work has been done to guide the bicycle designer in making good design decisions. But while it is clear that misconceptions about bicycle motion persist, many questions about bicycle dynamics and control have been answered in the past twenty years, using equations independently formulated that describe the important external and internal torques acting on a bicycle (13, 14). For example it has been established by several researchers that the inverted pendulum model gives a good explanation of bicycle stability in terms of the sideways capsize (20). Also many researchers have shown conclusively that gyroscopic effects cannot account for the stability of bicycles and clear explanations for the increased stability or rideability of bicycles at higher speeds have been proposed (2, 5, 20, 21).

This survey has been arranged into themes covering the following eight areas: early explanations for bicycle motion, development of the equations of motion, bicycle myths, experimental work, multibody dynamics, control engineering approaches, computer modelling of bicycles and chronological reviews of paper. The decision to use these themes was made because it was felt to be more relevant to discussing this dynamic problem than the more common chronological approach.

2.2. EARLY EXPLANATIONS OF BICYCLE MOTION

One of the earliest explanations for the stability of a bicycle in motion was proposed in 1869 by Rankine who argued that centrifugal forces resulted in sufficient torque to balance the gravitational overturning moment. He then described the inverted pendulum model for balance and the motion of a bicycle attempting to follow a straight course as *"the plain wavy line represents the actual track of the centre of mass."* This was the first time that this fundamentally important concept was described. He then gave a description of counter-steering stating *"it is obvious, that the first thing to*

be done is to incline the fore-wheel in the direction opposite to that of the intended curvature, in order that the base point may be displaced and give rise to centripetal force. The effect of this is to deflect the base-track away from the intended centre of curvature (22)."

Later towards the end of the nineteenth century, Bourlet wrote one of the earliest books on the design and analysis of bicycles and followed this up with a paper outlining a mathematical study of bicycle motion (23, 24). Bourlet described equations for a bicycle with a vertical steering axis and no trail. Much later Meijaard et al reviewed Bourlet's work as part of their history of bicycle steer and dynamic equations (14). They found that when linearized Bourlet's non-linear roll equations were correct except for omitting the front wheel gyroscopic term associated with the steer rate.

Sharp's book "Bicycles and Tricycles, An Elementary Treatise On Their Design And Construction" was an interesting and detailed description of early bicycle development up to the end of the 19th Century (7). This book discussed the science relevant to bicycles such as: statics, dynamics, material properties and system behaviour. He described basic bicycle stability equations that used centrifugal forces in the way proposed by Rankine in 1869. The author then examined bicycle stability, steering action, motion over rough surfaces and resistance to motion. The text included a detailed description of the development of bicycles from the first Hobbyhorse of 1817 up to the end of the 19th century, including the Rover Safety bicycle of 1885. The last section of this book examined specific technical developments in the areas of: gearing, tyres, pedals, brakes and frames.

In 1899 Whipple wrote a paper on bicycle dynamics in which he briefly discussed Bourlet's and McGraw's independent papers on bicycle stability (15, 23). Note that McGraw's paper published in the journal "Engineer" on 09 Dec 1898 has not been obtained and is not referenced. Whipple stated *"no satisfactory explanation on mathematical lines has been given of the practicality and ease of riding a bicycle."* He then developed non-linear equations of motion for a bicycle assuming that: the roll angles were small, the bicycle consisted of only two rigid bodies, the motion was steady and that any turns have large radii. From his nonlinear equations he developed linear equations of motion for a bicycle. These were analysed to find unstable roots and he identified four critical velocities which required different control input modes on the part of the rider in order to maintain stability. The highest critical velocity was v_1 (5.5 m/s), then v_2 (4.6 m/s), v_3 (3.8 m/s) and finally v_4 (3.3 m/s). Between v_1 and v_2 the bicycle was only stable by turning the front wheel into the roll or by moving the body away from the roll. Between v_2 and v_3 stability was achieved by moving the body into the roll. Below v_2 the bicycle was unstable if ridden with the hands off (i.e. a steering input is required for stability). Finally below the lowest critical velocity was v_4 (3.3 m/s) the rider must use a combination of body motion and steering input to remain upright. Meijaard et al recently reviewed Whipple's paper as part of their history of bicycle equations (14). They found that except for small errors, Whipple's non-linear governing equations were nearly correct.

2.3. DEVELOPMENT OF EQUATIONS OF MOTION

Little more was done in regards to bicycle dynamics until Timoshenko and Young included a short analysis in their classic engineering text “Advanced Dynamics” in 1948 (20). Their bicycle analysis produced equations of motion that could cope with large angles of yaw and roll and their work is much cited by researchers in this field. They described a model for balancing a bicycle similar to that of balancing an inverted pendulum in that the rider must steer the bicycle to make use of centrifugal forces to position the centre of mass over the tyres and so correct any capsize tendency. Their equations clearly showed that in order for the bicycle to remain upright the rider must steer the front wheel into the direction of any roll, exactly as proposed by Rankine, Sharp and Whipple. This model for stability is still thought to be valid as a simple analysis of straight-line travel. Their equations did not include many of the real life complications of bicycles such as the steering geometry variables that later researchers have added.

Psiaki wrote about the dynamics of bicycle and derived full non-linear equations for its motion (25). He conducted computer numerical analysis (using Fortran IV) and examined the effects on stability in a straight line using different design parameters. Secondly he solved the characteristic equation for the case of a steady turn. He studied stability by varying the following parameters: head tube angle, trail, wheelbase, height and longitudinal position of mass, speed and several moments of inertia, one at a time. Meijaard et al have compared Psiaki’s eigenvalues in a forward speed range with their model and have stated that his results agreed with theirs within plotting accuracy (14).

Lowell and McKell used Timoshenko and Young’s analysis as a starting basis for their investigation (20, 21). They simplified the equations by only considering small angles of yaw and roll and by modelling the steering geometry of their bicycle as a simple trailing castor wheel. They derived simplified equations for bicycle yaw and roll angles which were solved using a fourth order Runga-Kutta method to obtain numerical solutions, plotting angular responses against time. No damping term is included in their model and only the front wheel gyroscopic term due to yaw is included. The gyroscopic torque on the front wheel due to roll and the gyroscopic torque on the rear frame and rider due to cornering are neglected, potentially serious omissions which will be discussed later. As their results didn’t demonstrate counter-steering action or self-righting stability it is believed that their analysis is incorrect. Meijaard et al concludes “*when our equations are simplified to correspond to their model the equations do not agree... it is incorrect* (14).”

Hand presented new equations of motion for a bicycle with a model consisting of four rigid bodies (26). He used Lagrangian equations to develop linearized equations of motion for hands off riding i.e. with no steering input from the rider. He then applied the Routh Stability Criterion to establish stable and unstable combinations of design parameters. A PC based Fortran programme was developed to apply the Routh Stability Criterion stability to specific designs. According to Meijaard et al, Hand's equations agreed with their bench marked equations but Hand's Fortran program for calculating stability eigenvalues had errors (14).

Franke, Suhr and Rieß developed a general bicycle model with the following simplifying assumptions: a rigid bicycle frame, no tyre slip or friction, thin disc wheels, a level road and no wind (27). Their model allowed for the steering geometry of rake and trail and it had five rigid bodies; the frame, the rear wheel, the rider, the handlebar/front fork assembly and the front wheel. They investigated stable and unstable riding conditions and the ability of the bicycle to stabilise itself and their model only examined hands off riding with a zero input steering torque. The momentum approach was used to develop final equations of motion consisting of second derivatives for velocity, yaw and roll and these equations were solved by computer using the Runga-Kutta procedure which produced eigenvalues for the system. They concluded that gyroscopic wheel effects were essential for inherent stability though it is clear from other researchers' work that this is not the case. They also said that steering stability increased linearly with trail but it is known from the literature that too large a trail can cause an over correction of the front wheel and so can reduce stability (28).

Fajans described the equations of motion for bicycles and motorcycles and explained the phenomena of counter-steer and hip steer (12). A counter-steer manoeuvre (first described by Rankine) is when the steering wheel is initially turned away from the desired direction of turn causing the bicycle to lean into the corner (22). The three equations of motion Fajans developed describe the dynamic motion of the bicycle for specific steering inputs and were derived from the works of Timoshenko & Young and later Lowell & M^{c}Kell. These equations were dynamically unstable unless a small damping term was added. In practice this damping is due to the front tyre and the rider's arms (12, 29) The author then discussed the limitations of these equations because of the unaccounted for effects of tyre deformation, head tube angles and friction.

Fajans examined in: a road racing bicycle and a large motorcycle. With the exception of the driving power, motorcycle dynamics share many similarities with bicycle dynamics, therefore some studies of motorcycles are of relevance to this investigation. Input values for steering torque and various physical parameters such as mass and wheelbase length were selected and used to obtain the dynamic outputs of yaw and roll. The author concluded that gyroscopic effects only have a small part to play in assisting cornering and are not required for system stability. A no hands turn using hip steer was investigated and the oscillations that occur for "no hands" riding were modelled. These oscillations were usually suppressed by the mass and damping provided by the rider's arms.

Jackson and Dragovan also developed equations of motion that were derived from Timoshenko & Young and Lowell & M^{c}Kell (20, 21, 30). Their model allowed for more realistic steering geometries than other available models, for example Fajans (12). They stated they undertook experimental work that measured the motion of a bicycle, but their theoretical and experimental results were not included in the paper. Like many others they concluded that gyroscopic terms were unimportant for stability (12).

Fajans' equations were modified by Prince (the author of this thesis) by adding terms to account for changes in steering geometry due to head tube angle and front fork rake (31, 32). Two approaches were adopted to validate this modified model. First a simplified Simulink model was prepared that used exactly the same assumptions as Fajans: i.e. no Coriolis terms and the same head tube angle

and rake values. This model showed nearly identical results to Fajans in terms of: yaw vs. time and roll vs. time with identical time lags, rise times, amplitudes, overshoots, and oscillations. Next an experiment was carried out to measure the actual steering and roll angles of a moving bicycle. A bicycle was fitted with transducers to measure yaw and roll angles and a data logger recorded the results. The results of both validation procedures confirmed key parts of the theory and helped validate the model. The final complex Simulink model produced more realistic results and displayed more system stability than the Fajans model. As stated by many others the gyroscopic terms were shown to be insignificant and could not account for bicycle stability.

Meijaard, Papadopoulos, Ruina and Schwab developed linearized equations of motion for a rigid four body bicycle system (rear wheel, rear frame & rider, front fork and front wheel) including the use of realistic front wheel geometry (14). Their model used three degrees of freedom (roll, steer and forward velocity) and includes 25 parameters. They validated their theoretical approach using two different computer simulations: Spacar (in Fortran 77) and Autosim. The eigenvalues obtained from the linearized stability analysis of their bicycle model showed regions of stability and instability for different forward speeds and also the nature of any instability present e.g. capsize, wobble or weave. Capsize was defined as the bicycle toppling over, wobble is a high frequency vibration of the front wheel only and weave is a medium frequency rolling and yawing of the rear assembly of the bicycle (33). The authors spent some effort solving their final equations (using two different methods) and checking the results against previous researchers' work, eventually finding close agreement by both their methods. They reviewed the work of many previous researchers in the field and compared their approach to these researchers in a detailed supplementary appendix. They also compared their results to what had been achieved experimentally by Kooijman et al (34). As a result they were confident that their equations could be used as a benchmark against which other studies could be compared and verified. They aided such a benchmarking process by providing eigenvalues to an accuracy of 15 significant figures.

2.4. BICYCLE MYTHS

One of the most persistent myths about bicycle stability is the importance of gyroscopic effects. When discussing bicycle stability R. E. Klein mentions *"the often misunderstood role of gyroscopic effects* (5). Two Germans, mathematician F. Klein (famous for describing the Klein bottle) and physicist Sommerfeld wrote a four part treatise "On the Theory of Gyroscopes" which was published between 1897 and 1910. A review of this paper by Meijaard et al concludes that its general statement in reference to bicycles *"gyroscopic effects ...are indispensable for self-stability"* is not correct (16).

As recently as 1998 researchers have incorrectly explained the dynamic motion of bicycles and their stability by using the gyroscopic effects of their wheels (17, 27, 35). One example of such an incorrect explanation was made by Higbie who described the cornering motion of a motorcycles, particularly the counter-steer manoeuvre, entirely by using gyroscopic action (35). No other torques, internal or external, were mentioned by this author except for a brief mention of the effect of

gravitational torque on front wheel yaw. This was a simplistic and incomplete discussion and repeated the myth of the importance of the gyroscopic term.

Later on, Cox described the cornering motion of a motorcycles particularly the counter-steer manoeuvre, as being due to two effects, firstly the conical shape of the tyre caused the bicycle to roll around a central point and secondly the gyroscopic action of the wheels due to gravitational torque (17). Cox added the angular momentum vector from the steering torque to the angular momentum of the wheel and argued that this caused the bicycle to lean over. It is believed that this is not the correct way to apply gyroscopic theory to this physical problem. In addition it has been verified by computer modelling that the steering torque can be very small (e.g. in order of 0.5 Nm for a bicycle) and so would not cause the bicycle to lean over as was claimed (31). Cox correctly described the effect of gyroscopic torque on the front wheel but includes no other internal or external torques such as the inertia torque or castor torque.

Overall the role of gyroscopic effects in bicycle stability are often misunderstood and overstated (17). Such claims about the importance of gyroscopic effects have been shown by many other researchers to be incorrect both by mathematical modelling and by the use of experimental zero gyroscopic bicycles. It is very clear that gyroscopic forces are not essential for self-stability nor do they allow bicycles to be ridden (2, 36, 37). Jones was the first to demonstrate the unimportance of gyroscopic effects and R. E. Klein has further confirmed these findings experimentally several times (2, 4).

2.5. EXPERIMENTAL WORK

Surprisingly few experimental investigations of bicycles have been described in the open literature. One of the most cited was performed by Jones who examined the basic question of why is it possible to ride a bicycle and keep it upright and why it seems easier to balance it when riding at higher speeds (2). Jones demonstrated the relative unimportance of gyroscopic effects with his famous experiment (2, 38). He built a special bicycle that had a second wheel fitted alongside the front wheel. This wheel didn't touch the ground and was linked by gears to the front wheel so that it rotated at the same speed but in the opposite direction. As this second wheel was nearly identical to the original wheel almost all of the gyroscopic effects were cancelled out. Jones found that it was a simple matter to ride this zero gyroscopic bicycle and that it did not feel substantially different from an unmodified bicycle. Jones could successfully ride it without his hands on the steering handlebars, showing conclusively that gyroscopic effects are not required for the ride stability of bicycles.

Jones then considered the well-known observation that the front wheel of a bicycle turns into the direction of any roll (i.e. into the corner). He explained that this occurs because as the front wheel turns (due to a twisting gravitational torque) the bicycle lowers its centre of mass and so lowers its potential energy. Calculations were made to find this change in the height the mass for different roll and steering angles. These calculations showed that when the steering wheel is pointing straight ahead the twisting gravitational torque increases linearly for increased roll angles. It was concluded that as the roll angle increases the bicycle provides a greater twisting torque that steers the wheel

into the corner. This effect helps to counteract the leaning over of the bicycle due to the inverted pendulum effect. He also found that different steering geometries have different rates of increase in this twisting torque and he used these results to plot a graph indicating stable and unstable geometries. A stability criterion was proposed that is discussed in Chapter Six, Jones tested his ideas by purposely building another experimental bicycle designed to be unstable and as predicted he found that it was unstable. Finally Jones built a bicycle to investigate whether front wheels can self-centre. He concluded that far from self-centring the rest of the bicycle swung in behind the new altered track of the front wheel and continued on a new stable course. The experimental work of Jones has been widely referred to by many later researchers (12, 21, 39, 40).

Kirshner examined Jones' paper but disagreed with some of his conclusions (39). The Jones stability criterion was shown to be approximately equal to the trail of the bicycle allowing for the steer angle and roll angle. Kirshner disagreed as to the cause of the apparent self-centring effect Jones observed in his final experiment and concluded that Jones' theory for bicycle stability was not valid. Kirshner then concluded that gyroscopic effect of the front wheel does contribute to bicycle stability but did not provide any positive analysis to justify this claim other than to say *"we attempt to verify a nongyroscopic theory of bicycle stability and fail.*" Given the widespread experimental and theoretical support for Jones' conclusion about the unimportance of the gyroscopic effect it is hard to agree with Krishner.

Le Hénaff spent the first part of his paper discussing the history of research into bicycle stability including references to Jones' work (40). He discussed the Jones stability criterion and plotted dynamic stability curves of the "height of wheel hub / wheel radius" versus lean angle for different speeds (2). He concluded that these curves explain why a bicycle is more stable at higher speeds because they show that a smaller steering angle is required to generate the required stabilising centrifugal force. He also concluded that though gyroscopic forces on the wheel are *"negligible and unable by themselves to account for equilibrium"* they do enable a bicycle to be ridden hands off.

Hunt inspired by Jones' zero gyroscopic experiment, also showed that cancelling the gyroscopic component of the bicycle's front wheel made no difference to the rideability of the bicycle (36). Hunt fitted a second wheel to the front forks alongside the front wheel, arranged to spin in the opposite direction, hence cancelling the gyroscopic couple. Care was taken to align the gyroscopic vectors and to make sure that the gyroscopic torques were inline. A brass adaptor was made to perfectly align the front and counter rotating wheels. Extra weight was added to ensure that the moment of inertia of the counter rotating wheel was close to that of the front wheel. The second wheel was spun by hand at the desired speed and direction before starting to ride the bicycle. Hunt described the experiment and concluded that the addition of this reverse spinning wheel made no difference to the bicycle's rideability. He described in brief terms: balancing stability, steering and countering-steering and the only calculations given were basic but clearly showed that the magnitude of any gyroscopic couple was insignificant compared to the gravitational couple.

R.E. Klein is an Engineering Professor at the University of Illinois who has used the study of bicycles to teach students about dynamic systems. He has developed student projects that designed and

built interesting and unique bicycles that examined various dynamic issues. These have included numerous zero-gyroscopic bicycles, naive bicycles (with a 90^{o} head tube angle and no trail), easy to ride bicycles for beginners, rear steered bicycles and exaggerated gyroscopic bicycles (4, 5, 13, 37). Klein's work is covered in more detail in a later section in this Chapter on control engineering approaches.

Foale and Willoughby's well known book "Motorcycle Chassis Design: the Theory and the Practice" discussed experimental and empirical work on the subject of motorcycle design and handling performance (41). The book described in great detail many practical aspects of motorcycle chassis design with the use of: diagrams, photos and experimental work, though no mathematical analysis is provided. Front wheel speed wobbles were discussed as to the likely causes and solutions, but only in practical terms not in theoretical ones. One chapter discussed an experiment involving the radical modification of the front wheel geometry of a motorcycle and the effects on handling performance. They asked why the then current motorcycles used head tube angles of between 60^{o} and 65^{o}. They concluded that it is a combination of convenience of construction, lack of imagination and fear of customer resistance. Using a BMW R75/5 motorcycle (circa 1970) they increased its head tube angle from 63^{o} to 75^{o} and then to 90^{o} and also adjusted the rake from 49 mm to 0 mm and then to –49 mm so that the trail remained at a value of 89 mm for all three cases. Considerable road testing was done (over 3000 km) with five different riders and qualitative analysis was made of the riders' descriptive feedback though no quantitative analysis was made. The modified geometry showed increased stability but also insensitivity to and better damping of outside perturbations. The front fork suspension was also more effective but fork juddering occurred under heavy braking. The authors concluded that steering geometries other than those arrived at by rule of thumb and accepted practice may have advantages.

Lignoski completed an interesting experiment to determine whether the bicycle steering angle is proportional to the lean angle (42). This is a common assumption made by researchers to simplify their equations of motion (21, 43). Lignoski used Lowell and McKell's equations and treated the motion of a bicycle as a damped simple harmonic oscillator and the gyroscopic torque of the front and rear wheels due to rolling and due to cornering were not included in his model. Though the equations are overly simplified, the experiment and its purpose is interesting. It consisted of rigidly mounting a video camera to a post attached to a bicycle and videoing the bicycle and surrounding walls as the bicycle was ridden. From the video recording produced, the lean angle was determined from the difference between the camera's frame of reference and vertical lines marked on nearby walls. In a similar way the steering angle was calculated from the video by comparing the projected length of the handlebars to the projected length of the handlebars at several known angles. The resulting experiment recorded only one very short run of two seconds in duration and Lignoski had problems getting accurate results as lots of practical problems were experienced including signal noise which increased the uncertainty of the results. Lignoski's experiment, while ingenuous, appears inconclusive but he reached the tentative conclusion that steering angles were proportional to lean angles, with the constant of proportionality equal to 2.40 +/- 0.15.

Kooijman et al completed an experimental validation for a numerical model of an uncontrolled bicycle (34). Many theoretical models simplify the bicycle problem by ignoring effects such as frame and wheel flexibility, the play in bearings, tyre effects and wheel slip. This practical research examined whether these simplifications are valid, an important consideration. Their model had three stated degrees of freedom (roll of rear frame, steering angle of front wheel and rotation of rear wheel) and produced linearized equations of motion for the upright steady motion of a bicycle with only small outside perturbations. Their experiment consisted of a fully instrumented bicycle which recorded roll, yaw, steering angle and rear wheel rotation. The bicycle had no rider but was pushed along a dry level floor by a person running alongside it. A total of 76 experimental runs were made with a maximum run length of 40 metres. From the recorded results the bicycle's eigenvalues were found from the plotted data and these experimental eigenvalues compared well to the theoretical values. They concluded that the theoretical model was valid when compared to the experimental results and that the assumptions made to simplify the model were reasonable.

Further experiments by Koojiman et al involved an instrumented rider and bicycle on a road and later on a treadmill and concluded that the rider steers and stabilises the bicycle mainly by steering inputs via the arms and with very little upper body lean or knee movement (44). Only at very low speeds (1.4 m/s) was any lateral knee movement observed at all. The steering inputs were performed at a similar frequency to the pedalling frequency and their amplitude increased as forward speed decreased.

Moore et al also wished to test the hypotheses that riders principally use direct steering input for control and make little use of upper body movements to control the bicycle (45). To examine this question they used a motion capture technique to examine three different riders riding a bicycle on a large rolling road. The experiments examined a cyclist riding at steady speeds ranging from 2 to 30 km/hr. Matlab was used to analyse the riders' movements from the data collected by the motion capture cameras. The motions of different parts of the rider were examined using frequency analysis to determine whether they were contributing to steering control. They concluded that steering control was mainly done by the arms through the handlebars but at low speeds some steering control was exerted by a lateral knee motion, agreeing with Koojiman (44). No upper body lateral motion was observed contributing to steering control thereby proving their hypotheses.

Moore and Hubbard looked at the importance of front wheel diameter, head tube angle, trail and wheelbase on the self-stability of a bicycle (46). They used a mathematical model that they benchmarked to work of Meijaard et al [18]. They considered bicycle self-stability and assumed the rider to be a rigid body with no piloting or control action and investigated a narrow speed range of 12.9 - 17.6 km/hr and two instability modes, capsize and weave (but not the wobble mode). They found the stable speed range between the two modes (capsize and weave) for four main parameters (wheel diameter, head tube angle, trail and wheelbase). An interesting and unexpected result obtained was that the stable speed range was close to the minimum value when the front wheel diameter was 700 mm (which is very close to a standard road bicycle 700C wheel diameter). They found for such a 700 mm wheel the stable speed range was between 4 and 5.5 m/s. In fact common

empirical observations show that the stable speed range is much wider than this. They say "*a more robust assessment of handling qualities is needed."*

Later Moore et al conducted a series of interesting experiments to determine a range of physical parameters for the bicycle rider system including: mass, centres of mass, moments of inertia of the bicycle components (frame, front fork and wheels) and the rider properties (47). They used a combination of experimental measurement and the use of previously published data to determine these values. Comments were made about the practical difficulty of measuring the bicycle's physical parameters. For example the centres of mass of the bicycle are given as +/- 20mm accuracy which could be considered a significant error. Unfortunately the bicycle chosen for measurement was not a high performance bicycle. Therefore the results in this paper are not especially helpful for evaluating high performance handling, though the methods for obtaining them are interesting.

In addition to these studies of the bicycle system, experimental investigations of the human rider are of interest as about 80% of the mass of the bicycle rider system is contributed by the rider. One US Air Force sponsored study undertaken by Hanavan developed a mathematical model to calculate the properties of humans of different builds (48). More details of this and similar work are given in Chapter Five when discussing the formulation of key bicycle design parameters.

2.6. BICYCLE MULTI BODY DYNAMICS

Wilson's book "Bicycling Science Ergonomics and Mechanics" has become a standard reference for those interested in bicycles. The first edition co-authored with Whitt, covered general aspects of ergonomics and human power generation as applied to bicycles and other pedal powered vehicles (6). The coverage of bicycle mechanics included: resistance to motion (e.g. wind, rolling and friction resistance), braking, balancing and steering stability. Other topics included: bicycle frame materials, human powered vehicles (HPV) and future HPV developments. The section on balancing and steering briefly discusses many previously mentioned researchers (2, 15, 20, 49). It defined various terms and steering geometry parameters and gave formulae from both Davison and Bourlet that calculate a front wheel geometry which neither rises or falls when the front wheel is turned though no justification was provided as to why this geometry would be useful for stability (50, 51). The second edition, written only by Wilson, describes in detail Jones' paper and Lynch's computer simulation of bicycle motion (49). The third edition by Wilson (with contributions from Papadopoulos) discusses stability theories in more detail with good descriptions of: inverted pendulums, Jones' experiments, counter-steering and a short discussion of the work of Papadopoulos (52). Front wheel wobble (shimmy) is discussed in detail with references to Den Hartog (29).

Doebellin's text "System Modelling and Response: Theoretical and Experimental Approaches" contained a section that discussed the stability of four wheeled vehicles (53). The author described in detail how to build several different dynamic models of four wheeled vehicles from the general equations of motion. Care was taken to include such things as: tyre effects, inertia effects caused by roll (including suspension effects) and the effect of a shifting payload. The final developed models were analysed for steering response and instability using a CSMP (Continuous System Modelling

Programme) simulation. This work has relevance to this investigation as it clearly showed how equations of motion for multi body systems, like cars and bicycles, can be derived from fundamental first principles.

Cocco's book "Motorcycles Design and Technology: How and Why" included diagrams and equations to illustrate the principles of motorcycling design, riding techniques and handling performance and was based on the work of both R. S. Sharp and Prof Cossalter (8, 54), (55). The author examined the effects of changes to motorcycle design on performance. Specifically this book considered: balancing on two wheels, cornering, accelerating, braking, vibration, aerodynamics, engines, frame and suspension design. The approach taken by this author was to discuss the concepts with diagrams and terms at a basic level. Though the treatment uses many simplifying assumptions the anecdotal information was interesting. The descriptive section which discussed front wheel design, steering geometry, speed wobbles and weaves was relevant to this investigation. Basic formulae were given (sometimes without proof or references) which enable useful effects to be found such as the frequency of a high speed wobble and the amount of fork drop that occurs when turning the front wheel.

2.7. CONTROL ENGINEERING APPROACHES

Other researchers have looked at bicycles from a control engineering perspective with an emphasis on stability and rideability. Some such as R. E. Klein have treated the bicycle as an interesting engineering system worthy of study using the control engineering approach (4). Others such as Suryanarayanan et al, have designed bicycle autopilot controllers, (56). Another group have made use of control theory to investigate bicycle instability and to determine measures of rideability, such as Seffen (28).

According to R. E. Klein, *"the bicycle is not a trivial topic, as one might suppose at first glance, but it is a rather formidable subject worthy of study" (5)*. His paper discussed new ways to teach the concepts of dynamic systems using bicycle motion as a practical everyday problem to study. This approach to teaching undergraduate students used theory lectures and computer simulation techniques to cover the necessary control theory. Klein's paper concentrated on the effectiveness of this teaching approach and recommended it because it stimulated student interest in the field of control. Different aspects of bicycle motion are mentioned to give examples of how this teaching method worked in the classroom. Laboratories were also used to help students build up proficiency in the use of Fortran simulation e.g. modelling a bicycle counter-steering manoeuvre. Finally the students were required to write an original essay on a selected aspect of bicycle motion such as the relative importance of gyroscopic effects when riding a bicycle. Students also completed the construction and testing of various experimental bicycles of their own design e.g. rear steered, zero gyroscopic, and bicycles with accentuated gyroscopic effects. This construction assignment allowed students to test out original ideas that they had first generated from theory and computer simulation.

Another paper by Klein expanded on the use of bicycle motion to teach the concepts of dynamic systems (4). The paper described three basic transfer functions that could be used to build up a

model of bicycle dynamics, namely: the relationship of the steering angle to lean angle, an inverted pendulum model for balance and a steering control law for rider feedback. These were combined into a matrix algebra form to obtain three transfer functions. Block diagrams of the transfer functions were obtained and a computer simulation was undertaken. His simulation showed the response of a bicycle to an impulse force on the steering wheel, where a clear countering-steering action occurred before turning in the opposite direction.

Motorcycles share many similarities with bicycles and Cossalter et al described a detailed mathematical model for the steady state turning of two wheeled motorcycles (55). Steady state turning assumes that both the roll angle and the steering angle remain nearly constant and is simpler dynamically than counter-steering manoeuvres. Their model was complex and allowed for: four distinct rigid bodies, tyre effects, aerodynamic effects and pitching. The mathematical model used the standard equations of motion to describe the cornering manoeuvre and the final model was solved using an iterative computer process. The authors concluded that the rider controls the motorcycle largely with steering torque but also with changes in body position and vehicle speed. The steering torque required for a steady state turn depends on several terms of large magnitude both with positive and negative values. They concluded that tyre forces due to side slip and roll stiffness had a small effect on the steering torque, but that the tyre twisting torque made a large negative contribution especially at large roll angles. They found that fork design was critical to the required steering torque and that increasing the trail decreased the steering torque as did decreasing the steering head angle.

Meijaard and Popov also developed a complex model for a motorcycle including: tyre forces, aerodynamic forces, suspension, power train and proportional-integral rider control action. Their results described the interaction of many of these components for example aerodynamic forces tend to damp the wobble mode but accentuate the weave mode (57).

Getz and Marsden described the design and simulation of a bicycle controller which uses front wheel steering and rear wheel torque control (i.e. speed control) to maintain bicycle stability (58). Lagrangian equations of motion were developed for a simple bicycle model which had a perpendicular steering axis, no front wheel trail and simplified inertia and mass effects. The testing of the controller indicated that a large gain was necessary due to the large time derivatives. A series of bicycle simulations were run which showed that their controller could stabilise a bicycle after a perturbation or a steering input. Importantly, counter-steering behaviour was observed in their simulation results.

Seffen et al investigated the controllability of two wheeled vehicles when upright and running in a straight line (28). Their paper examined how a rider can remain upright by steering into the roll. A thorough review of the current state of knowledge examined instabilities such as capsize, weave and wobble. They concluded by describing a conventional model for a bicycle first described by Sharp (8). Their equations were derived from Lagrange and were used to produce four 2nd order differential equations of motion. These were recast as a set of coupled first order equations using the state space method with Matlab. A bicycle rideability index was developed which was used to

examine the effect of changing the: front wheel trail, moments of inertia and head tube angle had on controllability and this index is explained further in Chapter Six.

Suryanarayanan et al examined the system dynamics involved in the directional control of a two wheeled human powered vehicle (HPV) (56). HPVs are specialist bicycles designed to break specific straight line speed records such as the one hour HPV record (currently set at 91.55 km) and are regulated by either the World Human Powered Vehicle Association (WHPVA) or the International Human Powered Vehicle Association (IHPVA) (59). Typically HPVs place the rider in a prone position within a fairing to minimise aerodynamic drag. Manoeuvrability and handling are much less important than the ultimate top speed. But the very high speeds attained mean that high speed instabilities such as weave and wobble can be a problem.

Their objective was to design an autopilot for a HPV capable of speeds of 100-160 km/hr. Previous HPVs had experienced control problems at high speed due to their human pilots' limitations, principally their slow speed of response. These researchers concluded that using a steering wheel trail value similar to a conventional bicycle makes a HPV unstable in cross winds. They concluded that a lateral crosswind would induce a torque that would cause the front steering wheel to turn away from the wind leading to increased yaw and instability. Ideally a bicycle should lean into the wind and the front wheel should yaw into this roll. The rider can then easily balance the force of the crosswind on the bicycle by adjusting how much front wheel yaw is needed and hence maintain upright balance and steer a straight course. A HPV with an aerodynamic body fairing could use increased fin area at the rear of the bicycle in order to make the bicycle yaw into the wind. This places the aerodynamic centre of pressure aft of the centre of the tyre grip. However they concluded that this would only be effective within a limited speed range. Presumably this is because the aerodynamic forces on the fairing vary according to velocity squared so are subject to large variations. The authors speculate that by reducing or eliminating front wheel steering trail crosswind vulnerability would be reduced. However this would cause other directional stability problems due to the lack of feedback and would warrant automatic control. The authors mathematically modelled a bicycle using kinematic equations based on an inverted pendulum model. They then examined the yaw and roll dynamics for three different HPV designs; a conventional front wheel steered HPV with trail, a conventional front wheel steered HPV without trail and finally an unconventional rear wheel steered HPV. From the results of this modelling the authors designed a steering controller for a front wheel steered HPV suitable for a 16-160 km/hr speed range. They concluded that an automatic steering controller was feasible and that the front wheel steering configuration gave the best performance but they gave no details of the results of the different steering geometries. They also proved that the rear wheel steered bicycle was unstable under most conditions because it has an odd number of real unstable poles.

Chen et al produced bicycle equations with nine degrees of freedom (six for the rear frame and rider, two more rotational ones around both wheels and a ninth around the steering axis) using Lagrangian equations and the energy approach (60). They developed balancing and path tracking strategies for the bicycle using steering controllers with both PID and fuzzy logic control action and

details were given of the control schemes and rules table. Outputs using control action showed the bicycle roll angle, X & Y coordinate position and speed against time, but surprisingly not the yaw angle. It was stated that the bicycle path followed showed the model displayed counter-steering action but the scale of their graph makes this hard to discern. The controllers were successful in maintaining balance and following a desired path but the second controller was more able to accurately follow the desired path as it took the yaw angle of the bicycle into account.

A long article by Astrom et al examined in depth the issues of bicycle stability from a control engineering perspective (13). The authors have all used bicycles to teach undergraduate students control engineering in a way that combines theory with hands on experiments. The article discussed rider control, proportionality constants, transfer delays and gyroscopic effects. They developed several increasingly more realistic mathematical bicycle models including one that allowed for front wheel steering angle and trail, but neglected the stabilizing effects of the front fork and any gyroscopic effects. An early model demonstrated that bicycles are unstable without rider feedback or damping. This simple model was a naive bicycle that used a steering angle of 90^{o} just like the Fajans model discussed earlier (12). A piloting model was developed that assumed the rider was a proportional controller who balanced the bicycle by applying a steering torque proportional to the roll angle as proposed by Lignoski (42). They say that in practice riders also use lean actions, though results from Moore's experiments indicate otherwise (45).

Another of their bicycle models examined rear wheel steering and demonstrated why rear wheel steered bicycles are so difficult for riders to control. By examining the model carefully eventually a successful rear wheel steered bicycle was built by their students which could be ridden in some circumstances, demonstrating the value of a control engineering approach. This bicycle had the rider placed very high and very far forward, significantly changing the mass position. Also the bicycle needed to be ridden at some speed just as their equations had shown. This was presented as an interesting and instructive mathematical control problem. They discussed a series of bicycles built as student projects including zero gyroscopic bikes which again proved experimentally that a bicycle can be successfully ridden without gyroscopic assistance. Another section of this paper examined the difficulty of teaching young children to ride bicycles and trialled various modified bicycles designed to make learning easier.

Sharma and Umashankar designed a controller for a bicycle system that stabilises the roll of a bicycle by steering the bicycle into the roll using equations developed from Lowell and McKell (21, 43). Their aim was to see if a fuzzy controller could control an unstable system like a bicycle. Their controller used fifty fuzzy logic rules to determine the required control action for stabilisation. The computer simulation of their controller displayed only marginal stability and showed steady (not decaying) and substantial oscillations of the yaw and roll angles. Three separate very low speed values were used to test the controller (5.4 km/hr, 7.2 km/hr and 9 km/hr) and such low speeds were likely to be a hard test for a controller to achieve system stability. Their equations did not contain a front wheel twisting gravitational torque term and appear to repeat the errors of Lowell

and McKell (21). As their results didn't display any counter-steering action and it is thought that their investigation contains significant errors.

Ringwood and Feng wrote an interesting paper examining front wheel instability at high speeds (61). They used the bicycle equations of Astrom et al and spent some time obtaining experimentally the values for the position of centre of mass from actual road bicycles. Their model didn't include frame compliance, the mass of the front fork or any rider intervention such as feedback. They described the pole variations for different riding conditions and made suggestions regarding stability and this is discussed later in Chapter Six.

2.8. COMPUTER MODELLING

Lynch and Roland's aim was to simulate the motion of a bicycle using a computer and to use the results to generate realistic computer graphics of bicycle motion, an early example of computer animation (49). It was intended that the simulation and graphics could be used to assist in the design and development of new bicycle designs particularly with regard to stability and manoeuvrability. This study was one of the few financed by a bicycle company (the Schwinn Bicycle Company USA). They derived non-linear equations for a bicycle model which consisted of three rigid masses and ten degrees of freedom (six for the rear frame, two more rotational ones around both wheels, a ninth around the steering axis and the tenth for the rider about the roll axis) though they state there are only eight. It included 44 input parameters including: dimensions, masses, moments of inertia, gyroscopic effects, tyre side forces (slip and inclination) and tyre radial and lateral stiffness effects. Only basic details are given in this paper of their equations and no analysis of results is given. Their equations of motion contained several algebraic and typographical errors according to Meijaard et al. for example the side-slip angle of the front wheel did not contain the steering rate angle and this will have led to significant errors (14).

Their equations of motion were solved by computer using the Runga-Kutta procedure and were then used to generate a bicycle graphic animation. The paper showed the results of a bicycle undertaking a slalom manoeuvre and it was stated that the simulation compared well to full scale experimental results and this is shown in a series of figures and photos but no more details or quantification was provided. The authors stated that the limitations of the then available computers (1972) restricted the application of this model due to the high costs of producing a simulation. They stated that one useful outcome was that the generated graphic allowed nontechnical people to more easily understand the bicycle dynamics by observing the computer graphic of the bicycle's motion.

Donida et al developed a specific motorcycle computer model using ten packages from the Modelica Multibody software library (62). The equations of motion used in the model were based on both Cossalter's and Sharp's equations (8, 55). It is unclear from this paper how much these authors independently developed and how much was already available from the existing Motorcycle Dynamics library. Ten Modelica packages were used, namely: an eleven degrees of freedom (which are not defined in the paper) motorcycle package and other packages for: the chassis, suspension, rear swinging arm, wheels, tyre road interaction, braking systems, aerodynamics, road environment

and the driver. These ten packages were parametric, allowing a manufacturer to perform virtual prototyping of a proposed motorcycle design. This approach could be adapted and used for bicycle design.

2.9. CHRONOLOGICAL REVIEWS

At least two major papers chronologically reviewing studies into bicycle motion have been written.

Sharp's earlier paper was a chronological review of research into bicycle dynamics covering over a hundred years up until 1985 (8). It looks at forty five papers by researchers in this field including the author's other publications. It summarised the main contributions and conclusions of each paper but didn't present any numerical results or conclusions on bicycle stability or performance. It stated that at the time of writing (1985) a good understanding of bicycle dynamics had been achieved but that some important aspects were still not understood. The following areas that needed better understanding were mentioned: the rider bicycle interaction, the structural properties of the rider and frame flexibility.

More recently Meijaard et al reviewed the work of many researchers and over 70 papers in this field from 1866 till 2006 and compared historical equations and models to their own work in a detailed supplementary appendix (63). They conclude *"Although many reports, theses and papers have models at least almost as general as Whipple's model, and many of these are largely correct, as yet there is no consensus that any peer-reviewed paper in English has correct equations.*" As already mentioned they stated that their other work can be used to benchmark other researchers' bicycle models (14).

2.10. REMARKS

This literature survey concludes that there has been intensive research on bicycle dynamics and stability including the development of suitable equations of motion that can describe bicycle motion. Work on how various control methodologies can be made to pilot bicycles have been completed and some have had apparent success when applied to the experimental area. However the literature lacks information about how this available research can be used to develop proper design methodologies. Designers lack clear guidelines on how to improve and optimise their designs and so still rely on empirical observations and trial and error. Some of the studies into bicycle instability and the sensitivity of the bicycle to changes in key parameters are contradictory and need resolving. This is a major area of interest which will be examined further in this thesis. As most of today's evaluations of bicycle performance are subjective and not quantified, another objective is to develop methodologies that will define bicycle handling performance.

The following main points are raised:

1. The equations are complicated with some terms being important while others much less so. To make a suitable design methodology it is appropriate that only the critical terms be considered

2. The literature includes many examples of dynamic equations for the bicycle but these are not well correlated to design parameters.
3. The dynamic analysis of motion has not been looked at in detail in relation to bicycle design

2.11. INVESTIGATION OBJECTIVES

Considering the above remarks the main objectives of this work may be summarised as follows:

1. Investigate the possibility of developing a set of simplified yet still relatively accurate equations of motion with the flexibility to use in developing design methodologies. This is achieved by formulating an appropriate dynamic model which will be used to:
    a. look at the dynamic responses of the bicycle and to see how they relate to the rider
    b. investigate which terms in these equations are critical for the design process
    c. determine the effectiveness of the model in determining bicycle performance
    d. see if the bicycle can be optimised in terms of specific performance criteria
    e. simulate the above equations and validate them and then determine the realistic behaviour of the bicycle when using practical design parameters
2. Investigate the bicycle's performance in terms of its sensitivity to design parameters changes:
    a. first by formulating appropriate values for these design parameters which can then be used to develop an appropriate sensitivity methodology
    b. using this sensitivity methodology to identify critical design parameters and quantify their effects
    c. and determining which ones must be considered and which ones can be ignored so that the dynamic equations can be simplified while still maintaining a model that can accurately simulate bicycle behaviour
3. Develop a scientifically based design methodology which designers can use as a standard method, this includes:
    a. evaluation of alternative design methodologies including: criteria, tables, equations and charts
    b. developing and making appropriate recommendations for a suitable standardised design methodology
    c. and collecting design specifications from highly regarded bicycles for validation of this recommended design methodology

2.12. CLOSURE

In this Chapter a comprehensive literature survey has been completed which concluded with important remarks used to develop the objectives of this research. Chapter Three will continue this investigation by developing equations of motion for a bicycle that can be solved using a Simulink computer model. This model will be able to simulate different bicycle designs allowing key design parameters to be quantified in terms of their effect on handling performance. This analysis will then be used to develop a suitable design methodology.

3. BICYCLE MODEL FORMULATION

3.1. INTRODUCTION

This Chapter explains the theory behind the bicycle dynamic model used in this work. The assumptions used in the model are explained and justified. Finally it describes how the equations of motion for the model were developed, formulated and solved. One important feature of the proposed model is it can isolate and examine individual terms and design parameters allowing quantitative comparisons to be made. It is possible to easily adjust these individual terms in the model in order to undertake an evaluation of the significance of each torque term and a sensitivity study.

3.2. MODEL FORMULATION

A bicycle is a surprisingly complex problem which exhibits both yaw and significant roll, both of which are interrelated. It consists of at least six rigid bodies, see Figure 1:

1. front wheel
2. rear wheel
3. front fork and handlebar
4. main frame
5. lower part of rider
6. upper part of rider

However simplifying it down into two bodies is a common approach in the literature and this Chapter assumes the bicycle can be modelled as two bodies or assemblies A and B, see Figure 2 and Table 13 (12, 21, 37).

1. Assembly “A” consists of the front wheel, the front forks and the handlebars. These all turn and move together with one exception, the front wheel is free to rotate about its axle.
2. The other assembly “B” consists of the main triangular frame, the rear wheel and the rider. The frame and the rear wheel move together as one, except the rear wheel is free to rotate about its axle (12, 21, 30).

Assemblies A and B are linked by the steerer and head tubes acting as a hinge that is free to move about an axis defined by the head tube angle. Despite the rider not being a fixed body, it is common practice to treat the rider as a rigid body fixed to the rear frame and the justification for this was established experimentally by Kooijman et al (12, 21, 30, 44).

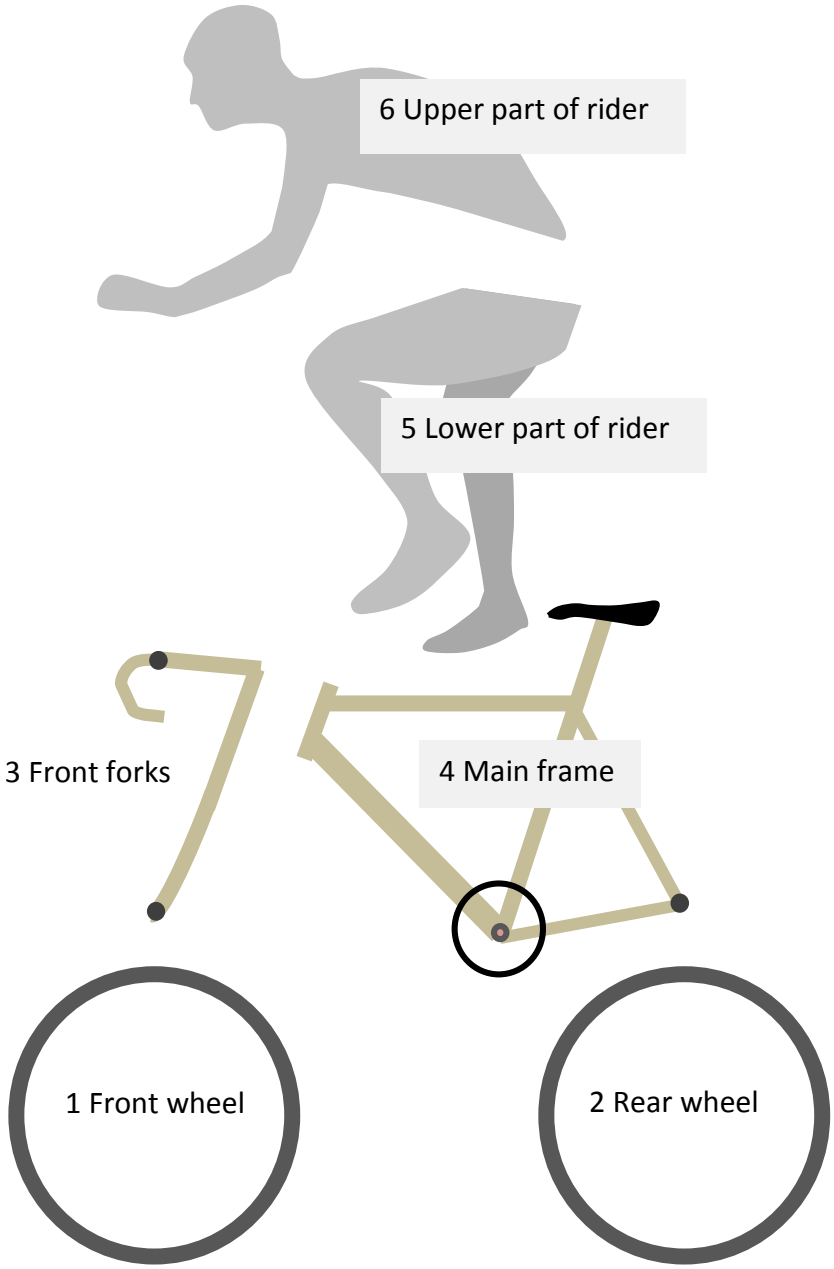

Figure 1 A six part bicycle rider model

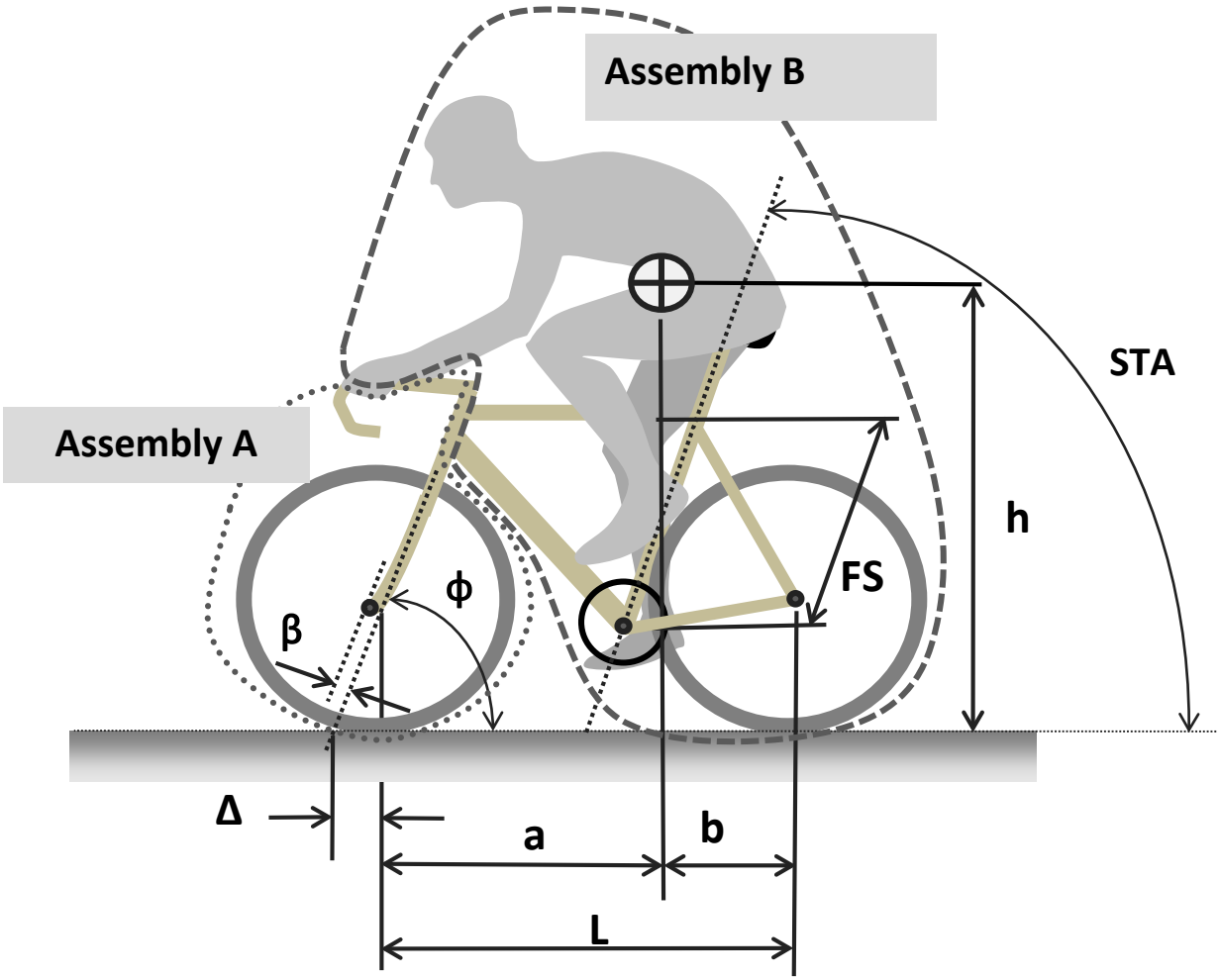

Figure 2 Bicycle terms for the selected model, see Table 5

Table 5 Bicycle model definitions, see Figure 2

	Symbol	Term Definition
1.	L	wheelbase
2.	a	horizontal distance from front wheel contact point to centre of mass
3.	b	horizontal distance from rear wheel contact point to centre of mass
4.	h	vertical distance from road surface to centre of mass
5.	ϕ	head tube angle (phi)
6.	β	fork rake also called offset (beta)
7.	Δ	front wheel trail (delta)
8.	FS	frame size
9.	STA	seat tube angle

3.3. MODEL ASSUMPTIONS

Due to the complexity of the bicycle rigid body model it is necessary to establish the following simplifying assumptions.

1. the bicycle consists of two rigid bodies assemblies A and B with the principal axes of inertia for each body lying along vertical and horizontal planes, see Figure 2
2. the rider is part of assembly B and is assumed to be rigid, therefore its centre of mass is fixed and all the mass of the system (both A and B) is concentrated at this point for the purposes of gravitational and centripetal effects
3. The three axes coordinate system for the bicycle model (Figure 3) conforms to the ISO standard 8855:2011 “Road vehicles -- Vehicle dynamics and road-holding ability – Vocabulary.” This standard from the International Organization for Standardization defines the principal terms used for road vehicle dynamics (1). These terms apply to passenger cars, buses and commercial vehicles but have been used in the literature for bicycle applications (37). The three axes coordinate system ha sits origin at the rear tyre contact point and moves with the bicycle.
4. the Coriolis effects of the front and rear assemblies (A and B) are included
5. the bicycle frame, front forks and both wheels are all rigid structures and do not distort in shape
6. all aerodynamic forces on the bicycle and rider are ignored
7. the road is smooth, level and uncambered

8. the bicycle is travelling at a constant speed, it is not pitching or bouncing and both the roll and steering angles are small i.e. less than 10 degrees
9. the tyres are thin and do not distort or slip sideways when cornering or slip in the direction of travel
10. all moments are assumed to be pure couples including steering torque which is applied by the rider and the bicycle is capable of undertaking a counter-steer cornering manoeuvre
11. the front tyre, rear tyre and centre of mass turn through the same radius when cornering
12. the radius of cornering is much larger than the bicycle wheelbase
13. realistic steering geometry can be used i.e. the fork rake and head tube angle can be varied to model realistic bicycles

Most of the above assumptions are self-explanatory, however some need clarification.The second assumption is that the human rider is a rigid body attached solidly to the rear frame (all of which is called assembly B). Kooijman et al have demonstrated that the rider steers and stabilises the bicycle mainly by steering inputs with very little upper body lean (44). Therefore no pedalling action and no counterbalancing using the rider's torso (called hip flick by Fajans) was considered in this model and the only piloting aspect of the human rider is that of a simple steering torque action (12).

To explain assumption six, the intention was to investigate the characteristics of the bicycle rider system and so it was not necessary to complicate the problem by considering external forces such as aerodynamic forces.

Regarding assumption nine, many researchers of road bicycles have assumed that the wheels to be thin discs and have ignored tyre effects (12-14, 21). Furthermore, after Koojiman et al ran an instrumented bicycle on a rolling road they concluded when referring to their maths model that *"the most dubious assumption that was validated in this model was the replacement of the tyres by knife edge wheels rolling without slipping"* (14, 34). On the other hand it is common for complex tyre models to be used when modelling motorcycles (33, 55, 62). Given that road bicycle tyres are much smaller in width (20 mm vs. 180 mm) and operate at higher inflation pressures than motorcycles (7 bar vs. 2 bar) it is reasonable to expect that they distort less and therefore could be modelled as thin discs. Experimental work by Dressel and Rahman found that the tyre relaxation length of a bicycle was only between 40 and 60 mm and this compares to the much larger tyre relaxation length of motorcycles which are between 100 and 500 mm (64). The tyre relaxation length is a measure of delay between when the front wheel is turned and when the tyre cornering force reaches a steady state value. The shorter this length, the shorter the delay and the more like a thin disc the wheel behaves.

However, previous work has indicated that the model requires some dampening for stability (12). Thus in this current work this tyre damping effect is included by adding a dampening term to the model.

Longitudinal wheel slip (in the direction of travel) has been ignored as it is assumed that such slip only occurs when braking or accelerating (65). Sideways tyre friction is present in the model and is essential in order for the bicycle to corner and to be stable. However, the current model ignores tyre rolling resistance as it is assumed that the speed is constant.

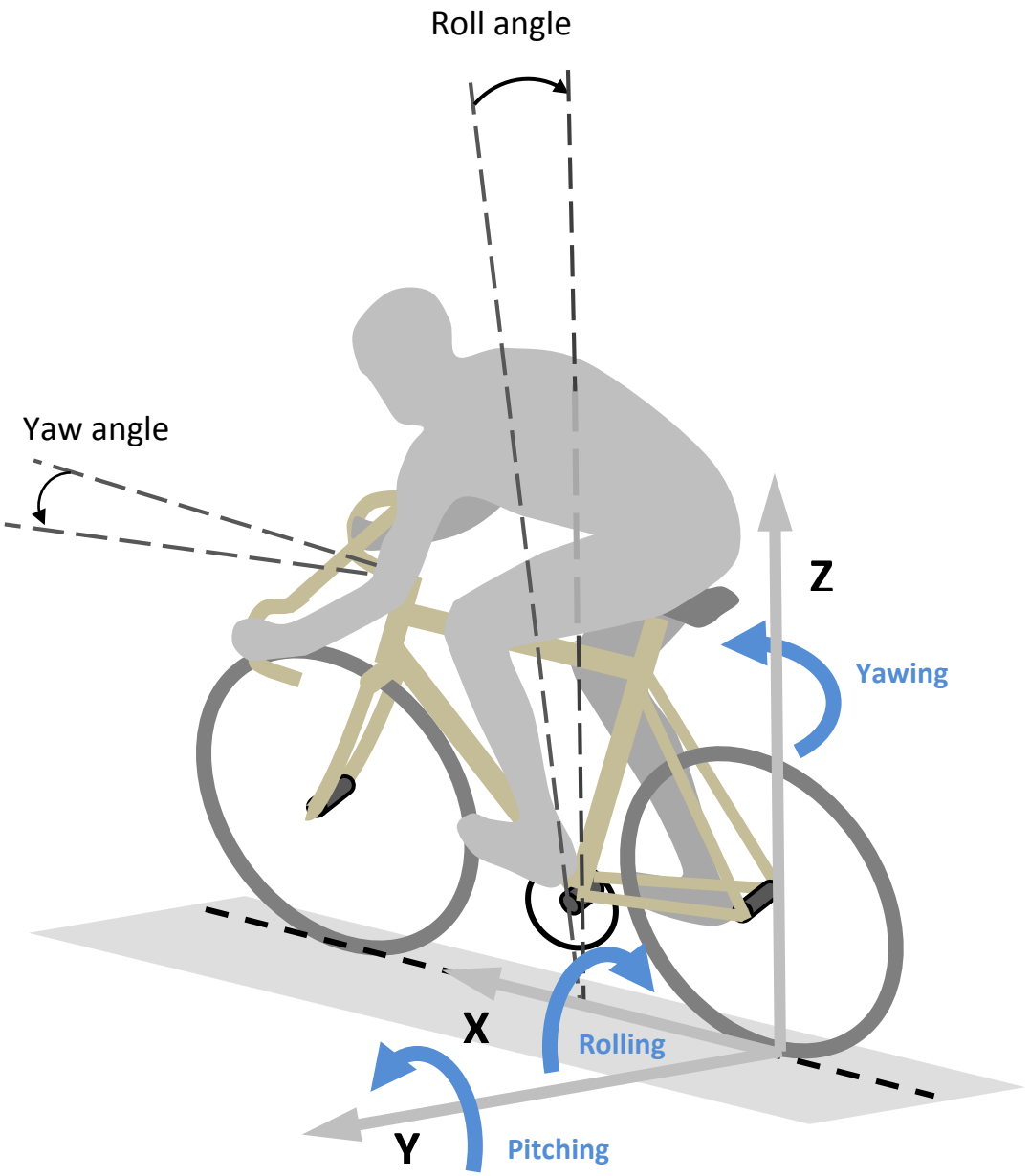

Figure 3 Bicycle axes for the selected model, positive directions shown, per ISO 8855 (1)

3.4. BICYCLE EQUATIONS OF MOTION

3.4.1.BASIC LAWS

In order to develop the equations of motion needed to solve the rigid body dynamics of the bicycle we begin with the Newton Laws of Motion and the General Equations of Motion and then by applying simplifying assumptions developed a suitable mathematical model for the bicycle.

For simplicity many of the parameters in this Section are defined in Table 5 and the remainder are explained in the Nomenclature and Glossary Sections (see also Table 6, Table 7 and Table 8). It is possible to apply the general momentum equations of motion in order to fully describe any three dimensional dynamic motion of a rigid body such as a bicycle (53, 66). For linear motion the equations of motion can be written in the three axes Cartesian coordinate system as (66):

$$\Sigma F_X = m_{XX}\dot{v}_X + \left(I_{ZZ} - I_{yy}\right)\omega_Y\omega_Z \tag{1}$$

$$\Sigma F_Y = m_{YY}\dot{v}_Y + \left(I_{ZZ} - I_{yy}\right)\omega_Y\omega_Z \tag{2}$$

$$\Sigma F_Z = m_{ZZ}\dot{v}_Z + \left(I_{ZZ} - I_{yy}\right)\omega_Y\omega_Z \tag{3}$$

Where F is force, m is mass, I is mass moment of inertia and ω is angular velocity and the Cartesian coordinate X, Y and Z system conforms to Figure 3, where X is the longitudinal direction, Y is the transverse and Z is the vertical direction. Similarly for the angular motion of a constant mass body the Momentum Equation applies:

$$\Sigma T = \dot{H} \tag{4}$$

Where T is the torque and $\dot{H}$ is the change in angular momentum. Now the general equations of motion for rigid body motion in the three axis Cartesian coordinate system (see Figure 3) attached to the body can be written:

$$\Sigma T_X = \dot{H}_X - H_Y\omega_Z + H_Z\omega_Y \tag{5}$$

$$\Sigma T_Y = \dot{H}_Y - H_Z\omega_X + H_X\omega_Z \tag{6}$$

$$\Sigma T_Z = \dot{H}_Z - H_X\omega_Y + H_Y\omega_X \tag{7}$$

Where the three components of angular momentum are:

$$\dot{H}_X = I_{XX}\dot{\omega}_X - I_{YZ}\dot{\omega}_Y - I_{ZX}\dot{\omega}_Z \tag{8}$$

$$\dot{H}_Y = -I_{XY}\dot{\omega}_X - I_{YY}\dot{\omega}_Y - I_{YZ}\dot{\omega}_Z \tag{9}$$

$$\dot{H}_Z = -I_{ZX}\dot{\omega}_X - I_{YZ}\dot{\omega}_Y + I_{ZZ}\dot{\omega}_Z \tag{10}$$

These equations state that the sum of the torques equal the change in angular momentum for bodies of constant mass.

3.4.2.THE EULER EQUATIONS OF MOTION

The principal axes of inertia of a body are defined as those about which the maximum values for the mass moments of inertia occur. For symmetrical bodies the principal axes occur on planes of symmetry (53, 66). In the case of body like a cylinder, as the body is symmetrical about the X, Y and Z axes they are all principal axes. And as the origin of the reference axes X, Y and Z coincide with the centre of mass, then the inertia tensors I_{XY}, I_{YZ} and I_{XZ} all equal zero and the General Equations of Motion simplify to the Euler Equations of Motion.

So if the bicycle model can be assumed to be symmetrical about X, Y and Z the three momentum equations of motion, (8 to (10 may be simplified into the Euler equations, but is this a reasonable proposition?

- Considering the rider alone (which is the dominant mass in the system) Hanavan records values for the inertia tensors as follows; I_{XZ} = -1.7218 kgm^2, $I_{XY} = I_{YZ}$ = 0 kgm.^{2}
- Similarly Meijaard et al records the following values the inertia tensors for their equivalent of assembly B, as I_{XZ} = 2.4 kgm^2, $I_{XY} = I_{YZ}$ = 0 kgm.^{2} (14, 48).
- Therefore in both these cases two of the three tensors equal zero and the third tensor I_{XZ} has a value of about 25% of the principal moment of inertia I_{XX}.
- Also the bicycle by itself (without a rider) is symmetrical about the longitudinal X axis and is approximately symmetrical about the vertical Z located through the centre of mass.

Therefore the assumption to use Euler Equations for the bicycle model can be justified and this greatly simplifies the equations of motion. Also it is common practice in the study of automobile vehicle dynamics to assume that the Euler equations apply (53).

The Euler Equation of Motion about the X axis is:

$$\Sigma T_X = I_{XX}\dot{\omega}_X + I_{ZZ}\omega_Y\omega_Z - I_{YY}\omega_Y\omega_Z \tag{11}$$

The first right hand term is the inertia torque, the second the gyroscopic torque and the third is torque due to Coriolis acceleration.

Similarly the Euler Equations of Motion about the Y and Z axes are:

$$\Sigma T_Y = I_{YY}\dot{\omega}_Y + I_{XX}\omega_X\omega_Z - I_{ZZ}\omega_X\omega_Z \tag{12}$$

$$\Sigma T_Z = I_{ZZ}\dot{\omega}_Z + I_{YY}\omega_Y\omega_X - I_{XX}\omega_Y\omega_X \tag{13}$$

3.4.3. GOVERNING EQUATION DEVELOPMENT

It is possible to deal with the six equations of motion previously detailed [i.e. equations (1) to (3) and (11) to (13)] however in this research our interest is focused on yawing and rolling of the bicycle. Therefore the following simplifications can be made:

1. Forces and linear motion in the X axis are neglected as the bicycle is assumed to be travelling at a constant forward linear speed with no acceleration or braking. Therefore, there are no linear accelerations along the X axis and this eliminates equation (1)
2. Forces and linear motion in the Y axis are also neglected as the tyres are assumed to have no side slip angle (so that the radius of cornering is equal to the wheelbase/steering angle R = L/σ, see Figure 4). Therefore, there are no linear accelerations along the Y axis so this eliminates equation (2)
3. Forces and linear motions in the Z axis are neglected as the road is assumed to be level and smooth, so there is no bouncing. Therefore, there are no linear accelerations along the Z axis eliminating equation (3)
4. All rotations about the Y axis are neglected (except for the gyroscopic torque due to the spinning of each wheel) as the road is assumed to be smooth and level therefore the bicycle is not pitching and this eliminates Euler equation (12). Note that the gyroscopic torque of each rotating wheel is accounted for by taking them about the central axis of each wheel and treating them as pure couples.

Thus the governing equations of motion to consider for the bicycle model are:

1. The sum of moments about the horizontal axis (X) for assembly A (producing rolling), refer to Euler equation (11) and Figure 3
2. The sum of moments about the horizontal axis (X) for assembly B (producing rolling), refer to Euler equation (11) and Figure 3
3. And the sum of moments about the vertical axis (Z) for assembly A (producing yawing), refer to Euler equation (13) and Figure 3

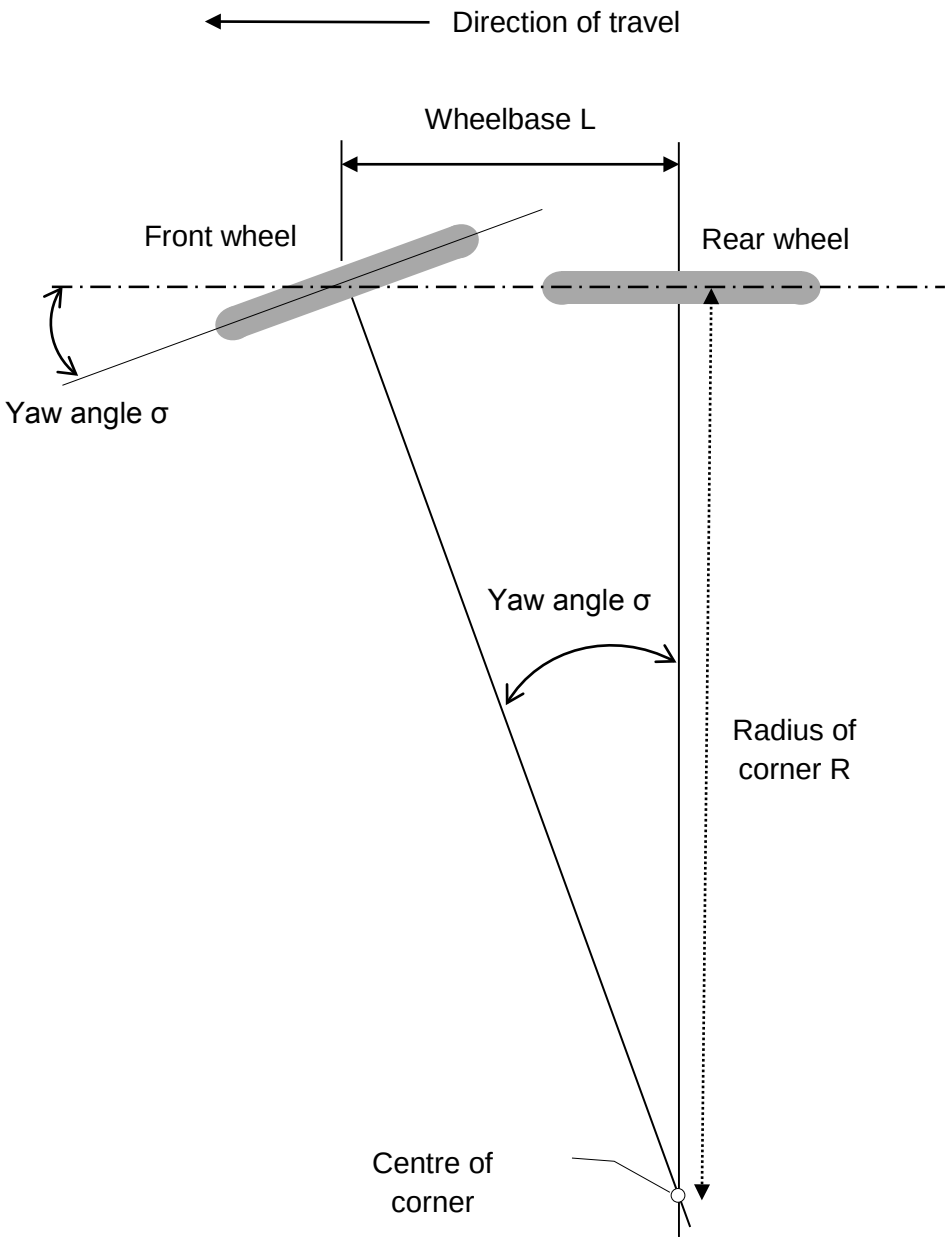

Figure 4 Cornering bicycle geometry indicated the relationships between L, σ and R

Now that the assumptions and definitions have been dealt with, the equations of motion for a bicycle dynamic model can be formulated. All the torque terms in the following equations are defined in Table 6, Table 7 and Table 8. Their derivations are available in the literature along with suitable freebody diagrams of the model (12, 21, 30). The first equation considers yawing moments about the vertical Z axis for the front assembly A (see Figure 2) and results in:

$$T_{inertia} + T_{gyro/roll} - T_{Coriolis} = T_{steer} - T_{Jones} - T_{castor} + T_{frame} - T_{damping} \tag{14}$$

Incorporating the bicycle X, Y, Z axes from Figure 3 this equation is expanded out to:

$$I_{ZA}\,\dot{\omega}_{ZA} + I_{YF}\,\omega_{YF}\omega_{XF} - I_{XF}\,\omega_{YF}\omega_{XF} = T_S\,sin\phi - Mg\frac{b}{L}sin\phi\Delta_e\,\lambda - M\frac{bv^2}{L^2}sin\phi\Delta_e\,\sigma + T_f\cos\phi - \Gamma\dot{\sigma} \tag{15}$$

And is further expanded to:

$$I_{ZA}\,sin\emptyset\ddot{\sigma} + I_{YF}\frac{v}{r}\dot{\lambda} - I_{XF}\frac{v}{r}\dot{\lambda} = T_S\,sin\phi - Mg\frac{b}{L}sin\phi\Delta_e\,\lambda - M\frac{bv^2}{L^2}sin\phi\Delta_e\,\sigma + T_f\cos\phi - \Gamma\dot{\sigma} \tag{16}$$

Then rearranged to make T_S sinϕ the subject:

$$T_S\,sin\phi = I_{ZA}sin\emptyset\ddot{\sigma} + I_{YF}\frac{v}{r}\dot{\lambda} - I_{XF}\frac{v}{r}\dot{\lambda} + Mg\frac{b}{L}sin\phi\Delta_e\,\lambda + M\frac{bv^2}{L^2}sin\phi\Delta_e\,\sigma - T_f\cos\phi + \Gamma\dot{\sigma} \tag{17}$$

Further simplification gives the first equation of motion:

$$T_S\,sin\phi = I_{ZA}sin\emptyset\ddot{\sigma} + \left(I_{YF}\frac{v}{r} - I_{XF}\frac{v}{r}\right)\dot{\lambda} + Mg\frac{b}{L}sin\phi\Delta_e\,\lambda + M\frac{bv^2}{L^2}sin\phi\Delta_e\,\sigma - T_f\cos\phi + \Gamma\dot{\sigma} \tag{18}$$

The second equation considers rolling moments about the horizontal X axis for the front assembly A and results in:

$$T_{inertia} + T_{Coriolis} - T_{gyro/yaw} = T_{frame} + T_{gyro/cornering} - T_{steer} + T_{castor} + T_{Jones} \tag{19}$$

This is expanded out to:

$$I_{XA}\,\dot{\omega}_{XA} + I_{ZF}\omega_{YF}\omega_{ZF} - I_{YF}\omega_{YF}\omega_{ZF} = T_f\,sin\phi + \frac{I_{YF}v^2 sin\phi}{rL}\sigma - T_S\cos\phi + M\frac{bv^2}{L^2}cos\phi\Delta_e\sigma + Mg\frac{b}{L}cos\phi\Delta_e\lambda \tag{20}$$

Using the bicycle X, Y, Z axes this equation is expanded out to:

$$I_{XA}\ddot{\lambda} + I_{ZF}\frac{v}{r}sin\phi\dot{\sigma} - I_{YF}\frac{v}{r}sin\phi\dot{\sigma} = T_f\, sin\phi + \frac{I_{YF}v^2 sin\phi}{rL}\sigma - T_s\cos\phi + M\frac{bv^2}{L^2}cos\phi\Delta_e\sigma + Mg\frac{b}{L}cos\phi\Delta_e\lambda$$

(21)

This is rearranged to make T_f sinϕ the subject:

$$T_f\, sin\phi = I_{XA}\ddot{\lambda} + I_{ZF}\frac{v}{r}sin\phi\dot{\sigma} - I_{YF}\frac{v}{r}sin\phi\dot{\sigma} - \frac{I_{YF}v^2 sin\phi}{rL}\sigma + T_s\cos\phi - M\frac{bv^2}{L^2}cos\phi\Delta_e\sigma - Mg\frac{b}{L}cos\phi\Delta_e\lambda$$

(22)

Simplification gives the second equation of motion:

$$T_f\, sin\phi = I_{XA}\ddot{\lambda} - Mg\frac{b}{L}cos\phi\Delta_e\lambda + \left[I_{ZF}\frac{v}{r}sin\phi - I_{YF}\frac{v}{r}sin\phi\right]\dot{\sigma} - \left[\frac{I_{YF}v^2 sin\phi}{rL} + M\frac{bv^2}{L^2}cos\phi\Delta_e\right]\sigma + T_s\cos\phi$$

(23)

Finally the third equation considers rolling moments about the horizontal X axis for the rear assembly B (see Figure 2) resulting in:

$$T_{inertia} + T_{Coriolis} - T_{gyro/cornering} = -T_{frame} + T_{centrifugal} + T_{gravity} + T_{kink}$$

(24)

Applying the bicycle X, Y, Z axes this equation is expanded out to:

$$I_{XB}\,\dot{\omega}_{XB} + I_{ZR}\omega_{YR}\omega_{ZR} - I_{YR}\omega_{YR}\omega_{ZR} = -T_f\sin\phi + \frac{Mv^2 sin\phi h}{L}cos\lambda\sigma + Mgh\sin\lambda + \frac{Mhbv}{L}\dot{\sigma}$$

(25)

And is further expanded to become the third equation of motion:

$$I_{XB}\ddot{\lambda} + I_{ZR}\frac{v}{r}\sigma - I_{YR}\frac{v^2}{rL}\sigma = -T_f\sin\phi + \frac{Mv^2 sin\phi h}{L}cos\lambda\sigma + Mgh\sin\lambda + \frac{\mathrm{Mhbv}}{\mathrm{L}}\dot{\sigma}$$

(26)

Equations (18), (23) and (26) have σ (sigma, yaw) and λ (lamda, roll) as the main outputs and T_S (steering torque) as the main input. Because T_f (frame torque) is the torque of interaction between assemblies A and B it can be eliminated in these preceding equations.

Now equations (18), (22) and (26) are similar to those developed by Fajans but have additional terms added (12). These additional terms allow for the Coriolis effect, the steering head tube angle and trail, as one of main objectives of this work was to investigate the significance of these additional terms. All of the torques in these three equations are self-explanatory except for the kink torque in equation (26) i.e. $\frac{Mhbv}{L}\dot{\sigma}$. As the second term on the left hand side of equation (26) i.e. $I_{ZR}\frac{v}{r}\sigma$, only accounts for the Coriolis Effect of the rear wheel, the kink torque term is required to allow for the remainder of the Coriolis torque on the assembly B, see Figure 5. If the front wheel is turned abruptly, both wheel contact points follow arcs, however, while the rear wheel trajectory smoothly transitions into a curved path the front wheel trajectory has a kink. Likewise the trajectory of the point halfway between the wheels has a similar kink and this results in the kink torque term. Of course the centre of mass doesn't turn straight away, it continues in a straight line and in comparison to the point half way between the wheels appears to be kicked out. For an abrupt change in the steering angle this kink requires an impulsive force which is different from the steady state centrifugal forces as these forces are not subject to such a kink. Fajans described the kink torque as being *"valid in a reference frame rotating at the instantaneous angular frequency V/R = (V/L) x σ"* (12).

Table 6 Terms in equation (14)

Term	Expanded term	Physical meaning
$T_{Inertia}$	$I_{ZA}\dot{\omega}_{ZA}$	Inertia torque due to the yawing of A
$T_{Gyro/roll}$	$I_{YF}\omega_{YF}\omega_{XF}$	Gyroscopic torque due to the rolling of A
$T_{Coriolis}$	$I_{XF}\omega_{YF}\omega_{XF}$	Coriolis torque of A
T_{Steer}	$T_S \sin\phi$	Steering torque input by rider, corrected for the head tube angle
T_{Jones}	$Mg\frac{B}{L}\sin\phi\Delta_e\lambda$	Jones torque or trail steer, causes the wheel to lean into the corner
T_{Castor}	$M\frac{bv^2}{L^2}\sin\phi\Delta_e\sigma$	Castor torque due to trail, tends to straight the wheel up
T_{Frame}	$T_f \cos\phi$	Torque of assembly B on A, corrected for the head tube angle
$T_{Damping}$	$\Gamma\dot{\sigma}$	Damping torque (if this term is zero the bicycle may be unstable)

Table 7 Terms in equation (19)

Term	Expanded term	Physical meaning
$T_{Inertia}$	$I_{XA}\dot{\omega}_{XA}$	Inertia torque of the front wheel due to rolling of A
$T_{Coriolis}$	$I_{ZF}\omega_{YF}\omega_{ZF}$	Coriolis Torque of A
$T_{Gyro/yaw}$	$I_{YF}\omega_{YF}\omega_{ZF}$	Gyroscopic torque of front wheel due to yawing of A
T_{Frame}	$T_f \sin\phi$	Torque Assembly B exerts on A corrected for the head tube angle
$T_{Gyro/cornering}$	$\mathrm{I_{YF}}\frac{\mathrm{v}^2 \sin\phi}{\mathrm{rL}}\sigma$	Gyroscopic torque of front wheel due to cornering
T_{Steer}	$T_S \cos\phi$	Steering Torque corrected for the head tube angle
T_{Castor}	$M\frac{bv^2}{L^2}\cos\phi\Delta_e\sigma$	Castor torque corrected for the head tube angle
T_{Jones}	$Mg\frac{b}{L}\cos\phi\Delta_e\lambda$	Jones torque corrected for the head tube angle

Table 8 Terms in equation (24)

Term	Expanded Term	Physical Meaning
$T_{Inertia}$	$I_{XB}\dot{\omega}_{XB}$	Inertia torque of frame , rider and rear wheel due to rolling of B
$T_{Coriolis}$	$I_{ZR}\omega_{YR}\omega_{ZR}$	Coriolis Torque of the rear wheel
$T_{Gyro/cornering}$	$I_{YR}\omega_{YR}\omega_{ZR}$	Gyroscopic torque of rear wheel due to cornering
T_{Frame}	$T_f \sin\phi$	Torque Assembly A exerts on Assembly B corrected for the head tube angle
$T_{Centrifugal}$	$M\frac{v^2 h \sin\phi}{L}\cos\lambda\sigma$	Centrifugal torque
$T_{Gravity}$	$Mgh\sin\lambda$	Gravitational torque
T_{Kink}	$\frac{Mhbv}{L}\dot{\sigma}$	Kink torque (Coriolis torque of assembly B less rear wheel)

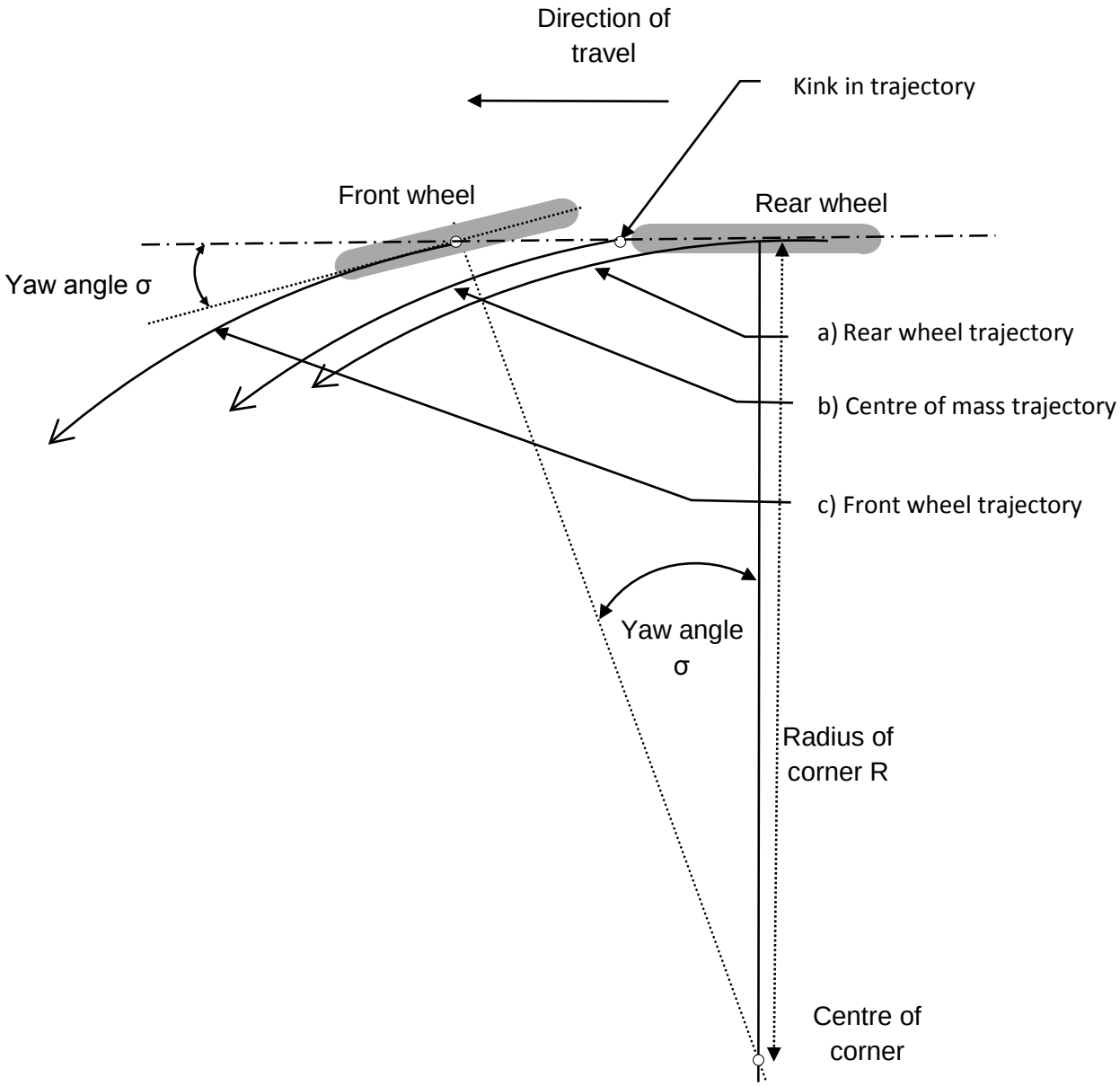

Figure 5 The kink torque results from three different trajectories a), b) and c)

3.5. SIMULINK EQUATIONS

There are many approaches that could be used to solve equations such as equations (18), (23) and (26), however we chose to use Simulink in a Matlab environment because by using this software it was easier correlate between individual equation terms, the bicycle design parameters and the performance in terms of handling.

In this Chapter the three bicycle equations of motion (18), (23) and (26) are used to formulate a mathematical model for dynamic motion which will be solved using Simulink. This section describes the development of these Simulink equations into a model that can accurately simulate bicycle dynamic behaviour.

Different inputs such as riding conditions and bicycle geometry were used in the model to quantify the effect they have on the dynamic behaviour. An important feature of this model was the ability to use different steering geometries in order to achieve optimum steering performance and it will be necessary to change design parameters to investigate their individual effect on the model. Also it was important to be able to isolate individual torque terms to determine their significance and to see which ones could be disregarded, so further simplifying the equations for other purposes.

The three governing equations of motion must first be rearranged so that they can be solved with Simulink to first find the rate of change of yaw ($\ddot{\sigma}$) and of roll ($\ddot{\lambda}$) of a bicycle and then plot the angles of front wheel yaw (σ) and bicycle roll (λ) against time, see Figure 3.

(14) considered the yawing moments about the vertical Z axis for the front assembly A and after considering the bicycle's physical parameters it reduces to equation (18). Now this equation by using the terms A1, A2…An (see Table 9) can be reduced further to:

$$A_3\ddot{\sigma} = T_s \sin\phi - A_1\dot{\lambda} - A_2\lambda - A_4\dot{\sigma} - A_5\sigma + A_6 \tag{27}$$

It is then rearranged to make $\ddot{\sigma}$ the subject:

$$\ddot{\sigma} = \frac{T_S \sin\phi}{A_3} - \frac{A_1\dot{\lambda}}{A_3} - \frac{A_2\lambda}{A_3} - \frac{A_4\dot{\sigma}}{A_3} - \frac{A_5\sigma}{A_3} + \frac{A_6}{A_3} \tag{28}$$

Similarly equations (19) and (22) which allow for the roll of assembly A about X, reduce to:

$$T_f \sin\phi = B_1\ddot{\lambda} - B_2\lambda + B_3\dot{\sigma} + B_4\sigma + T_s\cos\phi \tag{29}$$

Where terms B1, B2…Bn have been substituted (see Table 9)

Next equations (24) and (26) which allow for the roll of assembly B about X, can be reduced by using terms C1, C2…Cn (see Table 9) to:

$$T_f \sin\phi = -C_1\ddot{\lambda} - C_2\sigma + C_3\sin\lambda + C_4 cos\lambda\sigma + C_5\dot{\sigma} + C_6\sigma \tag{30}$$

Equating equations (29) and (30) gives:

$$B_1\ddot{\lambda} - B_2\lambda + B_3\dot{\sigma} + B_4\sigma + T_s\cos\phi = -C_1\ddot{\lambda} - C_2\sigma + C_3\sin\lambda + C_4 cos\lambda\sigma + C_5\dot{\sigma} + C_6\sigma \tag{31}$$

Which is rearranged to make $\ddot{\lambda}$ the subject giving:

$$\ddot{\lambda} = \frac{-C_2\sigma}{(B_1+C_1)} + \frac{B_2\lambda}{(B_1+C_1)} + \frac{C_3\sin\lambda}{(B_1+C_1)} + \frac{(C_5-B_3)\dot{\sigma}}{(B_1+C_1)} + \frac{(C_6-B_4)\sigma}{(B_1+C_1)} + \frac{C_4\cos\lambda\sigma}{(B_1+C_1)} - \frac{T_s\cos\phi}{(B_1+C_1)} \tag{32}$$

It is equations (28), (29) and (32) that Simulink will solve to find the dynamic behaviour of the bicycle.

3.6. CLOSURE

This Chapter has developed the three equations of motion that solve the rigid body dynamics for the bicycle, beginning with the Newton Laws of Motion and the General Equations of Motion. Euler equations were used in the bicycle model, which is reasonable as the bicycle is symmetrical about the X Z plane and is approximately symmetrical in the other planes. Suitable simplifying assumptions were made to develop a mathematical model for the bicycle leaving three equations left to be solved: one to consider yawing moments about the Z axis for the front assembly A, the second considering rolling moments about the X axis for front assembly A and the final third equation considering rolling moments about the X axis for rear assembly B. These equations were reframed into a suitable form for Simulink and in the next Chapter they will be solved.

Table 9 Coefficients An, Bn and Cn

Coefficient	Equal to
A_1	$\left(I_{YF}\frac{v}{r} - I_{XF}\frac{v}{r}\right)$
A_2	$Mg\frac{b}{L}\sin\phi\Delta_e$
A_3	$I_{ZA}\sin\emptyset$
A_4	Γ
A_5	$\frac{Mbv^2}{L^2}\sin\phi\Delta_e$
A_6	$T_S\sin\phi$
B_1	I_{XA}
B_2	$\frac{Mgb}{L}\cos\phi\Delta_e$
B_3	$\left\{\left(I_{ZF}\frac{v}{r}\sin\phi\right) - \left(I_{YF}\frac{v}{r}\sin\phi\right)\right\}$
B_4	$-\left(\frac{I_{XF}v^2\sin\phi}{rL}\right) - \left(M\frac{bv^2}{L^2}\cos\phi\Delta_e\right)$
C_1	I_{XB}
C_2	$I_{ZR}\frac{v}{r}$
C_3	Mgh
C_4	$\frac{Mv^2\sin\phi h}{L}$
C_5	$\frac{Mhbv}{L}$
C_6	$I_{YR}\frac{v^2}{rL}$

4. SIMULATION AND VALIDATION

4.1. INTRODUCTION AND OVERVIEW

Now that the equations of motion for a bicycle have been developed and reframed into a suitable form they can be solved using Simulink in a Matlab environment. This Chapter describes how the model based on equations (18), (23) and (26) from Chapter Three is solved using Simulink.

The Simulink model takes the input from the rider (the steering torque) and after applying appropriate variables and parameters (such as speed, bicycle total mass, wheelbase length, head tube angle, rake) it can find the dynamic response of the bicycle in terms of yaw and roll. An overview of the Simulink computer model is shown in Figure 6 and more detailed diagrams are described later in this Chapter (see also Appendix A).

The models' input variables and design parameters can be easily varied to determine their importance and simulate different manoeuvres, bicycles and riders. This is an important feature of the model as one of the main objectives of this research is to determine appropriate steering geometries in order to achieve optimum steering performance. In addition the damping term can be varied or disregarded to investigate its effect on stability and the results of this computer modelling will be shown in detail in Chapter Five. This Simulink model is made up of six distinct parts which are described below and are also shown in schematic form in Figure 7.

1. Model inputs
    a. The variable inputs (3 in number) see Table 10
        1. Steering torque from the rider (using a Simulink subassembly)
        2. Bicycle velocity
        3. Damping torque
    b. The bicycle parameters (13 terms) shown Table 11
2. Preliminary calculations of the: velocity, steering geometry and wheelbase terms
3. Calculations of the intermediate constants A_n ,B_n & C_n which are shown Table 9
4. Intermediate calculations to find terms for equations (28), (29) and (32)
5. Final calculations of equations (28), (29) and (32) that produce the bicycle model outputs of yaw and roll
6. Simulink bicycle model outputs plotting angles vs. time for:
    a. Yaw or σ
    b. Roll or λ
    c. Frame torque or T_F

The six parts are clearly shown in Figure 7 and they will now be explained more fully in this Chapter along with more detailed diagrams, see also Appendix A.

4.2. INPUT VARIABLE FORMULATION

As already mentioned it has been known for two hundred years that small changes to a bicycle's design have an enormous effect on performance (2, 6, 32, 61). But changes to these design parameters are still largely made on a trial and error basis. *"Bicycles are subject to such complex and variable forces that the bicycle can really only be designed through trial and error and not just by computer modelling (67)."* Therefore appropriate parameter and variable values must be selected for use in the model in order for any simulations to be meaningful.

The Simulink model has three variable inputs: steering torque, speed and damping, which are shown Table 10. The steering torque from the rider can be modelled as any type of common torque input (e.g. impulse, ramp and step) and Figure 8 shows a suitable torque consisting of two impulses (approximately so) the first initiates the turn while the second completes it and stabilises the bicycle in a new direction. A standard steering torque input used for many simulations consists of two small impulses of maximum magnitude + 0.45 Nm and - 0.414 Nm. These two values were found by trial and error to produce a reasonable cornering manoeuvre which returns the bicycle back to an upright position within a reasonable time frame (of 15 to 20 seconds) but of course other values could be used.

A simple Simulink subassembly that can produce this standard steering torque is shown in Figure 9. A second more adaptable subassembly was also developed to allow the steering torque to be easily adjusted in its amplitude and time lag values and details of this second assembly is shown in Appendix A.

Table 10 Model variable inputs

	Symbol	Variable inputs definition	Units
1.	T_{Steer}	Steering torque (from the rider)	Nm
2.	v	Velocity	m/s
3.	Γ	Damping torque	Js

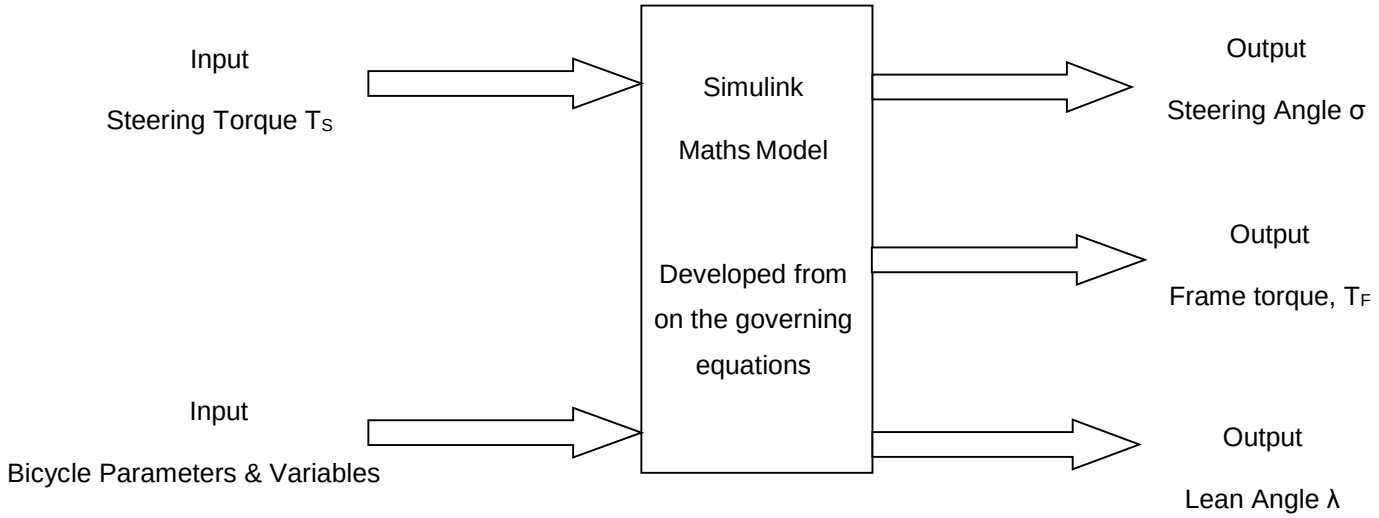

Figure 6 Overview of the Simulink Computer Simulation Model, showing the inputs and three outputs

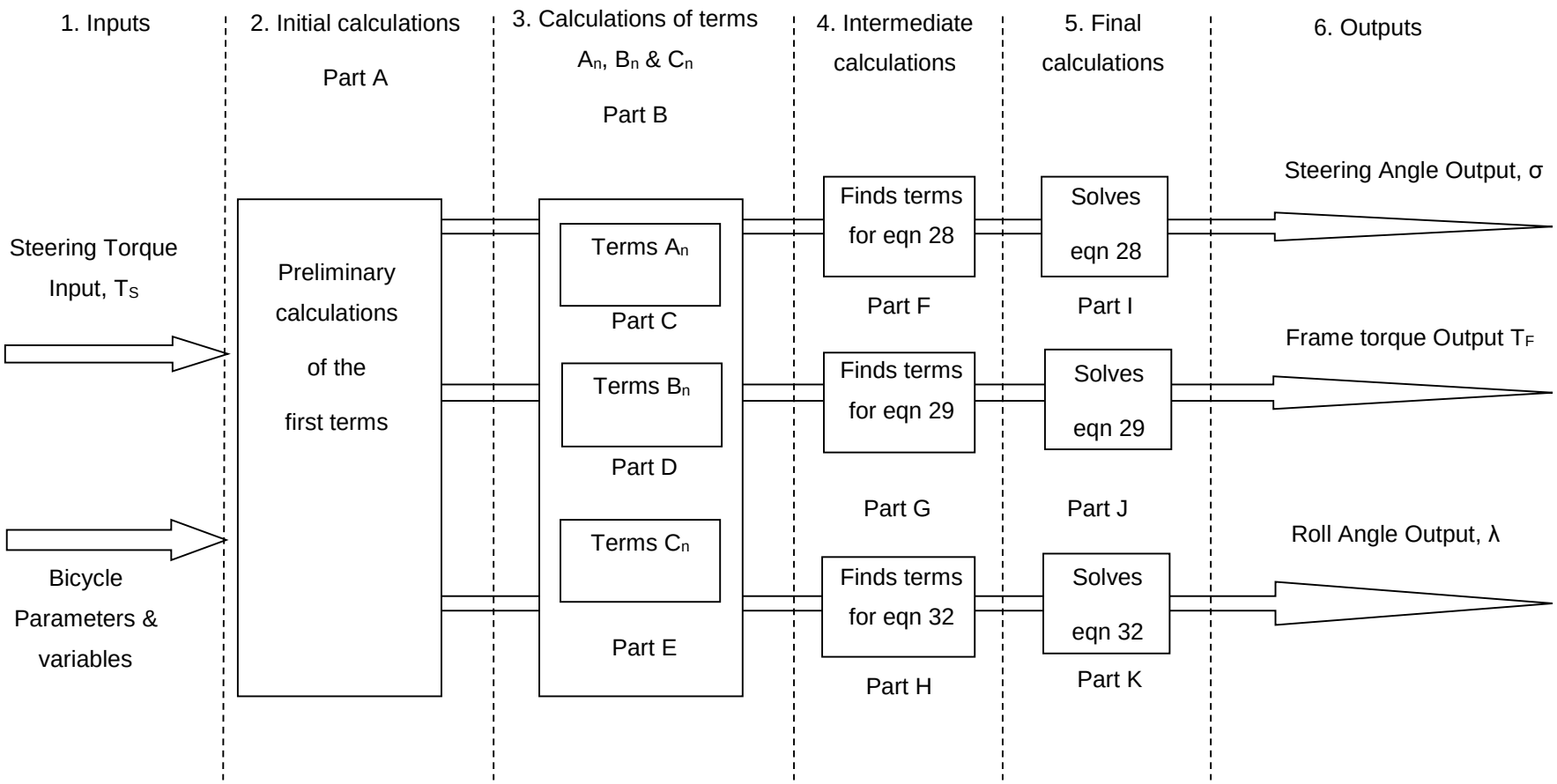

Figure 7 Schematic breakdown of the Simulink Model, showing the main elements or parts

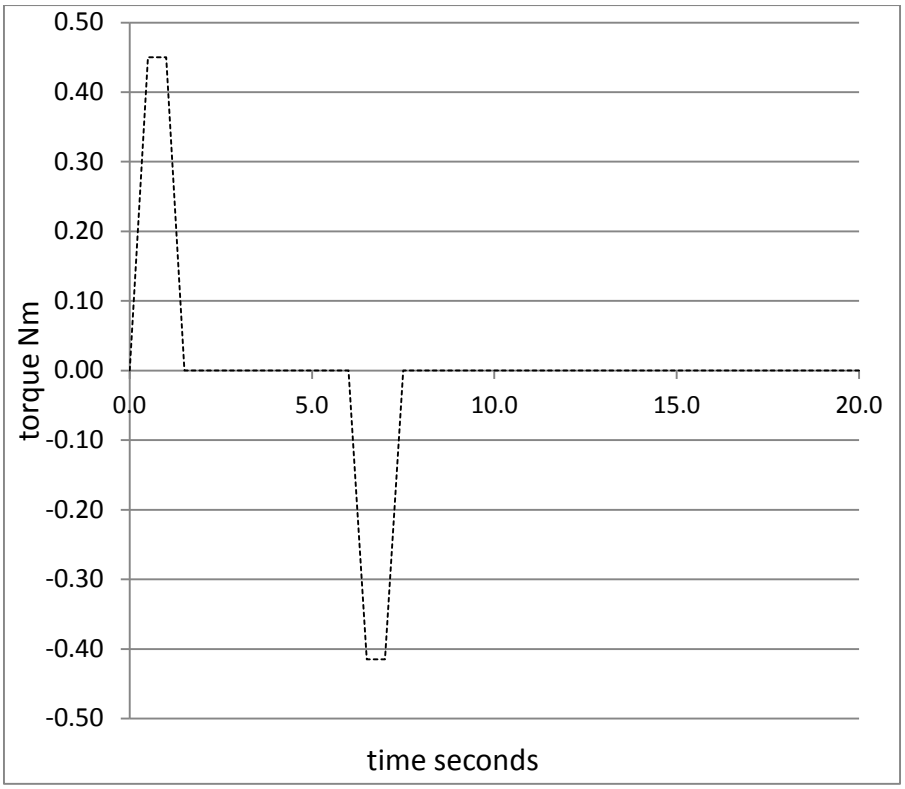

Figure 8 Bicycle handlebar steering torque input for the standard simulation

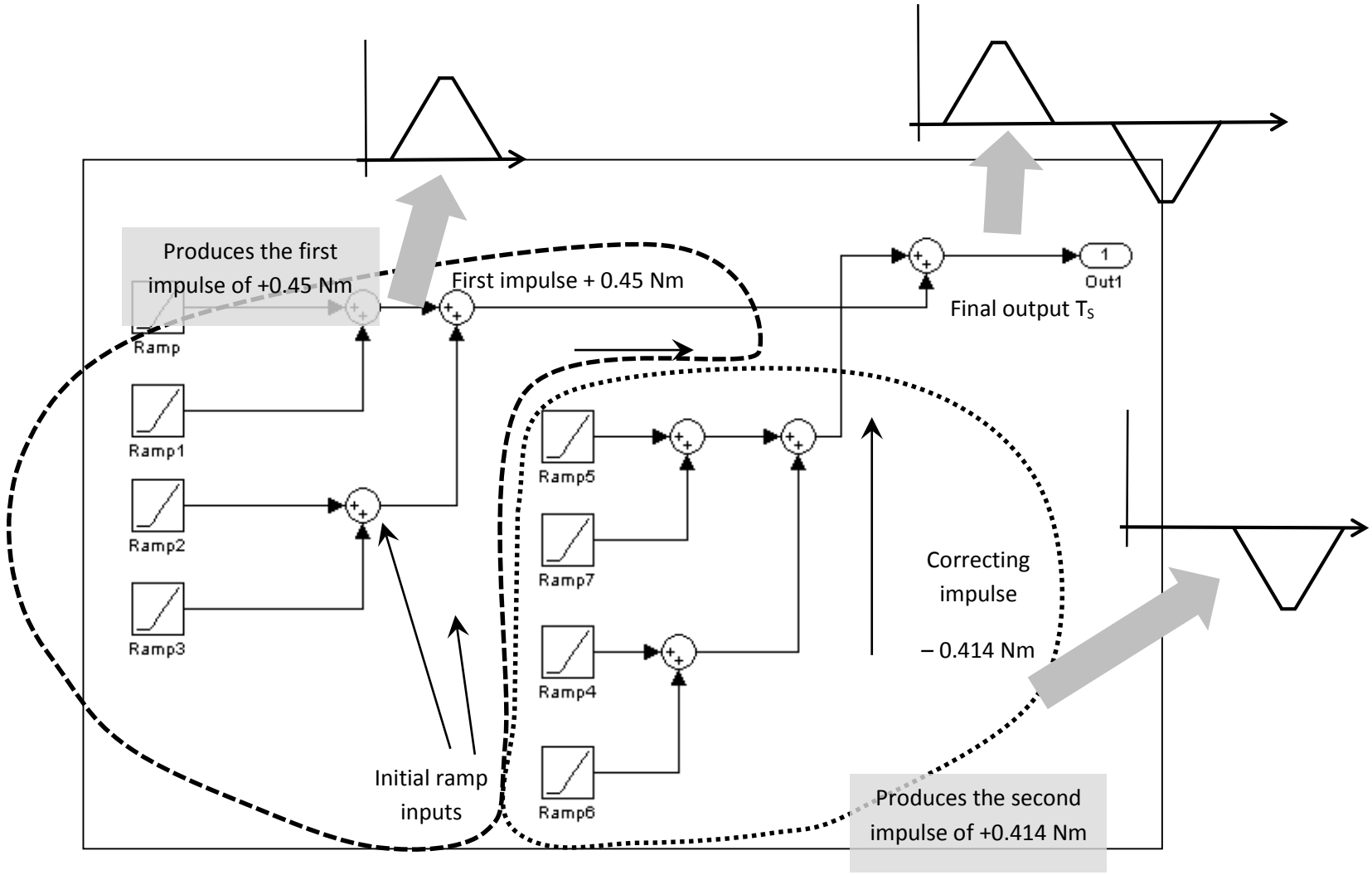

Figure 9 The steering torque subassembly that produces the standard steering torque shown in Figure 8

4.3. PARAMETER FORMULATION

As stated earlier the Simulink model uses thirteen bicycle parameters (eleven if only counting one moment of inertia for the wheels) and three variable inputs to model bicycle behaviour (Table 10 and Table 11). These terms are very familiar to designers and are the ones used when developing designs. An additional five secondary parameters are listed in Table 12, but these are not required for the Simulink model due to redundancy. However these secondary parameters are widely used within the bicycling fraternity and so need to be discussed.

Table 11 Bicycle parameters

	Symbol	Parameter definition	Units
1.	I_{XA}	Moment of inertia of assembly A about X axis (roll)	kgm^2
2.	I_{XB}	Moment of inertia of assembly B about X axis (roll)	kgm^2
3.	I_{ZA}	Moment of inertia of assembly A about Z axis (yaw)	kgm^2
4. & 5.	I_{XW} & $I_{ZW\ 1,\ 2}$	Moment of inertia of both wheels about X and Z axes	kgm^2
6.	$I_{YW\ 1,\ 2}$	Moment of inertia of both wheels about Y axis	
7.	L	Bicycle wheelbase	m
8.	b	Horizontal distance from the rear wheel hub to the centre	m
9.	h	Height of centre of mass	m
10.	D	Diameter of the bicycle wheel	m
11.	M	Mass	kg
12.	Φ	Head tube angle	degrees
13.	β	Fork rake (or offset)	m
Note 1 Due to symmetry the wheel moments of inertia have the following relationships: $I_{XW} = I_{ZW}$ and $I_{YW} = 2.I_{XW} = 2.I_{YW}$			
Note 2 Because the wheels on most bicycles are identical front and rear, it is convenient to consider both wheels together in the Simulink model as I_{XW}, I_{YW} & I_{ZW}, while in the equations of motion the front and rear wheels have been separated out and are referred to as I_{XF}, I_{YF}, I_{ZF} and I_{XR}, I_{YR}, I_{ZR}			

Table 12 Secondary parameters

	Symbol	Definition	Units	Comments
1.	FS	Frame size	m	defines the correct size of the bicycle for the rider
2.	STA (or γ)	Seat tube angle	m	related to the parameters b, h and L
3.	Δ	Trail	m	determined by Φ and β
4.	Δe	Effective trail	m	also determined by Φ and β
5.	a	Horizontal distance from front wheel hub to centre of mass	m	redundant dimension because, a = L – b

4.3.1.FRAME SIZE

Two of the parameters in Table 12 need further explanation, the frame size and seat tube angle. Frame size is needed because this is how bicycles are matched to people of different sizes. Frame size is traditionally measured parallel to the seat tube and is the distance from the centre of the bottom bracket to the centre of the top tube at its intersection with the seat tube as shown in Figure 11. The benchmark bicycle is based on a frame size of 550 mm and this was chosen because it is a common medium size for male riders and it is the correct size for a 1.84 m tall rider, a moderately tall male just below the 95th percentile (48). Many rule of thumb methods are used to determine the correct frame size for individual riders. One common and widely accepted method is to multiple the inside leg inseam measurement (in mm and shown in Figure 10) by 0.65 to give the correct frame size in mm (68-71).

Frame size is not required in the Simulink model as it is redundant, because of the use of the model parameters for the wheelbase and mass position (i.e. L, b and h, see Figure 2). These three parameters are proportional to the frame size and thereby already allow for it.

However it is no longer universal for all manufacturers to provide traditional frame size dimensions in their specifications. This is because many manufacturers have begun to make frames with a sloping top tube, angled downwards to the rear of the bicycle. This was first seen in the Giant TCR (Total Compact Road) bicycle of 1997 and this style of frame is shown in Figure 12 (72). This downward sloping top tube is used because of claimed advantages of reduced frame weight, improved handling and increased frame stiffness. It may also have a commercial advantage by allowing a manufacturer to cover the full range of rider sizes with a smaller number of bicycle models, hence reducing tooling, work in progress and stock costs. Unfortunately it is not possible to define these sloping frames using the traditional frame sizing system. The commonest alternative to the traditional method is to quote stack and reach dimensions, which are defined as follows:

- stack is the vertical distance from centre of the bottom bracket to centre of the head tube measured at its top end, see Figure 13
- and reach is the horizontal distance from centre of the bottom bracket to centre of the head tube measured at its top end, see Figure 13

This alternative sizing method is now used by many (but not all) manufacturers now that sloping frames have become common. But sizing methods are confusing to many riders and many are unsure as to which frame size they should purchase (73). Some sort of internationally recognised standardisation in frame sizing would appear desirable but this is outside the scope of this investigation.

4.3.2.SEAT TUBE ANGLE

The second parameter, seat tube angle, is the angle the seat tube makes relative to the horizontal plane see Figure 11. It is an important manufacturing parameter that enables easy fabrication of conventional frames and it also determines the seat and rider position. The seat tube angle is also a much discussed parameter within the bicycling fraternity and many claims are made as to its influence on handling and comfort, see later discussions in Chapter Seven (69, 74, 75). As with the frame size parameter, the Simulink model allows for the seat tube angle through the use of the terms “b” and “h” (that define the mass position). The seat tube angle can be related back to “b” and “h” by using a combination of trigonometry and empirically derived relationships and the full details of how this can be done is shown in the Appendix B.

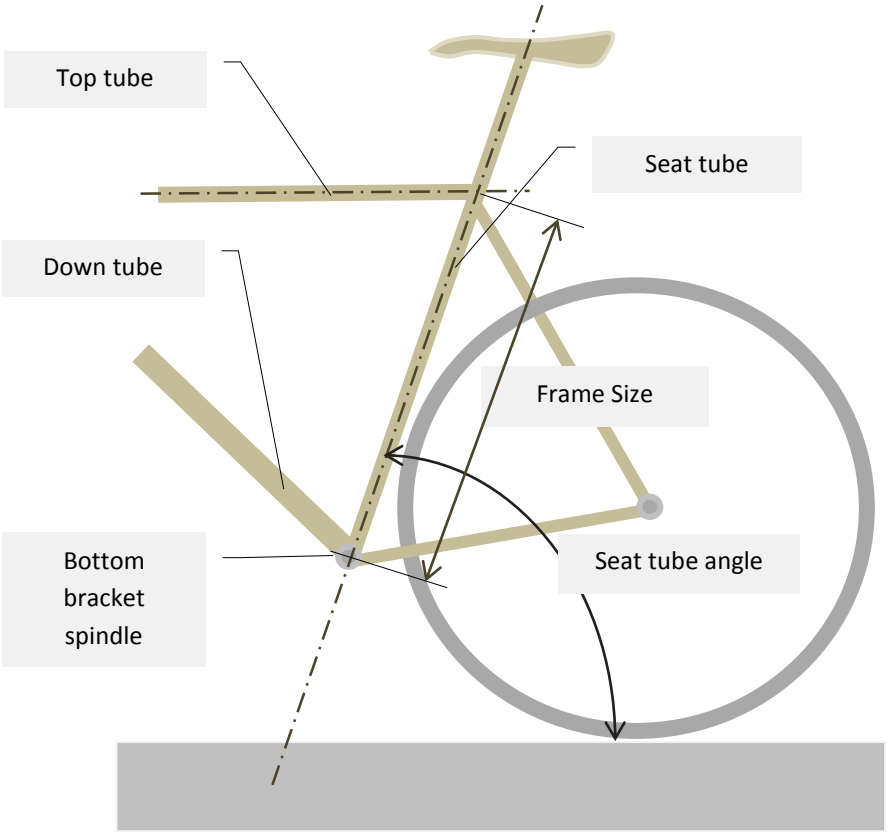

Figure 11 Defining a bicycle's frame size dimension and seat tube angle

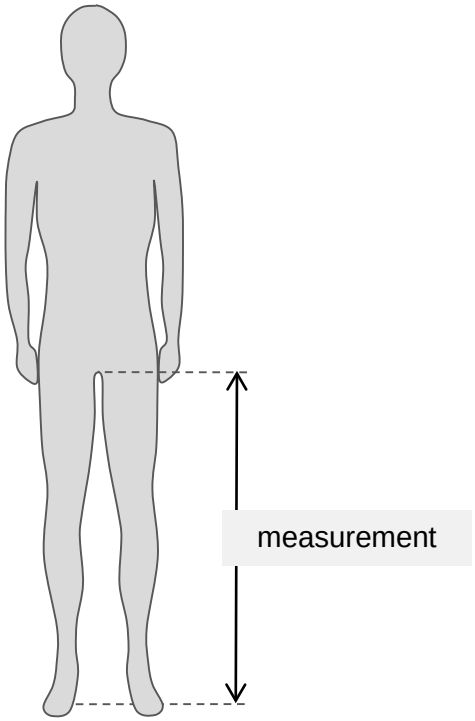

Figure 10 The cyclist's inseam measurement used to determine the correct bicycle size

Figure 12 Giant TCR bicycle frame of 1997 clearly showing the sloping top tube (76)

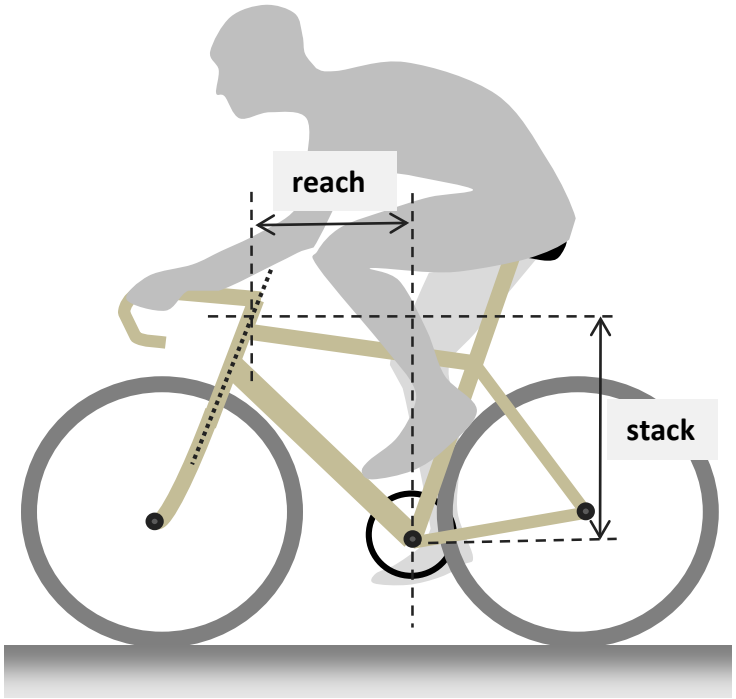

Figure 13 Defining a bicycle's stack and reach dimensions

4.4. BENCHMARK PARAMETERS

It is necessary to select appropriate values for all 13 parameters and 3 variables, ones that will be representative of modern high performing road bicycles in order that realistic simulations can be made. Appropriate values are also needed in order for the sensitivity study to be undertaken. Of particular importance was the choosing of appropriate and representative values for a reference point, the benchmark bicycle. The benchmark values are not intended to be thought of as optimum values but rather should be typical of well-designed road bicycles, somewhere in the middle of the range of values. The benchmark bicycle will also be useful when examining the differences between individual bicycle designs (such as the Tour de France bicycles examined in Chapter Seven) as it can be a datum point. Also the four bicycle design charts developed and discussed later in Chapter Six, all use iso-handling lines referenced back to the benchmark bicycle's iso-handling line.

4.4.1. SUPPORTING EVIDENCE FOR PARAMETER SELECTION

The following comments are supporting evidence as to why particular benchmark values were selected.

- First a review of the literature was undertaken to find out what parameter values other researchers had used. Moore et al determined a range of values for physical bicycle parameters including: mass, the position of the mass, moments of inertia of bicycle components (frame, front fork, wheels and rider). They were found by experimental measurement and from previously published data. (47). The bicycle they chose to measure was a 2008 Batavus Browser and from the details given it is clear this is not a high performance bicycle. For example the total bicycle weight is given as 23.5 kg, which is very high when compared to a top road bicycle such as a Trek Madone 7.7 weighing only 6.54 kg (77). Also the Batavus also has a very long wheelbase (1.120 m) and a shallow head tube angle (68.5^{o}). Similarly when measuring the human rider they have chosen a subject weighing 72 kg but give no indication of their height or body mass index, so it is hard to know how representative they are of the riding population. Therefore the results given in this paper need to be considered with these comments in mind.
- Ringwood and Feng's paper obtained experimentally values for the position of centres of mass of actual road bicycles e.g. Trek 5200, Trek 1000, Trek Madone, Klein and Litespeed (61). When finding the vertical centre of mass position they assumed that the bicycle rider system was a simple pendulum when it is actually a compound pendulum. As a consequence their estimate for the vertical position of the centre of mass has a significant error and places it about 160 mm too low.
- Fajans' paper on the motion of bicycles and motorcycles used several values for centres of mass and moments of inertia (12). He referenced some sources but said others were inferred, but did not include any details. Using these values in his derived equations Fajans examined in detail a road racing bicycle and a large motorcycle.

- Chen's paper on bicycle balancing and path tracking strategies used parameter values which they found experimentally but no details of how this was done was given (60). The wheel masses are very high at 2.09 and 3.93 kg (front and rear respectively) and this was because the bicycle was not a high performance design and also a rotary encoder was attached to the front wheel.

- Damavandi et al presented a short report that summaries seven methods for finding the moments of inertia of a human subject (78). This has relevance when determining moments of inertia and mass and its position of the bicycle rider system. This is a difficult theoretical and experimental problem due to the wide range of human body shapes and the difficulty of measuring and defining the human body. Their purpose was to find the most efficient way of determining an individual's moments of inertia for clinical evaluations. The usual method is to estimate these values from anthropomorphic tables but this has problems because the tables do not accurately describe adolescent, obese or elderly populations. They did not describe the theory or procedures employed with any of the seven methods they listed. The report concluded that the inverse dynamic pendulum and the angular momentum methods gave results within the average of the others, but this was not quantified precisely. They recommended that these two methods could be used with confidence in the clinical environment to estimate the moments of inertia for individual subjects.

- Dempster undertook a three year long United States Air Force sponsored investigation published in 1955, whose purpose was to determine the space requirements for seated male air crew (79). It was also hoped that the kinematic information would assist in designing ergonomic controls and cockpits so that under extreme conditions of flight, effective control would still be possible. Dempster undertook the detailed examination of eight male cadavers (all older males of slight build). This involved the examination of dissected body parts (torso, head, upper and lower limbs). He measured and recorded details of: dimensions, volumes, masses, centre of mass positions and moments of inertia. The centres of mass were found by the suspension method and moments of inertia by the compound pendulum method. The resulting data was arranged in tables of anthropomorphic data listed for each body segment but was not combined into a complete mathematical model of the human body. Therefore it cannot be used for this current study unless further work was done. His information could be used to construct a simple mathematical model of a person in any posture that could calculate mass, mass position and moments of inertia. But because the cadavers were older males (ranging from 52 to 83 years) and of slight build (50 to 70 kg) they are not representative of young, athletic male bicycle riders nor female riders. Therefore this information is considered to have limited use for this study other than as a comparison with other results.

- Hanavan's United States Air Force study developed a complete mathematical model that can find masses, centres of mass, products and moments of inertia for humans of different builds and in different postures (48). The study's purpose was to determine the inertial properties for space crew to help design equipment for the weightless environment

of outer space (such as self-manoeuvring units for extra-vehicular work). His mathematical model breaks the body down into fifteen segments that are simplified as easily calculated hemispherical, cylindrical or conical shapes. These are then used to calculate the required properties for a complete human body. Importantly and usefully he summarised these human body properties into a design guide. His guide lists different combinations of standing and sitting positions (with limbs in various positions). In total the mass and inertial properties for 31 different body positions are included in his design guide. For each position full values for composite subjects of the 5th, 25th, 50th, 75th and 95th percentile groups are given. Hanavan body position number 18 closely approaches that of a rider in the seated pedalling position and those results are used in this study, see Figure 14. The Hanavan model was validated by comparing it to existing data available from the previous research of Hansen and Cornog (not cited) that had measured 66 subjects (US Air Force male flight crew of the 1950's). The Hanavan mathematical model was found to be accurate within 18 mm for the position of the centre of mass and generally within 10% for the moments of inertia when compared with anthropomorphic data. Full details of the computer programme written in Fortran II & IV code are supplied in Hanavan's report.

4.4.2.BENCHMARK VALUES

The choice of the benchmark values was made after considering experimental measurements and calculations, other researchers' work and manufacturers' published specifications about their own bicycles. For the developed Simulink model in this study, the benchmark parameter values selected are listed in Table 13. These selected benchmark parameter values are not proposed as highly precise values but they are believed to be sufficiently true and accurate for their purpose as defined by ISO standard 5725-1. Rounding has been used on the benchmark values, generally to 2 significant figures. According to ISO standard 5725-1, the international standard defining the vocabulary of metrology, the terms trueness and precision have a specific meaning when describing the accuracy of a measurement process (80). Precision refers to the closeness of agreement within series of individual measurements while trueness is the closeness of the average of a series of measurements to the true value. Consequently accuracy refers to both trueness and precision and to be accurate a series of measurements must be sufficiently true and precise for the purpose.

Justification for why these values were selected are summarised in Table 14 and Table 15 (parts I and II) and these two tables show a complete picture of the range of these values, so that decisions about future variations to the model can be made with knowledge and confidence. As already noted many researchers have used values which are not representative of high performing bicycles. This can be attributed to the fact that many of the bicycles used for experiments are of average or below average design and construction. Also some researchers deliberately exaggerated some values, for example wheel mass, in order to investigate the effect of individual terms such as gyroscopic effects (14). Typically values are overly heavy and in the case of dimensions such as wheel diameters and wheelbases are inaccurate.

Reflecting on this it was decided that it was necessary to apply rigour in order to obtain appropriate values for this study and a combination of experiments, calculations and extensive reference to the literature has allowed this to be achieved with some confidence. Engineering calculations were possible on some components, namely the moments of inertia of wheels, front forks, bicycle frame and rider, see Appendix C. These calculations had close agreement to the experimental values which allows confidence in advancing the selected values for the benchmark bicycle shown in Table 13.

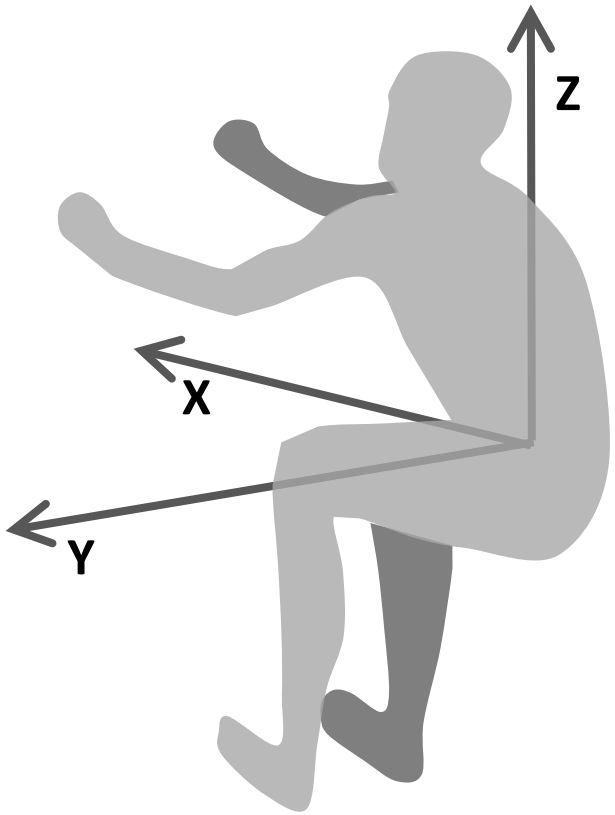

Figure 14 Hanavan's Report lists the above position as # 18 (positive X Y Z directions indicated)

Table 13 Benchmark bicycle parameters and other terms

	Symbol	Parameter Definition	BM Value [1]	Units	Source
1.	I_{XA}	Moment of inertia of assembly A about XA axis (roll)	0.2	kgm^2	from calculation and comparison to Fajans (12)
2.	I_{XB}	Moment of inertia of assembly B about XB axis (roll)	100	kgm^2	from calculation and comparison to Fajans (12)
3.	I_{ZA}	Moment of inertia of assembly A about ZA axis (yaw)	0.08	kgm^2	from calculation and comparison to Fajans (12)
4.	I_{XW}	Moment of inertia of both wheels about X axis (roll)	0.05	kgm^2	from experimental measurement, see Appendix C
5.	I_{YW}	Moment of inertia of both wheels about Y axis (rotational)	0.10	kgm^2	from experimental measurement, see Appendix C
6.	I_{ZW}	Moment of inertia of both wheels about Z axis (yaw)	0.05	kgm^2	from experimental measurement, see Appendix C
7.	L	bicycle wheelbase	1.0	m	selected from comparison to database, see Chapter Seven
8.	b	Horizontal distance from centre of rear wheel to centre of mass	0.33	m	from calculation and comparison to Fajans & Ringwood (12)
9.	h	Height of centre of mass	1.1	m	from calculation and comparison to Fajans & Ringwood (12)
10.	D	Diameter of the bicycle wheel	0.675	m	from manufacturers' data, see Appendix E
11.	M	Mass	80.0	kg	based on a bicycle of 7kg and a rider of 73kg see Appendix F
12.	Φ	Head tube angle	73.0	degrees	selected from comparison to database, see Appendix F
13.	β	Fork rake	0.045	m	selected from comparison to database, see Appendix F
		Secondary Parameter Definition			
1.	FS	Frame Size	0.55	m	Not a model input but estimated from L and h
2.	STA	Seat tube angle	74.0	degrees	Not a model input but estimated from L and h
3.	Δ	Trail	0.05613	m	Not a model input but calculated using the trail formula from the head tube angle and rake
4.	Δ_e	Effective trail	0.05368	m	Not a model input but calculated using the trail formula from the head tube angle and rake
5.	a	Horizontal distance from centre of front wheel to centre of mass	0.67	m	Not a model input but calculated from L and b
		Variable Definition			
1.	T_{Steer}	Steering torque [2]	variable	Nm	from selection and comparison to Fajans (12)
2.	v	Velocity	25	km/hr	A selected value, but other values have been used in some simulations and this is made clear in the text
3.	Γ	Damping torque term	0.65	Js	see Fajans (12)
		Other Definition			
	g	Acceleration due to gravity	9.81	m/s^2	A constant at the standard value

Note 1 BM or benchmark bicycle value

Note 2 variable term which can be adjusted in the Simulink model as required

Table 14 Comparison of parameters from various sources, part I

	Symbol	Model Parameter Definition	Values from references	Minimum value	Maximum value	Experimentally derived values See Appendix C	Calculated values See Appendix C	Selected benchmark value	Units
1.	I_{XA}	MOI of A about XA axis (roll) wheel included	0.0546 (14) no wheel included 0.080 (37) no wheel included 0.084 (12) 0.086 (34) no wheel included 0.345 (44) no wheel included	0.0546	0.086	N/A	0.22506 (0.0713 with no wheel included)	0.200	kgm^2
2.	I_{XB}	MOI of B about XB axis (roll) wheel included	163 (12)	163	163	N/A	100 to 155 depends on assumptions	100	kgm^2
3.	I_{ZA}	MOI of A about ZA axis (yaw) wheel included	0.079 (12) 0.0114 (14) no wheel included 0.020 (37) no wheel included 0.065 (34) no wheel included	0.020	0.079	N/A	0.07578	0.080	kgm^2
4.	I_{XW} & I_{ZW}	MOI of front & rear wheel about X (roll) and Z (yaw) axes	0.0458 (28) 0.0475 (12) 0.700 (37) 0.078 & 0.081 (14) 0.109 (60) 0.060 & 0.140 (34)	0.0458	0.109	0.0421 to 0.05713	0.0473	0.050	kgm^2
5.	I_{YW}	MOI of front & rear wheel about Y axis (rotational)	0.095 (12) 0.1034 (28) 0.140 (37) 0.156 & 0.162 (14) 0.218 (60) 0.120 & 0.280 (34)	0.095	0.280	0.0845 to 0.1095	0.092	0.100	kgm^2
6.	L	Bicycle wheelbase	2013 Tour de France bicycles all 30 models see Appendix C 0.990 average	0.978	1.014	1.010 (Trek 1500)	N/A	1.000	m
7.	b	Horizontal distance from centre of rear wheel to centre of mass	0.300 (14) 0.300 (34) 0.330 (12, 21) 0.430 (61) 0.492 (37)	0.300	0.492	N/A	0.310	0.330	m

Table 15 Comparison of parameters from various sources continued, part II

	Symbol	Model Parameter Definition	Values from references	Minimum value	Maximum value	Experimentally derived values See Appendix C	Calculated values See Appendix C	Selected benchmark value	Units
8.	h	Height of centre of mass	0.867 (61) 0.900 (14) 1.08 (34) 1.028 (37) 1.25 (12) 1.5 (21)	0.867	1.500	1.030	1.090	1.100	m
9.	D	Diameter of the bicycle wheel 700C x25 wheel	0.67004 (81) 0.67959 (64) (0.6748 average)	0.67004	0.67959	0.675	N/A	0.675	m
10.	M	Mass made up of the bicycle and the rider	27.9 bicycle only (34) 81.6 bicycle & rider (21) 87 bicycle & rider (14) 88.5 bicycle & rider (37) 100 bicycle & rider (12)	81.6	100.0	N/A	N/A	80	kg
			Bicycle only 6.8 kg min UCI weight (3)	6.8	7.3	8.5 (Trek 1500)	N/A	7.0	
			Tour de France 2013 Riders Average weight 68.83 kg for all 219 riders (82) See Appendix C	56.0	84.0	N/A	N/A	73.0	
11.	Φ	Head tube angle	2013 Tour de France bicycles all 30 models see Appendix C 73.2 average	71.9	74.0	N/A	N/A	73.0	degrees
12.	β	Fork rake	2013 Tour de France bicycles all 30 models see Appendix C 0.0449 average	0.039	0.053	N/A	N/A	0.045	m
13.	Δ_e	Effective trail	2013 Tour de France bicycles all 30 models see Appendix C 0.05515 average	0.0447	0.06342	N/A	N/A	0.05368	m

4.5. PRELIMINARY CALCULATIONS – PART A

After the parameters and variables have been formulated, some preliminary calculations are required to find the first terms in the model. The purpose of this first step is to convert values such as velocity, wheel radius, head tube angle and wheelbase into the necessary terms and units before the first major step in the modelling process occurs (which is to find the constants: A_n, B_n, and C_n) see Figure 15.

It would have been possible to have eliminated these preliminary calculations by using SI units for all parameters and variables. For example velocity could have been defined in metres/sec rather than km/hour and angles in radians not degrees. But by defining the parameters in common units, the simulation model is more easily used, as it allows quick comparisons between individual simulations to be made and allows manufacturers' information about bicycle designs to be easily related to the model.

In Figure 15 the top element of the model shows how the velocity terms of v, v^2 and v/r (all in fundamental SI units) are calculated from an initial velocity input in units of km/hr. The middle element finds the wheel radius, effective trail and sinΦ and cosΦ terms from the steering geometry parameters. Finally the third element simply changes the wheelbase input into L^2.

The five parts of the Simulink model (parts A to E) are shown in Table 16 which summarises what each part's purpose is and identifies the relevant figure number for each part.

Table 16 Details of Simulink Parts A to E

Model Part	Purpose	Figure number
A	Preliminary calculations of the velocity, steering geometry and wheelbase terms	Figure 15
B	Finding the coefficients A_n, B_n and C_n	Figure 16
C	Finding the coefficients A_1, A_2, A_3, A_4 and A_5	Figure 17
D	Finding the coefficients B_2, B_3 and B_4	Figure 18
E	Finding the coefficients C_2, C_3, C_4, C_5 and C_6	Figure 19

4.6. INTERMEDIATE CONSTANTS – PARTS B, C, D & E

After the preliminary calculation steps have been completed the next step can proceed. This first major modelling step calculates the intermediate constants, A_n, B_n, and C_n which have been defined in Table 9 (and an overview of these steps is shown in Figure 16). These intermediate constants are required in order to solve the equations of motion. This step is further broken down into three subparts: C, D and E, details of which are shown in Figure 17, Figure 18 and Figure 19. Note that not all the A_n, B_n, and C_n constants have to be calculated as the following three constants are already known ($A_4 = \Gamma$, $B_1 = I_{XA}$ and $C_1 = I_{XB}$).

In Figure 15 the top element (Part C) finds the coefficients A1, A2, A3 and A5 which will be used to help solve (28, Part C is shown in more detail in Figure 17. The middle element is Part D which calculates coefficients B2, B3 and B4 to solve equation (29) more details of which are shown in Figure 18. The final element of Figure 15 is Part E used to calculate coefficients C2, C3, C4, C5 and C6 which will be used to solve equation (32) and Part E is also shown Figure 19.

4.7. INTERMEDIATE CALCULATIONS – PARTS F, G & H

Once the constants (An, Bn and Cn) have been found the intermediate calculations can proceed. There are three parts (F, G and H) to these intermediate calculations which are listed in Table 17. Each part takes one group of the intermediate constants, A_n or B_n, or C_n (plus any necessary initial terms) and calculates the further individual terms required for each of equations (28), (29) and (32) (see also Figure 20, Figure 21 and Figure 23).

Table 17 Details of Parts F, G and H

Model Part	Purpose	Figure
F	Finding the terms for (28	Figure 20
G	Finding the terms for (29	Figure 21
H	Finding the terms for (32	Figure 22

In Figure 20 which shows Part F, coefficients A_1, A_2, A_3, A_4, A_5 and A_6 and other terms are used to produce the individual terms of equation (28). Next in Figure 21, Part G, coefficients B_1, B_2, B_3 and B_4 and other terms are used to produce the individual terms of equation (29). Finally in Figure 22, Part H, coefficients B_1, B_2, B_3 and B_4 and coefficients C_1, C_2, C_3, C_4, C_5 and C_6 plus other terms are used to produce the individual terms of equation (32).

4.8. FINAL CALCULATIONS – PARTS I, J & K

The last step in the Simulink model is to take all the previously calculated terms and use them to find the bicycle dynamic response in terms of yaw and roll. The three parts that do this are I, J and K and their purposes are described in the (see also Table 18, Figure 23, Figure 24 and Figure 25).

Table 18 Details of Parts I, J and K

Model Part	Purpose	Figure
I	Finds the yaw angle of the front wheel (σ)	Figure 23
J	Finds the frame torque ($T_f \sin \Phi$)	Figure 24
K	Finds the roll angle (λ)	Figure 25

The final steps are shown in next three figures starting with Figure 23 (Part I) which using the terms from equation (28) finds the yaw angle of the front wheel. Then in Figure 24 (Part J) the frame torque is found from equation (29). The last Figure 25 (Part K) finds the roll angle using equation (32).

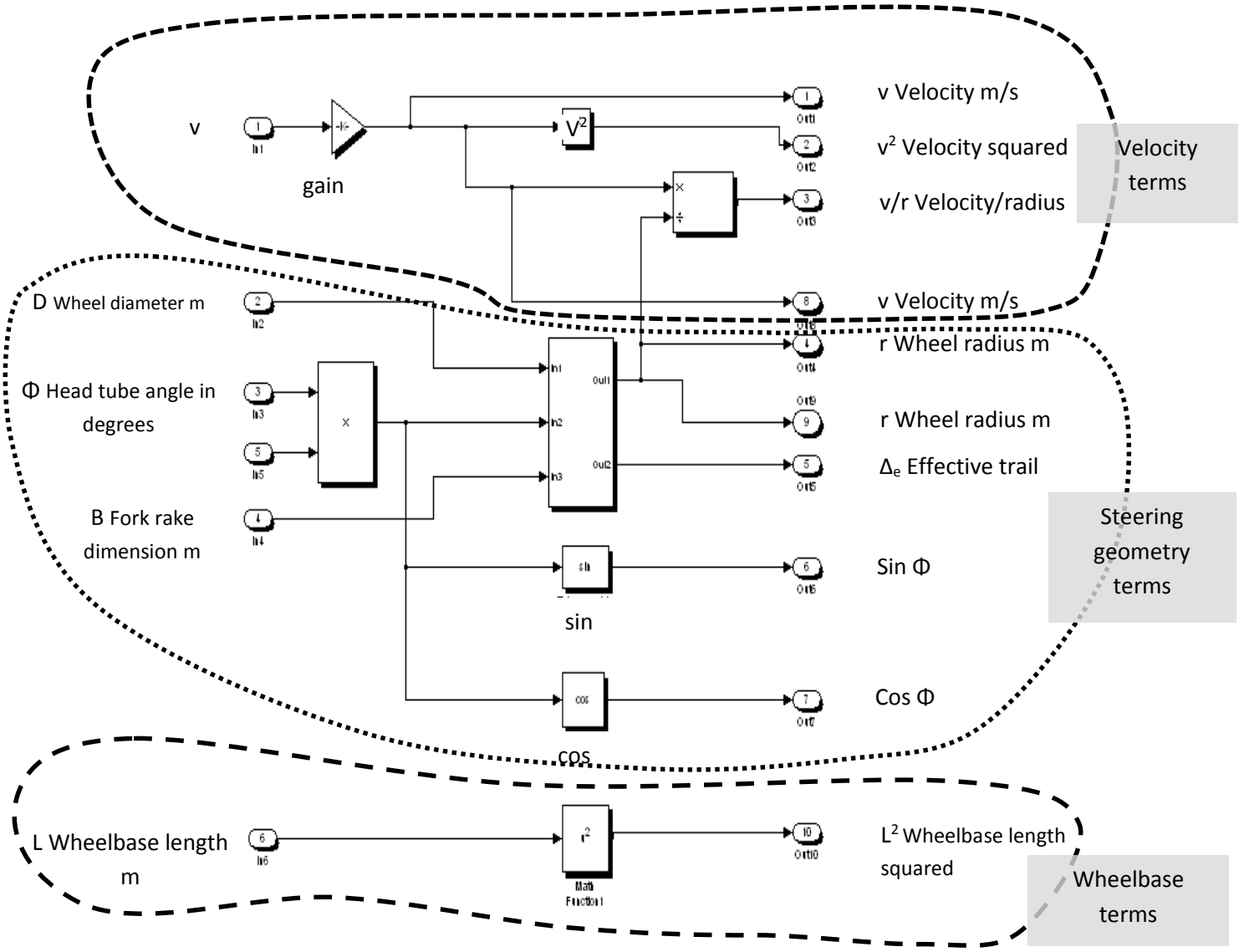

Figure 15 Part A, showing the initial calculations using Simulink

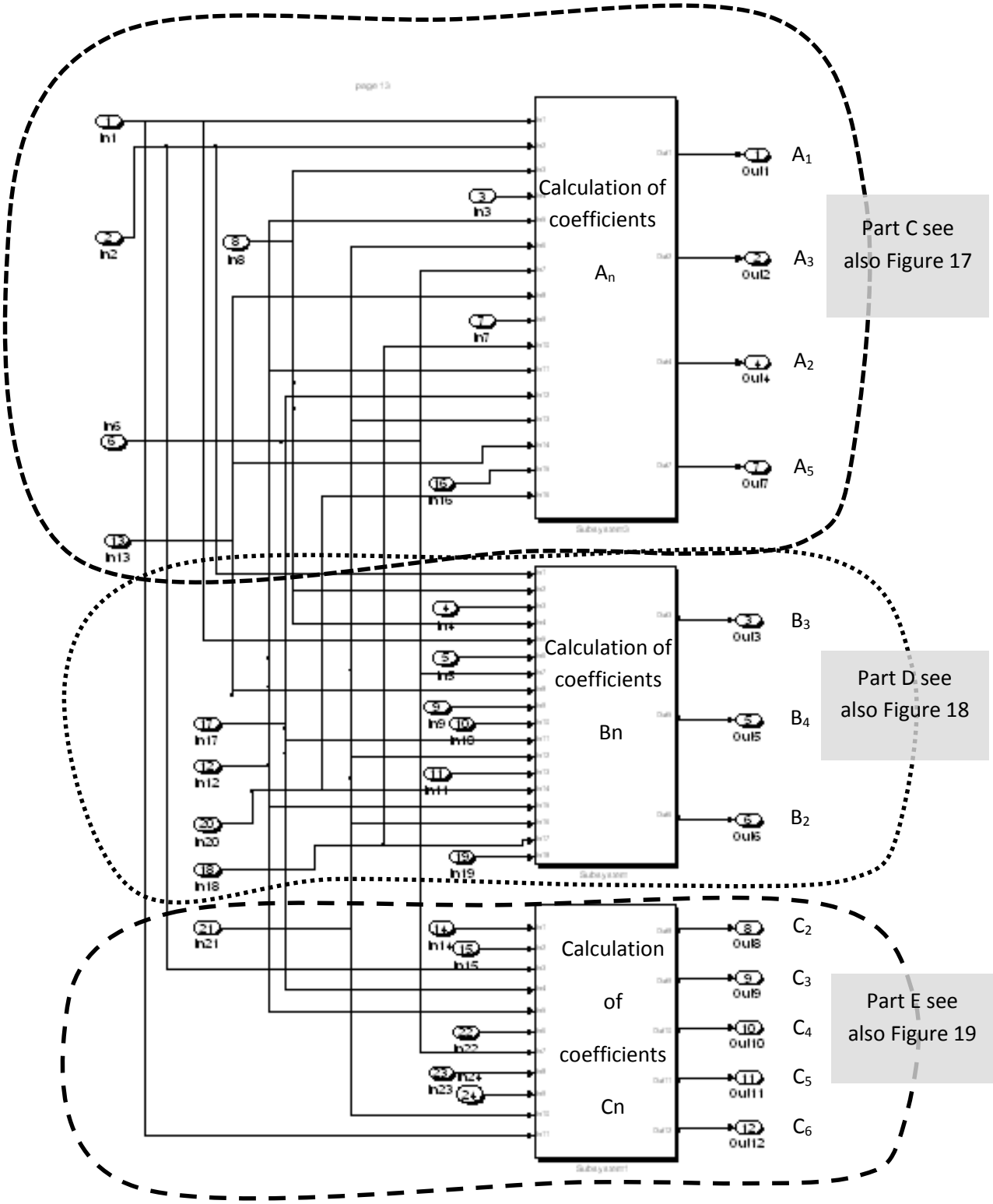

Figure 16 Part B, showing an overview of the Simulink calculations of coefficients A_n, B_n & C_n

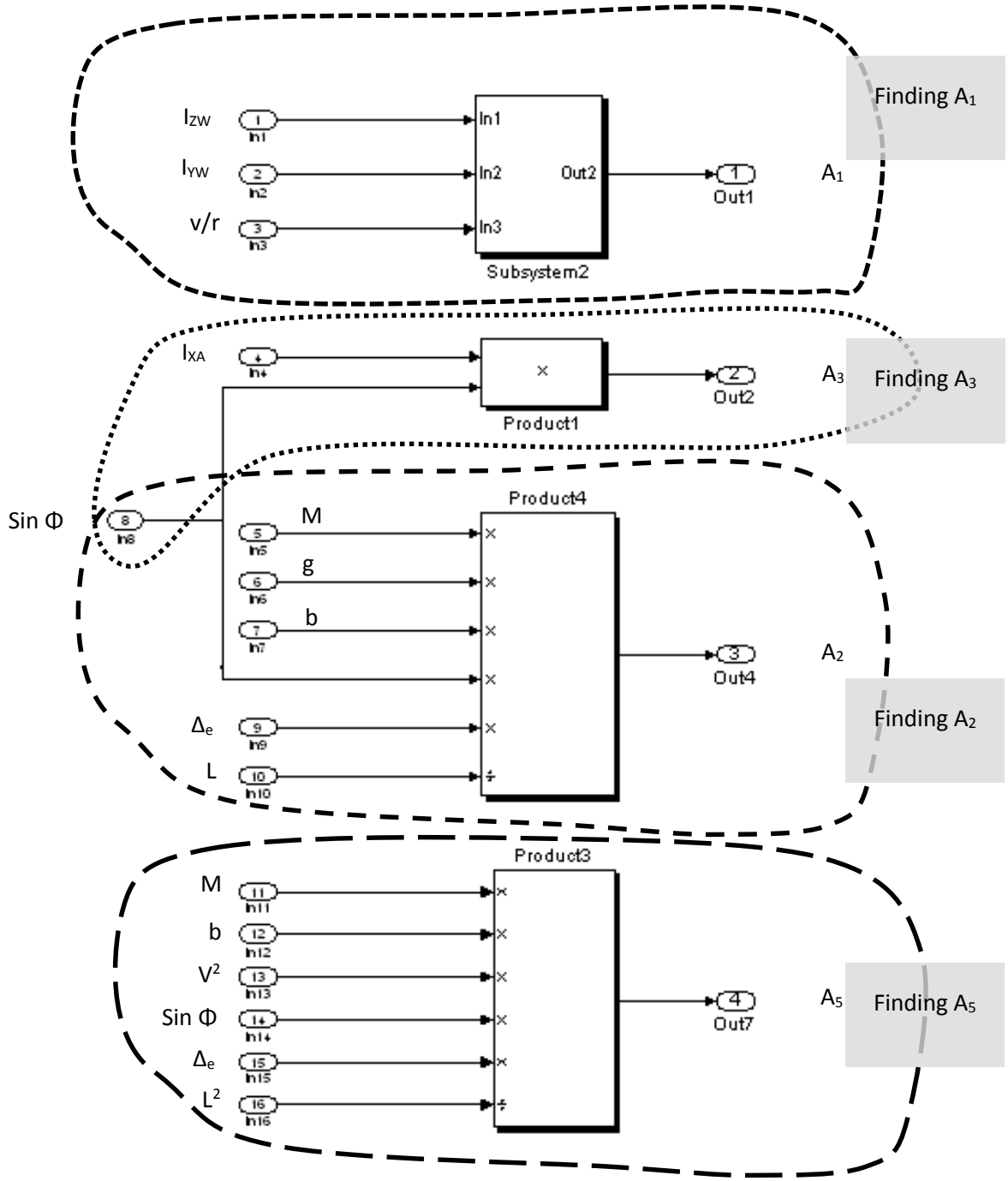

Figure 17 Part C, showing Simulink calculations of coefficients A_1, A_2, A_3 & A_5

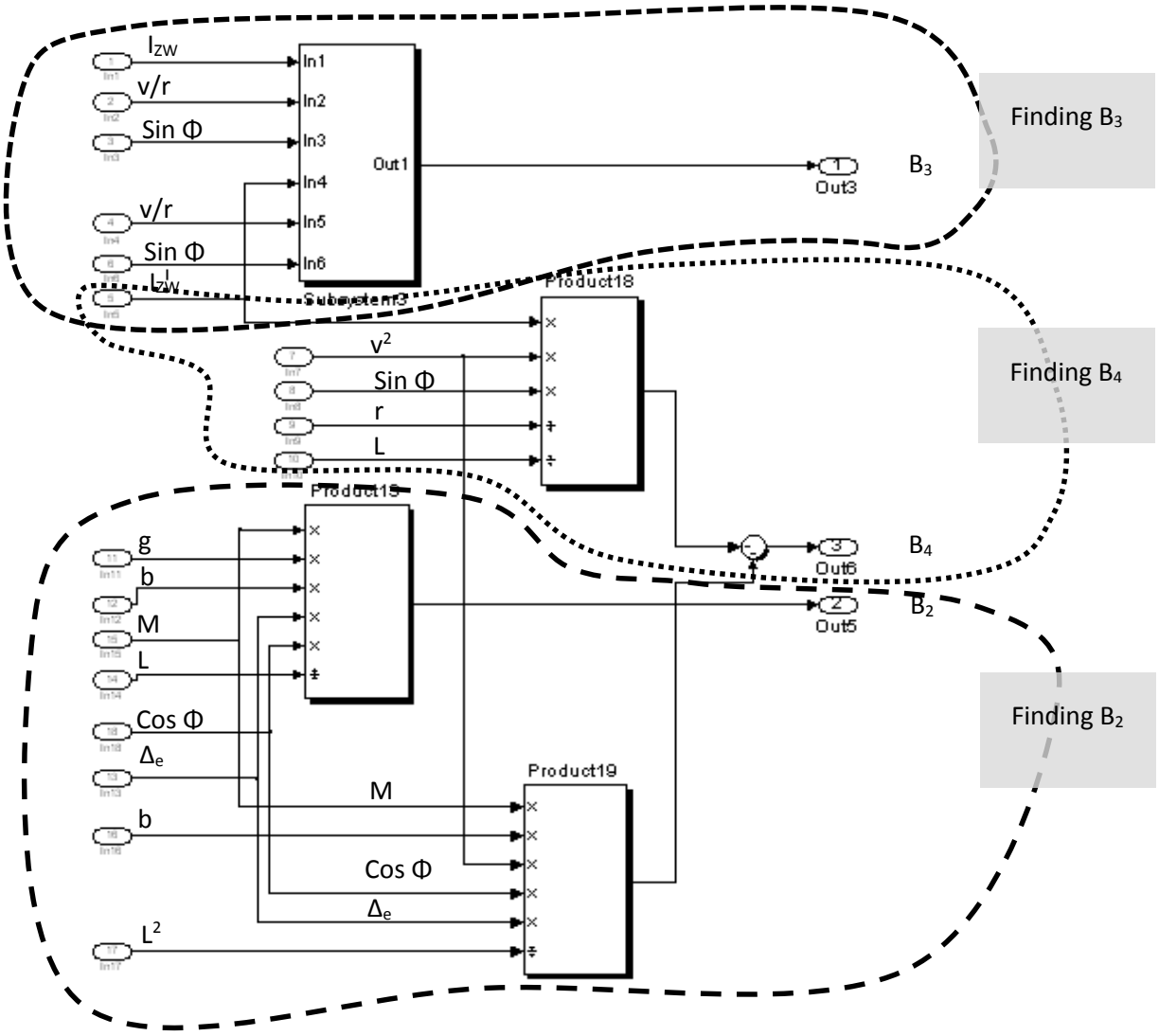

Figure 18 Part D, showing the Simulink calculations of coefficients B_2, B_3 & B_4

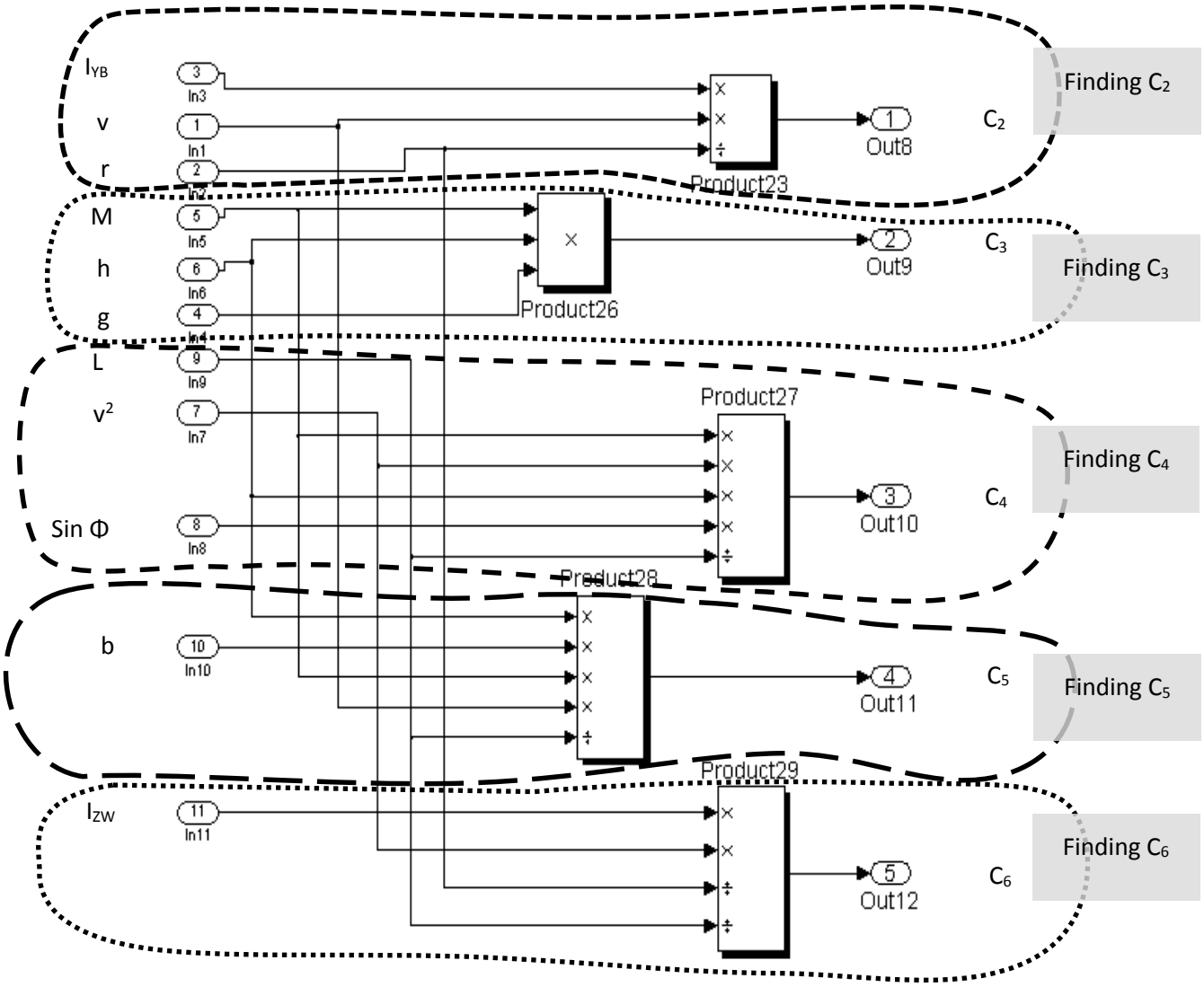

Figure 19 Part E, showing the Simulink calculations of coefficients C_2, C_3, C_4, C_5 & C_6

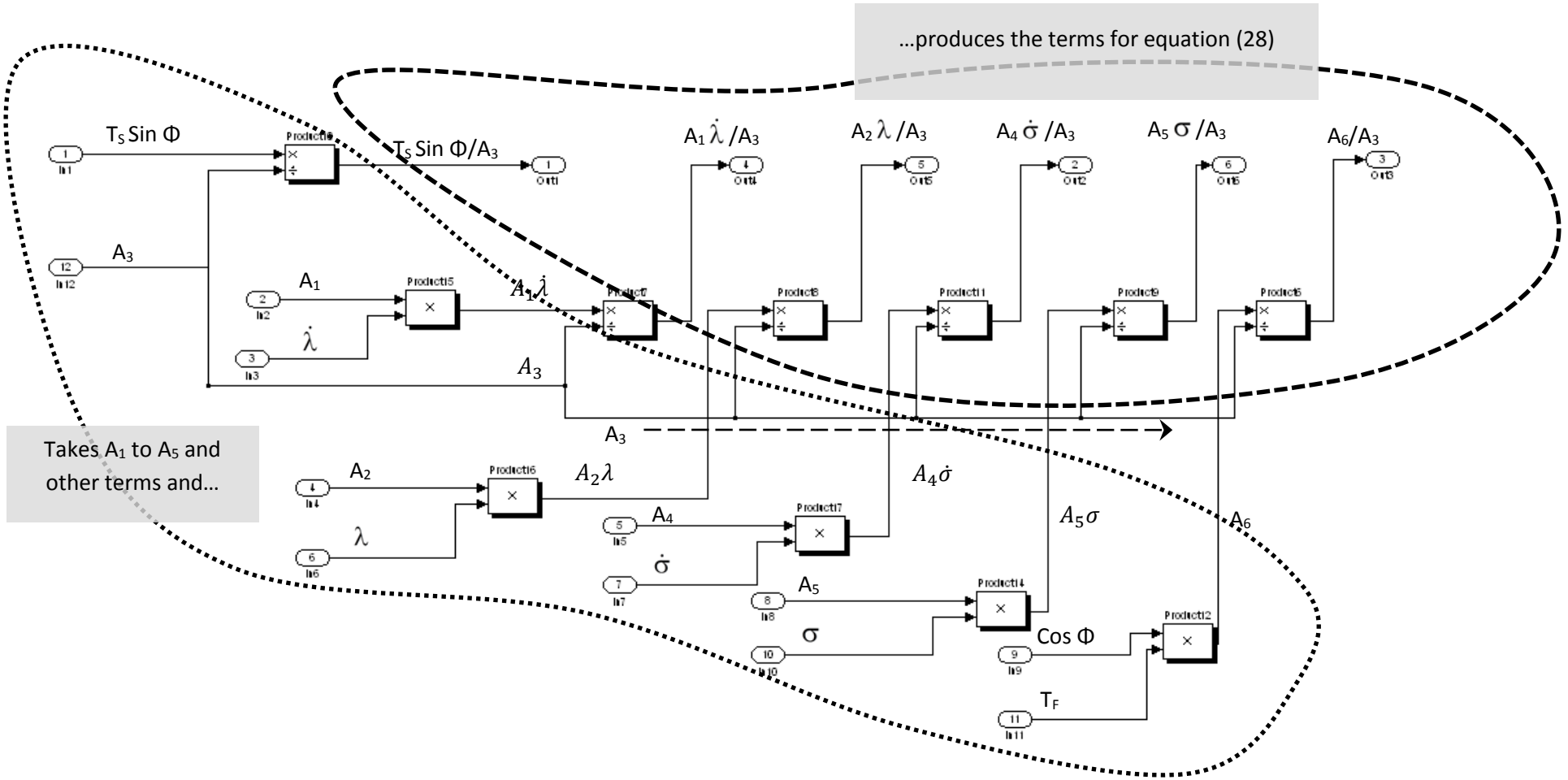

Figure 20 Simulink Part F, outlining the calculations of the terms required for equation (28)

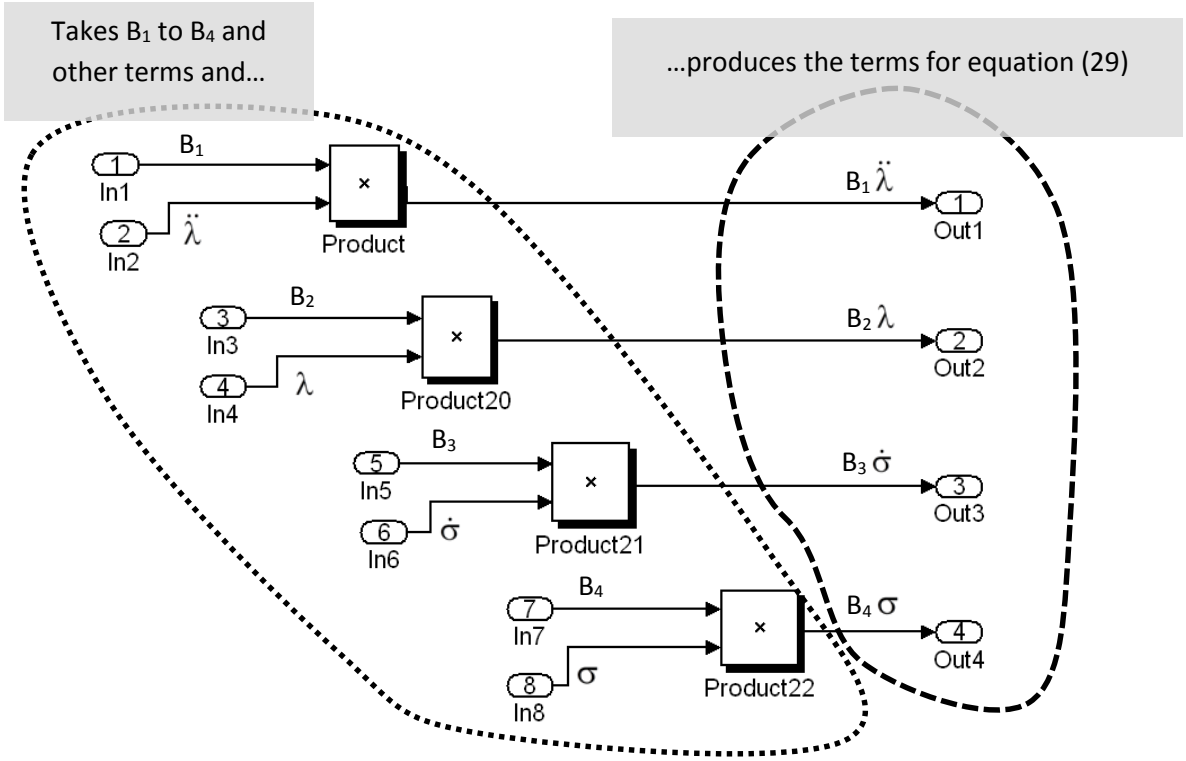

Figure 21 Simulink Part G, outlining the calculations of the terms required for equation (29)

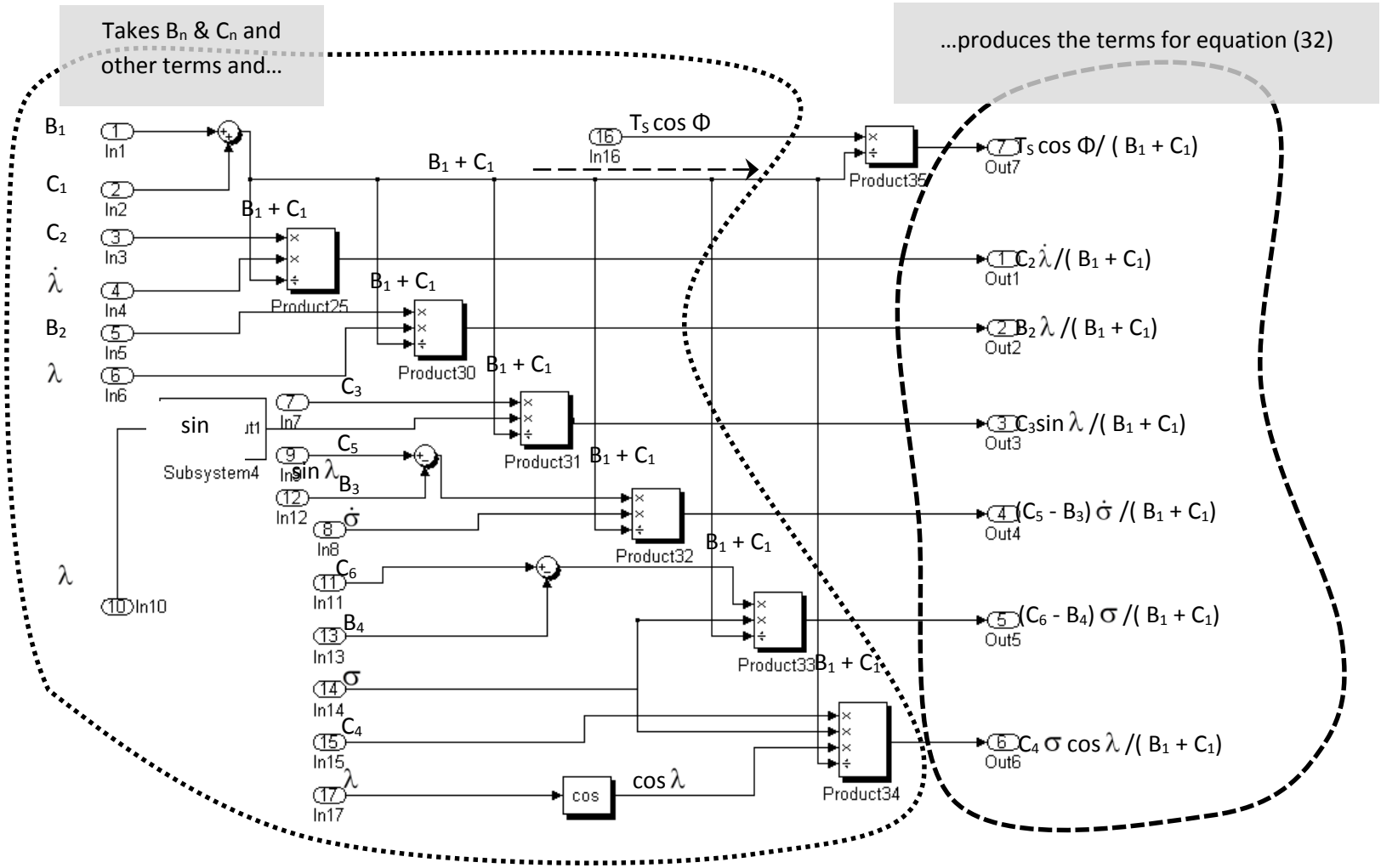

Figure 22 Simulink Part H, outlining the calculations of the terms required for equation (32)

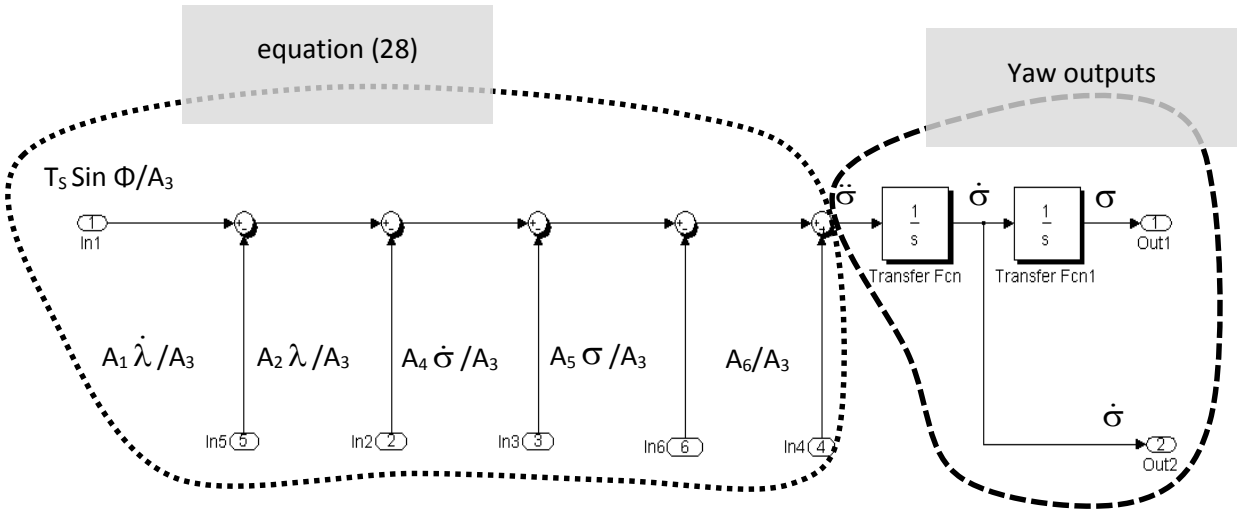

Figure 23 Simulink Part I, calculation of yaw σ terms

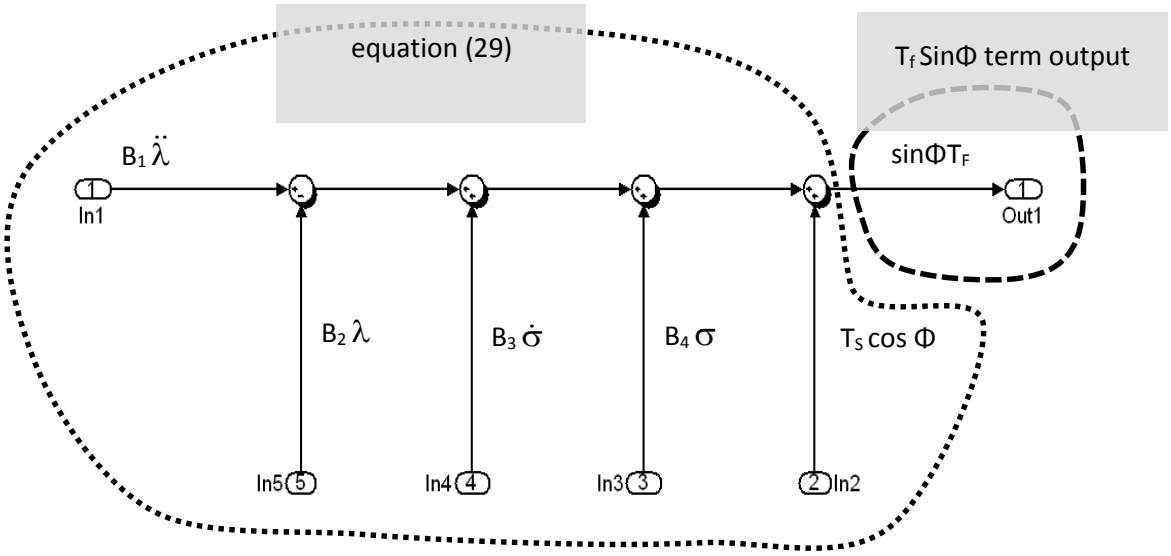

Figure 24 Simulink Part J, calculation of frame torque T_F

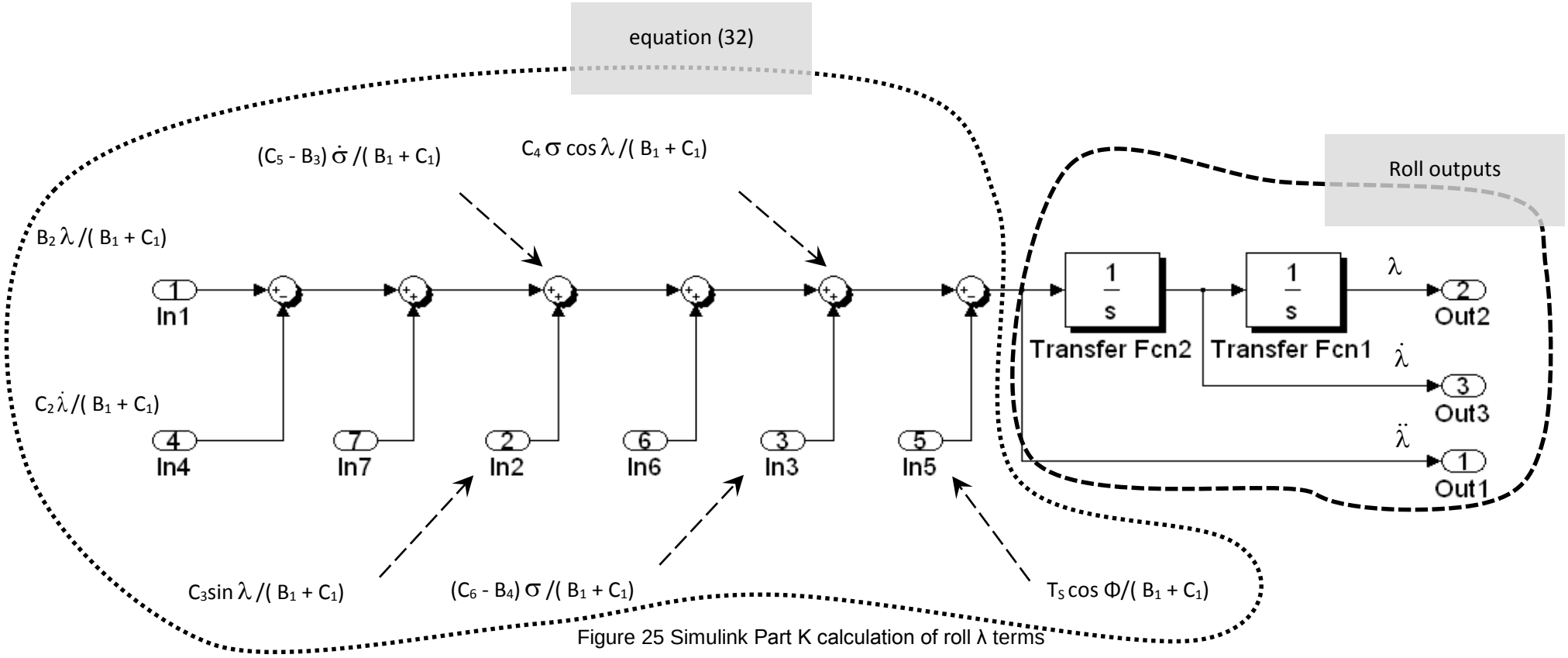

Figure 25 Simulink Part K calculation of roll λ terms

4.9. SIMULINK OUTPUTS

Once all the Simulink calculations have been completed, two final outputs are obtained: the front wheel yaw (σ) and bicycle roll (λ) with respect to time and these can be plotted on a Simulink Scope or saved to a Matlab workspace file for further analysis and processing. In Figure 26 a typical output of yaw and roll angles is shown plotted against time for the benchmark bicycle using a standard steering torque input (as per Figure 8).

The counter-steer cornering manoeuvre was described in Chapter Two when discussing the literature (12, 41, 54). To review this manoeuvre, consider the situation where a bicycle is required to corner to the right, the rider first has to turn the front wheel very slightly to the left, which is opposite to the direction of the turn. This small movement of the wheel will initiate a very small turn to the left. As the bicycle starts this small left hand turn, the centrifugal force induced on the bicycle and rider mass causes the bicycle to roll to the right. Once this happens, both the Jones and castor torques combine to cause the front wheel to now turn rightwards into the roll. The bicycle will now turn right and complete the desired right hand turning manoeuvre (2, 12, 41, 54). Clear evidence of such a counter-steering action is evident at the start of the simulation in Figure 26, where for the first 2 seconds the front wheel has yawed in a positive direction (to the left) before the desired negative (or right hand) yaw occurs.

Counter-steering is a counter-intuitive action and this may be one reason why it is hard for people to learn to ride bicycles, as it is not possible to corner a bicycle without initially turning the steering in the opposite direction. This action is something that most bicycle riders eventually will learn to do instinctively without consciously realising they are doing it. In fact it is common when discussing this topic even for experienced riders to claim that they do not countersteer when cornering.

4.10. ADDITIONAL MODEL FEATURES

Two additional features were added to the Simulink model which assisted the detailed analysis of various characteristics.

1. Parameter gain blocks

   The physical parameters were linked via gain blocks to the model in order to allow easy adjustment of their values for both sensitivity and stability analysis. Details of these gain blocks are shown in Appendix A. The Simulink model is therefore able to be run using different physical parameters so that model assumptions could be very quickly changed as required. This capability enables:

   - The model to be more easily checked against other work in this area
   - A variety of different bicycle manoeuvres to be tested and evaluated
   - Different designs to be quickly compared

2. Torque term examination

   Additional elements were added to the model allowing individual torque terms to be isolated and examined (that is all 23 torques from each of the three equations of motion). This enabled suggestions to be made as to which terms could be neglected from the equations of motion without affecting the model's accuracy. After considering this it was seen that at least 5 terms could ignored without affecting accuracy and it is possible that as many as 11 terms can be ignored for some applications. For more discussion on this topic see Section 5.3, also the details of these additional elements are shown in Appendix A.

Now that the model has been formulated, it must be validated before further use and two approaches are used to do this: comparing to existing literature and experimental validation. Both of which will be discussed in the following two sections.

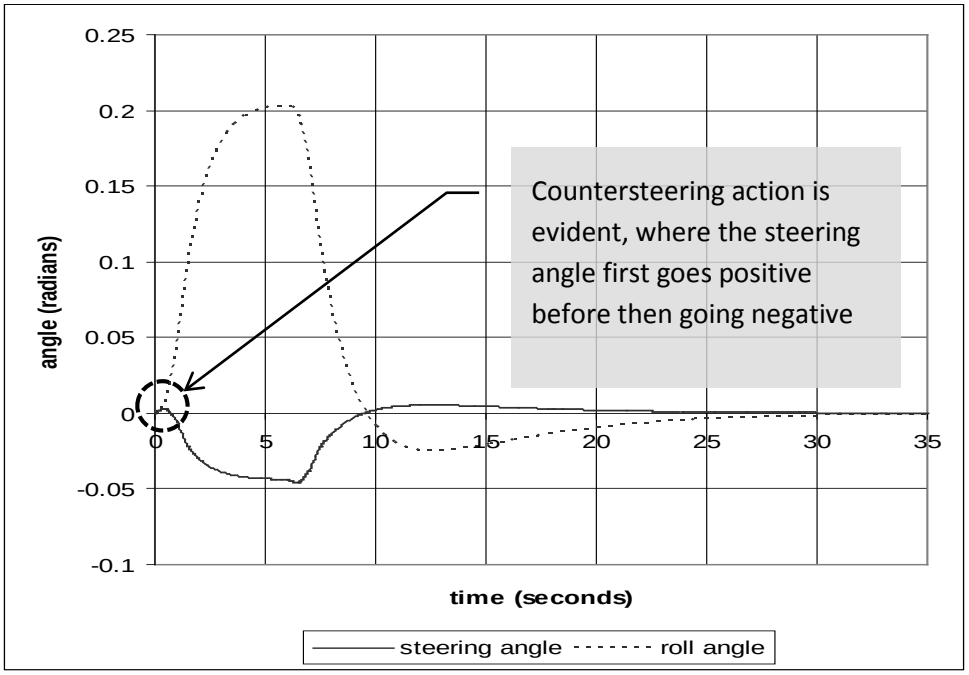

Figure 26 A typical Simulink simulation with outputs of yaw (steering angle) and roll angles

.

4.11. VALIDATION WITH LITERATURE

Now that a computer simulation model has been developed it needs to be validated and the theoretical approach chosen was to compare it with the literature. This was done by running a simplified Simulink model that used the same assumptions as Fajans, that is setting the new terms that allowed for Coriolis effects and the steering head tube angle to zero and using the same values for input torques, parameters and variables, see Table 19 (12). The key differences between Fajans and the more complex Simulink model are summarised as follows:

1. The Fajans steering head tube angle is set at 90 degrees i.e. the axis is vertical, whereas in the benchmark model it is set at 73 degrees with typical ranges for road bicycles being between 71.5 to 76 degrees. Because of its simplified steering geometry the Fajans model cannot be used to optimise steering geometry, a critical area of bicycle design.
2. Fajans uses a negative rake to provide the required trail, where in practice road bicycles have positive values of between 33 and 60 mm, see Chapter Seven.
3. Fajans neglects all the Coriolis torque terms, whereas the complete Simulink model includes all Coriolis torque terms.

Table 19 shows these assumptions for all three models and drawings of the steering geometries for a Fajans bicycle and a typical road bicycle are displayed Figure 28 and Figure 27.

Table 19 Model Assumptions

Assumptions	The Fajans model	Simplified Simulink model	Complex Simulink model
HTA degrees	90.0	89.9_1	73.0
Rake mm	-20.0	-19.42	45.0
Trail mm	20.0	20.0	56.13
Coriolis terms included	no	no	yes
Note 1, the model could not run with a 90 degree HTA angle, so 89.9 degrees was used instead as being the closest practical value			

A simulation using this simplified model was run and then compared with Fajans with the simplified model showing nearly identical output responses in terms of yaw and roll to Fajans, with very similar time lags, rise times, amplitudes, overshoots and oscillations, see Figure 29 (note that the simplified Simulink results are offset by 5 seconds to make the comparison clearer). The differences between them are quantified in Figure 30 where it can be seen that for most of the manoeuvre the yaw difference is within 2.5% (0.001/0.4) and the roll difference within 1% (0.002/0.2). This confirms agreement between this Simulink model's basic assumptions and Fajans but doesn't say anything about the validity of the added terms or other modifications. Simulink is a mature programme and it is reasonable to have a high degree of confidence in these

results. When using the default “adaptive step size” as was done in this case, the answer Simulink provides with such a comparison is as accurate as is practically possible.

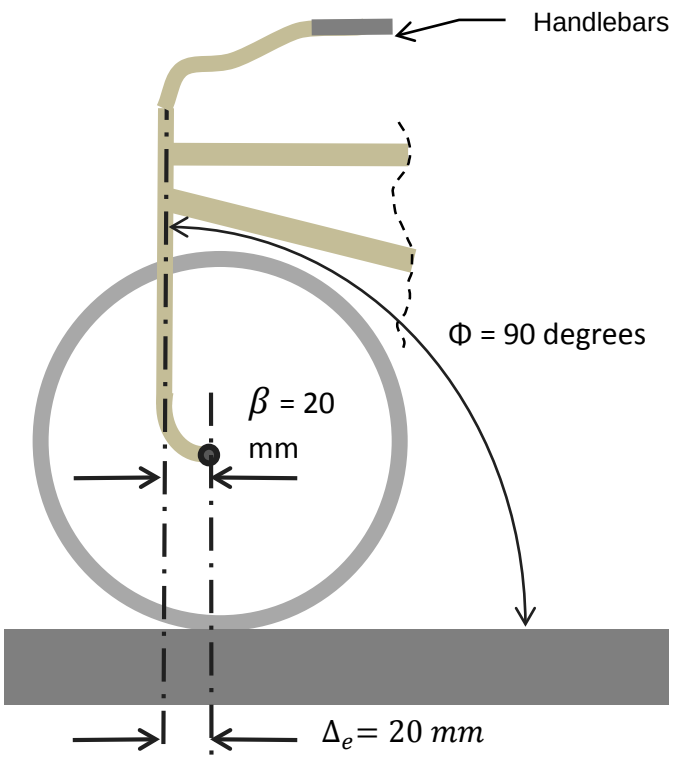

Figure 28 Fajans’ simple bicycle steering geometry

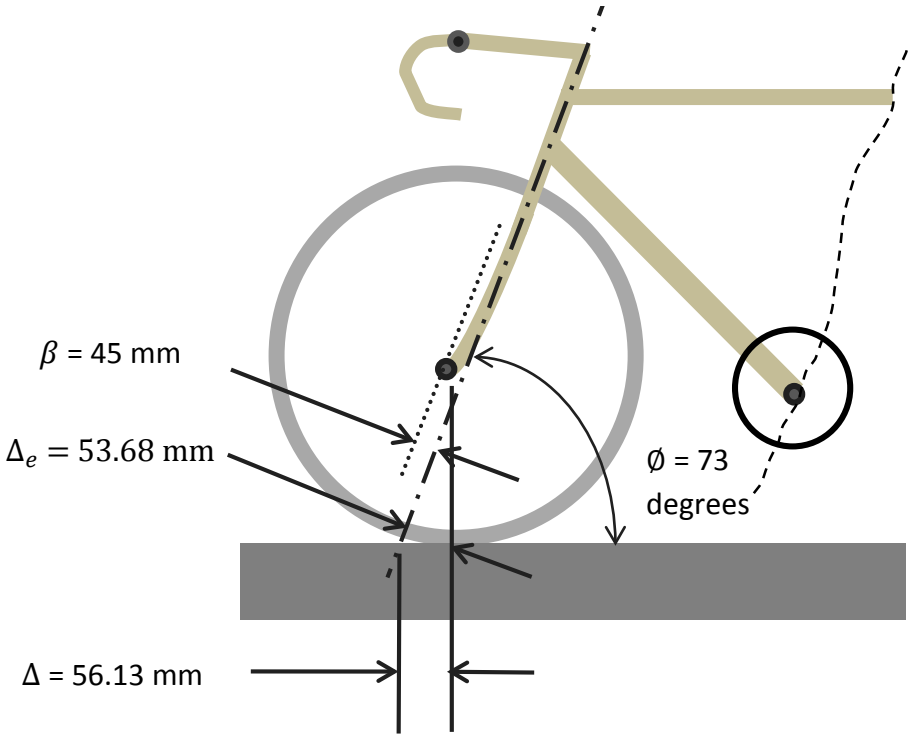

Figure 27 The benchmark bicycle’s steering geometry

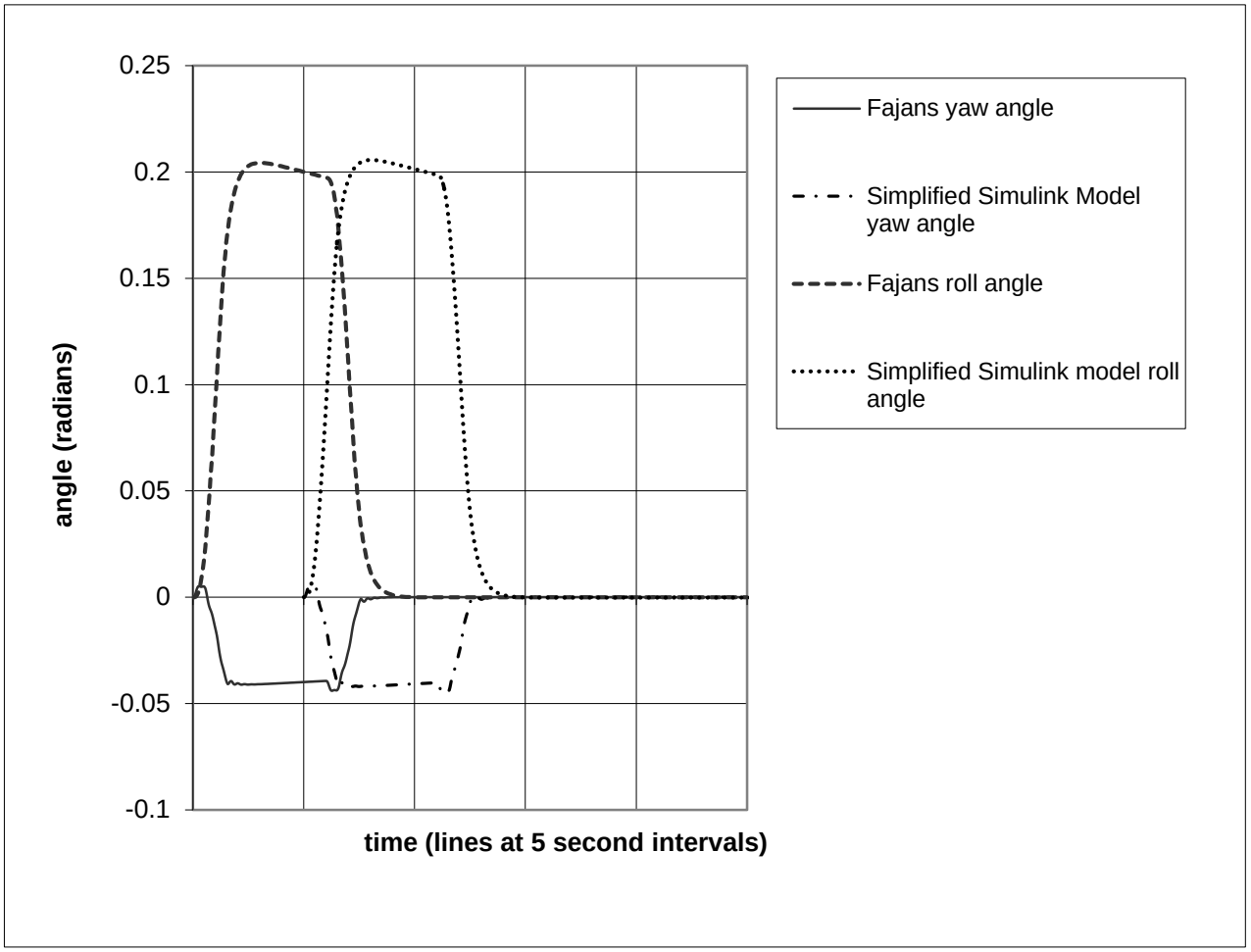

Figure 29 Comparison of the Simplified Simulink and Fajans models (with the Simulink results offset by 5 sec)

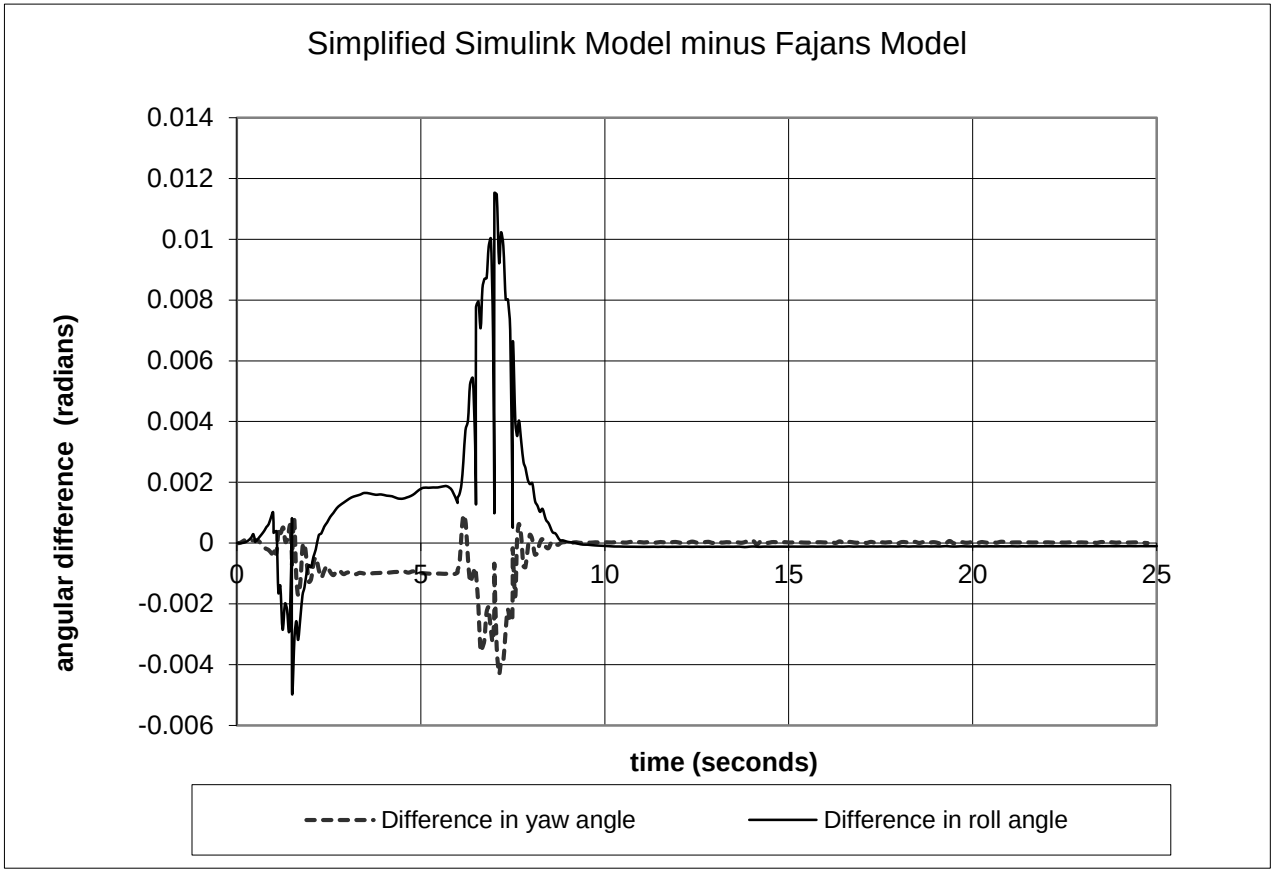

Figure 30 Difference between the yaw and roll angles of the Simplified Simulink and Fajans models

4.12. EXPERIMENTAL VALIDATION

In addition to the theoretical validation the Simulink model was validated by comparing it to an experimental investigation (31). In this part of the investigation a bicycle was adapted for experimental work by being fitted with transducers to measure front wheel yaw (or steering angle) and roll angles while a data logger recorded the results. This experimental bicycle test rig could record yaw and roll angles against time for test runs of up to 30 seconds and this rig is illustrated in Figure 31, Figure 32 and Figure 33.

The yaw angle was measured using a rotary electrical potentiometer with its input shaft directly attached to the steering stem by a simple coupling, see Figure 33. The potentiometer's output was proportional to the front wheel's yaw angle.

The roll angle was measured using a custom made infra-red (IR) distance measuring sensor mounted on a short bracket at the rear of the bicycle, see Figure 32. A pulse of IR light was emitted from the sensor and travelled downwards and once it hit the road surface it was reflected back. The reflected IR light returned to the sensor at a different angle from the transmitted angle and this angle was proportional to the distance to the road surface, as in Figure 34. As the bicycle rolled, the IR sensor detected a change in the angle of the reflected light beam and this was used to determine the roll angle, shown in Figure 35. For more details of this experiment and the apparatus used see Appendix C.

Using this bicycle different experimental scenarios were investigated under controlled conditions, first counter-steered cornering was considered which showed exactly the same characteristics for roll and yaw as predicted by the computer simulation. A counter-steered manoeuvre was always preceded by the tell-tale yaw of the front wheel in the opposite direction to the turn, followed by a quick yaw reversal as the turn continues. It can also be noted that the same effect occurs during the correcting part of the manoeuvre as the bicycle comes back to a straight course and this is clearly indicated in Figure 36 through to Figure 41. A total of 68 experimental runs were undertaken and the best and most representative runs are presented in this Chapter as a summary of the results.

To get good experimental results, it was necessary to take care to ride the bicycle as smoothly and upright as possible, prior to making the turn. The turn should be a slow gentle sweeping manoeuvre through at least 180 degrees as smaller, tighter turns were hard to interpret amongst the background signals of normal riding.

A second series of experiments involved testing on the road. From these tests it is apparent that constant steering corrections are required for balance when riding along the uneven surface of a typical road. As most road surfaces are highly irregular, changes in yaw and roll of the bicycle must cope with this irregularity, while the bicycle/rider system must obey the inverted pendulum rule in order to remain upright. The rider must constantly correct for changes in the bicycle's roll angle by using the yaw of the front wheel to steer the wheels under the centre of mass, this is

particularly evident in Figure 40 and Figure 41. A careful comparison of these figures shows that the maximum positive values of roll match the maximum negative values of yaw and vice versa.

Figure 31 Experimental bicycle setup used to validate Simulink model

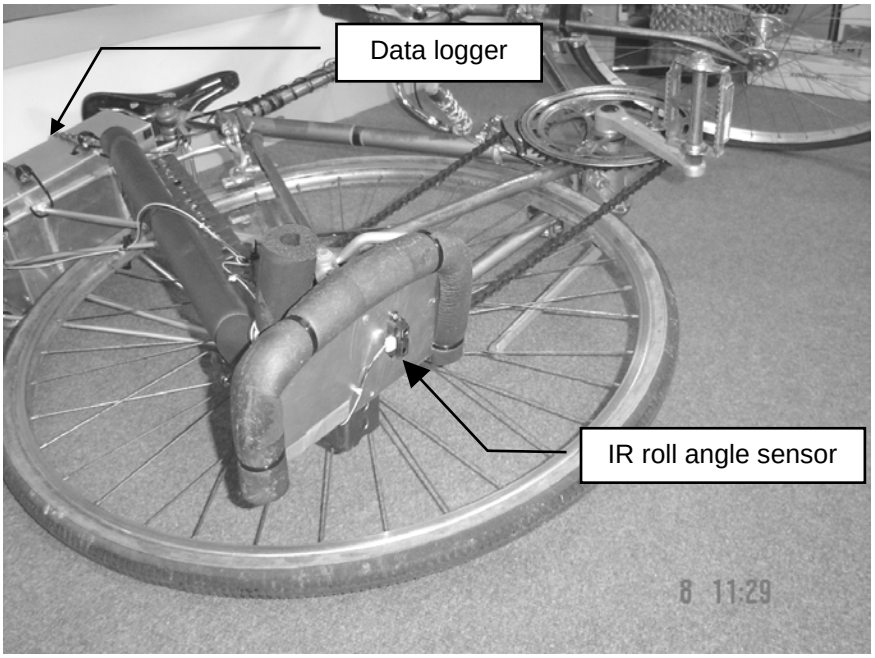

Figure 32 IR sensor and data logger used to measure the roll angle

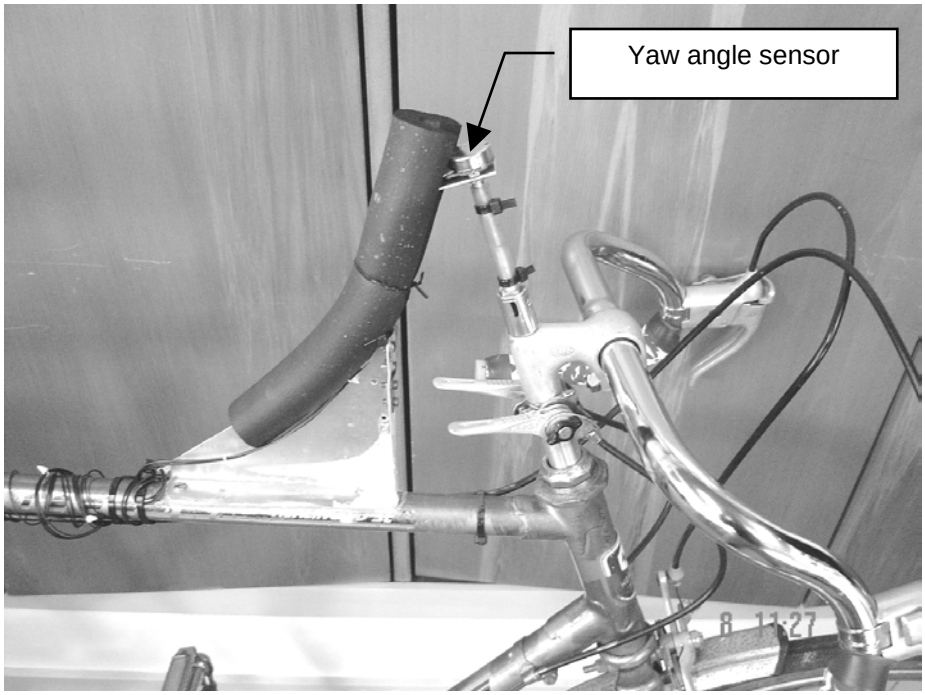

Figure 33 Yaw angle sensor measuring front wheel yaw

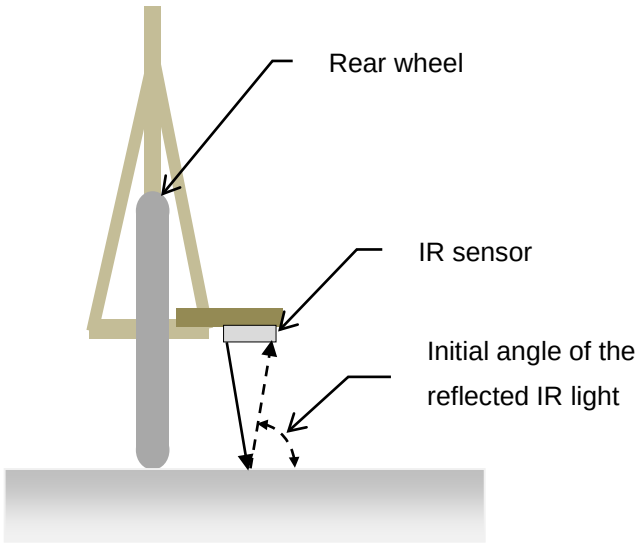

Figure 34 Bicycle roll sensor emits and receives IR light

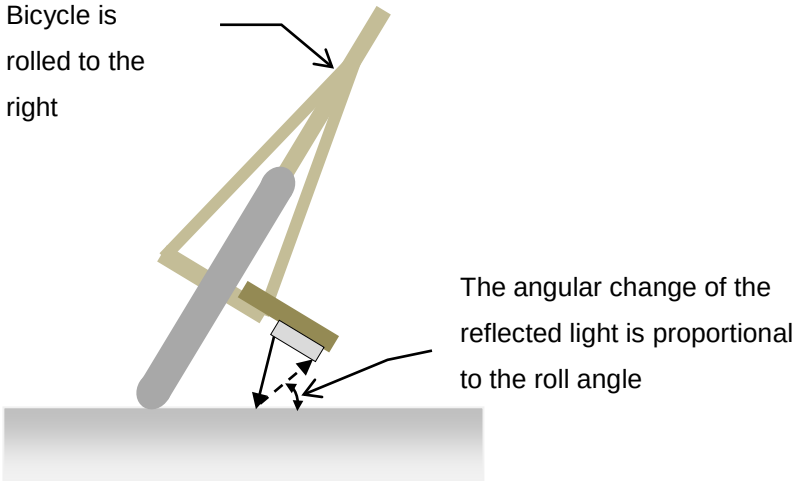

Figure 35 Roll angle is determined from the changed angle of the reflected light

In principle, this series of experiments illustrates trends (e.g. the counter-steering action) as it was very difficult to statistically correlate the data due to the irregular road surface and the large measurement noise and error signals that resulted. However, the results of the experiments and the comparison with other work indicate that the present computer model is acceptable to study bicycle dynamics [10].

From the results obtained it was possible to comment on the validity of the Simulink model. Both the theoretical and experimental validation shows the expected dynamic responses to a steering input. One very interesting point is that the yaw angle shows the same type of counter-steer both at the start and the end of the cornering manoeuvre, as the model. The roll angle also varies at the same rate as yaw and mirrors the model's response with regards to trends. It was not possible to quantify these responses with regards to the steering torque as the torque was not recorded. In fact the problem of recording steering torque is not a simple one, as the steering forces are very small compared to the vertical forces exerted on the handlebar by the rider.

4.13. REMARKS

This Chapter has described the structure and main elements of a Simulink model that can solve the equations of motion developed in Chapter Three. The model takes the rider's steering torque input and after applying appropriate physical parameters (such as mass, wheelbase length, head tube angle, rake and trail distance) finds the yaw and roll responses of the bicycle.

This Chapter also describes the validation of the model using both theoretical and experimental approaches. The theoretical approach to validate this model was to compare it with Fajans using identical parameters and variables and from the results obtained it can be seen that it showed nearly identical responses to Fajans.

The Simulink model was also validated by comparing it to the results of the experimental investigation where a bicycle was fitted with transducers to measure yaw and roll angles recorded on a data logger. From the results obtained it was possible to comment on the validity of the Simulink model as the experiments showed the expected dynamic responses to a steering input.

The model is now ready to be used for a detailed analysis of bicycle dynamic behaviour and this is described in the next Chapter.

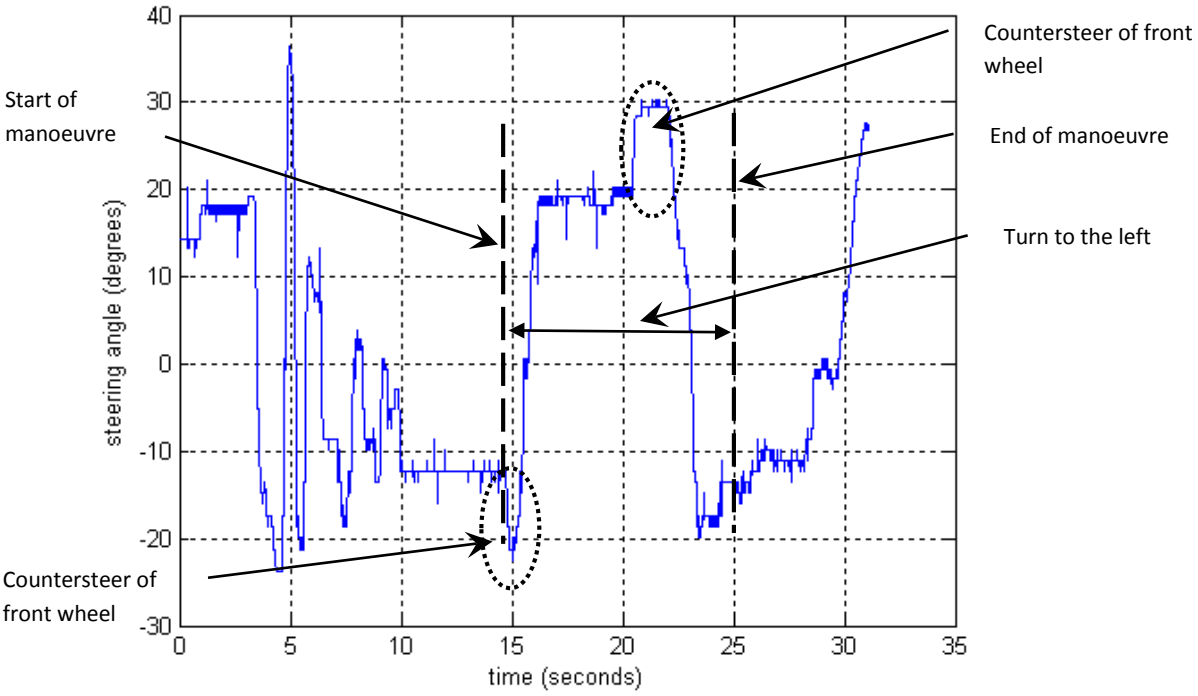

Figure 36 Yaw (steer) angle output during an experimental counter-steer cornering manoeuvre

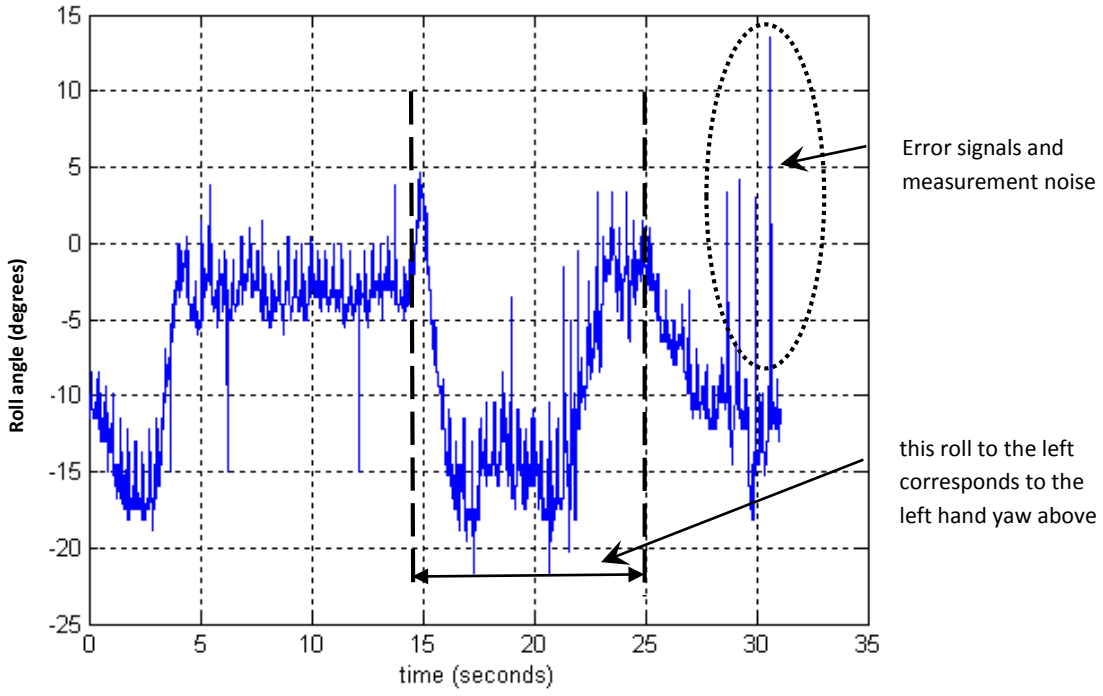

Figure 37 Roll angle output during the same experimental counter-steer cornering manoeuvre

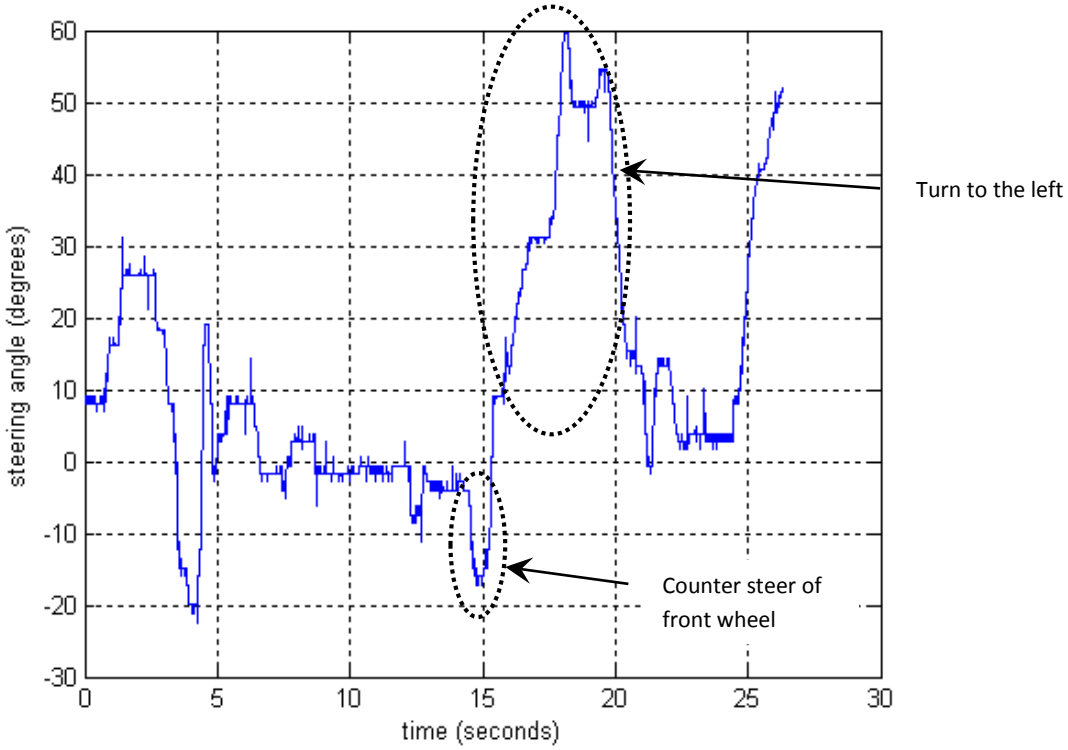

Figure 38 Yaw (steer) angle output for a second experimental counter-steer cornering manoeuvre

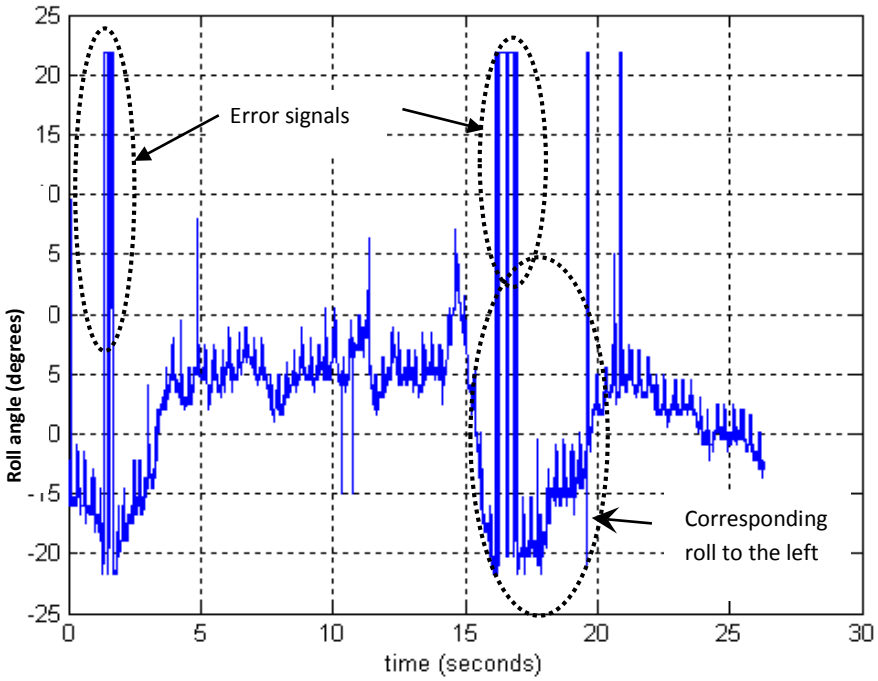

Figure 39 Roll angle output during the second experimental counter-steer manoeuvre

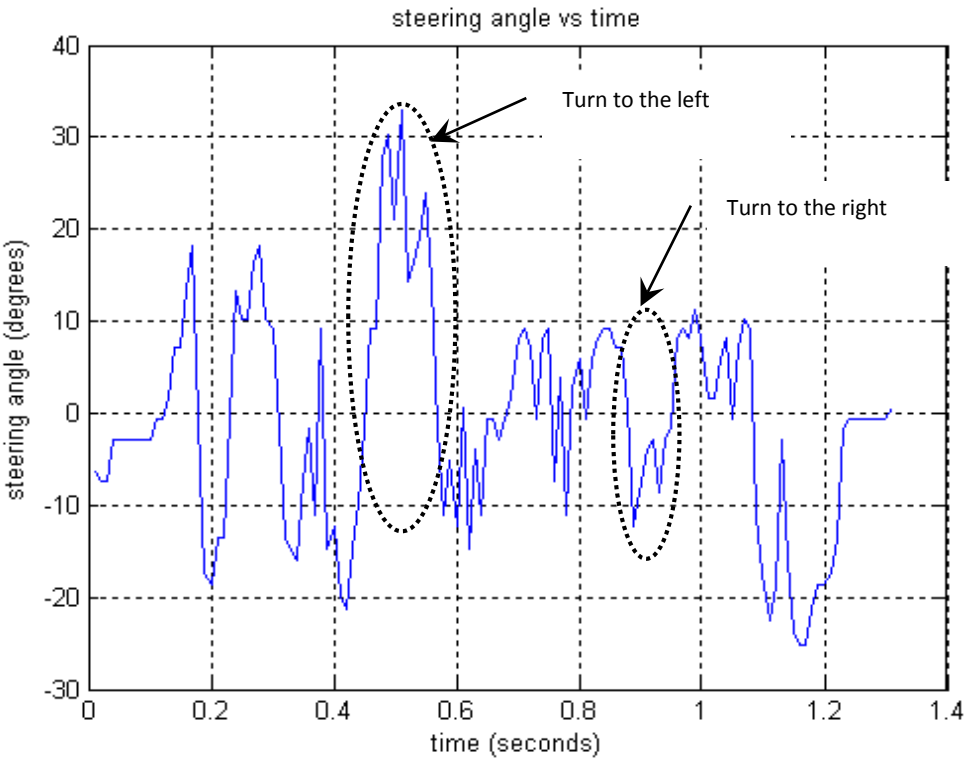

Figure 40 Yaw (steer) angle output for part of a typical experimental road ride

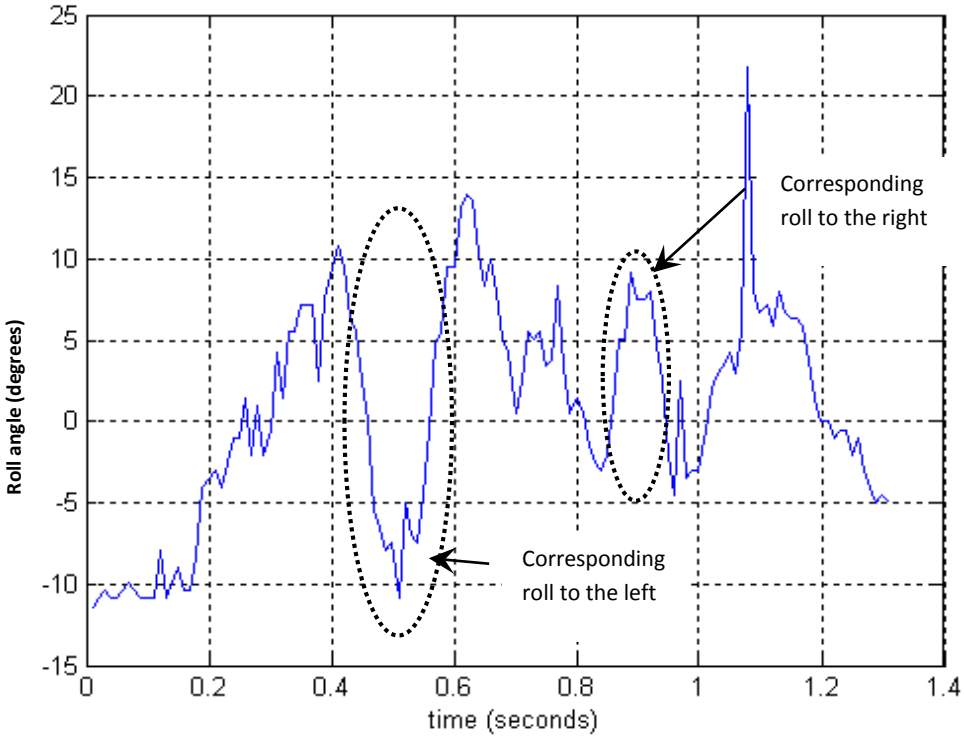

Figure 41 Roll angle output during the same experimental road ride

5. BICYCLE MODEL ANALYSIS

5.1. INTRODUCTION

This Chapter considers the bicycle design process and asks how it can be correlated with the model in Chapter Four? Given the large number of terms and parameters in the equations, what sort of simplifications and manipulations can be justified? Since a design process in most cases is based on approximations and empirical approaches it is logical to simplify the equations of motion to obtain a more practical and useful formulation. There is no sense in having long and overly complicated equations if the final design process later on requires significant simplifications and approximations. Furthermore as there are no unique values for the design parameters such approximations are normally acceptable. But before these simplifications can occur we need to determine how sensitive the analysis is to changes in these parameters. This Chapter uses the bicycle dynamic model developed and described in Chapters Three and Four to investigate and understand the following issues:

1. the effectiveness of the model in determining bicycle dynamic behaviour
2. the importance and significance of each torque term in the equations of motion
3. the sensitivity of the bicycle's performance to changes in design parameters

We ask the following important questions. How can the bicycle be optimised in terms of specific performance criteria? Can the equations of motion be simplified by ignoring any of the torque terms? It is important to understand how sensitive the bicycle is to changes in assumptions and parameter values. Finally how stable is the bicycle dynamically and is it possible to identify and avoid unstable design regions? Such questions need to be systematically examined and to provide answers the Simulink model was used to conduct the following:

1. Bicycle performance simulations

   The purpose of these simulations was to demonstrate the basic capabilities of the model and to see if it could effectively reproduce realistic bicycle dynamic behaviour, especially the reactions of the bicycle to changes in steering geometry, damping, speed and steering torque.

2. Torque term evaluations

   The significance and importance of individual torque terms in the dynamic model was examined by analysing the results of Simulink trials. By focusing on individual torque terms it was possible to determine the significant and insignificant terms so that recommendations about simplifications to the equations of motion could be made.

3. Sensitivity study

   This study identified critical design parameters and quantified their effects on bicycle handling performance. It determined their minimum and maximum acceptable limits and examined their relative importance in terms of their overall effects. These results are later used in Chapter Six to develop practical design charts for designers.

4. Stability study using the characteristic equation

   For completeness in this study the characteristic equation of the bicycle system was found as its roots determine the character of the time response and the natural transient response of the system, hence why it is called the characteristic equation. A necessary requirement for stability is for all of the roots of the characteristic equation to have negative real parts. Once the characteristic equation has been found the Routh Stability Criterion can be used to find out if it has any unstable roots without actually solving them and this procedure is shown in Appendix D.

5.2. BICYCLE PERFORMANCE SIMULATIONS

This section describes the results of a series of Simulink simulations that demonstrated the model's basic capability. These simulations demonstrate the application of the model and reproduce realistic bicycle dynamic behaviour, especially the reactions of the bicycle to changes in key parameters. Does the model show the same sort of results as expected from the literature and previous experiments? This section examines the following two areas of interest in order to understand bicycle performance:

1. the steering geometry terms (head tube angle, rake and trail) and the damping term
2. and speed and steering torque

5.2.1. STEERING GEOMETRY AND DAMPING

First consider the effect of steering geometry and damping, how do they affect each other? It is well known that steering geometry is a critically important factor in bicycle design (10, 83). This geometry is defined by: the wheel radius, head tube angle and rake values, from which the trail (and effective trail) can be calculated using the four equations below [equations (33 to (36)] see also Table 20 and Figure 42.

Trail equation

$$\Delta = \frac{r - \frac{\beta}{\cos \emptyset}}{\tan \emptyset} \tag{33}$$

Alternative trail equation

$$\Delta = \frac{r \cos \emptyset - \beta}{\sin \emptyset} \tag{34}$$

Effective trail equation

$$\Delta_e = \Delta \sin \emptyset \tag{35}$$

Alternative effective trail equation

$$\Delta_e = r \cos \emptyset - \beta \tag{36}$$

Table 20 Steering geometry terms:

Symbol	Steering geometry definition	Units
Φ	Head tube angle	degrees
β	Fork rake (or offset)	m
r	Wheel radius	m
Δ	Trail	m
Δ_e	Effective trail	m

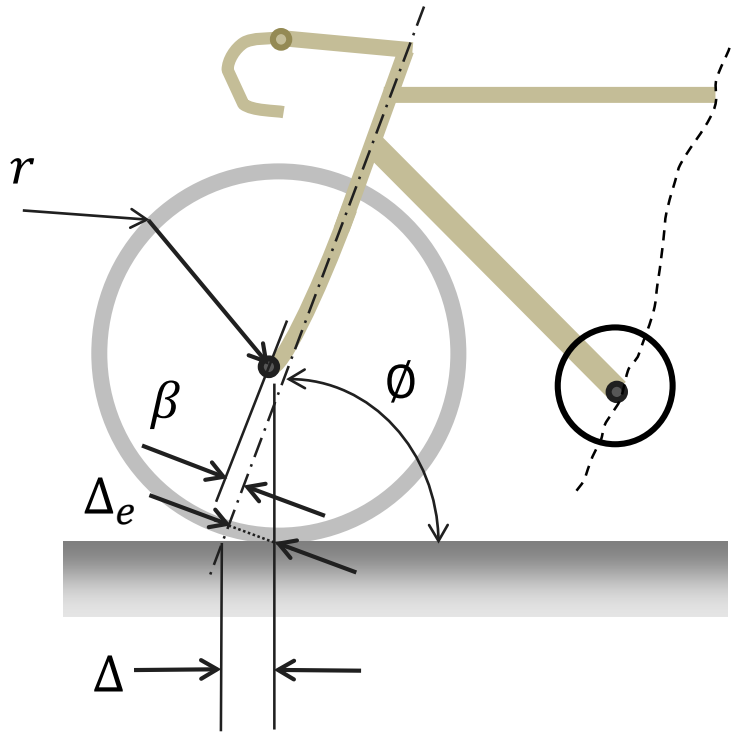

Figure 42 Bicycle steering geometry terms for the front wheel

In this section, five different steering geometry cases are examined and their dynamic responses are compared with one another (their specific geometries are shown in Table 21).

Table 21 Steering geometry cases

Case No	Head tube angle degrees	Rake mm	Trail mm	Comments	Outcomes	Relevant figures
One	73	45	56.128	Benchmark bicycle[1]	Stable even with no damping	Figure 43, Figure 48, Figure 51, Figure 52 and Figure 53
Two	73	75	24.757	reduced trail	Marginal, requires a precise steering input	Figure 45
Three	73	15	87.499	Increased trail	Highly unstable	Figure 46
Four	90	-20	20.000	Fajans bicycle	Unstable at low damping values	Figure 44 Figure 47
Five	89	-50	55.899	Fajans with increased trail	Marginal stability with low damping	Figure 49 Figure 50
Note 1 the benchmark bicycle has the standard geometry						
Unless otherwise noted the standard steering torque of +0.45/-0.414 Nm is used (see Figure 8						

First consider the effects of trail with the first three cases.

- For case one (the benchmark bicycle) when using a standard steering torque, the bicycle successfully completed a counter-steered manoeuvre and exhibited acceptable behaviour, with a rapid steering response and small overshoots and this is displayed in Figure 43. This means that this bicycle is easy to precisely control and steer. As discussed in Chapter Three the Simulink model (i.e. case one) includes new terms often ignored by others. With these new terms the dynamic results differed to the Fajans model and others, though the fundamental aspects remained (12). Overall, case one shows a slower cornering response with greater time lags and slower rates of change than Fajans, see Figure 44. The graph shapes are more rounded and less angular, which is what would be intuitively expected and this shows the significance of using assumptions previously not considered, such as realistic steering geometry.

- For case two with a reduced trail, the bicycle now exhibits large yaw and roll overshoots, seen in Figure 45. To compensate for this a rider would need to be able to sensitively apply and control a very small steering torque in order that the response of the bicycle is kept to acceptable values of yaw and roll. Therefore this bicycle is harder to control and requires more skill due to its tendency to overshoot, but it may not be unstable.
- In case three the bicycle uses a larger trail and this geometry proved to be unstable with exponentially increasing yaw and roll angles, see Figure 46. It would probably not be possible to control this bicycle even with very fine and skilful steering control actions.

Now consider what effect damping has and how it interacts with the steering geometry. The damping term (Γ, units Js) was found by Fajans to be necessary to ensure stability and it is provided by the passive resistance and active responses of the rider's arms (12). Also the hysteresis in the tyre contact patch and tyre wall provides an additional dampening effect (84).

- For case four (the Fajans bicycle) with a damping term of 0.65 Js, this bicycle can successfully complete a counter-steered turn (see Figure 44) but as damping is reduced yaw and roll oscillations increase rapidly. As damping approaches 0.05 Js, these oscillations start to grow exponentially, showing the bicycle to be uncontrollable as shown by Figure 47.
- Now consider the benchmark bicycle (case one) where it is interesting to see that for the same low damping term of 0.05 Js the bicycle was still completely stable, see Figure 48.
- Finally for the case five bicycle (which is similar to Fajans but with an increased trail) even at quite low damping terms (0.05 Js) it was still stable and was only just starting to show signs of oscillation, see Figure 49. Finally by reducing damping to 0.005 Js this bicycle becomes unstable, see Figure 50. This damping value is an order of magnitude below the minimum requirement for case four, clearly showing the effect that trail has on stability and the importance of the interaction of the steering geometry and damping terms.

These different simulations show the importance of selecting the correct steering geometry in order to achieve a satisfactory steering performance. Immediately we can see how a reduced trail increases overshoots (Figure 45) while an increased trail can result in instability (Figure 46). Perhaps cases three to five are still rideable with sufficient practice and skill but obviously the controlling steering torque would need to be finely adjusted. In conclusion a design can have too much trail as well as too little. These are important findings showing that if the correct geometry is selected, damping is not so critical to the stability of the system. Modern bicycle steering geometries reduce the need for damping, improve stability and reduce the dependence on precise, fine steering inputs to maintain control.

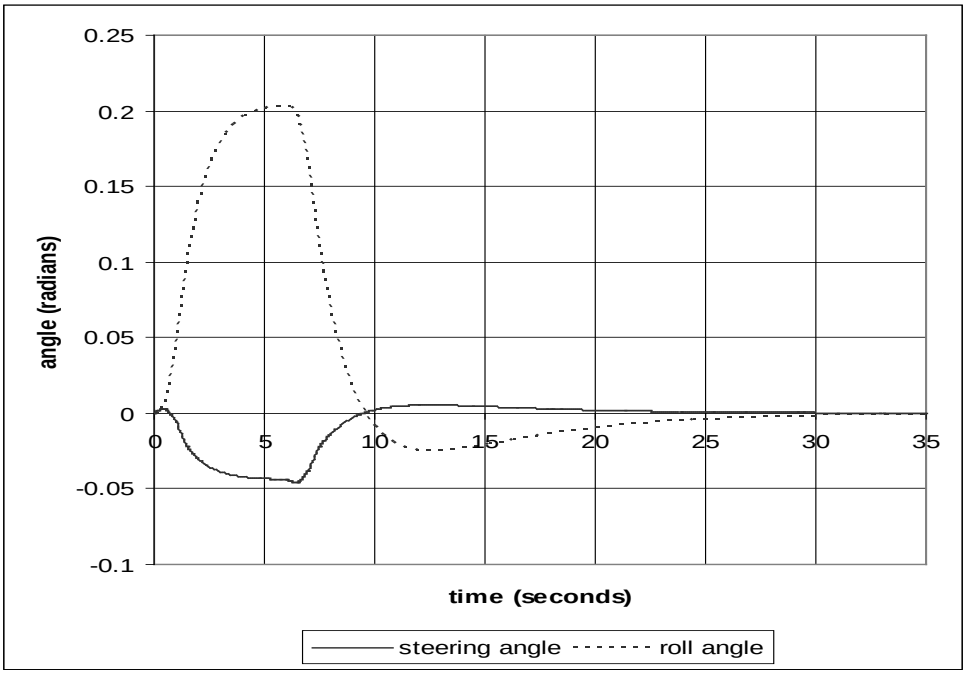

Figure 43 Simulink result for the benchmark bicycle on a standard run, case one

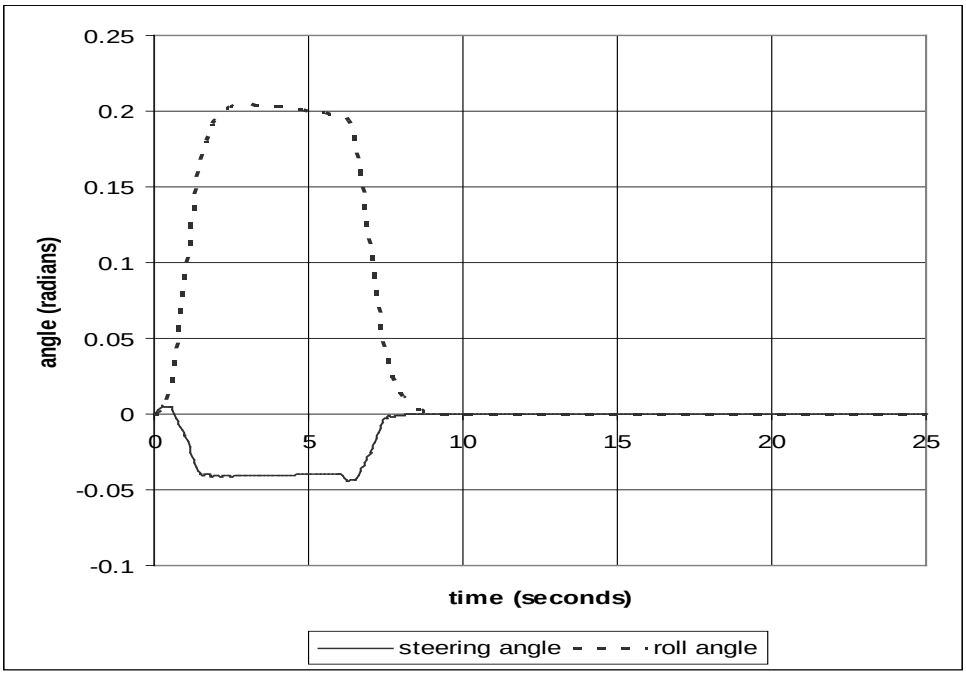

Figure 44 Fajans model for a standard simulation

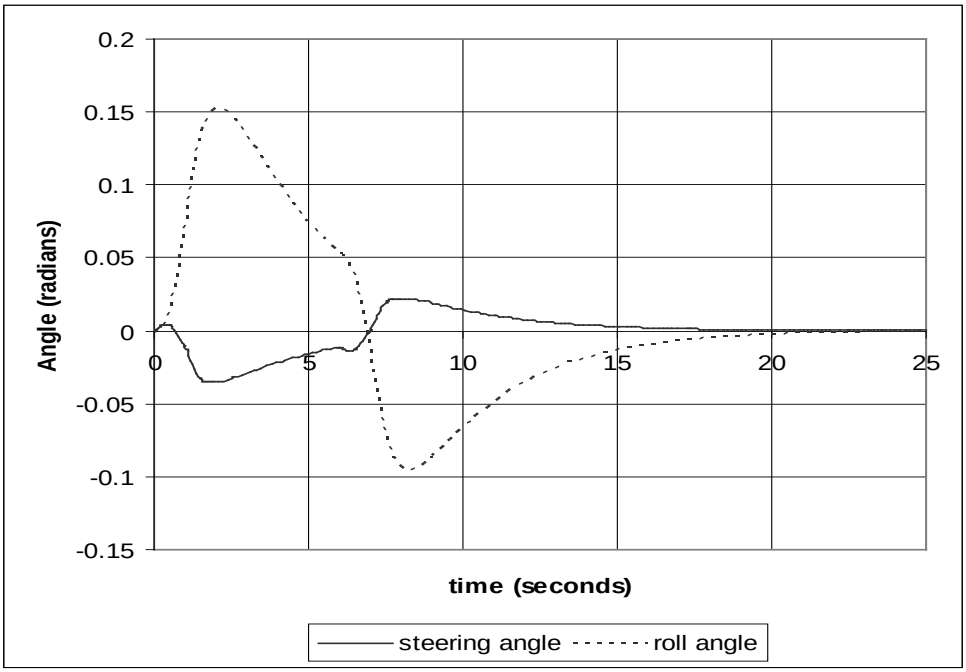

Figure 45 Case two simulation with reduced trail

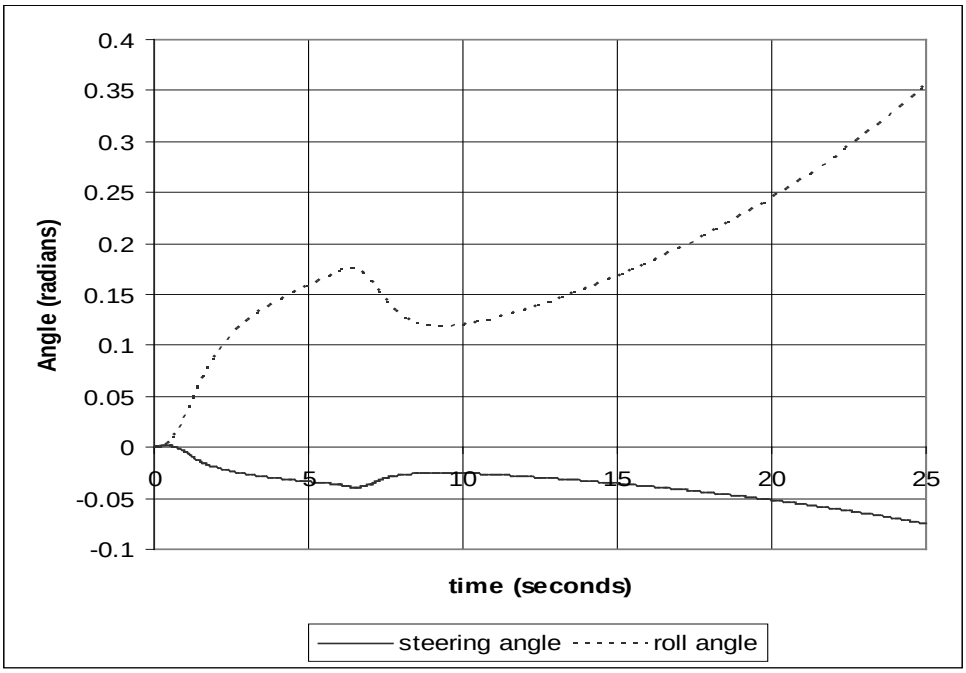

Figure 46 Case three simulation with increased trail

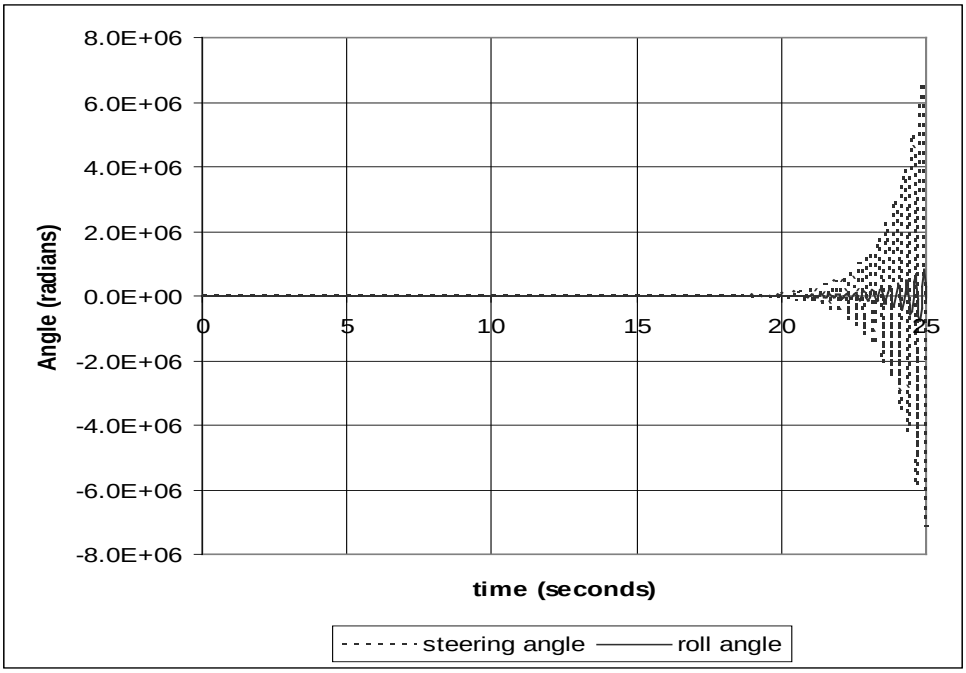

Figure 47 Case four simulation with low damping of Γ = 0.05 Js

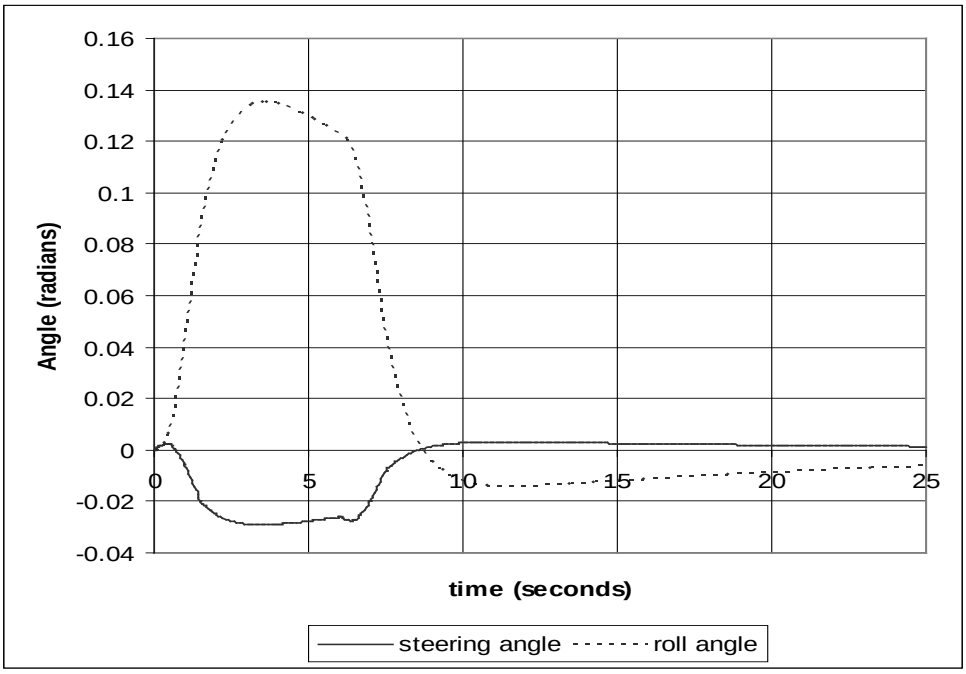

Figure 48 Case one simulation with low damping of Γ = 0.05 Js

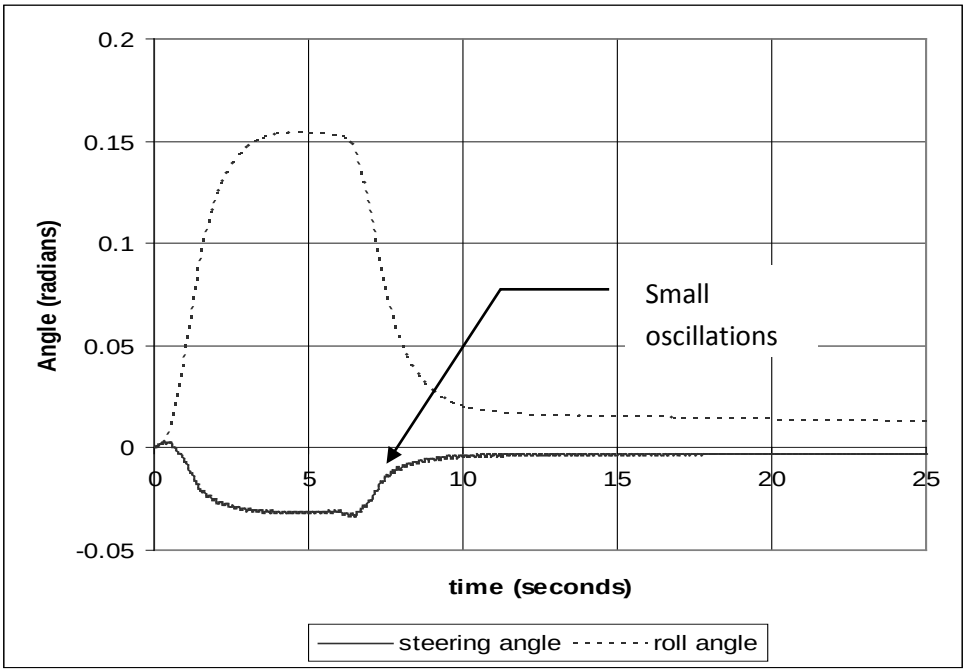

Figure 49 Case five simulation with a low damping of Γ = 0.05 Js

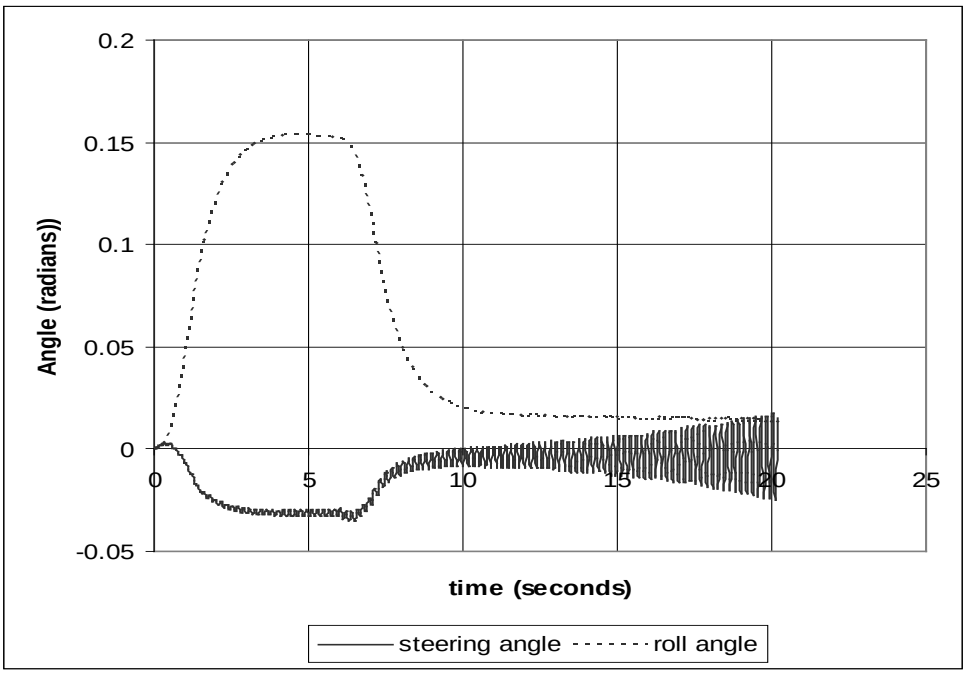

Figure 50 Case five simulation with very low damping of Γ = 0.005 Js

5.2.2.SPEED AND STEERING TORQUE

It is commonly reported that bicycles are more stable at higher speeds (2, 5, 20, 21). But does the model developed show this behaviour? This investigation now considers the effect of speed and the associated steering torque required for control.

- For case one with all terms in the model unchanged, except for speed, it was found that at 5 km/hr the bicycle became unstable when the steering torque remained at the standard value (+0.45 / -0.414 Nm) see Figure 51.
- Only by reducing the steering torque down to +/- 0.0025 Nm (or 0.6% of the standard value) was it possible to control the case one bicycle at this lower speed, see Figure 52. This torque is equivalent to a couple comprising of two oppositely opposed 0.57 gram forces set 450 mm apart on the handlebars. Of course such a very small torque value would be difficult for a rider to apply and control but it is not impossible with practice. Therefore it is concluded that as the speed reduces the steering torque required to control the bicycle must also dramatically reduce.
- Conversely as the speed increases above 25 km/hr the torque required to steer the bicycle around a corner increased. When speed increased to 85 km/hr (with all other terms unchanged) it was found that the bicycle became incredible stable in a straight line. The standard steering torque of +0.45 / -0.414 Nm, only produced very small yaw and roll responses of 0.06^0 (0.001 radians) and 3.2^0 (0.055 radians) respectively, in other words the steering input hardly produced a change in direction and this is shown Figure 53.

This supports the common empirical observation that bicycles are more stable and easier to ride at higher speeds (2, 5, 20, 21). It also means that to undertake a large course variation at high speed a large steering torque is required. In addition outside perturbations have less effect on bicycles and will not affect their course as much and so the bicycle is more self-stable.

An important objective for this study was to find ways to optimise bicycle steering geometry and to improve performance. After consideration of the five cases just examined it can be seen that careful selection of the steering geometry parameters is critical, also as they are interrelated wrong combinations can dramatically affect the steering response and stability. The advantage of the Simulink model is it allows different geometries to be checked for any potential stability problems before a design is built.

By plotting the trail and the head tube angle onto a chart it will be possible to indicate unstable regions and such a chart could be used to design successful geometries and avoid mistakes. In Figure 54 such a chart is drawn and on it is displayed lines of constant rake. Cases one to five from Table 21 have been plotted on this chart.

A region of stability is approximately indicated within the dotted line. At this stage the boundary between stable and unstable geometries is not precisely known. Obviously the negative trail region is completely unstable and has not been plotted. Though the exact boundaries between stable

and unstable regions are not yet known this will be explored by further investigations in Chapters Six and Seven. Out of interest the 1817 Hobbyhorse is also plotted, with a head tube angle of 90 degree, 0 mm trail and 0 mm rake, it is marginally unstable according to the chart but in practice is still rideable.

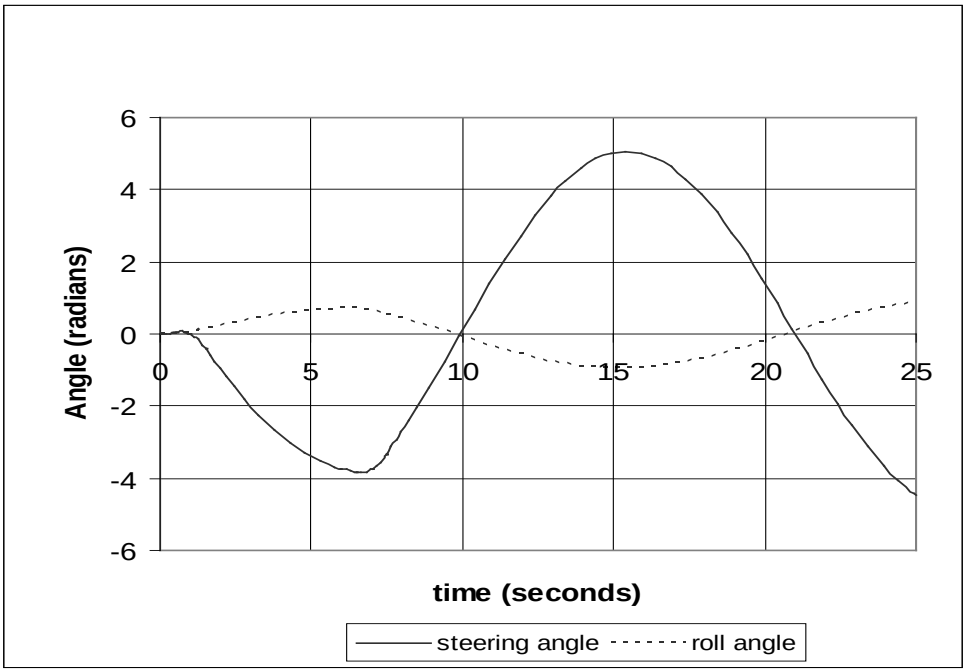

Figure 51 Case one low speed simulation v = 5 km/hr and $T_S \approx$ +/- 0.45 Nm

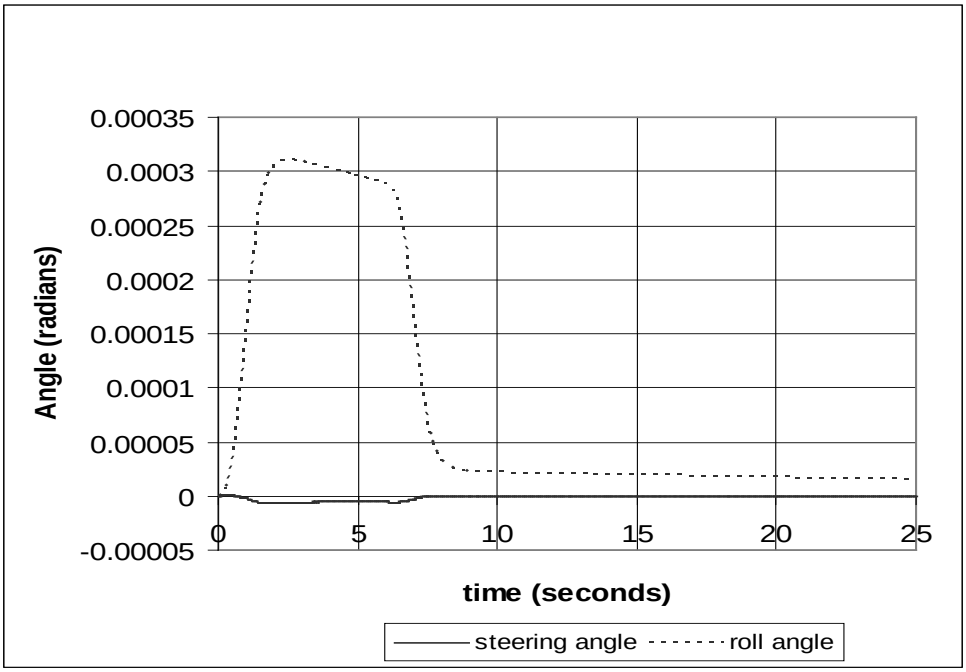

Figure 52 Case one low speed simulation v = 5 km/hr and $T_S \approx$ +/- 0.0025 Nm

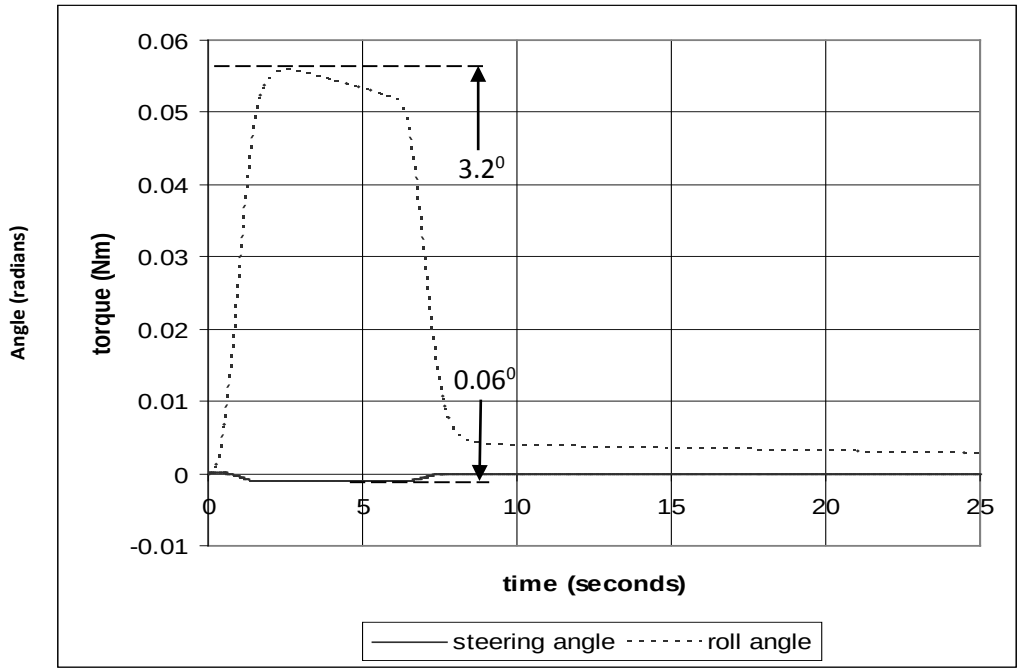

Figure 53 Case one high speed simulation v = 85 km/hr and $T_S \approx$ +/- 0.45 Nm

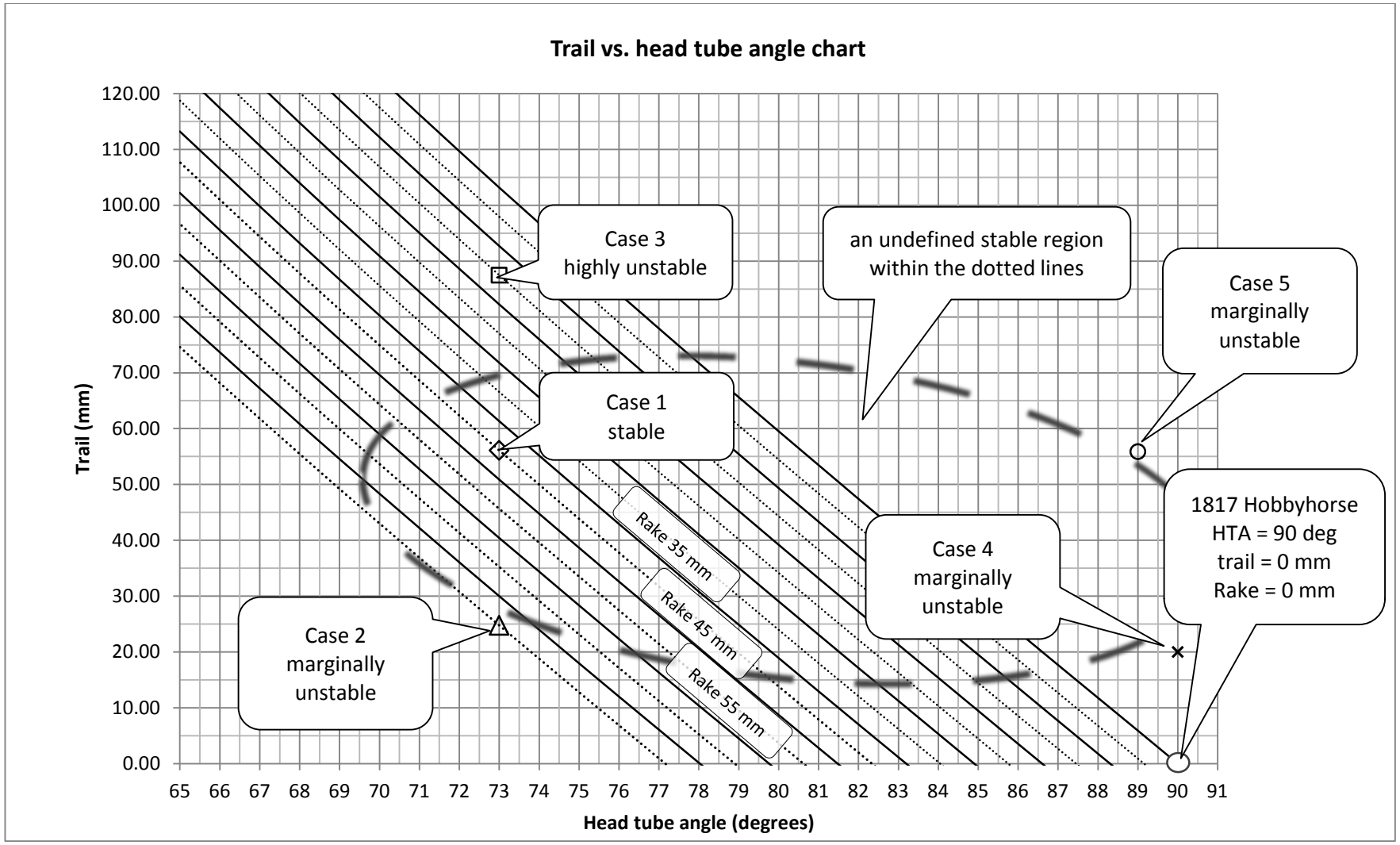

Figure 54 Trail vs. head tube angle front wheel geometry chart (wheel dia. all 675 mm & rake lines at 5 mm intervals)

5.3. SIGNIFICANCE OF TORQUE TERMS

An evaluation of the significance of each torque term is important because the full equations of motion [equations (14, (19 and (24)] are complicated (having a total of 23 individual torque terms even after our simplifying assumptions) and it would be difficult to use these equations for design purposes without further simplification. Simplification is also justified because the design process itself is an approximation process that can tolerate small variations. So we need to find out which terms can be ignored without affecting the dynamic model results.

In order to determine this the terms were isolated within the Simulink model without affecting its functionality and simulations were run so the magnitude of each torque could be compared and decisions made as to which are the most significant and which could be ignored from the model. If some torques can be ignored without adversely affecting the accuracy of the dynamic modelling this would simplify further analysis. Also a very simplified set of equations would enable more appropriate equations to be used for some purposes. For example undergraduate teaching, because though the problem of bicycle motion engages students, the current complicated equations interfere with many worthwhile educational outcomes.

Each of the three fundamental equations of motion [i.e. equations (18, (23 and (26)] are now examined in turn and suggestions as to appropriate simplifications are made.

5.3.1. FIRST EQUATION – MOMENTS ABOUT THE YAW AXIS FOR A

The first equation (18) considers the yawing about the vertical Z axis for the front assembly A. It has eight torques terms in total, two of which are new compared to the Fajans model (the Coriolis and frame torques) but which torques can be ignored? First the peak values for each individual torque term were found and torque with the largest peak value was identified. Then the peak values of each torque were compared to this maximum torque term. It was decided to consider excluding any torque which had a peak value of 10% or less of that of the maximum torque term's peak value, unless there was a good reason to include it. This is an order of magnitude less than the maximum torque's value. The suggestions as to which terms in equation (18) to ignore are shown in Table 22 and comments about this now follows:

- the castor torque, Jones torque and the steering torque input from the rider are of major importance and are shown in Figure 55
- the castor and Jones torques are by far the most significant terms in this equation and dominate the yaw of assembly A
- the gyroscopic torque of the front wheel due to rolling, the Coriolis torque and the frame torque that B exerts on A are an order of magnitude less than the most important terms and have a minor effect, they are shown in Figure 56
- the Coriolis and frame torque are new terms introduced into this model

- note that the gyroscopic term is almost counteracted by the Coriolis torque and this shows the unimportance of the gyroscopic effect, but as it is well known and so of interest it could be included in a study
- the frame torque of B on A follows the same shape as the castor and Jones torques, but is smaller
- all of these three minor torque terms could be ignored without compromising model accuracy
- the least important terms are the inertia torque due to yawing of assembly A and the damping torque
- these terms are two orders of magnitude smaller than the most important torques and are shown in Figure 57
- the damping torque is small but should not be ignored because as shown in previous modelling it can have a significant effect on stability (at least for some steering geometries)
- the inertia torque could be ignored but as it is well known and so of interest it may be included

In conclusion, for equation (18) of the original eight torques, for the purposes of the characteristic equation, two could be ignored (Coriolis and frame torques) and for a more simplified set of equations a further two more could be ignored (the inertia and gyroscopic/roll torques).

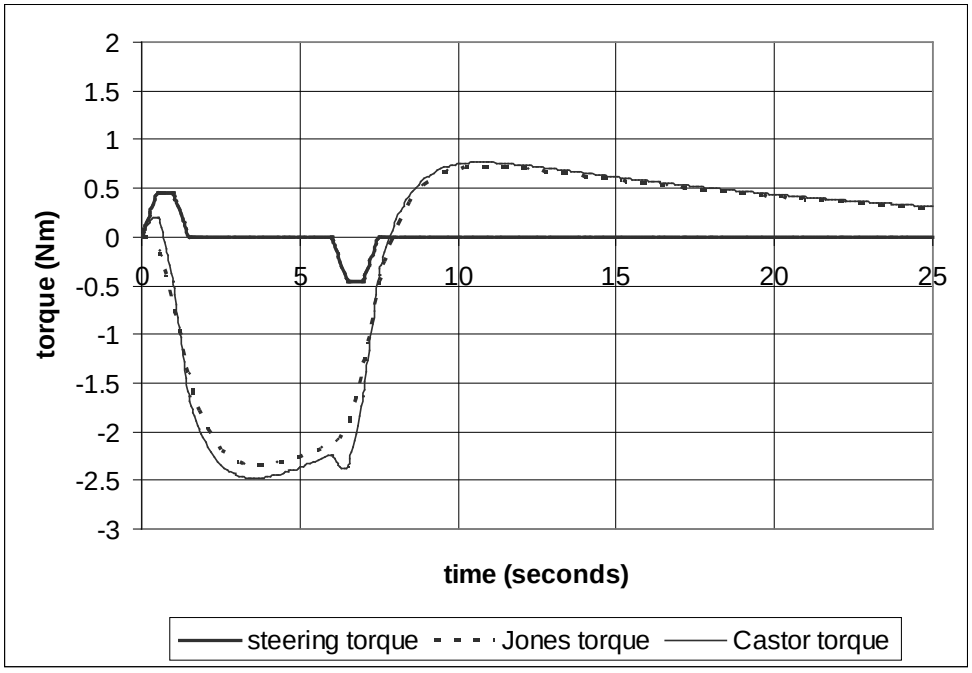

Figure 55 Major torque terms from equation (18)

Table 22 The terms from equation (18) and their significance

	Torque	Expanded term	Relevant figure number	Description and comments	Max torque value Nm (%)	Assumptions	Significance of the term
1.	$T_{Inertia}$	$I_{ZA}\dot{\omega}_{ZA}$	Figure 57	Inertia torque due to the yawing of A	+/- 0.023 (0.92%)	very small and could be ignored but included as it is well known and so of interest	negligible effect
2.	$T_{Gyro/roll}$	$I_{YF}\omega_{YF}\omega_{XF}$	Figure 56	Gyroscopic torque due to the rolling of A	+ 0.2 (8%)	small and could be ignored but included as it is well known and so of interest	minor effect
3.	$T_{Coriolis}$	$I_{XF}\omega_{YF}\omega_{XF}$	Figure 56	Coriolis torque of A	+ 0.09 (3.6%)	can be ignored	minor effect
4.	T_{Steer}	$T_S \sin\phi$	Figure 55	Steering torque input by rider, corrected for the head tube angle	+ 0.45 (18%)	must be included	major effect
5.	T_{Jones}	$Mg\frac{B}{L}\sin\phi\Delta_e\lambda$	Figure 55	Jones' torque or trail steer, causes the wheel to lean into the corner	+ 2.3 (92%)	must be included	major effect
6.	T_{Castor}	$M\frac{bv^2}{L^2}\sin\phi\Delta_e\sigma$	Figure 55	Castor torque due to trail, tends to straight the wheel up	- 2.5 (100%)	the maximum torque and must of course be included	major effect
7.	T_{Frame}	$T_f \cos\phi$	Figure 56	Torque of assembly B on A, corrected for the head tube angle	+ 0.125 (5%)	can be ignored	minor effect
8.	$T_{Damping}$	$\Gamma\dot{\sigma}$	Figure 57	Damping torque (if this term is zero the bicycle may be unstable)	+/- 0.018 (0.72%)	small but included as found to be essential for dynamic stability	negligible effect

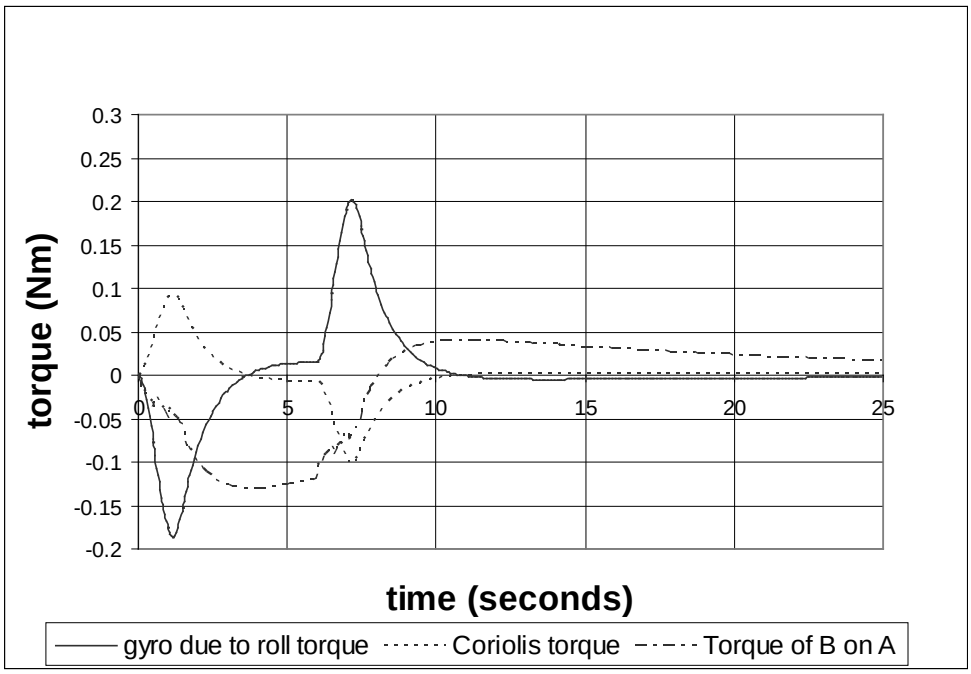

Figure 56 Minor torque terms from equation (18)

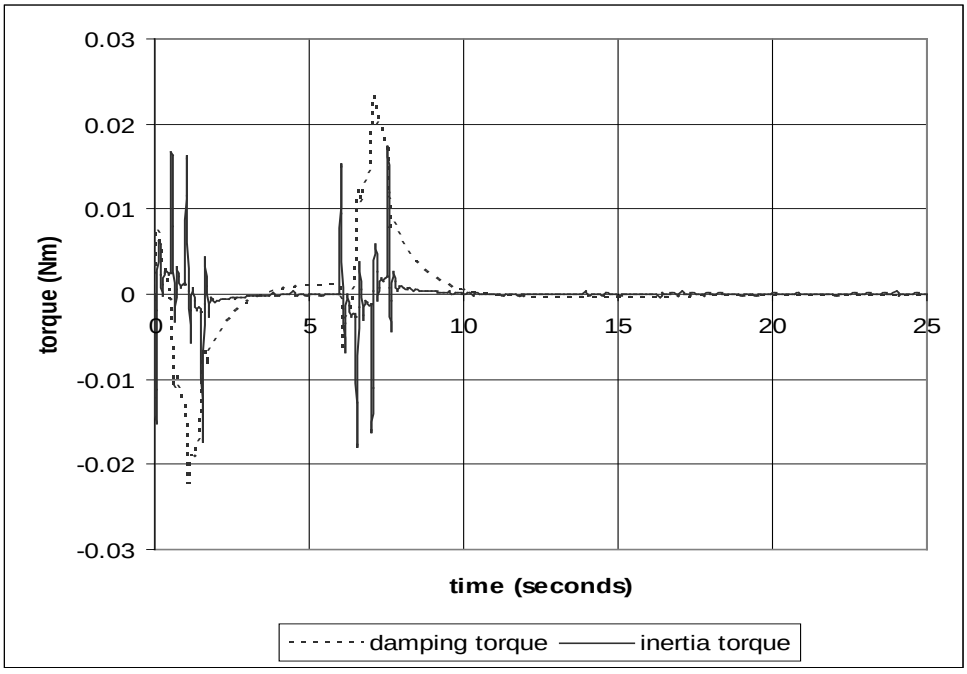

Figure 57 Negligible torque terms from equation (18)

5.3.2.SECOND EQUATION - MOMENTS ABOUT THE ROLL AXIS FOR A

The second equation considers the rolling moments about the horizontal X axis for the front assembly A [equation (23)] and has eight terms in total, four of which are new: the Coriolis, steer, castor and Jones torques (the last three were added to account for realistic steering geometry). The suggestions as to which terms in equation (23) to ignore are shown in Table 23, along with the following comments:

- the major terms are: the gyroscopic torque of front wheel due to cornering, castor torque, Jones torque and the frame torque of B on A, shown in Figure 58
- this is one case where a gyroscopic torque has a major effect, but on its own it still does not account for the stability of the bicycle
- two of these terms, the castor torque and the Jones torque are new ones introduced due to considerations of steering geometry and they both oppose and more than counteract the gyroscopic term due to cornering
- the next most important terms in order of magnitude are the minor torques of: steering torque and the inertia torque of assembly A due to rolling, see Figure 59
- the steering torque is new and was introduced due to considerations of steering geometry
- both these torques (steering torque and Inertia torque) could be ignored
- the least important terms are: the Coriolis torque and gyroscopic torque of front wheel due to yawing (refer to Figure 60) and the Coriolis term is a new torque added to this model
- again this shows the unimportance of the gyroscopic effect and both these terms are negligible in their effect and could be ignored

In conclusion, for equation (23) of the original eight torques, for the application of the characteristic equation, two could be ignored (Coriolis and steer torques) and for a more simplified set of equations a further two more could be ignored (the inertia and gyroscopic/corner torques).

Table 23 The terms from equation (23) and their significance

	Torque	Expanded term	Relevant figure number	Description and comments	Max torque value Nm (%)	Assumptions	Significance of the term
1.	$T_{Inertia}$	$I_{XA}\dot{\omega}_{XA}$	Figure 59	Inertia torque of the front wheel due to rolling of A	+/- 0.12 (10.0%)	small and could be ignored but included as it is well known and so of interest	minor effect
2.	$T_{Coriolis}$	$I_{ZF}\omega_{YF}\omega_{ZF}$	Figure 60	Coriolis Torque of A	+/- 0.035 (2.92%)	could be ignored	negligible effect
3.	$T_{Gyro/yaw}$	$I_{YF}\omega_{YF}\omega_{ZF}$	Figure 60	Gyroscopic torque of front wheel due to yawing of A	+ 0.07 (5.8%)	small and could be ignored but included as it is well known and so of interest	negligible effect
4.	T_{Frame}	$T_f \sin\phi$	Figure 58	Torque Assembly B exerts on A corrected for the head tube angle	+ 0.4 (33.3%)	must be included	major effect
5.	$T_{Gyro/cornering}$	$\mathrm{I_{YF}}\frac{\mathrm{v}^2 \sin\phi}{\mathrm{rL}}\sigma$	Figure 58	Gyroscopic torque of front wheel due to cornering	+ 1.2 (100%)	maximum torque, unusually for a gyro term it has a major effect	major effect
6.	T_{Steer}	$T_S \cos\phi$	Figure 59	Steering Torque corrected for the head tube angle	+/- 0.13 (10.8%)	could be ignored	minor effect
7.	T_{Castor}	$M\frac{bv^2}{L^2}\cos\phi\Delta_e\sigma$	Figure 58	Castor torque corrected for the head tube angle	- 0.75 (62.5%)	must be included	major effect
8.	T_{Jones}	$Mg\frac{b}{L}\cos\phi\Delta_e\lambda$	Figure 58	Jones torque corrected for the head tube angle	- 0.7 (58.3%)	must be included	major effect

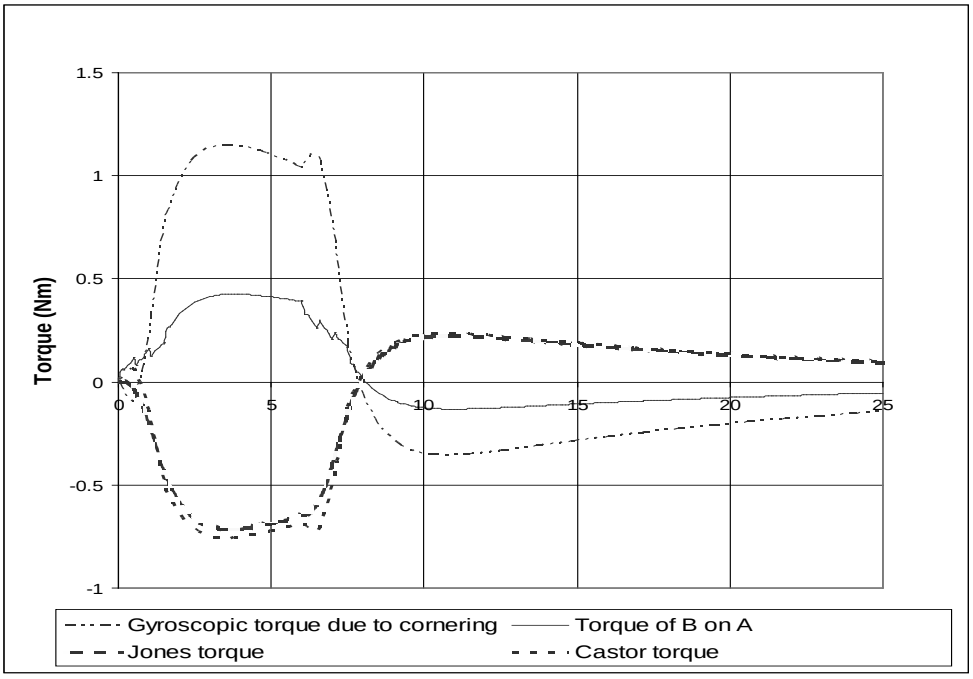

Figure 58 Major torque terms from equation (23)

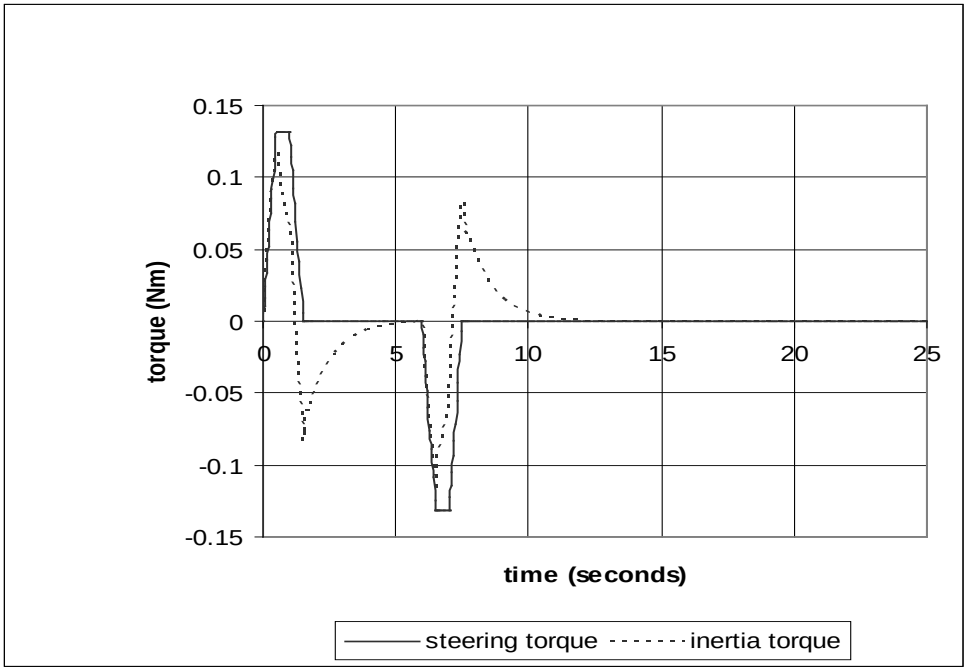

Figure 59 Minor torque terms from equation (23)

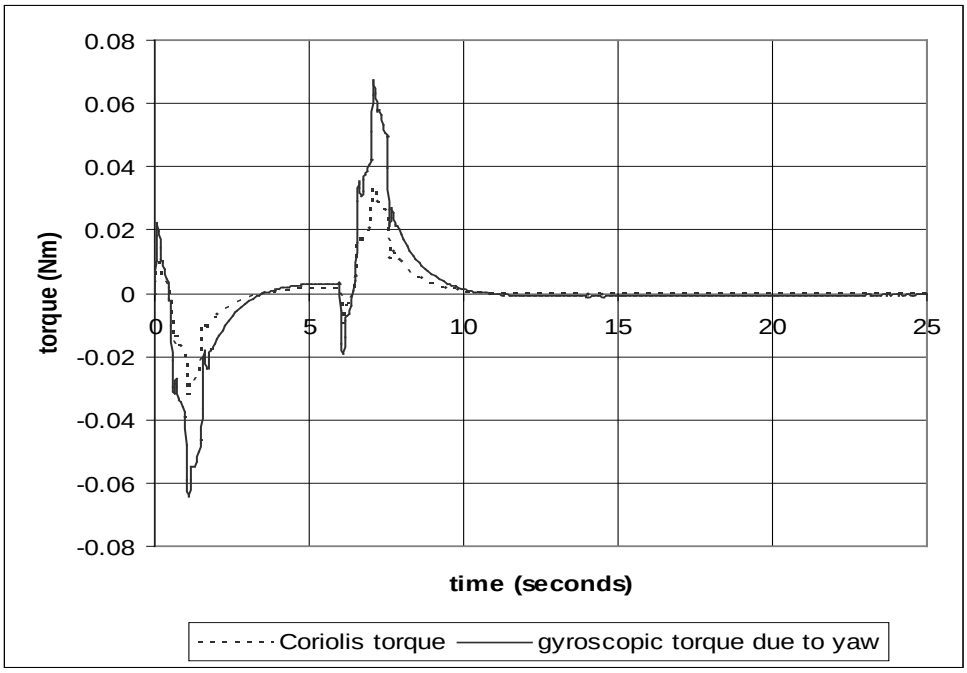

Figure 60 Negligible torque terms from equation (23)

5.3.3.EQUATION THREE - MOMENTS ABOUT THE ROLL AXIS FOR B

Finally the third equation deals with the rolling moments about the horizontal X axis for the rear assembly B [equation (24)] and this third equation currently has seven terms, one of which is new, the Coriolis torque. The suggestions as to which terms to ignore are shown in Table 24 and other comments are shown below:

- the most important terms in this equation in order of magnitude are: the centrifugal torque due to cornering and the gravitational torque due to rolling and these major torques are shown in Figure 61, these two torques must balance each other during the cornering manoeuvre to enable cornering to occur without capsizing or falling over occurring
- the next most important terms in order of magnitude are: the inertia torque of assembly B due to rolling and the kink torque, see Figure 62, these are of an order magnitude less than the most important terms, however they are not insignificant and should be considered
- the least important terms in order of magnitude are: frame torque of A on B, gyroscopic torque of the rear wheel due to cornering (yawing) and the Coriolis torque of assembly B
- these three negligible torques are shown in for the standard simulation run in Figure 63
- again the gyroscopic effect is unimportant
- these are all very small terms that are four orders of magnitude smaller than the most important torques and can be ignored
- the Coriolis term is the only new torque added to this model

In conclusion, for equation (24) of the original seven torques, for the purposes of the characteristic equation, one could be ignored (the Coriolis torque) and for a more simplified set of equations two more could be ignored (the frame torque and the gyroscopic torque of the rear wheel due to cornering).

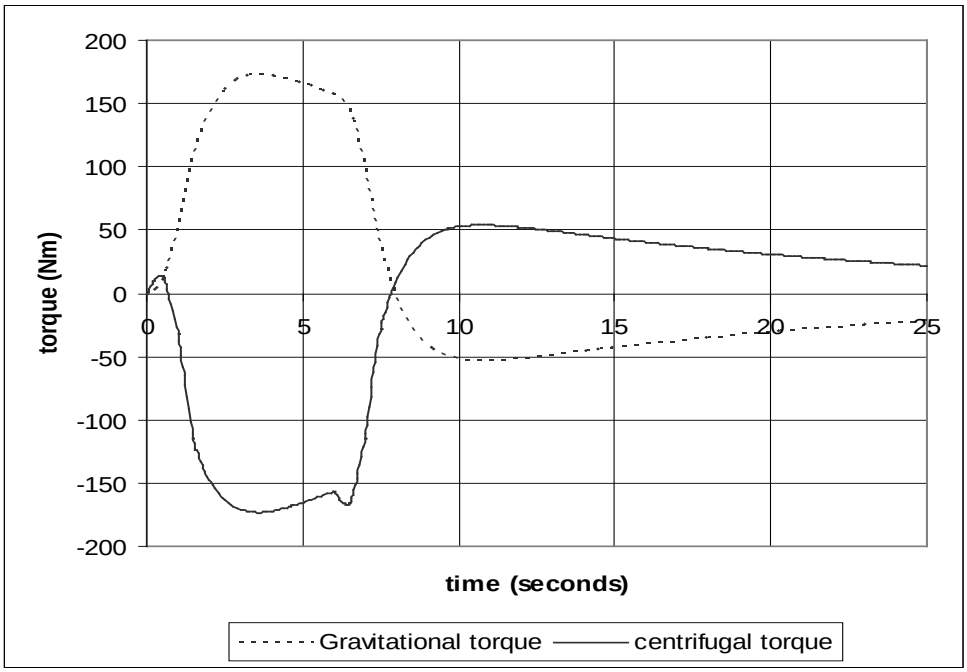

Figure 61 Major torque terms from equation (26)

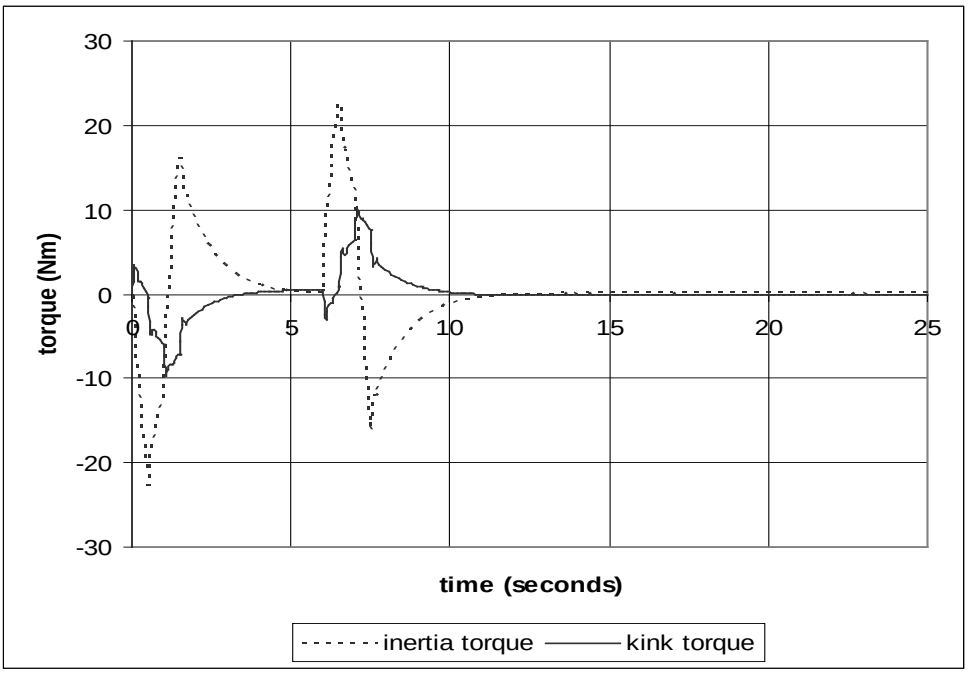

Figure 62 Minor torque terms from equation (26)

Table 24 The terms from equation (26) and their significance

	Torque	Expanded term	Relevant figure number	Description and comments	Max torque value Nm (%)	Assumptions	Significance of the term
1.	$T_{Inertia}$	$I_{XB}\dot{\omega}_{XB}$	Figure 62	Inertia torque of frame , rider and rear wheel due to rolling of B	+/- 23.0 (13.1%)	must be included	Minor effect
2.	$T_{Coriolis}$	$I_{ZR}\omega_{YR}\omega_{ZR}$	Figure 63	Coriolis Torque of the rear wheel	+/- 0.10 (0.06%)	can be ignored	Negligible effect
3.	$T_{Gyro/cornering}$	$I_{YR}\omega_{YR}\omega_{ZR}$	Figure 63	Gyroscopic torque of rear wheel due to cornering	- 0.40 (0.23%)	very small and could be ignored but included as it is well known and so of interest	Negligible effect
4.	T_{Frame}	$T_f \sin\phi$	Figure 63	Torque Assembly A exerts on Assembly B corrected for the head tube angle	+ 0.40 (0.23%)	could be ignored for some purposes	Negligible effect
5.	$T_{Centrifugal}$	$M\frac{v^2 h \sin\phi}{L}\cos\lambda\sigma$	Figure 61	Centrifugal torque	- 175.0 (100%)	maximum torque	Major effect
6.	$T_{Gravity}$	$Mgh\sin\lambda$	Figure 61	Gravitational torque	+ 175.0 (100%)	maximum torque	Major effect
7.	T_{Kink}	$\frac{Mhbv}{L}\dot{\sigma}$	Figure 62	Kink torque (Coriolis torque of assembly B less rear wheel)	+/- 10.0 (5.7%)	could be included	Minor effect

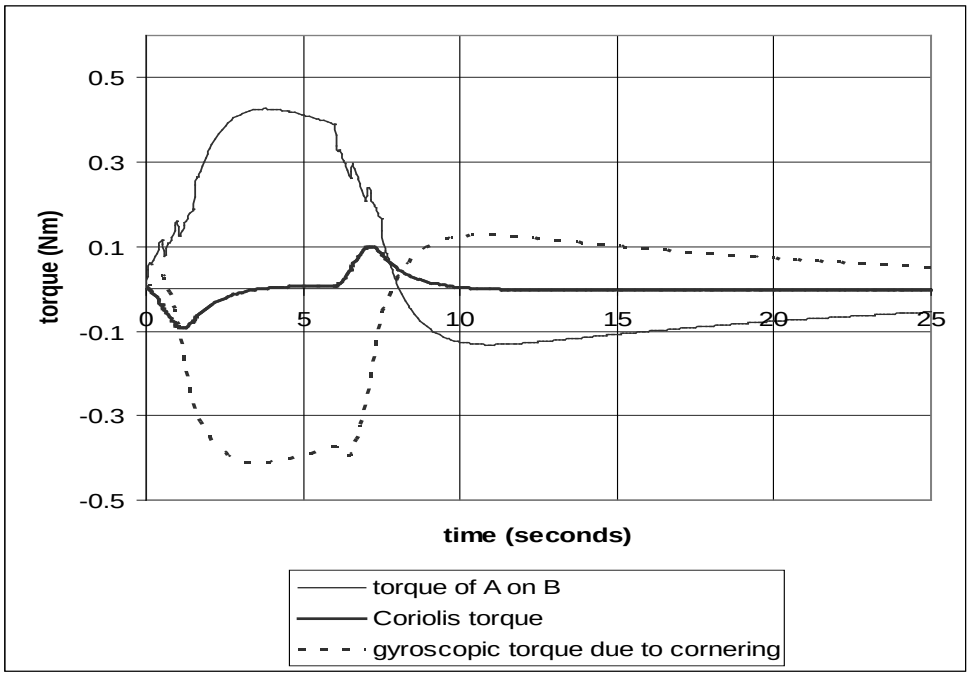

Figure 63 Negligible torque terms from equation (26)

5.3.4.TORQUE SIGNIFICANCE REMARKS

From this evaluation the following remarks are made:

- a summary of the effects of all torques and suggestions as to which ones to ignore are included in Table 22, Table 23 and Table 24
- the newly introduced torques for the Coriolis effects are all insignificant and could all be ignored without compromising the model
- it can be seen that as stated by many previous researchers the gyroscopic terms are insignificant and cannot account for bicycle stability
- most gyroscopic terms can be neglected from the equations except for the gyroscopic torque of front wheel due to cornering in equation (23) which is a major term
- the influence of steering geometry can be seen as significant, particularly the major terms added in equation (18) of the Jones and castor torque allowing for the head tube angle and they have a significant effect on steering stability

From the original set of 23 torques we can see that the Characteristic Equation could be reduced to 18 terms (dropping 5) to simplify finding its solution. A further more simplified set of equations suitable say for undergraduate teaching, could drop a total of 11 terms to end up with only 12 torques, see Table 25 for details. Such simplified equations would be more manageable without compromising the ability of the equations to explain the dynamic behaviour effectively.

Table 25 Summary of number of torque terms used

Equations of motion	**All terms from original equations**	**Terms used in characteristic equation**	**Further simplified set of equations** [1]
equation (14)	8	6	4
equation (19)	8	6	4
equation (24)	7	6	4
Total	23	18	12
Note 1 this simplified set of equations could be suitable for some design purposes such when only considering the effects of the most important design parameters			

5.4. SENSITIVITY STUDY

Now that the benchmark parameter values have been determined in Chapter Four, the Simulink modelling can proceed to the sensitivity study. The object of this study is to determine the significance of each parameter so that recommendations can be made about optimising bicycle designs. Which parameters are most important to the designer and how can their significance be quantified?

In order to study parameter sensitivity it is necessary to be able to vary them one at a time without changing the other parameters in order to see their individual effect on the model's dynamic responses. In practice changing one parameter would usually affect several others. For example fitting larger diameter wheels to an existing bicycle would immediately increase the height of the mass and moments of inertia. But it is possible to imagine a theoretical bicycle being fitted with larger diameter wheels which would not affect other parameters. This could be done by changing the frame geometry and wheel rim construction so as to ensure that all other parameters remain unaltered and this scenario is shown in Figure 64. Similarly for most of the remaining parameters it is possible to imagine (at least theoretically) a bicycle which only changes parameters one at a time. Hence the Simulink model was arranged so that each parameter could be individually isolated and incrementally changed to highlight their effect on bicycle performance and to indicate the bicycle's sensitivity to them.

In order to quantify sensitivity, an appropriate approach to measuring handling performance is needed. A key issue is to determine what sort of handling performance is desirable and then to define it. According to Minorsky *"It is an old adage that a stable ship is hard to steer" (85)*. In other words too much directional stability in a ship (or a bicycle) is as much a problem as too little. A beginner wants a stable, insensitive bicycle that easily holds a straight course, but the expert rider wants a bicycle that can respond quickly to a steering input, for example when taking rapid evasive action to avoid a hazard.

What is of interest in this study is the sort of handling expected of a top performing road racing bicycle as anticipated by top level riders. To the best of the author's knowledge no quantitative research has been done to find out what sort of handling top riders expect. The only information on this topic at all is qualitative and is discussed in Chapter Seven and what this reveals is the desire for a bicycle with highly responsive handling consistent with stability, particularly at speed. Riders expect to be able to react quickly to avoid an obstacle, such as a rider in the peleton falling over in front of them (the peleton is a large group of riders) but also handling that is predictable to give them confidence to ride at speed around corners. Riding comfort and maximum directional stability are not attributes that are desired by this group of riders.

The best way of measuring bicycle handling performance was determined to be an impulse response test. An impulse test closely resembles a realistic sudden input on the bicycle and is also a useful "test signal" for investigating unknown systems, since all frequencies are excited equally and the true nature of the system is revealed by the response (86). This is because the

intrinsic behaviour of a system can be discovered by abruptly disturbing the system when it is at rest with an impulse (87). Theoretically an impulse has infinite magnitude over zero time which while mathematically possible, is not physically achievable. In practice an impulse of sufficiently large magnitude and of a very short time duration can be considered to be an impulse response (88). *"The impracticality of the impulse response differs only in degree, not kind, from that of as step response, they are both approximations to reality when used to model the behaviour of real systems* (53)."

The impulse response has value in terms of bicycles because most of the disturbances that occur when riding initiate from sudden external yaw perturbations to the front wheel. This can be due to changes in the road surface such as bumps and hollows etc. Roll perturbations also occur but these are less common in practice and are mainly due to side winds causing the bicycle to suddenly roll. As this model assumes there are no aerodynamic forces or windage it follows that there are no side winds, so it is reasonable in this model to ignore the roll response.

An impulse where the area "A" under the graph is equal to "1" is called the unit impulse function and is written as $\delta(t)$, see Figure 65 (53). If the unit impulse is known, then the response to an impulse of any strength "A" is equal to "$\mathrm{A}\delta(\mathrm{t})$" (53). So by subjecting the bicycle model to a unit impulse input and measuring the response, the true dynamic characteristics of the bicycle can be studied. For example it can indicate how quickly the front wheel will stabilise after a sudden external steering torque perturbation. This stabilisation is best indicated by the settling time as this shows how quickly the front wheel yaw decays back towards the steady state position. Settling time is defined as the time taken for the response to fall to a within either 5% or 2% of the initial peak response. The 2% settling time was chosen because although the relative difference between two bicycles will be the same whether using a 5% or a 2 % settling time, the lower value (2%) was preferred because it is closer to the eventual steady state position of a zero angle.

Simulink can quickly find the front wheel yaw response (and its sensitivity) to an impulse by using Simulink's linear analysis capability, which calculates and plots the unit impulse response and finds the 2% settling time. It was necessary to do this multiple times for all the eleven parameters investigated.

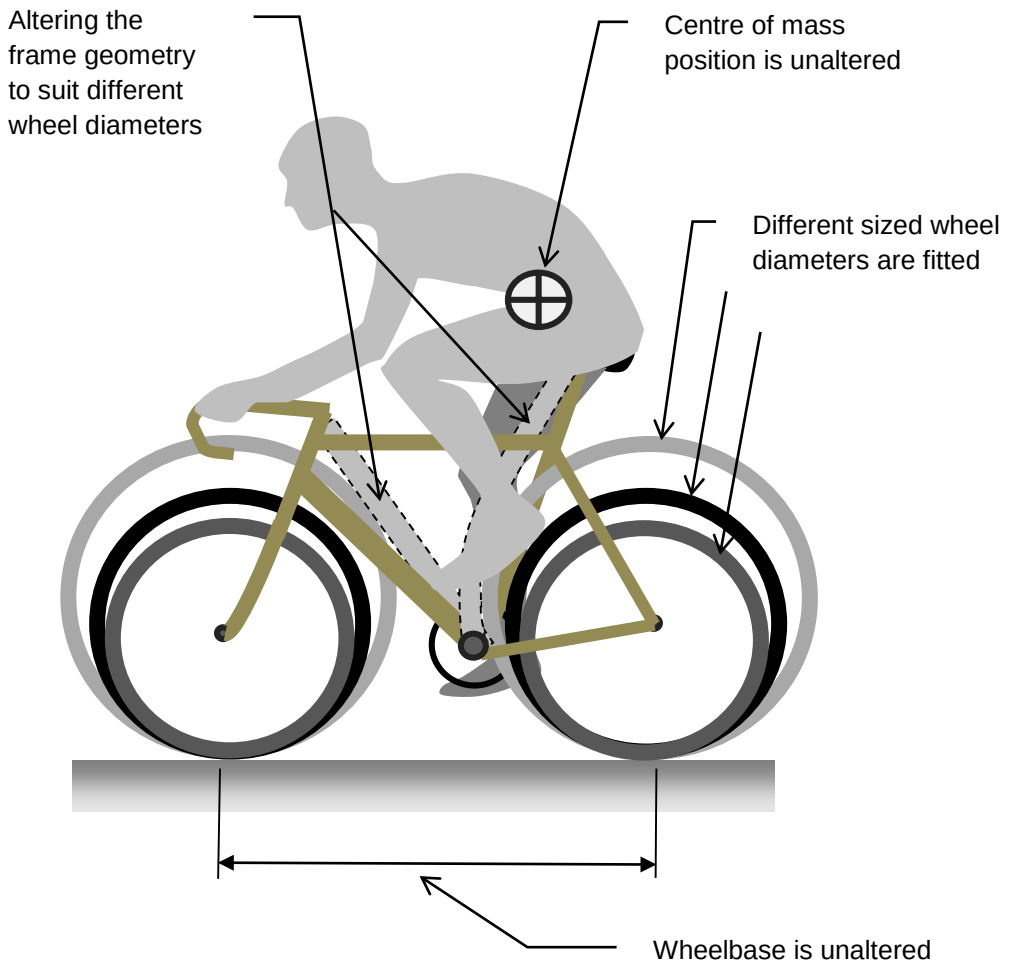

Figure 64 Illustrating how larger wheels could be fitted to the bicycle model without altering other parameters

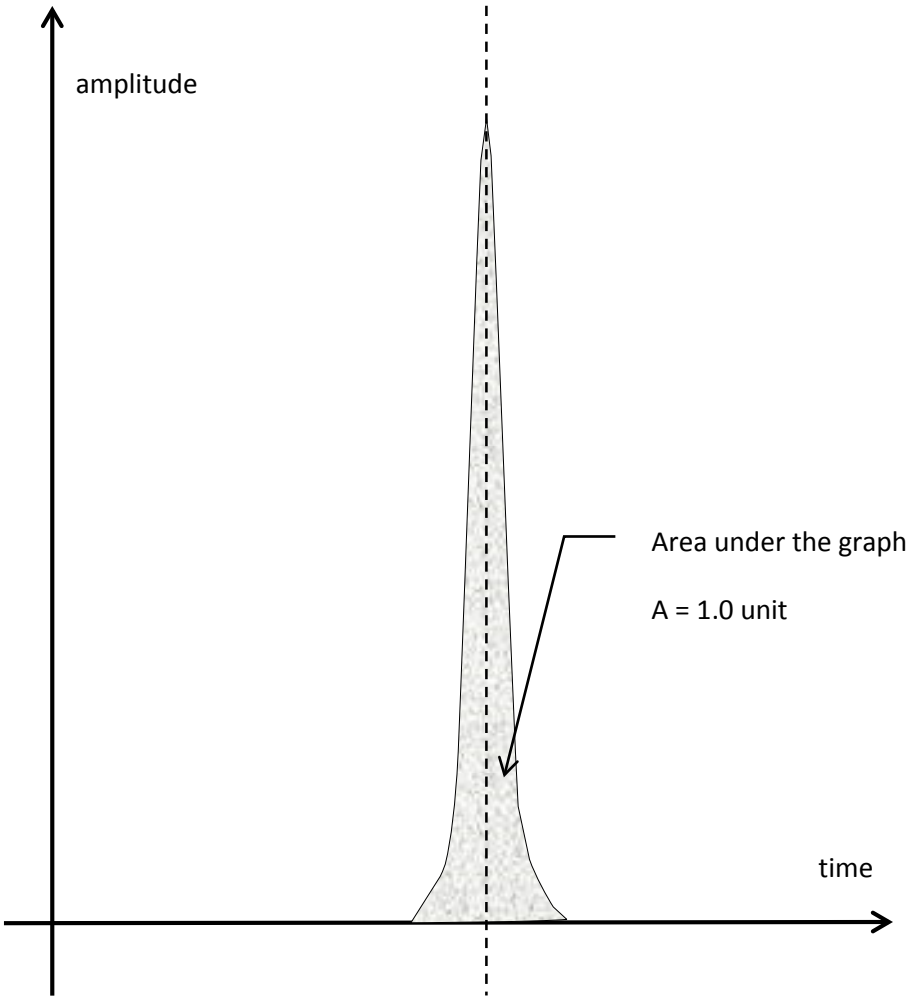

Figure 65 The unit impulse function

5.4.1.WHEEL DIAMETER

To undertake this sensitivity study, multiple Simulink trials for all eleven bicycle parameters were needed. But for reasons of brevity the methodology used will be described for one parameter only, wheel diameter. The remaining ten parameters were studied in the same way and the full results for all parameters are presented in this Chapter.

When considering the wheel diameter first we must refer to the internationally accepted standard wheel and tyre system for road bicycles, designated as ISO 700C (6). The 700C designation means that the nominal wheel diameter is 700 mm (though the actual diameter is smaller than this). The benchmark bicycle uses an ISO 700C x 25 wheel and tyre where 25 refers to the tyre width (in this case of 25 mm). The 700C x 25 wheel was found by direct measurement to have an actual outside diameter of 675 mm, but small variations in diameters for between different tyres and different manufacturers do occur. Two manufacturers did record slightly different diameter values for a 700 C x 25 tyre (one slightly higher and the other lower) but when averaged out they are consistent with the experimentally measured value of 675 mm shown in Table 26.

Now that the actual benchmark wheel diameter has been determined it is possible to vary diameters and record the different settling times that the Simulink model calculates. A series of unit impulse responses was found for a range of diameters from 697.5 mm (90% of the benchmark) up to 742.5 mm (110%).

Simulink was used find the front wheel yaw response (and its sensitivity) to an impulse by using Simulink's linear analysis capability, which calculates and plots the unit impulse response and finds the 2% (or other selected value) settling time. The linear analysis capability computes a linear system from the non-linear Simulink bicycle model and plots a linear unit impulse response between the specified input and output points.

The 2% settling time was calculated and recorded for each change in diameter and these are shown in Table 27. The impulse response for the benchmark wheel (675 mm diameter) produced a 2% settling time of 10.1 seconds which is shown in Figure 66. The different diameters were referenced to the benchmark and the change in settling time across the range of diameters was plotted on a graph, see Figure 67. A line of best fit for the data points was plotted and its slope is an indication of model's sensitivity to the parameter and is expressed as the % response change per 1% change of the parameter, making the analysis non-dimensional. For each 1% increase in wheel diameter it was found that the settling time increased on average by 5.75% (across a +/- 10% range with a R^2 value of 0.936) making this a significant parameter. This high sensitivity of the bicycle to changes in wheel diameter is an unexpected and interesting result.

Table 26 Typical road bicycle tyre values (64, 81)

ISO/ETRTO Code	Tyre width mm	D Actual wheel diameter mm [1]	D/D_{BM} [2]
700 X 18C	18	658.90	0.976
700 X 19C	19	662.09	0.981
700 X 20C	20	666.22	0.987
700 X 23C	23	671.79	0.995
700 X 25C	**25**	**674.82** [3]	**1.000**
700 X 28C	28	682.14	1.011
700 X 30C	30	685.32	1.015
700 X 32C	32	688.35	1.020
700 X 35C	35	692.80	1.026
700 X 37C	37	700.28	1.037
700 X 38C	38	693.92	1.028
700 X 40C	40	703.47	1.042
ETRTO (European Tyre and Rim Technical Organisation)			
Note 1 these are the averaged results from two manufacturers see Appendix E (64, 81)			
Note 2 D_{BM} = benchmark diameter			
Note 3 rounded up to 675.00 mm in this study			

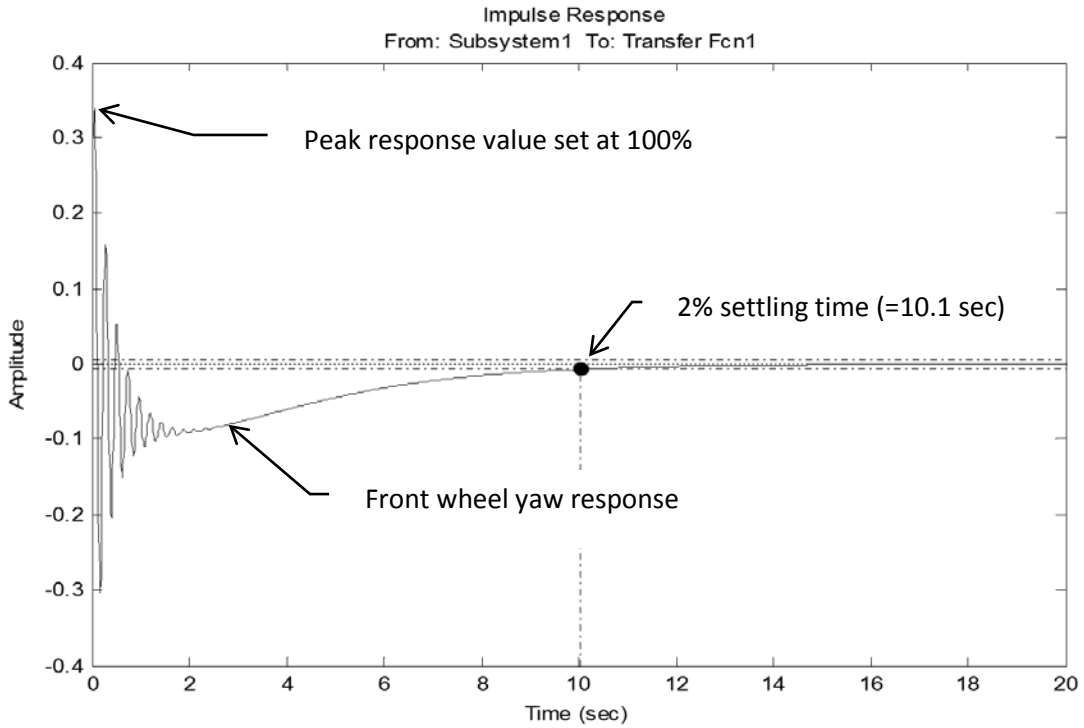

Figure 66 The front wheel yaw response (for the benchmark bicycle) to a unit impulse found using Simulink's linear analysis capability

Table 27 Wheel diameter settling times, used to plot Figure 67

Wheel diameter %	D Wheel dia. mm	S 2% settling time seconds	$S/S_{BM\ 1}$
90	607.5	6.58	0.65
91	614.3	6.83	0.68
92	621.0	7.09	0.70
93	627.8	7.37	0.73
94	634.5	7.67	0.76
95	641.3	7.99	0.79
96	648.0	8.34	0.83
97	654.8	8.72	0.86
98	661.5	9.12	0.90
99	668.3	9.57	0.95
100_2	**675.0**	**10.10**	**1.00**
101	681.8	10.60	1.05
102	688.5	11.20	1.11
103	695.3	11.80	1.17
104	702.0	12.50	1.24
105	708.8	13.30	1.32
106	715.5	14.20	1.41
107	722.3	15.20	1.50
108	729.0	16.30	1.61
109	735.8	17.60	1.74
110	742.5	19.10	1.89
Note 1 S/S_{BM} = 2% settling time/2% settling time of benchmark wheel			
Note 2 benchmark wheel diameter (675 mm = 100%)			

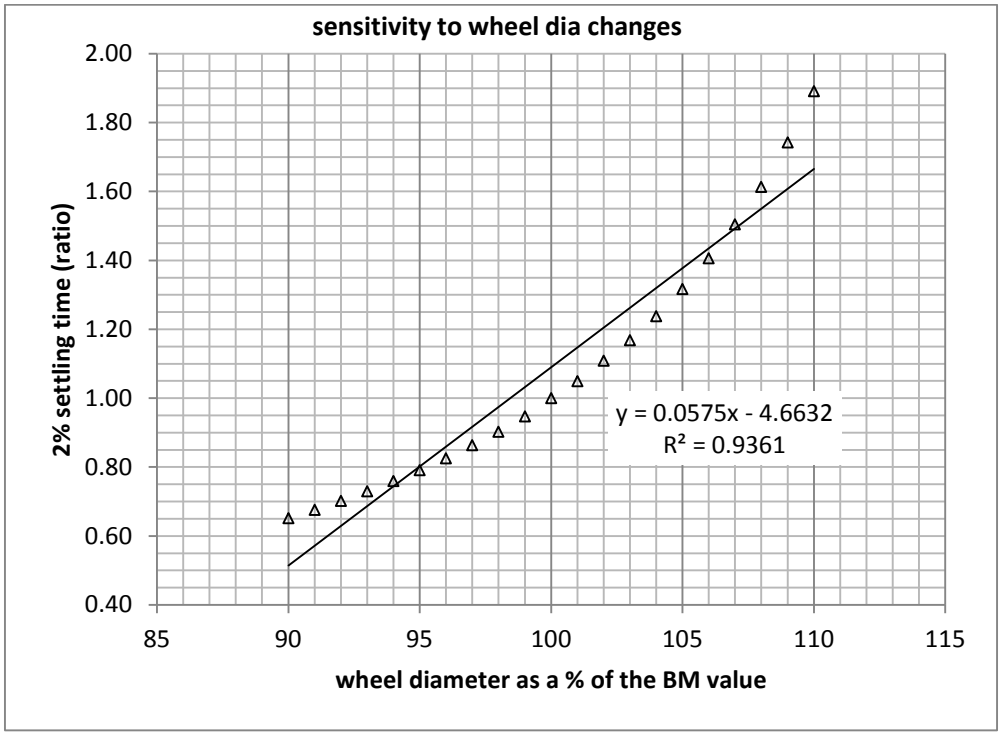

Figure 67 The 2% settling times for wheels of different diameters (with line of best fit equation and R^2 value)

5.4.2.REMAINING PARAMETERS

This section now presents the full results of the sensitivity study for all eleven parameters. After the wheel diameter sensitivity was determined all the remaining ten parameters were analysed in the same way and full results are shown in Table 28 and Figure 67 through to Figure 77.

Figure 77From these results several critical design parameters were identified and their effects quantified. The parameters have also been collated into four groups:

1. Steering geometry parameters
2. Wheel parameters
3. Mass and wheelbase parameters
4. All others

Steering geometry parameters

As expected and reported by many other researchers the parameters defining the steering geometry are important (head tube angle and rake) and the study of their effects was a major goal of this investigation (2, 13, 32, 55). It was found that:

- For a 1% increase in head tube angle (Φ) the front wheel yaw 2% settling time decreased by a significant 5.93% (across a -2% to + 10% range with a determination coefficient R^2 value of 0.830) see Figure 68.
- Similarly for a 1% increase in rake (β) it was found that the settling time decreased by a moderately significant 1.41% (across a +/- 10% range with a R^2 value of 0.996) see Figure 73.
- This is perhaps an unexpectedly small value for rake but when the steering geometry equations are inspected more closely the reason is immediately apparent. A 10% change in head tube angle causes the effective trail to change by about 75% whereas a 10% change in rake only changes the effective trail by 8%.
- As the effective trail (which is a function of wheel radius, head tube angle and rake) appears in four of the twenty three torque terms of the equations of motion it is no surprise the model is highly sensitive to changes in trail and the single parameter (head tube angle) that most affects it.

Wheel properties parameters

- As just determined the wheel diameter is a significant parameter, see Figure 67. A 1% increase in wheel diameter increased the settling time by a significant 5.75% (for a -10% to + 10% range and a R^2 of 0.936)
- A 1% increase in the wheel moment of inertia decreased the settling time by a moderately significant 2.02% (for a -10% to + 10% range and a R^2 of 0.982) see Figure 70.

- Because of the symmetry of the wheels it was unnecessary to isolate the moments of inertia about X, Y and Z axes (and it is not physically or theoretically possible to do so). So all three moments of inertia are linked and vary together ($I_{WX} + I_{WZ} = I_{WY}$, due to the parallel axis theorem).

Mass position and wheelbase parameters

An interesting result is the obvious interaction of the parameters defining the magnitude and position of the mass (M, b and h) and a fourth parameter defining the wheelbase (L).

- For a 1% increase in the longitudinal position "b" of the mass the 2% settling time increased by a moderately significant 2.07% (for a -10% to + 10% range and a R^2 of 0.995) see Figure 69
- A 1% increase in the magnitude of the mass the 2% settling time increased by a moderately significant 1.98% (for a -10% to + 10% range with a R^2 of 0.994) see Figure 71
- A 1% increase in the wheelbase "L" the 2% settling time decreased by 1.57% (for a -10% to + 10% range with a R^2 of 0.986) which is moderately significant, see Figure 72
- Surprisingly a 1% increase in the height of the mass "h" the 2% settling time only increased by 0.27% (for a -10% to + 10% range with a R^2 of 0.983) which is not significant, see Figure 74
- The interaction between these parameters opens the possibility of tuning a rider's position to optimise handling performance. For example, reducing a downhill mountain bicycle's settling time could be achieved by reducing the mass and moving it lower and to the rear and increasing the wheelbase.
- Note that the secondary parameters of frame size and seat tube angle can be linked to the parameters h, b and L, see Appendix B.

Finally considering the remaining three parameters (all others)

- For a 1% increase in the I_{XB} parameter the 2% settling time decreased by a not significant 0.11% (for a -10% to + 10% range and a R^2 of 0.857) see Figure 75
- For a 1% increase in the I_{ZA} parameter the 2% settling time increased by a not significant 0.10% (for a -10% to + 10% range and a R^2 of 0.857) see Figure 76
- Finally for a 1% increase in the IXA parameter the 2% settling time increased by a not significant 0.06% (for a -10% to + 10% range and a R2 of 0.668) see Figure 77

Full details of each parameter's significance and the sensitivity of the bicycle model to any changes is shown in Table 28 where they are ranked in order of significance.

For some parameters, stepping is evident in the graphs which occurs when several settling times apparently share the same value and then suddenly steps up to another value (see I_{XA}, I_{XB}, I_{ZA}

and h). This occurred because the Simulink analysis “only” gave settling time results within an accuracy of 1/100ths of a second and it was not possible to obtain a more precise result when the values were very low, as they were in these 4 cases. But as these are insignificant parameters it doesn’t affect the validity of the study.

The only significant parameter which exhibits strong nonlinearity was the head tube angle (with an $R^2 = 0.830$) and this is why its limits were set at between -2% to +10% which corresponded to the most linear part of its response. Three other insignificant parameters (I_{XA}, I_{XB}, and I_{ZA}) also had low R^2 values recording 0.668, 0.857 and 0.857 respectively, but this is not of great interest.

Table 28 Sensitivity results

Ranking	Symbol	Definition	Benchmark Value/s	Units	C_1	C/C_{HTA} [2]	R^2 Value [3]	Comments [4]
1.	Φ	Head tube angle	73	degrees	-5.93%	1.0000	0.830	significant term
2.	D	Diameter of the wheel	0.675	m	+5.75%	0.9696	0.936	significant term
3.	b	Horizontal distance from rear wheel hub to centre of mass	0.33	m	+2.07%	0.3491	0.955	moderately significant
4.	I_{W} [5]	MOI of wheels	0.05/010	kgm^2	-2.02%	0.3406	0.982	moderately significant
5.	M	Mass	80	kg	+1.98%	0.3339	0.994	moderately significant
6.	L	Wheelbase	1	m	-1.57%	0.2648	0.986	moderately significant
7.	β	Rake	0.045	m	-1.41%	0.2378	0.996	moderately significant
8.	h	Height of centre of mass	1.1	m	+0.27%	0.0455	0.995	not significant
9.	I_{XB}	MOI of B about X axis (roll)	100	kgm^2	-0.11%	0.0185	0.857	not significant
10.	I_{ZA}	MOI of A about Z axis (yaw)	0.08	kgm^2	+0.10%	0.0169	0.857	not significant
11.	I_{XA}	MOI of A about X axis (roll)	0.2	kgm^2	0.06%	0.0100	0.668	not significant

The parameters are ranked in order of greatest sensitivity

Note 1 C is the % change in the 2% settling time for each 1% increase of a parameter

Note 2 C/C_{HTA} is C referenced to the head tube angle parameter (absolute values)

Note 3 R^2 is the coefficient of determination, a measure of the strength of the linear relationship between two variables

Note 4 significant is defined as a change in C greater than 3%, moderately significant means a change between 1 and 3% and not significant means less than a 1% change

Note 5 due to symmetry, the wheel MOI have the following relationships, $I_X = I_Z$ and $I_Y = 2I_X = 2I_Z$, therefore the wheels' MOI has been included once and not three times

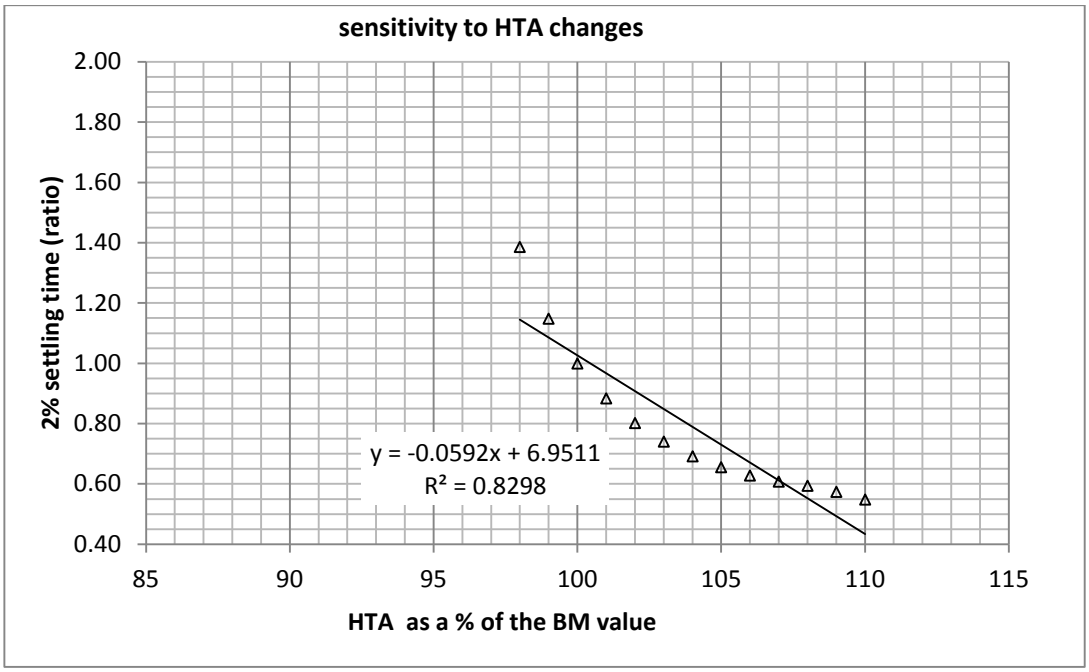

Figure 68 Settling time results for different head tube angles (with line of best fit equation, R^2 value)

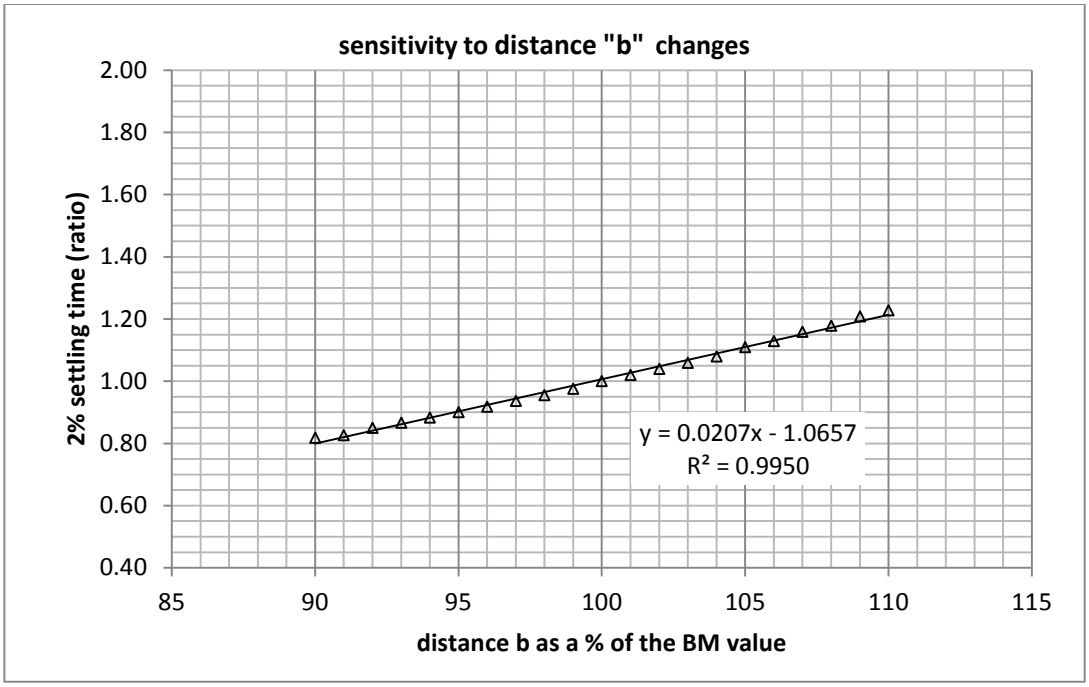

Figure 69 Settling time results for different distances “b”

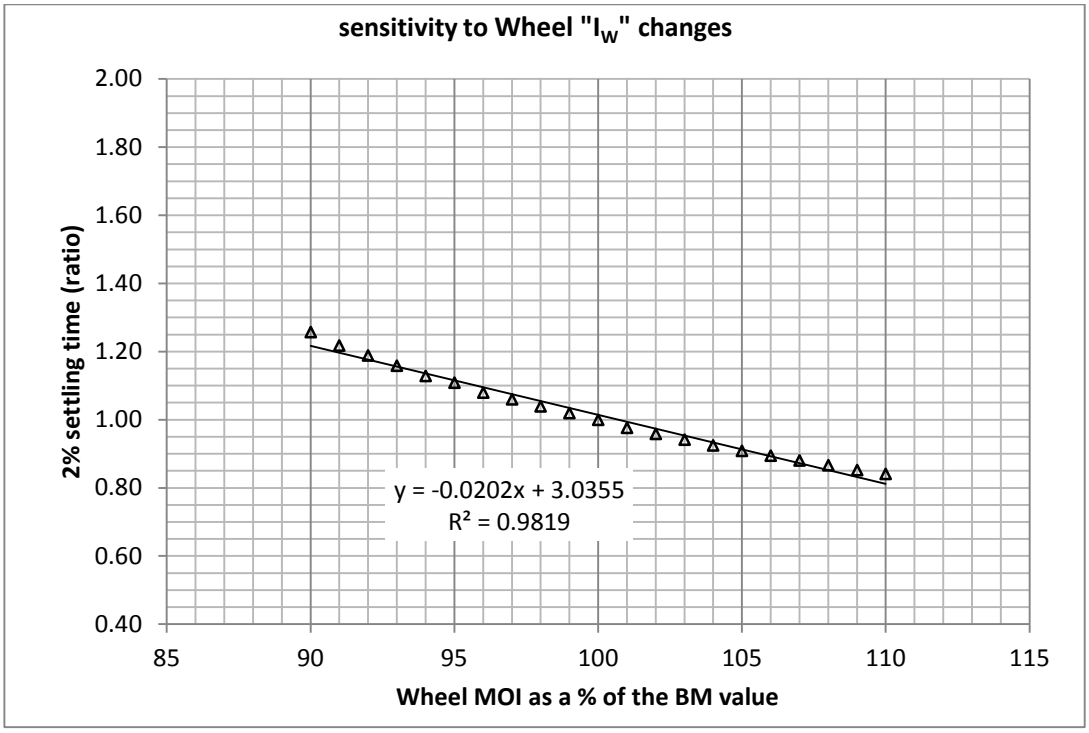

Figure 70 Settling time results for different moments of inertia for the wheels

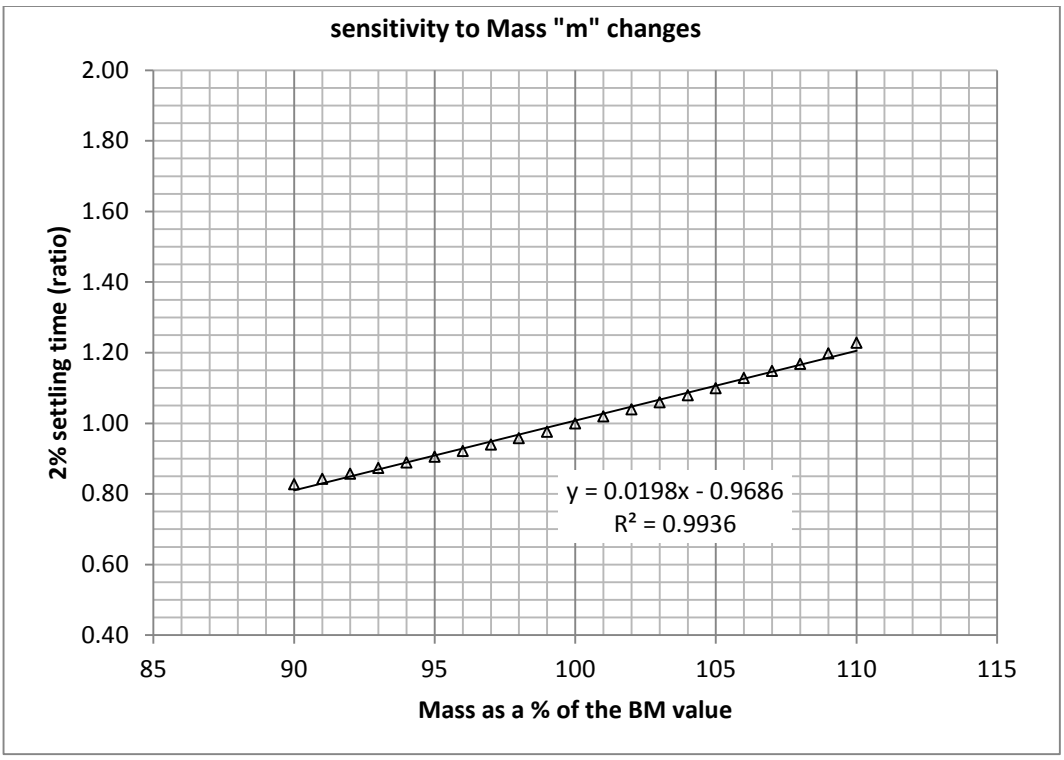

Figure 71 Settling time results for different masses

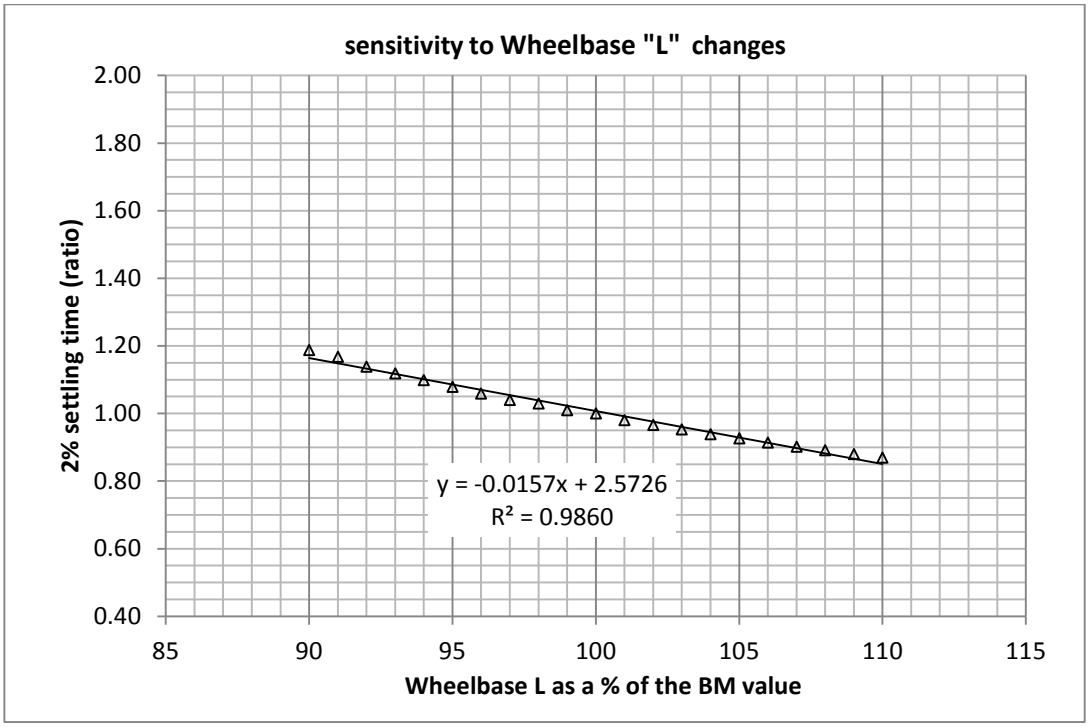

Figure 72 Settling time results for different wheelbases

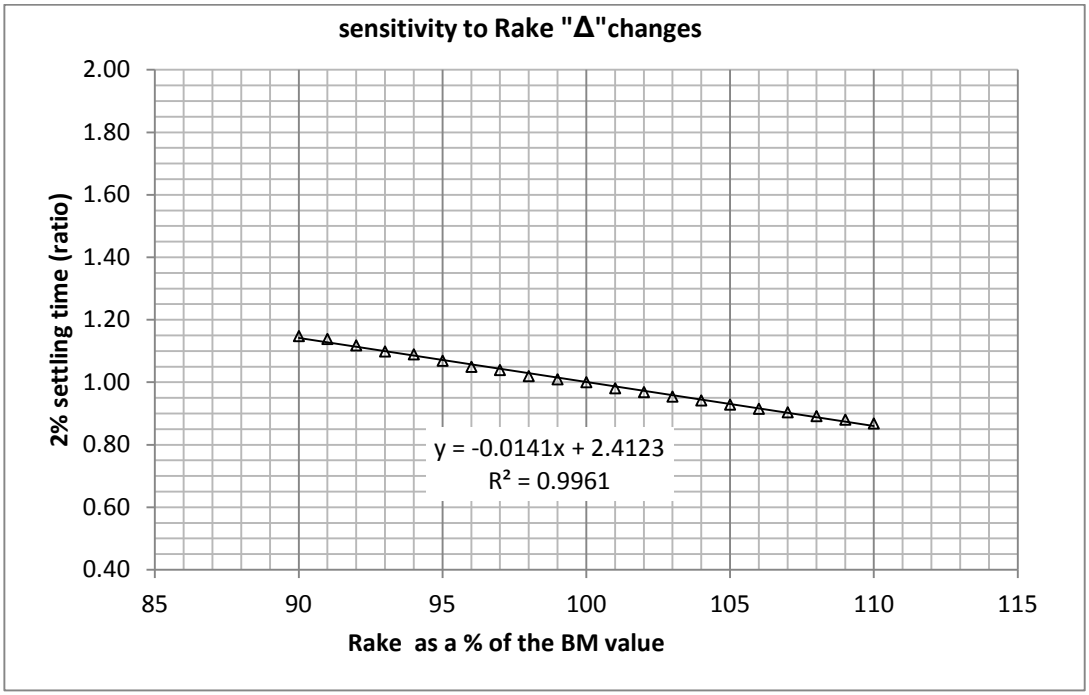

Figure 73 Settling time results for different rakes

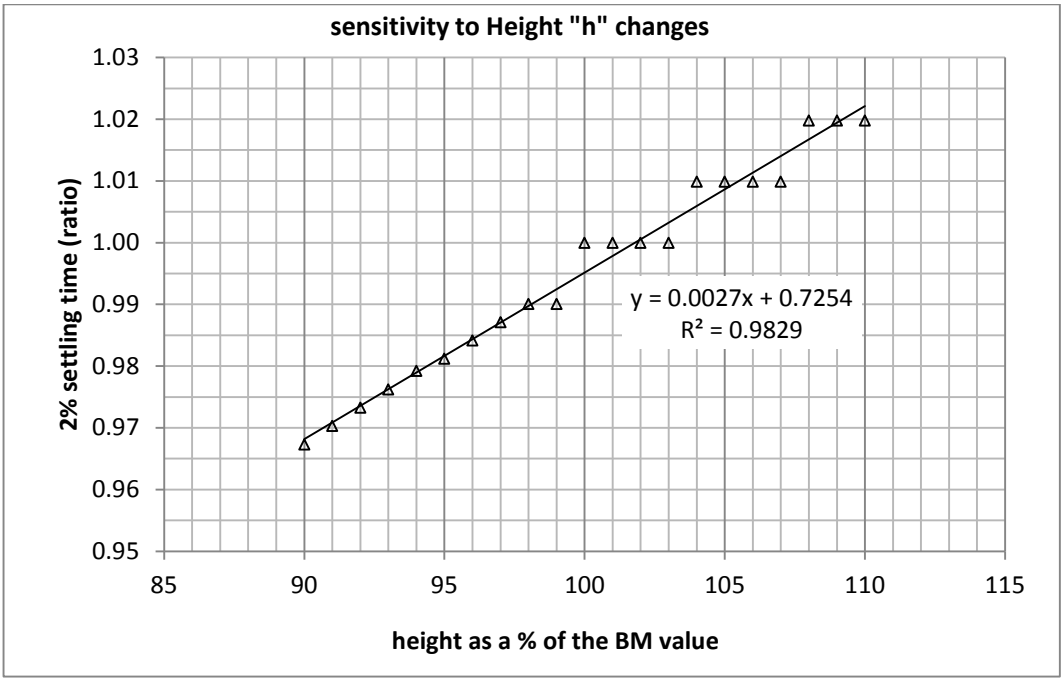

Figure 74 Settling time results for different distances “h” (note the stepping)

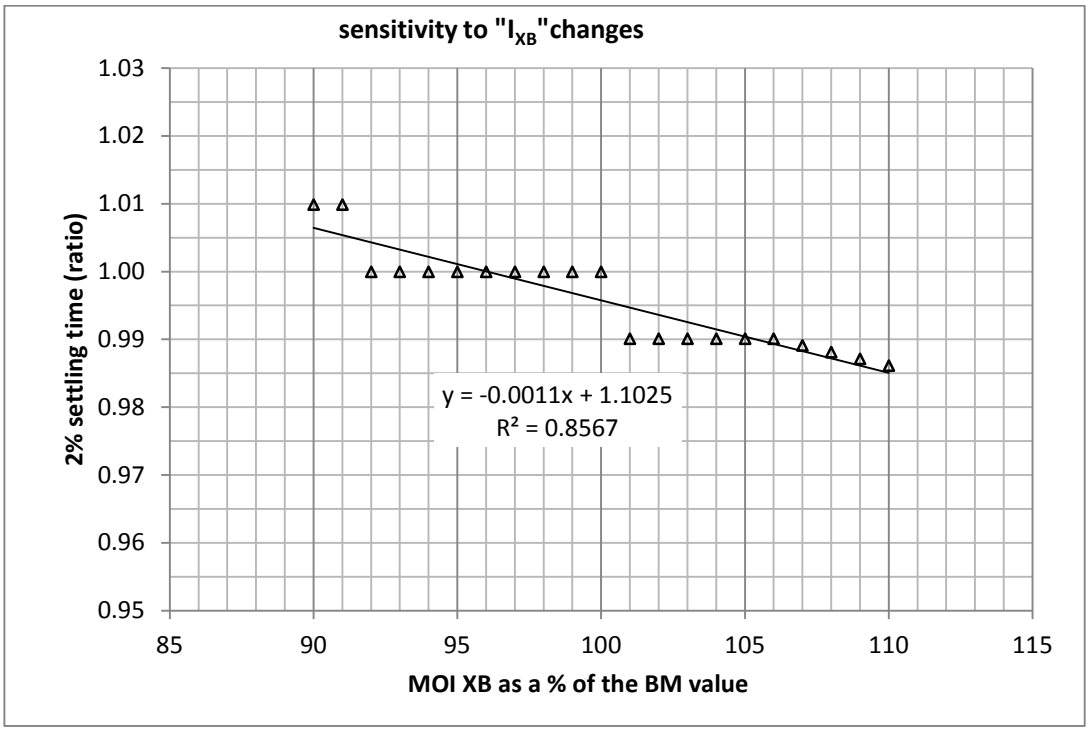

Figure 75 Settling time results for different moments of inertia of B about the X axis (note stepping)

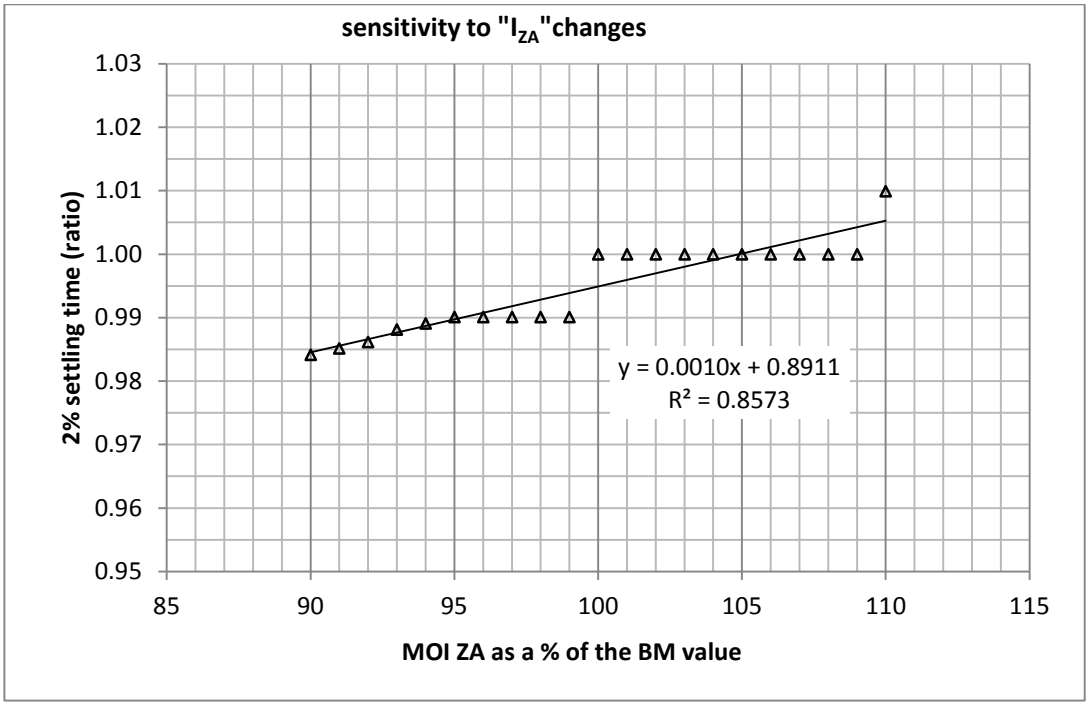

Figure 76 Settling time results for different moments of inertia of A about the Z axis (note stepping)

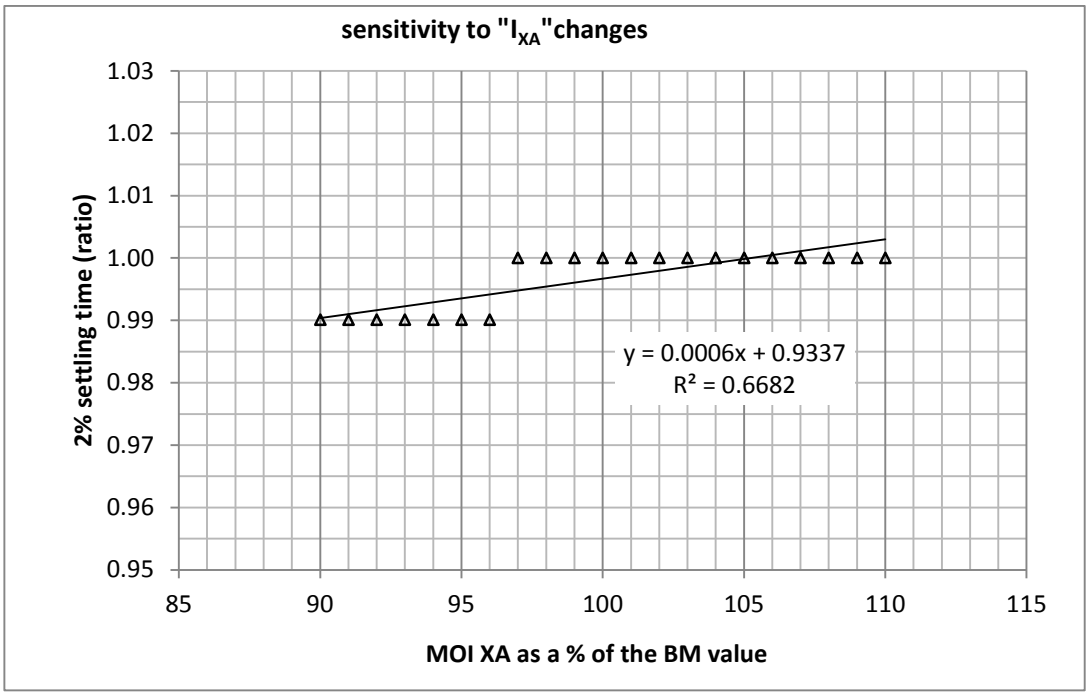

Figure 77 Settling time results for different moments of inertia of A about the X axis (note stepping)

5.4.3.SENSITIVITY REMARKS

This sensitivity study has quantified the effects of all eleven parameters and classified them as either significant, moderately significant or not significant and this quantification and classification is shown in Table 28. Significant parameters are defined as having a value of C of 3% or more (C is the % change in settling time for each 1% change in the parameter). Moderately significant parameters have a C of between 1% and 3%, and insignificant parameters have a C of less than 1%.

From this sensitivity study the significant parameters in order of most importance are:

1. Head tube angle
2. Wheel diameter

The moderately significant parameters are:

3. Mass horizontal distance from rear wheel hub “b”
4. Wheel moment of inertia
5. Mass
6. Wheelbase
7. Rake

And the other parameters that are not significant are:

8. Height of mass “h”
9. Moment of inertia of B about X (roll)
10. Moment of inertia of A about Z (yaw)
11. Moment of inertia of A about X (roll)

What this physically means is illustrated by the case of an existing bicycle with a handling problem. In such a case only a few options are practical, as all the design parameters are fixed except for those affected by wheel, tyre and front fork properties. So if new tyres are fitted it is possible to change the wheel diameter and perhaps wheel moments of inertia. If new wheels of a different construction are fitted this can affect the wheel’s moments of inertia. Finally if a new fork is fitted (a more expensive solution but possibly worth considering) it can change the rake value. So the wheel diameter, moments of inertia and possibly fork rake are the only possibilities to adjust. Small adjustments to the rider’s position (changing h and b) are also possible but they will be too small to have any significant effect. Therefore the following broad recommendations can be made to deal with a bicycle handling problem (first assuming that the bicycle is in good mechanical order).

If a bicycle has been found to have sluggish steering (with a slow settling time) then:

1. it would be worth trying a slightly smaller tyre to decrease the diameter
2. alternatively increasing the wheel moments of inertia will help

But doing both at once though may cancel each other out, So careful wheel and tyre selection is necessary in order to have an positive combined effect.

3. for example a sufficiently smaller diameter tyre and a new wheel with a heavier rim could reduce settling times, as wheel MOI's vary by at least +/- 10% and typical road bicycle tyre diameters by +/- 12% this is possibly an effective solution, see Chapter Six for details on how this can be systematically done using the Design Charts
4. a more radical (and expensive) solution would be to fit a new fork with less rake which increases trail, e.g.changing from a 40 mm to a 45 mm rake (a increase of 12.5%) reduces settling time by nearly 18%

Conversly if there is too quick a steering response and we wish to increase the settling times, the advice is reversed, that is add a larger diameter tyre with a lighter rim wheel and decrease the fork rake.

Completing this sensitivity study allows a scientifically based design methodology to be developed and this will be presented in the Chapter Six and this will make it possible to guide design decisions for new bicycles. It will give designers a practical means to determine what effect design changes have on bicycle handling.

This study can also be used to make practical suggestions on how to troubleshoot and cure steering problems with existing bicycles. Individual bicycles and riders can be experimentally measured to find actual values of mass, wheelbase, moments of inertia, etc. Then the Simulink™ model could be used to investigate the stability or instability of each particular case and small changes in key individual parameters may give insights on how to cure an existing problem.

For completeness in this sensitivity study the characteristic equation of the bicycle system was determined and the Routh Stability Criterion then used to find out if any unstable roots exist. Details of this procedure and the results are shown in Appendix D and they give the range of stability for the current system.

5.5. REMARKS

This chapter has examined the bicycle dynamic model and investigated:

1. the effectiveness of the model in determining bicycle performance
2. the significance of each torque term in the equations of motion
3. the sensitivity of the bicycle's performance to changes in design parameter

From this work it was found that:

1. Bicycle performance simulations demonstrated the capabilities of the model which was able to reproduce realistic bicycle dynamic behaviour.
2. Torque term evaluation determined the significant and insignificant terms and recommendations about simplifications of the equations of motion were made.

3. The sensitivity study identified the critical design parameters and quantified their effects on bicycle handling performance. It determined their minimum and maximum acceptable limits and examined their relative importance in terms of their overall effects. These results will later be used in Chapter Six to develop practical design charts for designers.

Now it remains to use the results of this Chapter, particularly the sensitivity study to develop a suitable design methodology for bicycles and the next Chapter continues this work.

6. BICYCLE DESIGN METHODOLOGY

6.1. INTRODUCTION

One objective of this investigation was to develop a suitable design methodology that manufacturers and designers could use to guide their bicycle design decisions. The current lack of a suitable methodology means that most manufacturers rely heavily on empirical rules of thumb, a practice which may stifle development. "*Because bicycle design has been based on tinkering rather than equations, there has been little scrutiny of bicycle analyses* (14)."

Design methodologies are common in engineering and can be in the form of: criteria, tables, equations and charts, all of which can be used when designing products. All these methodologies consider critical design parameters and prescribe ways of adjusting them within acceptable limits. A variety of methodologies will be examined in this Chapter to consider their suitability for designing road bicycles. These methodologies will be based on the sensitivity study from Chapter Five which identified critical design parameters. These methodologies will be discussed, evaluated and then a recommendation will be made as to the best approach.

As demonstrated in Chapter Five, bicycles are highly sensitive to changes in: the head tube angle, fork rake and the wheel diameter. Also significant is the wheel moment of inertia about the axis of rotation. The mass and its longitudinal position are moderately important but the mass height is less so. Designers need to consider these parameters when designing and comparing new designs and need to try to optimise their values for particular applications.

6.2. CURRENT APPROACHES

Most designers currently use a combination of experience and empirical evidence to design new bicycles. But the literature does have some suggestions as to how to approach this issue, mostly of a highly theoretical nature.

Meijaard et al obtained eigenvalues from their modelling which they say can be used to check alternative designs and which indicate critical speeds for three modes of instability (front wheel wobble, rear end wobble and capsize). In our view the level of mathematical understanding required would limit how useful most designers would find this approach.

Ringwood et al devised some design guidelines to indicate when an unstable condition is being approached particularly with regard to a front wheel high speed wobble (61). They suggested that stability decreased when any one of the following occurred: the bicycle frame got larger, the centre of mass moved to the rear, the centre of mass moved higher and the velocity increased. Their suggestion that stability decreased as velocity increased contradicts many popular observations but it is important to remember that the instability they investigated was a high speed front wheel wobble, so this may be a valid proposition. However the lack of an easy way to convert their work onto recommendations about appropriate parameter values means their approach is incomplete as a practical design tool.

Seffen et al proposed a bicycle rideability index which was used to quantify the effect of changing the front wheel parameters of trail, moment of inertia and head tube angle on controllability (28). Their index was plotted against velocity for different parameter values and compared with a benchmark bicycle to quantify how easy it would be to ride a specific bicycle. They found that for a given speed, as trail increases, rideability improved up to an optimum value and then deteriorated. Importantly they found that no single value of trail gave optimum rideability across all speeds. They also concluded that rideability improved as speed increased which contrasts with Ringwood. Their rideability index has no simple physical meaning as it is the square root of the ratio of the maximum and minimum singularity values of a complex matrix derived from the equations of motion. While their rideability index was useful from a theoretical engineering point of view, this measure of bicycle stability would not be a helpful aid for designers seeking to understand their designs or wishing to describe the attributes of their products to customers. The difficulty of explaining the mathematical concepts behind the rideability index and relating the index to observable physical effects limits its usefulness as a design tool.

Jones is a much cited author in this field which is remarkable given the length of time since his article was written and its brevity (2). His practical experiments have obviously captured people's attention in a way that a purely mathematical treatment would have failed to do. He proposed a steering stability parameter, based on the drop in height of the front wheel hub, the steering angle and the roll angle. Wilson's second edition of his text "Bicycling Science Ergonomics and Mechanics" describes in detail Jones' paper and calls his stability parameter, the Jones stability criterion or "u" (2, 10). He continues with a discussion about common steering geometries for a variety of bicycles and calculates "u" values for them. The third edition of this text discusses stability theories in more detail and contains good descriptions of: inverted pendulums, Jones' experiments, counter-steering and the work of Papadopoulos et al (52). The Jones stability criterion is commented on as follows, *"to sum up, Jones' experiments were very revealing, but his premise was faulty. Nonetheless "u" can be recognized as a very important stability quantity among bicycles with two wheels of the same size (52)."* Confusingly it then says the Jones stability criterion formula given in the second edition is wrong, but does not provide a clear correction (10). Despite this, some frame builders continue to find the "u" equation from Wilson's second edition useful. BikeCAD (a computer aided bicycle design programme) continues to calculate values for the Jones stability criterion despite the possible formula errors "*some users of BikeCAD Pro have requested that it be left in as they have already developed a sense of what Jones stability values work for them."* (89). This statement shows the real need for some practical and scientific way of determining stability and quantifying handling performance.

6.3. ALTERNATIVE DESIGN METHODOLOGIES

Several design methodologies are now considered and evaluated to determine their suitability for practical use. All these methodologies consider critical design parameters and describe ways of adjusting them and setting acceptable limits using practical and straightforward methods. The following alternative design methodologies were evaluated as to their suitability:

1. Design Criteria
2. Design Tables
3. Design Equation
4. Design Charts

The final recommendation as to a preferred method is made later in this Chapter and is based on a number of practical factors, as each method has different advantages and disadvantages. Each alternative method is a stand-alone technique that could be used together with or independently of the others.

6.3.1. DESIGN CRITERIA

The first alternative we considered was a Design Criteria methodology, which is a method intended to provide designers with a summary of the empirical knowledge including acceptable values and limits for key design parameters. A designer would consult a series of Design Criteria and systematically adjust the key parameters until it was judged that an acceptable solution had been reached. The final judgement would be based on past experience and the degree of willingness to push close to or beyond any boundaries.

The sensitivity study identified several key parameters which have significant effects on bicycle handling (e.g. head tube angle, rake, wheel diameter, wheel polar moment of inertia, wheelbase, mass and the mass position). The Design Criteria rules for setting values for these parameters were made after examining the database of Tour de France (TdF) road bicycles described in Appendix F. Where possible parameter recommendations are based on the equations for lines of best fit from the plotted values of these bicycles. The resulting Design Criteria methodology is shown in Table 29 and follows the procedural steps outlined in Table 30.

The advantages of the Design Criteria approach include:

- it codifies current knowledge and experience so that it can be retained and passed on
- it can be adapted and changed to reflect empirical improvements
- it is simple to follow and easy to explain
- it is conservative, safe and unlikely to result in poor designs

However its disadvantages are:

- it makes no allowance for the interaction of several parameters, a major limitation
- it has no scientific or mathematical rationale beyond line fitting equations from the TdF bicycle database
- it is silent on what happens if a design strays beyond the maximum or minimum limits
- it can't indicate likely or worthwhile areas for design innovation
- it is by nature conservative so it must follow design trends rather that assist in innovation, therefore it may inhibit improvements and advances in design

Table 29 Bicycle Design Criteria

Variable	Definition	Design Criterion	Approaching the min value	Approaching the max value
FS	Frame size [1]	$FS = IS \times 0.65 \pm 10\ mm$ (68, 69) • this is based on the size of the rider (an ergonomic rule (68)) • the normal advice if the ideal size is between two sizes is to select the smaller size (69)	• a smaller, more compact and lighter bike results in more lively steering but with less directional stability • may cause problems achieving the correct ergonomic position, typically if the frame is too small the rider will be hunched over	• a larger and heavier bike will be used and this will be more stable but is also more sluggish in its handling response
L	wheelbase	L (mm) = 0.3077 FS (mm) + 822.5 (mm) +/- 20 mm • this is based empirically on 2013 TdF road bicycles, see Appendix F and Figure 124	• quicker response possibly becoming unstable at some point	• more stable but also a more sluggish response with larger overshoots and longer settling times
D	Wheel diameter	• road bicycles are almost universally based on 700C wheels • note that different sized 700C tyres may have a noticeable effect see Appendix E and Table 26 (64, 69, 74, 81)	• sluggish response with large overshoot and long settling time	• quicker response becoming more unstable
I_{YW}	Moment of inertia of both wheels about the axis of rotation	• different wheel and tyre combinations have different handling effects • consult Table 26 for the MOI values for common wheels and tyres also Appendices C and E	• Every 1% decrease in wheel MOI decreases the settling time by 5.75% • increases the speed of response making the bicycle less stable but more lively	• every 1% increase in wheel MOI increases the settling time by 5.75%

		• the wheel's MOI can be determined by a compound pendulum experiment	• at some point instability will occur	• reduces the speed of response making the bicycle more stable but less lively
Delta Δ	Trail	Δ (mm) = - 0.035 FS (mm) + 76.3 (mm) +/- 10 mm • based on Appendix F, see Figure 126	• quicker response becoming possibly unstable at some point	• more stable but also more sluggish response with larger overshoots and longer settling times
Beta β	Fork rake (or offset)	β (mm) = 45.3 mm +/- 3.5 mm min 40.0 mm max 53.0 mm • based on Appendix F and Table 72	• sluggish response with larger overshoots and a longer settling time	• quicker response but becoming more unstable
Phi Φ	Head tube angle	Φ (^{o}) = 0.074 FS (mm) + 68.8^o +/- 1.5^o • based on Appendix F and Figure 125	• sluggish response with larger overshoots and a longer settling time	• quicker response but becoming more unstable
STA	Seat tube angle [2]	STA (^{o}) = 73.3^o +/- 1.1^o, min 69.2^o mm max 75.5^o • based on Appendix F see Table 72	• sluggish response with large overshoot and long settling time	• quicker response but becoming more unstable
Note 1 Frame size (FS) is explained in Chapter Four				
Note 2 Seat tube angle (STA) is explained in Chapter Four				

Table 30 Design Criteria Procedure

Procedural step	Comments
1. Select the bicycle frame size (FS)	• the bicycle's basic size is set by the frame size (FS), see Appendix B • this is determined ergonomically from the rider's inseam measurement, FS = IS x 0.65 (68, 69) • the correct FS allows the rider to pedal efficiently
2. Determine the wheelbase (L)	• the wheelbase (L) is determined empirically from Appendix F • a longer L increases stability but reduces the speed of response (75) • the wheelbase also influences the top tube length which has ergonomic & aerodynamic significance (69)
3. Determine the head tube angle and rake	• the two parameters of steering geometry: the head tube angle (HTA or Φ) and rake (β) determine the trail (Δ) which is a critical parameter
4. Determine the seat tube angle	• the seat tube angle (STA) completes the basic design of the frame geometry • a steeper seat tube angle increases steering liveliness but reduces rider comfort (75)
5. Consider the wheel properties	• the wheel diameter (D) of most road bicycles is set to the ISO 700C standard (nominally 700 mm) (74) • in practice different sized tyres vary the actual diameter (660 to 690 mm see Table 26) • the bicycle is surprisingly sensitive to different wheel diameters • the wheel's moment of inertia about the rotational axis has been found to have some importance and can be determined by a compound pendulum experiment

6.3.2.DESIGN TABLES

The purpose of a Design Table is to summarise design information into a tabular format (for example from a set of design criteria). Tables set out a series of recommendations in a codified way that are easy to interpret. They can be constructed in a similar way to the Design Criteria methodology by making use of empirical knowledge and experience. The difference is that the information is presented in its final form and doesn't require any calculations or interpretation.

An example of such a Design Table Series is shown in Appendix G, one Table of which is reproduced as Table 31. This Design Table Series covers a range of five frame sizes from 490 to 610 mm and the values listed in each Table (for target, minimum and maximum values) were found by using the Design Criteria rules set out in Table 29. To use this Series first use the rider's inseam measurement to find the correct frame size and hence choose the correct Table. Then use the selected Table to make decisions about the wheelbase, fork rake, head tube angle and seat tube angle values. In Table 31 below the parameter values for a 550 mm frame are shown and such a frame size is suitable for a rider with an inseam measurement of 846 mm.

Table 31 Road Bicycle Design Table - 550 mm frame size

Variable	Definition	Target value	Min value	Max value
IS	Rider inseam measurement	846	823	869
Δ	Trail (critical)	57 mm	47 mm	67 mm
L	wheelbase	992 mm	972 mm	1012 mm
beta	Fork rake (or offset)	45.5 mm	42.5 mm	53 mm
phi	Head tube angle	73.0^{o}	71.5^{o}	74.5^{o}
STA	Seat tube angle	73.6^{o}	71.5^{o}	74.8^{o}
Assumptions		• performance road bicycle • 550 mm frame size • based on 700C wheels • criteria based on Table 30		

If any of the assumptions in the Table are changed then amended tables would be needed. For instance if 650C wheels were used (instead of 700C) then changes to the head tube angle and rake recommendations would be required to compensate for this change.

The advantages of using Design Tables include:

- they require minimal calculations as the target, minimum and maximum values are all given to the user
- all the information for each parameter is listed so they are very clear and easy to use

The disadvantages are:

- just like the Design Criteria method they makes no allowance for the interaction of parameters which is a major limitation
- they offers no guidance as to the likely effect on handling if certain limits are reached or exceeded

Apart from these points they share all the advantages and disadvantages of the Design Criteria method that have been mentioned.

6.3.3.DESIGN EQUATIONS

An attempt was made to develop a closed form equation for quantifying handling performance but it was unhelpful. The equation was based on the results of the sensitivity study but after evaluation it was decided that this approach was unsuitable. A brief description is included for completeness in Appendix G.

6.4. DESIGN CHARTS

Design charts are commonly used by engineers and plot important parameters and indicate performance in some manner. For example a Pump Selection Design Chart plots pump head against flow rate and is used to select the best pump for a specific application. Once a pump selection has been made, the correct impellor size, power requirements, efficiencies and other parameters can be read directly from the Design Chart and its associated charts. Design Charts are constructed by first selecting the most appropriate parameters to combine on two (or more) axes and often include lines of constant parameter value drawn across them (e.g. lines of constant pump efficiency).

After considering all the other proposed design methodologies it was decided to develop and recommend the Design Chart concept because of its clear advantages (i.e. ease of use, ability to consider multiple parameters and scientific basis). The advantages and disadvantages of Design Charts are listed below.

Their advantages include:

- they are scientifically based and justified
- they are relatively easy to use with the minimum of calculations required
- they enable a wide audience to understand the design process and its outcomes
- they allow several parameters can be concurrently considered, so interactions can be studied

- a wider range of design decisions can be contemplated at once
- scientifically based iso-handling lines can be plotted on the chart to indicate handling performance
- the effect of moving a design in a particular direction on the chart is clearly shown i.e. it becomes more or less stable
- it may be possible to develop 3-D or contour style Design Charts, allowing even more parameters to be concurrently assessed

While their disadvantages include:

- assumptions have to be clearly known and adhered to
- design boundaries may be hard to define and so unsafe designs may be produced (so the design charts are not necessarily conservative)

The use of Design Charts for bicycles will allow a wide range of people to participate in and understand the design process and its outcomes as these Charts can be easily interpreted and can provide quantifiable evaluation of individual bicycles such as a settling time value. Individual bicycles design specifications can be plotted onto the Charts and this can provide riders with an easy way to compare new designs to bicycles they are already familiar with. Bicycles close to boundaries or limits on the charts are inevitably in grey areas and further methods are needed to determine exactly where the boundaries are. The Charts will allow designers to understand and quantify in meaningful ways any design changes they are considering and they need not be used in conjunction with any of the other methodologies discussed (that is criteria or tables or equations).

To produce relevant Design Charts, it was first necessary to examine the sensitivity study to see which parameters are the most important and also to consider which ones the cycling fraternity consider to be significant. From the results of the sensitivity study we can see in Table 32 that key parameters can be logically grouped together in terms of their interaction and overall significance (see also Table 28).

The first group are the terms that define the steering geometry, that is the head tube angle and rake (the head tube angle is commonly known to be highly significant). These two terms give the important third term trail (again considered highly significant by manufacturers) from a simple geometrical relationship. The second group concern the wheel diameter and wheel moments of inertia which the sensitivity study show to be important. The third group relates to the important area of frame geometry and considers the vertical and longitudinal position of the mass (h and b) and the wheelbase. These terms can be used to indirectly define the seat tube angle which is held to be a very significant term by the bicycle fraternity (73). The last group covers the related terms of mass and the moment of inertia of the rear assembly B. These two parameters have the least significance of the terms we are considering. This leaves two remaining parameters out of the original eleven, the two moments of inertia for the front assembly A (about the yaw and roll axes) which have been shown to be insignificant and therefore are not incorporated into a Chart.

In summary the four proposed Design Charts cover the design areas of:

1. Steering geometry (head tube angle, rake and trail)
2. Wheel properties (wheel diameter and moment of inertia)
3. Frame geometry (vertical and longitudinal position of the mass, wheelbase and seat tube angle)
4. Mass and roll inertia (mass and moment of inertia of B)

These four Design Charts are ranked above (from 1 to 4) according to their parameter sensitivity (as per Table 32) and they can be used together or independently as appropriate to the circumstances. But in the case of a new bicycle design probably the first two (steering geometry and wheel properties) would initially be heavily scrutinised. Followed by consideration of the frame geometry and mass and roll inertia Charts.

Table 32 Design Chart parameters

Relevant design chart	Symbol	Parameter definition	Benchmark value/s	Units	C % change [1]	Comments [2]
1. Steering Geometry Design Chart	Φ	head tube angle	73	degrees	5.93%	significant term
	β	fork rake	0.045	m	1.41%	moderately significant
2. Wheel Properties Design Chart	D	diameter of the bicycle wheel	0.675	m	5.75%	significant term
	I_W	MOI of wheels about X, Y and Z [3]	0.10	kgm^2	2.02%	moderately significant
3. Frame Geometry Design Chart [4]	b	horizontal distance of rear wheel hub centre to the centre of mass	0.330	m	2.07%	moderately significant
	L	bicycle wheelbase	1.000	m	1.57%	moderately significant
	h	height of centre of mass	1.100	m	0.27%	not significant
4. Mass and Roll Inertia Design Chart	M	mass	80.0	kg	1.98%	moderately significant
	I_{XB}	MOI of B about XB axis (roll)	100.0	kgm^2	0.11%	not significant
Parameters not considered	I_{ZA}	MOI of A about ZA axis (yaw)	0.08	kgm^2	0.10%	not significant
	I_{XA}	MOI of A about XA axis (roll)	0.20	kgm^2	0.06%	not significant

Note 1 C = % change in the 2% settling time for each 1% increase in the parameter

Note 2 definitions of the importance of each parameter

significant is defined as a greater than 3% change for each 1% increase in the parameter (of C)

moderately significant is between a 0.5% and 3% change of C

not significant is less than a 0.5% change of C

Note 3 due to symmetry of both wheels, $I_X = I_Y$ and $I_Z = 2I_X = 2I_Y$, therefore the wheel's moment of inertia property has been included once not three times

Note 4 this chart also includes the seat tube angle (STA) secondary parameter

6.4.1.DEVELOPMENT

Once the main parameters for the Charts had been decided upon in Table 32, a decision must be made as to which one is the independent variable and which the dependent variable. For the Steering Geometry Design Chart the independent variable is the head tube angle (plotted on the x axis) and the dependent variable is trail (the Y axis). Consideration was given as to what other possible parameters could be displayed in order to make each Chart as useful as possible. In the case of the Frame Geometry Design Chart the independent variable is b and the dependent variable is h, also plotted are lines of constant wheelbase and seat tube angle. So the Frame Geometry Chart contains four parameters (b, h, L and STA) and additionally has two boundaries defined by the UCI 5 cm rule and the toe overlap limit.

In Chapter Five the settling time of the unit impulse response was used as a measure of handling and this indicates how the bicycle will react to a sudden front wheel steering yaw perturbation. The unit impulse response of the benchmark bicycle was found to have a 2% settling time of 10.1 seconds which was equated to 100% and all other responses were referenced to this, making the study non-dimensional. Given that this was the bicycle's response to a unit impulse of infinite value across zero time, it is not surprising that the relatively long settling time of 10.1 seconds was obtained for the benchmark. In practice when using a jerk impulse of 0.5 Nm over 1.25 sec, a very similar 2% settling time of 10 seconds was obtained. But the analysis was not based on this jerk input because the torque was arbitrarily selected and it is felt that the Simulink unit impulse approach is more universal as well as being quicker to execute.

Initially the 2% settling time was recorded in seconds for a range of discrete parameter points in the early versions of the Design Charts. But this produced iso-handling line values with values in seconds. Therefore it was necessary to non-dimensionalise Chart settling times to make them universally applicable. From these initial charts it was possible to interpolate between the known points of trail and head tube angles to find any desired settling time value and therefore it was possible to convert the settling times from seconds to any desired percentage of the benchmark bicycle. An iterative process was used to complete all the charts in this manner.

This process resulted in the four Design Charts now presented, which display iso-handling lines expressed as percentages of the benchmark response (e.g. 70 % to 140%). This gives manufacturers a practical means to determine what effect a design change will have. In Chapter Seven different road bicycles will be plotted onto these Design Charts to compare current practice with Chart predictions about handling.

6.4.2. STEERING GEOMETRY DESIGN CHART

This first Chart examines the effect of different steering geometries on bicycle handling. The Chart plots the geometric relationships of head tube angle, trail and rake and the relevant steering geometry equations and definitions are now repeated (90).

Tail equation

$$\Delta = \frac{r\cos\emptyset - \beta}{\sin\emptyset} \tag{34}$$

Effective trail equation

$$\Delta_e = r\cos\emptyset - \beta \tag{36}$$

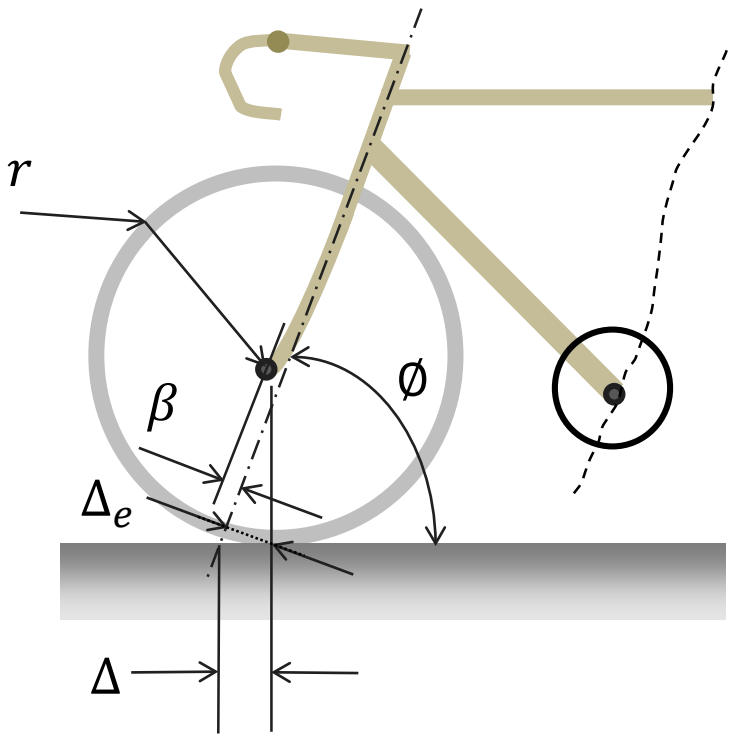

Figure 78 Bicycle steering geometry parameters defined

Somewhat similar charts to the proposed Steering Geometry Design Chart are available in the literature (2, 90, 91). For example, van der Plas includes several in his text “Bicycle Technology” see Figure 79 (90). Van der Plas arranges the axes differently to show rake vs. trail for lines of constant head tube angle. Though he states that stability increases with trail, this is a simplification and is only true for a small range of trail, as above a certain trail value an instability mode appears (28). He discusses the significance of the effective trail versus trail claiming that the effective trail gives a more accurate indication of stability, but he does not quantify this in any way.

As discussed earlier Jones devised a stability criterion and developed an interesting chart, see Figure 81, showing the drop in height of the front fork due to changes in the steering angle and roll (note roll is referred to as lean and a different notation has been used in his graphs). His second chart shows the head tube angle vs. front projection, plotted on lines of constant stability, Figure 82. Where front projection is a modified rake term expressed as a fraction of the wheel radius and is shown in Figure 80. The lines of constant stability are equal to $dH^2/d\sigma d\lambda$, (H = front fork height, σ = yaw angle and λ = roll angle) and are the rate at which the front wheel drops in height due to changes in yaw and roll angles (10). These lines are referred to as the Jones stability criterion (u) by Wilson in his second edition and are defined by a calculation, though the third edition states this earlier calculation was incorrect (10, 52, 92).

Meijaard et al have cast doubt on Jones’ analysis of bicycle stability (16). They point out that Jones has ignored the effect of the mass of the front assembly. They claim this can be important and may either be a negative or positive torque depending on the lever arm of the assembly’s centre of mass. In their view a more important objection is that Jones assumes the torque on a leaning front wheel is the same whether the bicycle is stationary or moving. But the ground reaction forces on the wheel change direction when the bicycle starts to move forward and this will change the twisting torque, so the Jones Charts cannot be completely correct,.

One significant practical problem with the Jones stability graph is that it is not expressed in terms of head tube angle, rake or trail. Rather it is based on the distance the front wheel fork drops in height due to the roll and steering angles. As Jones says *“it turns out that defining the height of the fork points of a bicycle in terms of steering geometry and angles of lean and steer is a remarkably tricky little problem.”* So either a computer solution is required (iteratively solving the simultaneous trigonometric equations) or an experimental procedure is called for to measure a bicycle’s fork point drop as the bicycle rolls and yaws. From practical experience we can state that such an experiment is not easy to perform with any accuracy without a custom built measuring rig being used.

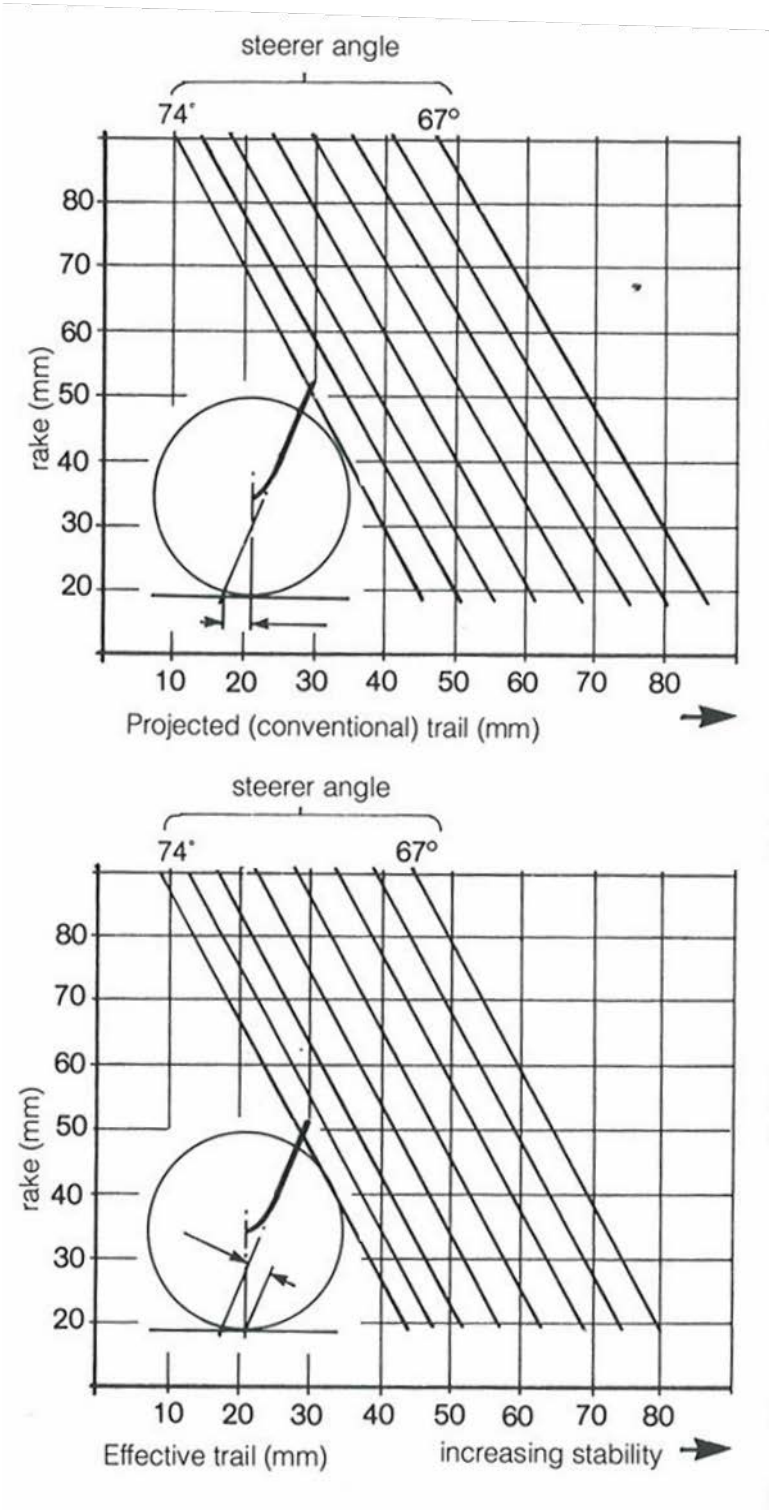

Figure 79 van der Plas steering geometry charts for the front wheel

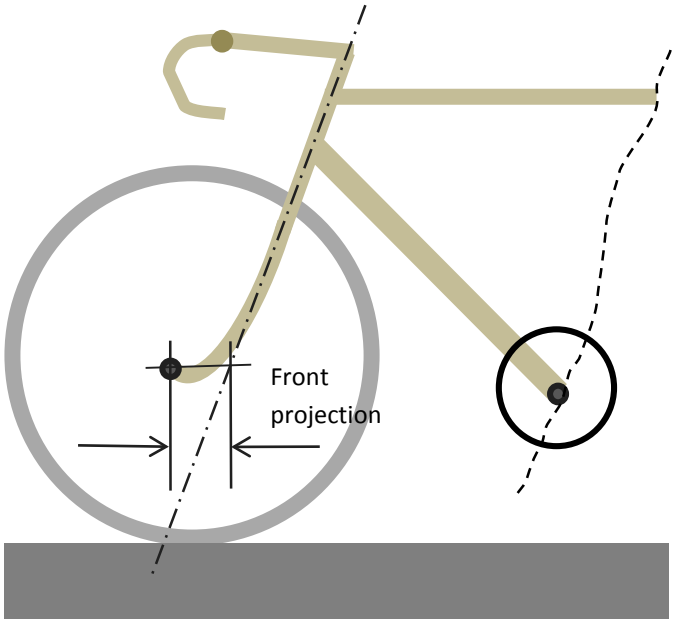

Figure 80 The front projection term defined by Jones

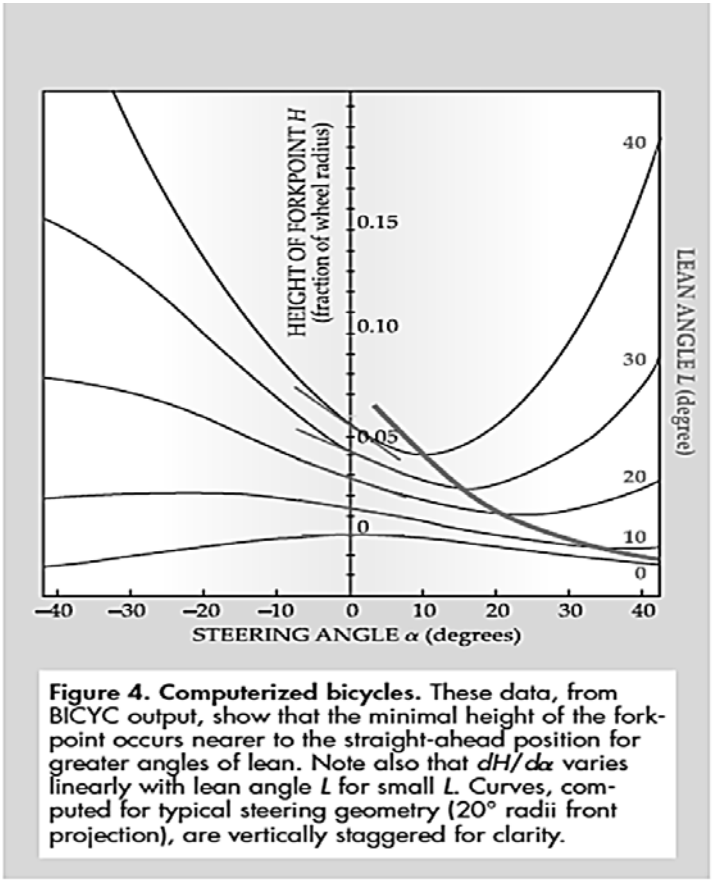

Figure 4. Computerized bicycles. These data, from BICYC output, show that the minimal height of the fork-point occurs nearer to the straight-ahead position for greater angles of lean. Note also that $dH/d\alpha$ varies linearly with lean angle L for small L. Curves, computed for typical steering geometry (20° radii front projection), are vertically staggered for clarity.

Figure 81 Front fork drop due to yaw and roll angle changes

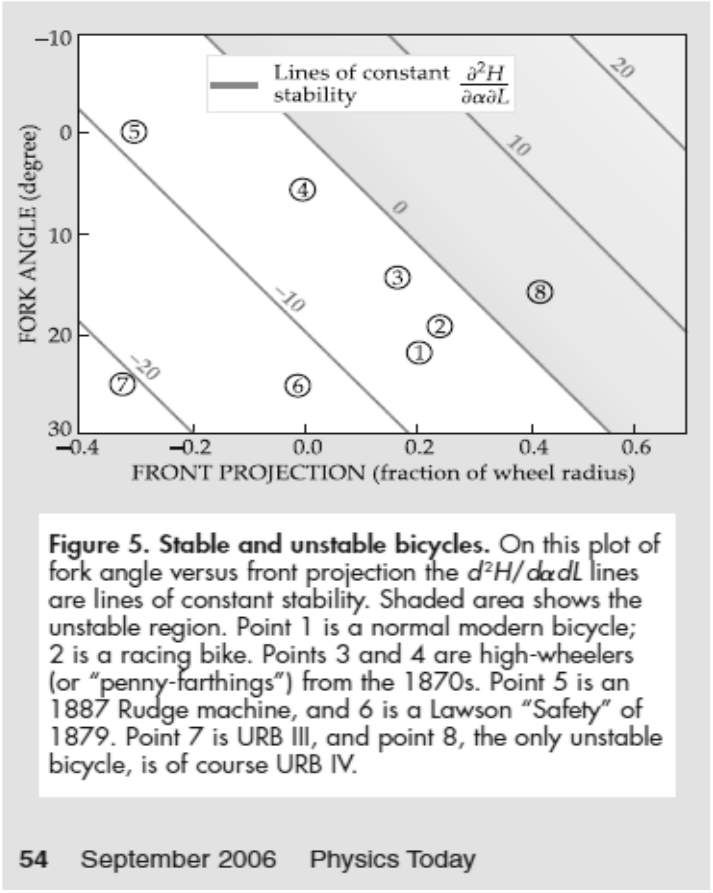

Figure 5. Stable and unstable bicycles. On this plot of fork angle versus front projection the $d^2H/d\alpha dL$ lines are lines of constant stability. Shaded area shows the unstable region. Point 1 is a normal modern bicycle; 2 is a racing bike. Points 3 and 4 are high-wheelers (or "penny-farthings") from the 1870s. Point 5 is an 1887 Rudge machine, and 6 is a Lawson "Safety" of 1879. Point 7 is URB III, and point 8, the only unstable bicycle, is of course URB IV.

Figure 82 Head tube angle vs. front projection with Jones stability criterion lines

Moulton, a well-known but now retired frame builder (based in the UK and USA) has produced the interesting steering geometry chart shown in Figure 83. Moulton's bicycles have been used in top international competitions including the Tour de France and the Olympics. A frequent writer with his own web blog about bicycles, he describes this chart in one of his 2010 entries (91). The axes orientation he chose are reversed from our proposed Design Chart. On his chart is displayed a line of "ideal handling" (this passes a point defined by a 73^{O} head tube angle, a 35 mm rake giving a 67.3 mm trail). Interestingly his line is very close to the 140% iso-handling line on the proposed Design Chart. No supporting analysis or evidence as to the selection of this particular line is included other than mentioning his empirical observations about steering geometry. *"In time I found there was an "optimum handling" line that I could draw on my graph, that would show me the fork rake needed for a given head angle (91)."*

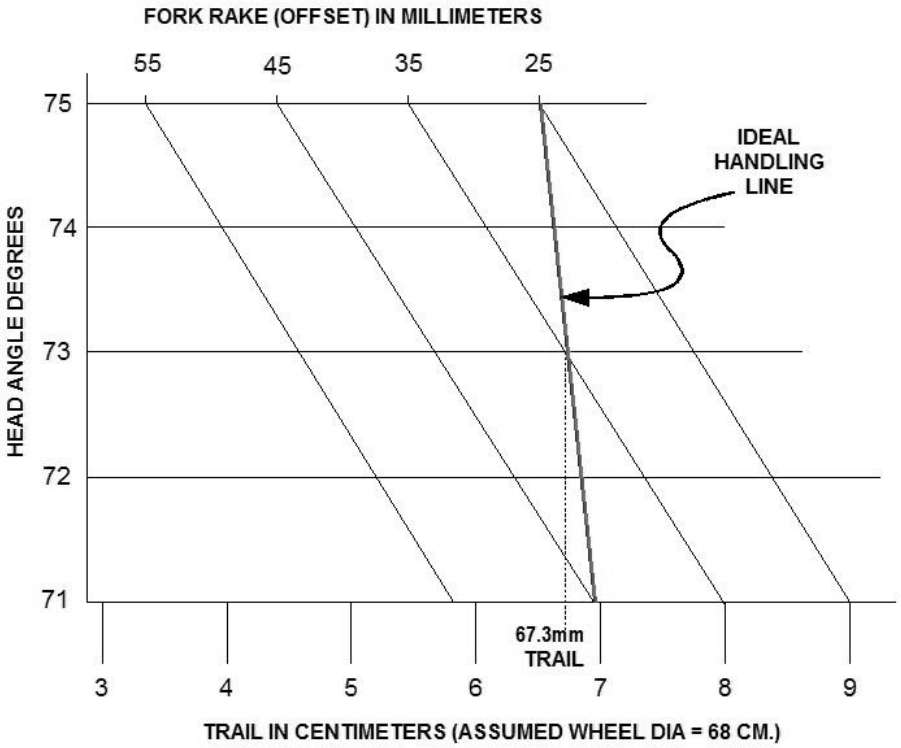

Figure 83 Moulton's proposed head tube angle vs. trail chart and ideal handling line

The proposed Steering Geometry Design Chart began as a chart showing trail vs. head tube angles plotted along lines of constant rake, similar to both the van der Plas and Moulton Charts, see Figure 79, Figure 83 and Figure 84 (90, 91). What is new about this Chart is the addition of a series of iso-handling lines (spaced at 10% intervals from 50 % to 150%). Each iso-handling lines connects points of constant settling time (based on the Simulink unit impulse response 2% settling time) and so indicates the bicycle's handling performance. The Chart assumes that all other design parameters are constant (that is wheelbase, mass, position of mass, moments of inertia, speed and wheel diameter). The iso-handling lines only indicate equivalent performances, they don't indicate any optimum design position. But they do allow easy and meaningful comparisons of individual bicycles and they can be used to compare design solutions quantitatively.

It is possible to plot existing designs onto the Chart to gain an insight as to what the different regions of the Chart will mean in terms of performance and by plotting successful bicycle geometries a suitable design envelope can be proposed.

The Chart in Figure 84 displays trail and head tube angle values that range from 0 to 120 mm and 62 to 80 degrees respectively with rake dimensions ranging from 0 to 75 mm. Of course it is the combination and interaction of these three parameters which is interest and this is what this Chart clearly displays.

Eleven iso-handling lines are drawn covering the area of interest, that is head tube angles between 69 and 77 degrees and trail values between 20 and 70 mm. The iso-handling line that passes through the benchmark bicycle is labelled the 100% line and it connects geometry combinations which have the same settling time and the other iso-handling lines are referenced to this 100% line. The overall trend is that as the trail increases (and rake decreases) the settling times increase or in the terms of van der Plas, stability has increased. But is this always a good thing? Sometimes a certain amount of sensitivity in handling (or instability) is desirable.

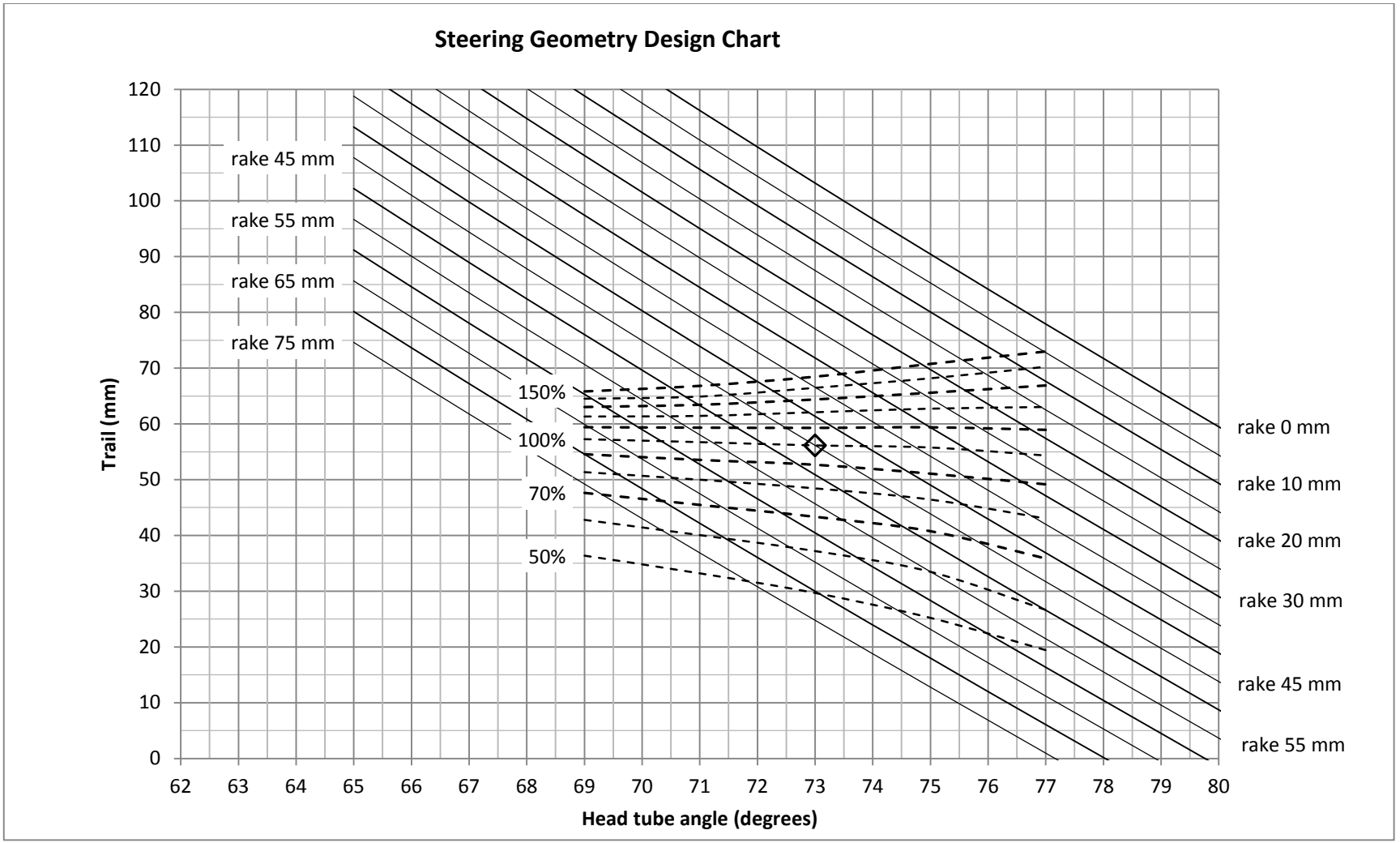

Figure 84 Steering Geometry Design Chart with iso-handling and constant rake lines (675 mm wheel dia.)

Consider the five different bicycles in Table 33 all with different geometries. On the enlarged Steering Geometry Design Chart in Figure 85 these three bicycles (cases A, B and C) with different combinations of head tube angles and rake all lie along the 100% iso-handling line. Assuming all other parameters are the same (wheelbase, mass, speed, mass position and moments of inertia) they will all have the same 2% settling time.

Consider a second scenario, where the benchmark bicycle's geometry (case A) is changed slightly. First keep the head tube angle unchanged at 73 degrees but change the rake from 45 mm to 50 mm (thus causing the trail to decrease to 50.9 mm) this is case D in Table 33 and Figure 85. This new geometry moves from the 100% iso-handling line to approximately 85%, which is a 15% drop. Next, in case E, keep the rake unchanged but change the head tube angle from 73 to 73.5 degrees this causes the settling time to drop from the 100% line to just above 90%, a decrease of nearly 10%. In both cases D and E, the rider would experience a much quicker settling down after a disturbance, which is a good thing up to a point. But the downside is both bikes would be more sensitive to disturbances. What this physically means is that for the benchmark bicycle (case A) and cases B and C under a unit impulse they would all take 10.1 sec (100%) to settle down to 2% of the maximum response. But for case D, such a bicycle would take 8.585 sec (85%) to settle and for case E it would take 9.09 sec (90%) to settle down after a unit impulse.

Chapter Seven will have a detailed discussion as to the application of this Chart to the elite road bicycles used in the Tour de France 2013 race.

Table 33 Five bicycles plotted in Figure 85.

Case	Head tube angle degrees	Rake mm	Trail mm	C 2% settling time	Marker
A	73.0	45	56.130	100%	diamond (benchmark)
B	69.0	67	57.300	100%	circle
C	77.0	23	54.310	100%	triangle
D	73.0	50	50.900	85%	cross
E	73.5	45	53.039	90%	square

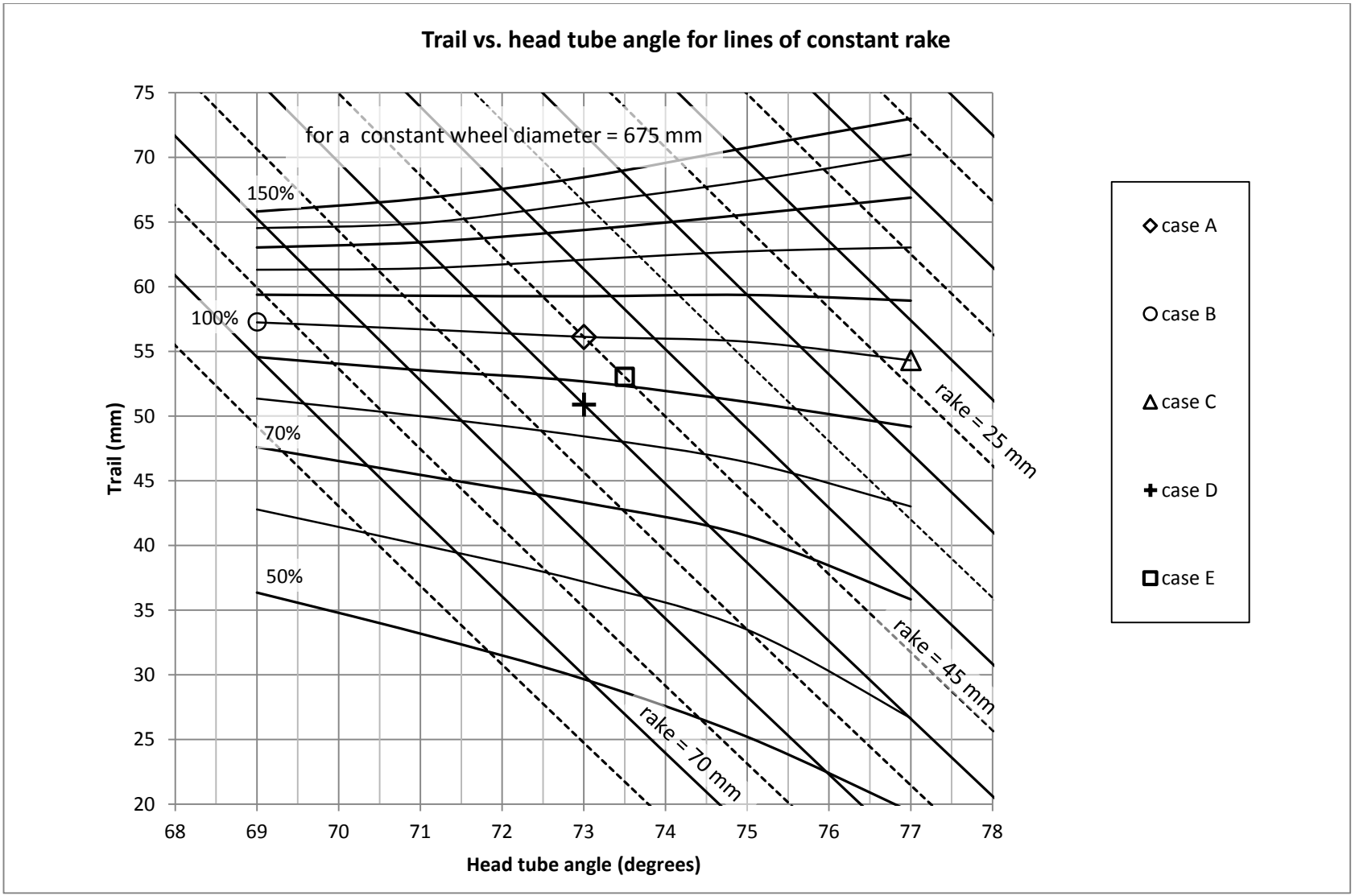

Figure 85 Steering Geometry Design Chart with five bicycles (cases A to E) plotted from Table 33

6.4.3. WHEEL PROPERTIES DESIGN CHART

The second proposed Chart shows the effect and interaction of the two important wheel properties, namely diameter and the moment of inertia about the rotational or polar axis Y, see Figure 89. These two wheel properties have a significant effect on settling time with bicycles being surprisingly sensitive to different wheel diameters (every 1% increase increasing the settling time by 5.75%). Also the wheel's moment of inertia about Y is important with every 1% increase, decreasing the settling time by 2.02%. However these effects tend to cancel each other out because increasing the wheel diameter usually increases its moment of inertia. So if the wheel diameter was increased but no change to its construction was made (i.e. materials, rim wall thickness and rim width to depth ratio all unchanged) the result may be that no change in handling occurs. The Wheel Properties Design Chart illustrates this interaction and gives guidance of how a handling may be improved by careful wheel selection. As far as is known, no similar chart to this has been proposed in the literature.

The Wheel Properties Design Chart was prepared using equations relating wheel diameter to the polar moment of inertia and making basic assumptions about wheel construction and material. Again, iso-handling lines of constant settling time are plotted and referenced to the benchmark wheel and they indicate equivalent performance, but they don't indicate an optimum wheel design. This Chart assumes the head tube angle, trail, rake, mass (and its position) speed and all other moments of inertia are constant.

To construct the Chart the following assumptions were made:

1. The contribution of the rim to overall moment of inertia is assumed to be 50% (experimentally this has been shown to be between 45% and 50% of the total). Hence the contribution of the tyre to the moment of inertia is allowed for by using this ratio. The hub and spoke moments of inertia contribution are small, typically in the order of 0.5% of the total and hence they can be ignored (see Figure 86).
2. The rim section is a hollow rectangular box of constant wall thickness (t) and material
3. The ratio of the rim section depth (P) to rim width (w) is defined by the P/w ratio (Figure 87) and ranges from 0.5 to 2.5 are shown on the Chart
4. The rim material and its density are known (e.g. 6106 series aluminium is a typical rim alloy with a density of 2700 kg/m^2)
5. The rim section width (w) is known, assumed to be 25 mm
6. The rim wall thickness (t) is known, assumed to be 1 mm
7. The tyre diameter (td) is known and the actual wheel diameter is given by:

$$actual\ wheel\ diameter = 1.8925\ X\ td + 627.27 \quad \text{(mm)} \tag{37}$$

This equation was found from manufacturers' supplied specifications (which are detailed in Appendix E) which were used to establish the relationship between the tyre width and the actual outside wheel diameter (as opposed to the nominal diameter). Tyre diameters of between 18 mm and 35 mm only are used, see Figure 90.

8. The wheel rim's moment of inertia is calculated using the standard formula for a hollow annulus of known thickness, width and inside/outside diameters

$$I_{wheel} = {}^{1}/_{2}\, M_1(R_1^2 + r_1^2) - {}^{1}/_{2}\, M_2(R_2^2 + r_2^2) \quad (38)$$

Where M = rim mass, R = outside radius, r = inside radius, subscript 1 refers to the outside rim shape and subscript 2 to the hollow inside rim, see Figure 88

Using these eight assumptions the Design Chart in Figure 89 was drawn, showing the wheel polar moment of inertia vs. wheel diameter plotted along lines of constant P/w ratio. The position of the benchmark bicycle is indicated as is usual by a diamond marker. From this Chart it can be seen that for a wheel of constant outside diameter as the rim depth P gets larger the moment of inertia increases. Similarly for a constant P/w ratio as the outside diameter increases so does the moment of inertia. This Chart covers a far wider range of wheel diameters from 525 to 800 mm (a 275 mm range) than usually occurs in practice. For example road bicycle wheel diameters normally vary between 660 and 690 mm (see Table 34) so redrawing the Chart as per Figure 90 is useful. The values for any of these assumptions can be easily changed to create other Wheel Properties Design Charts if required.

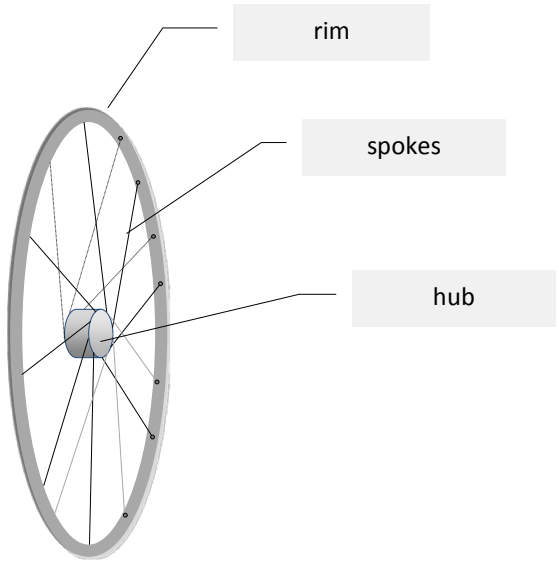

Figure 86 Parts of the wheel that are used to determine its moment of inertia

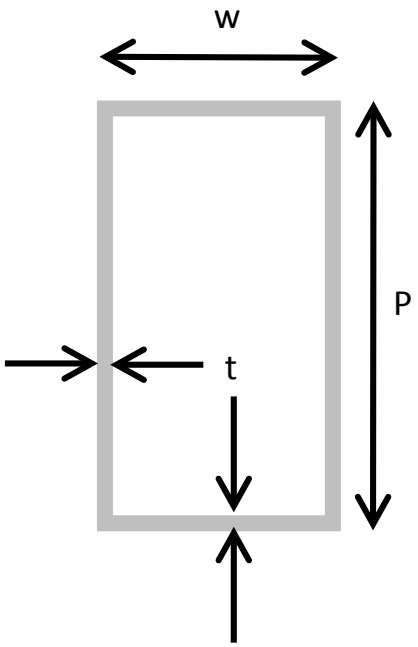

Figure 87 Wheel rim definitions of w, P and t

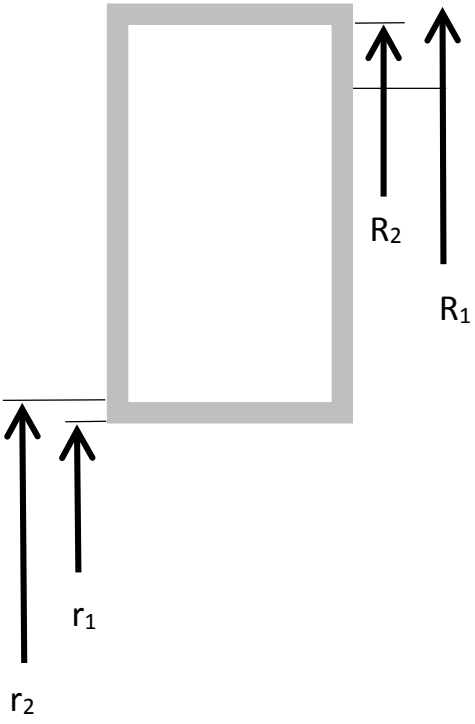

Figure 88 Additional wheel rim definitions of R_1, R_2, r_1 and r_2

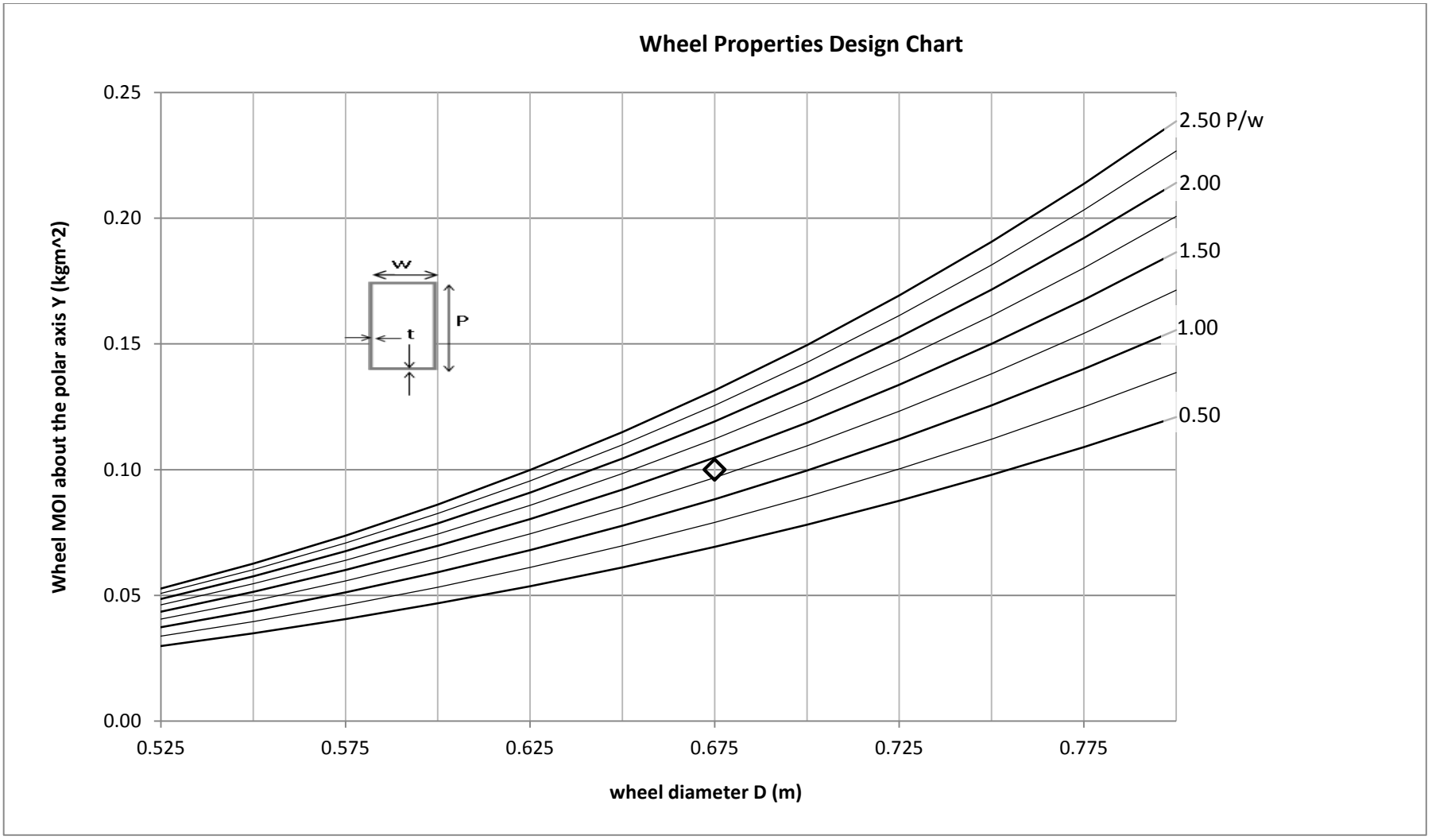

Figure 89 Wheel Properties Design Chart, wheel moment of inertia vs. diameter and rim shape P/w

The Chart in Figure 90 plots several wheels that have been measured experimentally and their details are shown in Table 34. This Table and Chart clearly shows how the settling times vary from 75% to a maximum of 135% of the benchmark wheel, also that the wheel outside diameters range from 675 mm to 687.8 mm and the P/w ratio from approximately 0.50 to 2.5.

Table 34 Tyre and wheel experimental values

Wheel type	**Front/Rear**	**Tyre**	**MOI Y axis kgm^2**	**D Actual Wheel Outside Diameter mm**	**C % settling time [1]**	**Approx P/w Ratio [2]**
Mavic SUP Open Pro	F	700C x 23	0.0871	675.00	135%	0.50
Altx 2800	F	700C x 23	0.0845	675.00	125%	0.75
Altx 2800	R	700C x 23	0.0979	675.00	105%	1.50
Benchmark wheel	F	700C x 25	0.1000	675.00	100%	1.50
Airline Vuelta	F	700C x 23	0.1006	675.00	100%	1.50
Mavic SUP	R	700C x 23	0.1017	675.00	95%	1.75
Mavic Aksium	R	700C x 23	0.1020	675.00	95%	1.75
Shimano 105	R	700C x 23	0.1054	675.00	95%	2.00
Mavic MA3	F	700C x 23	0.1077	675.00	90%	2.25
Shimano 105	F	700C x 23	0.1095	675.00	85%	2.30
Mavic MA3	F	700C x 28	0.1213	680.30	80%	2.50
Mavic MA3	F	700C x 32	0.1304	687.80	75%	2.25
Note 1 C given to the nearest 5%						
Note 2 P/w given to nearest 0.25						

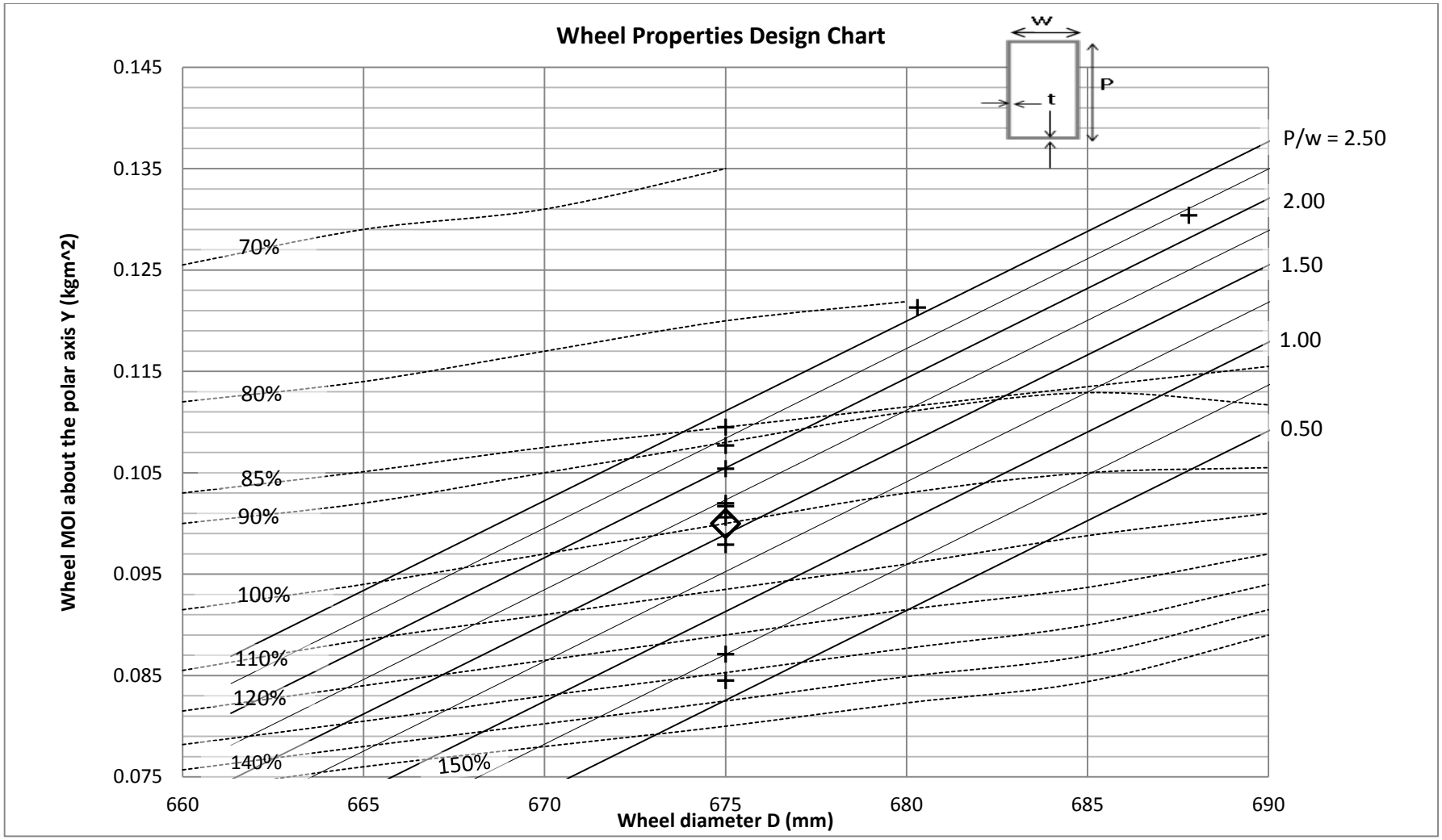

Figure 90 Wheel Properties Design Chart, plotting the wheels (experimental values) from Table 34, iso-handling lines shown

6.4.4.FRAME GEOMETRY DESIGN CHART

The third proposed Design Chart examining frame geometry looks at a new aspect of design and as far as is known is entirely new and original. This Chart shows the effect of the mass position (vertically and longitudinally) and its interaction with the wheelbase and seat tube angle. The proposed Design Chart applies to road bicycles but could be adapted to apply to other types of bicycles such as mountain bicycles.

In order to draw this Chart it was necessary to establish relationships between the mass position, the wheel base and the seat tube angle. This was done by using frame relationships derived from geometric and empirical relationships, and is fully explained in Appendices B and F. Many of the assumptions about these relationships were made using the benchmark bicycle as a starting point.

The first important relationship to examine is between the mass position (b and h) and the seat tube angle. It has been frequently claimed that a steeper seat tube angle results in a bicycle that is more compact and lively (but also less stable) (69, 74). Next to consider is the relationship between these three parameters (b, h and STA) and the wheelbase. The Chart's assumptions regarding seat tube angle, wheel base and mass position are as follows:

1. A standard road bicycle 700C x 25 wheel is used (with an actual diameter of 675 mm) (74)
2. The distance between the centreline of the seat tube and the outer circumference of the rear wheel is set at 32.5 mm and this allows for a suitable clearance between the seat tube and the tyre. Smaller values are sometimes used but can present construction and operational difficulties as road debris can become trapped between the seat tube and the tyre.
3. In order to minimise the wheelbase the seat tube angle is the steepest angle that can be fitted against the rear wheel while still conforming to assumptions 1 & 2 (75)
4. The bottom bracket drop is 67.5 mm, making the distance between the bottom bracket spindle and the road 270 mm (this is a standard value, see Appendix F)
5. The centre of mass position is defined by the main parameters h and b (already defined) and the additional terms k and j, which are defined in Appendix B
6. The ratio k/P is set at 0.2099, where P is the saddle height, this k/P value was selected to conform to the benchmark bicycle's known centre of mass position
7. And ratio j/P is 0.0912, again selected to conform to the benchmark bicycle's known centre of mass position
8. The relationship of wheelbase L (mm) to saddle height P (mm) is given by the empirical relationship, justified in Appendix B and F

$$L = 0.3077 \times P + 822.5 \pm 20 \quad (39)$$

The Frame Geometry Design Chart in Figure 91 shows the vertical mass position vs. horizontal mass position (h vs. b) plotted along lines of constant seat tube angle (STA) and constant wheelbase (L). Once again the position of the benchmark bicycle is indicated by a diamond marker and this Chart assumes that all other parameters are constant (head tube angle, rake, mass, moments of inertia, speed and wheel diameter).

The next stage in developing the Frame Geometry Design Chart is to plot two important boundaries or limits. These limits not determined by the model dynamics but are nonetheless important design considerations and are:

1. The Union Cycliste Internationale (UCI) 5 cm limit, which restricts the maximum seat tube angle that is permitted for any bicycle competing in UCI sanctioned races
2. The toe overlap limit, which is an ergonomics consideration important for smaller riders

6.4.4.1. UCI 5 CM LIMIT

The Union Cycliste International (UCI) is the international body authorised to regulate, control and run the majority of cycle sports (3). The main exceptions to their authority being human powered vehicle record attempts (covered by two independent bodies, IHVPA and WHPVA (59, 93)) and triathlon events, covered by the International Triathlon Union (94).

The UCI 5cm limit is determined by UCI Regulation 1.3.013 "Saddle Setback" which states that "*the peak of the saddle should be a minimum of 5 cm to the rear of a vertical plane passing through the bottom bracket spindle*" (95). In other words there is a maximum seat tube angle that must not be exceeded and this varies with the wheelbase and this is made clear by examining Figure 92. The intention of this regulation (and several other UCI rules) is to ensure that bicycles conform to a basic double triangle design and it prohibits what the UCI considers to be extreme designs, such as the one hour record and time trial bicycles of the 1990's.

The maximum seat tube angle given by this UCI Regulation can found from the following equation (see Appendix B).

$$STA = 90 - \sin^{-1}(5 + seat\ extension)/saddle\ height \qquad \textit{(in centimetres and degrees)} \tag{40}$$

This equation was used to plot the UCI 5 cm limit on the right hand side of the Design Chart Figure 94. The equation give the maximum seat tube angle for any given saddle height and then this is related to the position of the mass (h and b) using the relationships defined in Appendix B.

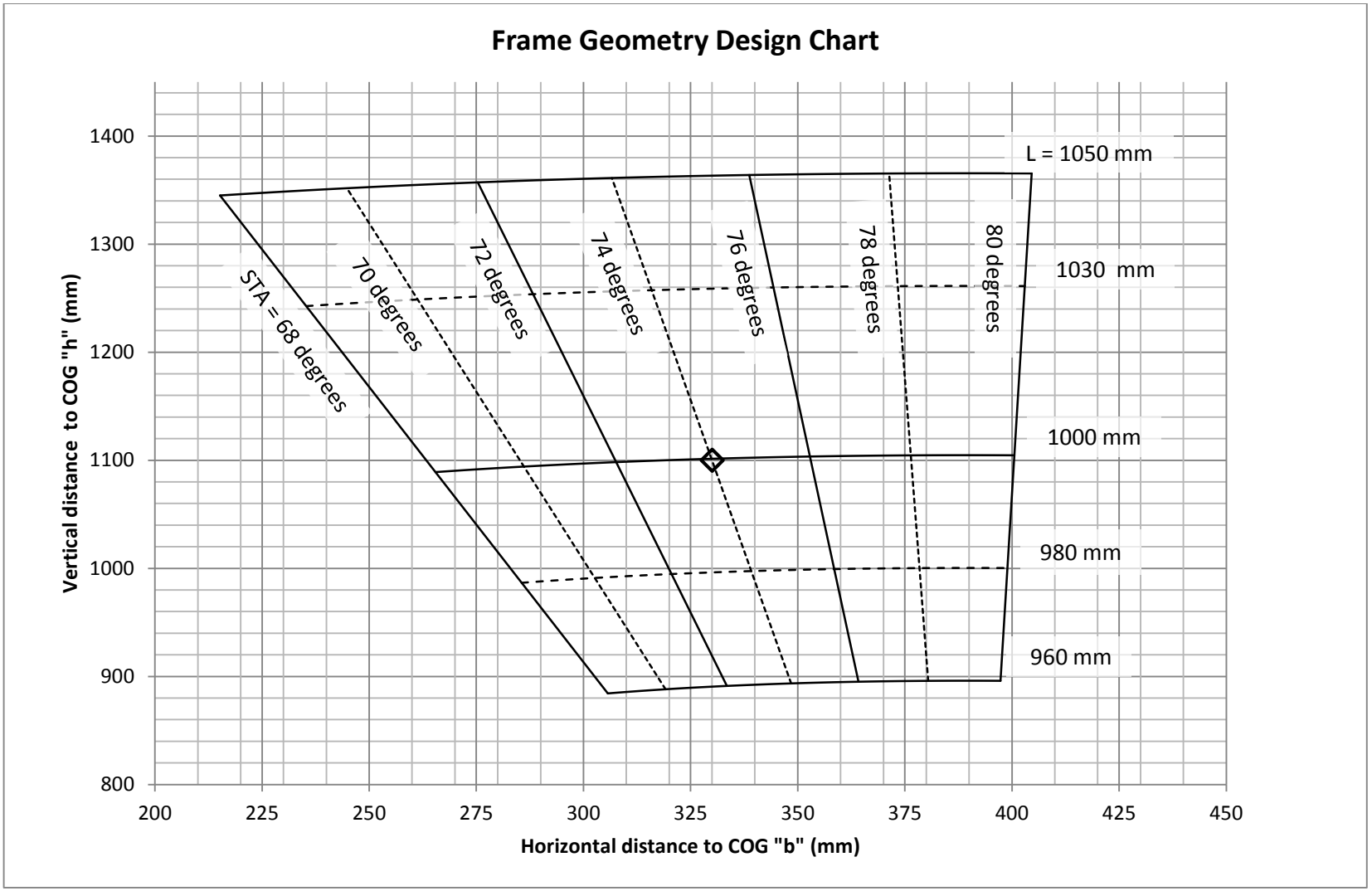

Figure 91 Frame Geometry Design Chart relating seat tube angle, wheelbase and mass position (distances b & h)

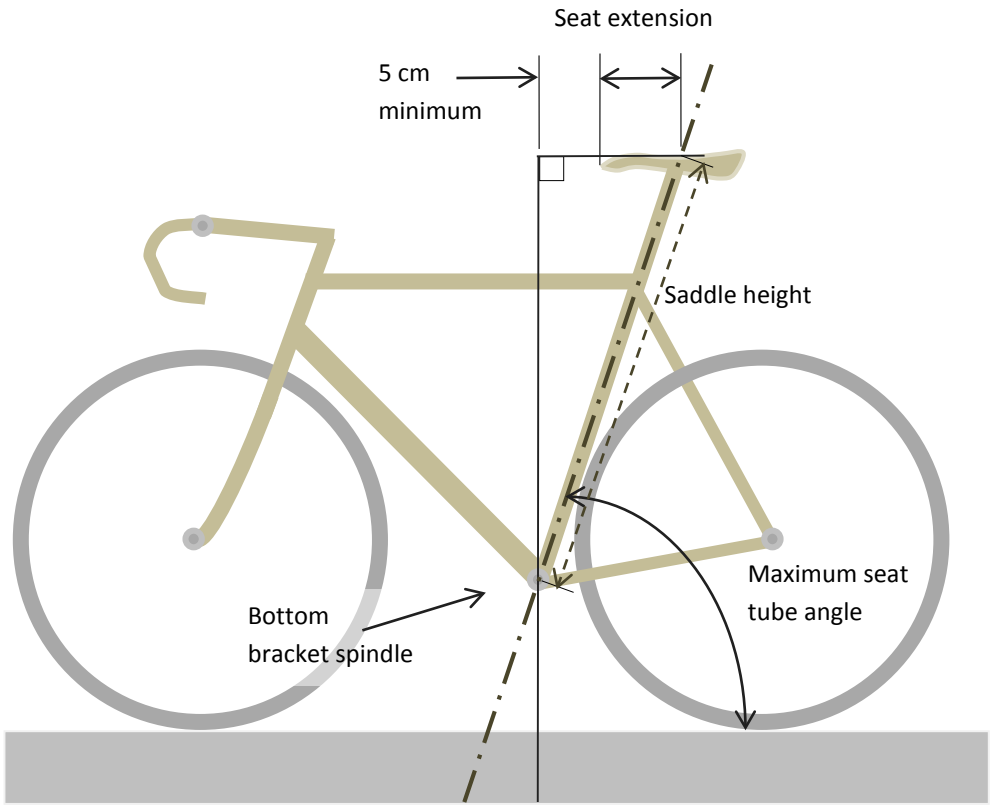

Figure 92 The UCI 5 cm rule defines the maximum seat tube angle permitted

6.4.4.2. TOE OVERLAP LIMIT

This second limit is an ergonomic consideration that is relevant to smaller riders. Toe overlap can be a significant problem for riders especially when frame sizes are below 52 cm and is commented in the literature (96, 97). When a pedal crank is in the 9 o'clock position a toe overlap exists if the front wheel overlaps the rider's toe. When the handlebar is turned this will contact the shoe and can cause the rider to lose control and crash, shown in Figure 93. The degree of overlap that can be tolerated seems to vary between individuals with some claiming no overlap at all is tolerable and others saying up to 25 mm is tolerable (96).

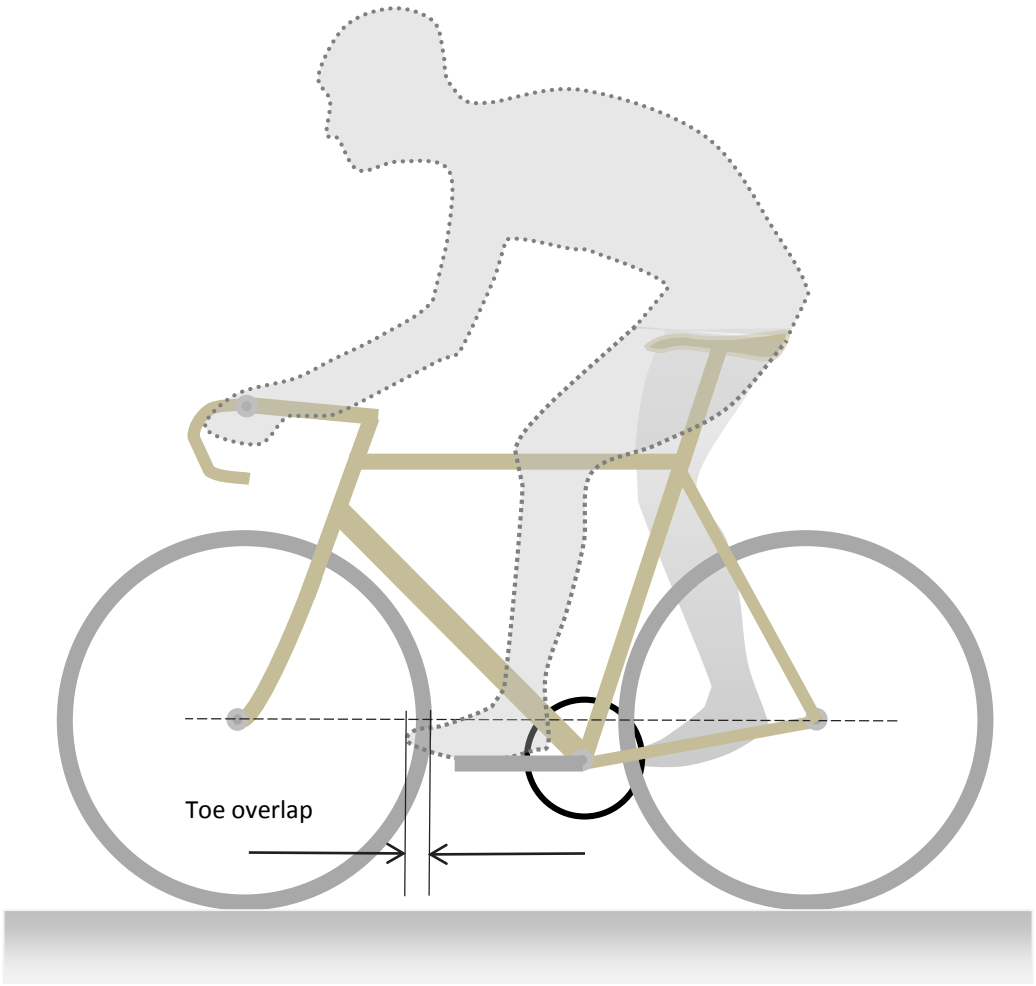

Figure 93 A toe overlap between the front wheel and shoe can exist for small bicycle frames

The amount of toe overlap that exists is determined by the steepness of seat tube angle and by how short the wheelbase is. In order to plot this second limit the saddle height has to be related to the wheelbase, which means combining a parameter determined by ergonomics (saddle height) with one that is not (wheelbase). The best way to do this is to recognise that the rider's inseam measurement determines saddle height and also determines the bicycle frame size, see Appendix B. Using the bicycle database (Appendix F) a relationship between the wheelbase and frame size was determined using the equation of the line of best fit. Combining these relationships makes it possible to determine the wheelbase (within a tolerance band) for a given saddle height. The equations and terms used to determine these values are given below in Table 35.

Table 35 Terms for wheelbase and saddle height relationship

Parameter	Symbol	Units
Wheelbase	L	mm
Frame size	FS	mm
Saddle height	P	mm
Rider inseam	IS	mm

The relationships derived fully in Appendix B are summarised below:

$$P = 0.885 \times IS \text{ (68, 69)} \tag{41}$$

$$FS = 0.65 \times IS \text{ (68, 69)} \tag{42}$$

Therefore:

$$IS = {}^{P}/_{0.885} \tag{43}$$

Substituting gives:

$$FS = 0.65 \times \frac{P}{0.885} \tag{44}$$

This gives:

$$FS = 0.735 \times P \tag{45}$$

Considering the 2013 Tour de France road bicycles in Appendix F, the empirical relationship between frame size and wheelbase was found and this gives the following equation, see Figure 124

$$L = 0.3077 \times FS + 822.5 \pm 20 \qquad R^2 = 0.652$$

(39)

For the benchmark bicycle with a 550 mm frame size this equation gives a wheelbase of 991.74 mm (-/+ 20 mm) or between 971.74 and 1011.74 mm) which is close to the chosen benchmark wheelbase of 1000 mm, see below.

$$L = 0.3077 \times 550\ mm + 822.5\ mm \pm 20\ mm$$

$$L = 991.74\ mm \pm 20\ mm$$

By substituting equation (45) for the saddle height P equation (39) becomes:

$$L = 0.3077 \times (0.735 \times P) + 822.5 \pm 20$$

(46)

Which gives the final equation necessary to find the toe overlap boundary:

$$L = 0.226 \times P + 822.5 \pm 20$$

(47)

To plot the toe limit line the following seven assumptions were used (explanations of these particular assumptions is given in Appendix B):

1. Actual wheel diameter D is 675 mm
2. Bottom bracket drop is 67.5 mm
3. Clearance between seat tube centreline and rear wheel is 32.5 mm
4. Crank length is 165 mm (measured experimentally)
5. Shoe extension in front of the pedal spindle centreline is 120 mm (measured experimentally)
6. Centreline of shoe is 130 mm from centreline of bicycle in a transverse direction (measured experimentally)
7. Maximum permitted overlap between wheel and shoe is 10 mm (96)

Using these equations and assumptions gives the toe overlap limit shown on the Design Chart in Figure 94. This final version of the Frame Geometry Design Chart includes a series of iso-handling lines (from 60 % to 160%) connecting points of constant 2% settling time. Again these iso-handling lines indicate equivalent settling times and show the important interacting effect of changing the position of the mass (h and b), the wheel base and the seat tube angle all on one Chart.

It has been claimed for a long time that a steeper seat tube angle means the bicycle is more compact and lively (but also less stable) (68, 69, 74, 75). But this Frame Geometry Design Chart is indicating that as the seat tube angle gets steeper the settling time actually increases which appears contradictory.

Perhaps what the literature is referring to is that a more favourable front wheel/rear wheel weight distribution is achieved as the seat tube angle steepens and this would mean the bicycle would have a lower moment of inertia about the yaw axis and so would be more easily turned about this axis. This investigation did not examine this aspect of bicycle dynamics and so this needs more study. But in terms of the Simulink impulse response it is clear that steeper seat tube angles cause settling times to increase.

This raises again the issue of what is desirable in terms of bicycle handling. Is it longitudinal stability meaning a high degree of self-stability and directional stability in a straight line? Or is it the speed of response and the ability to quickly take evasive action to avoid an obstacle? Is it predictability and the lack of unpleasant surprises such as sudden or increasing front wheel oscillations? Or is it a short settling time and the ability to settle down quickly after a disturbance? Finally is it a quick yaw response (the ability to corner) which is related to a low moment of inertia about the vertical axis road and the resistance of the tyres skidding sideways? It must inevitably involve a compromise of many of these attributes and of course will vary according to the type of bicycle and rider involved. This is an important area which needs close examination.

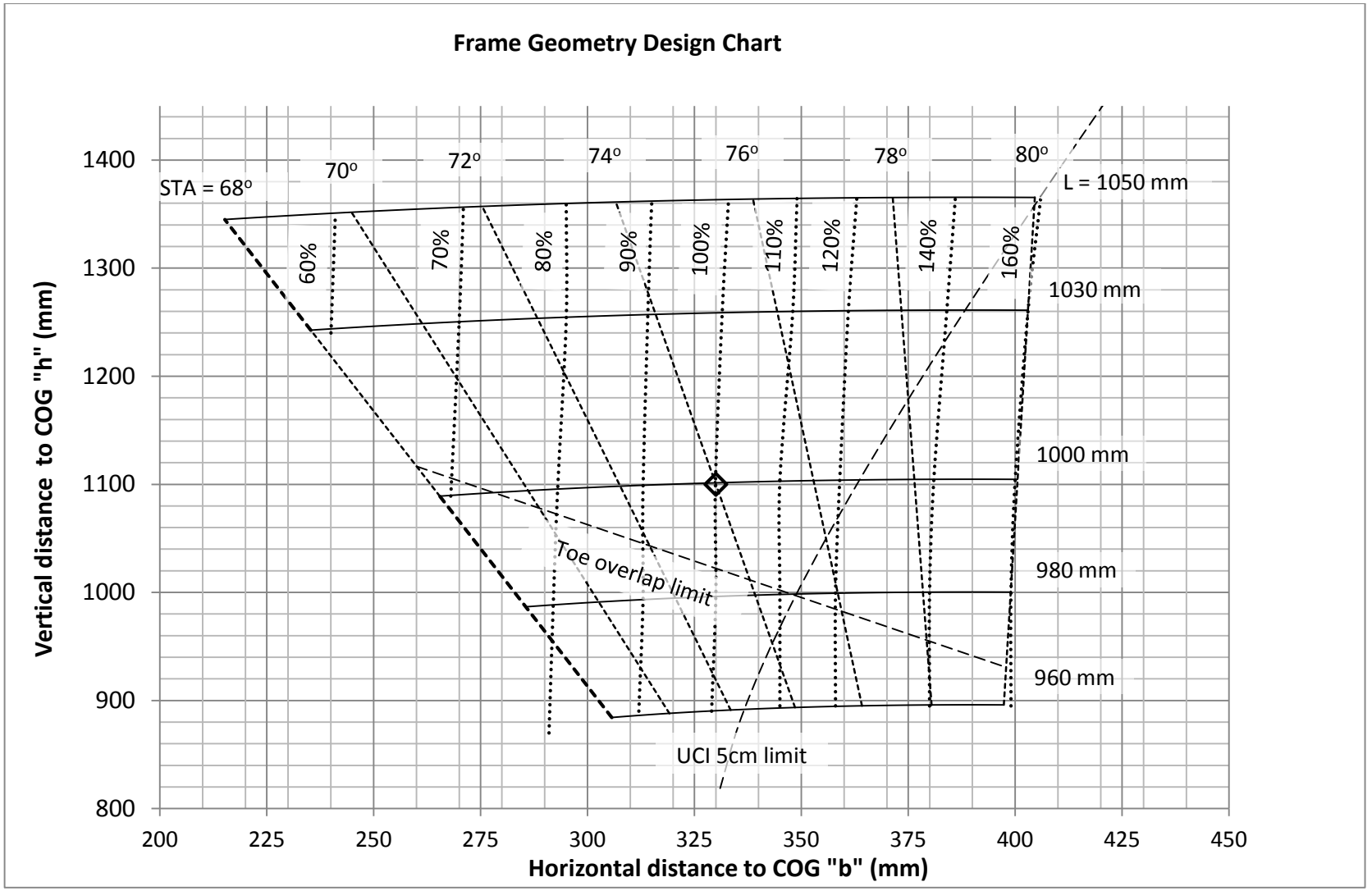

Figure 94 Frame Geometry Design Chart, indicating iso-handling lines, also UCI 5cm and toe overlap limits

6.4.5.MASS AND ROLL INERTIA DESIGN CHART

The fourth and last Design Chart examines the relationship between the bicycle's total mass (M), its vertical height (h) and the moment of inertia of rear assembly B about the roll axis (I_{XB}). This Chart completes the proposed design methodology and examines the last moderately significant parameter, mass. The sensitivity study shows that while the bicycle's mass is moderately significant, but both the mass vertical height and moment of inertia I_{XB} are not significant, see Table 36.

Table 36 Sensitivity of M, I_{XB} and h

Relevant design chart	Symbol	Parameter definition	Benchmark value/s	Units	C% change [1]	Comments
Mass and Roll Inertia Design Chart	M	Mass	80	kg	+1.98%	moderately significant
	h	Height of centre of mass	1.1	m	- 0.27%	not significant
	I_{XB}	MOI of B about XB axis (roll)	100	kgm^2	+0.11%	not significant
Note 1 C is the % change in the 2% settling time for each 1% increase in the parameter						

In order to draw this Chart it was necessary to find a way to easily calculate I_{XB}. After investigation it was found that a reasonable approximation was to assume that I_{XB} is equal to Mh^2 and this is justified in the following calculations. Consider a bicycle with a mass of 80 kg with a vertical height h of 1.100 m (i.e. the benchmark bicycle) if it is assumed that I_{XB} is equal to Mh^2 we get:

$$I_{XB} = Mh^2 \tag{48}$$

$$I_{XB} = 80(kg)1.1(m)^2$$

$$I_{XB} = 96.8\ kgm^2$$

A more complex calculation could assume that the parallel axis theorem applies and make use of the experimental values of Appendix C and Hanavan to give a second answer (48).

Table 37 Second moment of inertia values

Symbol	Parameter definition	Value	Units	Source
M_{Rider}	Mass of rider	73.0	kg	Chapter 4
h_{Rider}	Height of centre of mass of rider	1.100	m	Chapter 4
I_{XRider}	MOI rider about their centre of mass	8.0	kgm^2	(48)
$M_{Bicycle}$	Mass of bike (less forks & front wheel)	5.0	kg	Chapter 4
$h_{Bicycle}$	Height of centre of mass of bike (less forks & front wheel)	0.600	m	from experiments see Appendix C
$I_{XBicycle}$	MOI of bike (less forks & front wheel) about centre of mass of B	2.0	kgm^2	from experiments see Appendix C

Using the values in Table 37 we get:

$$I_{XB} = I_{Rider} + I_{Bicycle}$$

$$I_{XB} = (I_{Rider} + Mh^2) + \left(I_{Bicycle} + Mh^2\right)$$

(49)

$$I_{XB} = (8 + 73 \times 1.1^2) + (2 + 5 \times 0.6^2)$$

$$I_{XB} = 100.13\ kgm^2$$

This second answer of 100.13 kgm^2 is within 3.5% of the first calculated result of 96.8 kgm^2 and this shows that the use of Mh^2 is an acceptable way to find I_{XB}.

The completed Mass and Roll Inertia Design Chart in Figure 95 shows lines of constant mass height (h) drawn on a Chart plotting I_{XB} vs. mass. The iso-handling lines show the effect on handling caused by varying the mass and its height, clearly showing that while mass has a moderately significant effect on handling changing, height and moment of inertia have much less effect and are not significant.

Different vertical positions of the mass can be due to factors such as:

- changes in seat positions
- different front steering stem lengths and heights
- changes to the rider's posture
- the carrying of higher loads on the rider (such as water bottles, nutrition, back packs etc.)

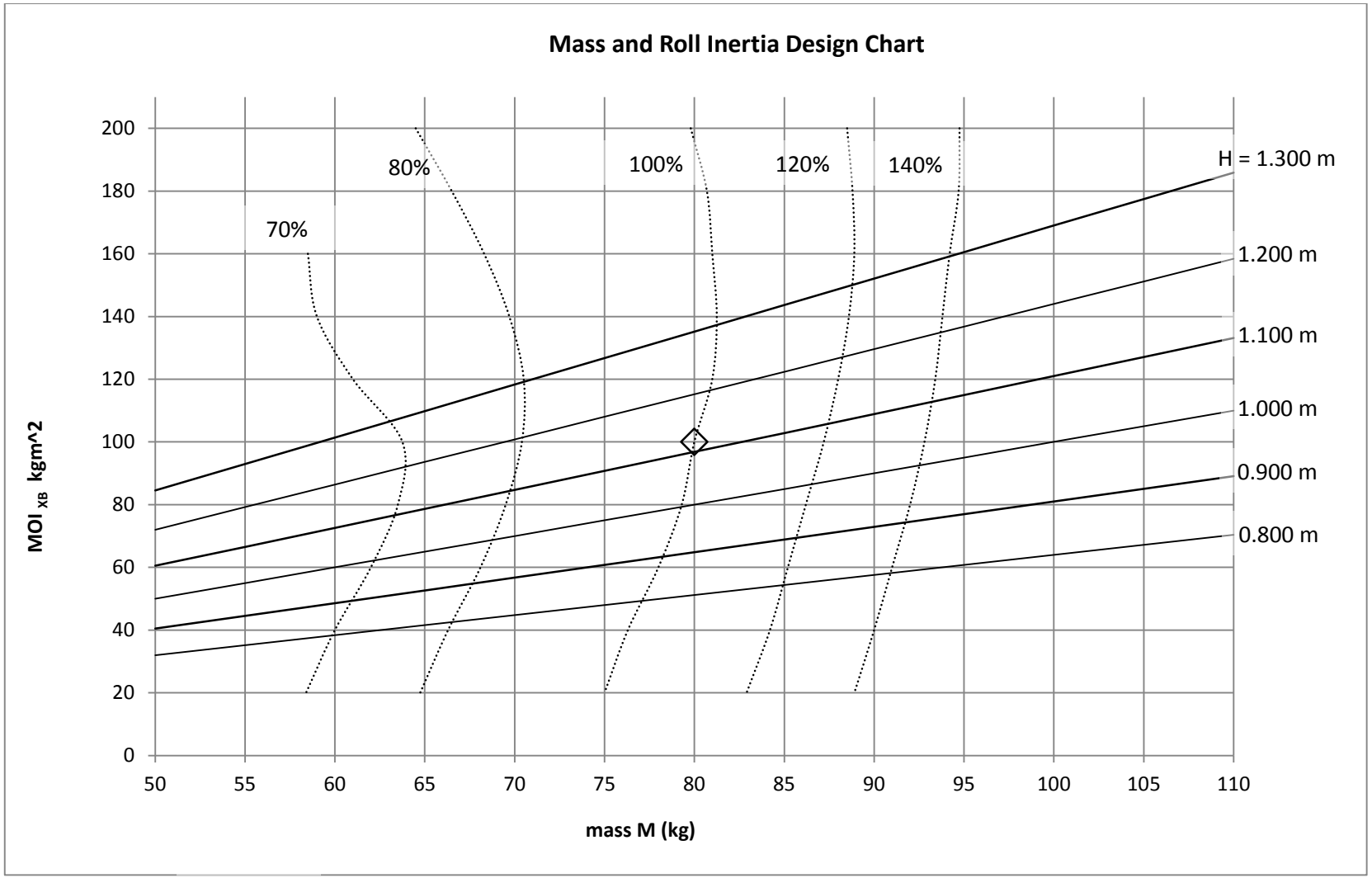

Figure 95 Mass and Roll Inertia Design Chart, for lines of constant mass height (h) also iso-handling lines shown

6.5. DESIGN CHART REMARKS

The four Design Charts described in this Chapter make use of the high level mathematical analysis of the Simulink model and present handling information (as iso-handling lines) in a way that is suitable for the bicycle fraternity to interpret. Use of these Design Charts allows bicycle designers to explore the implications of design choices with more confidence about the outcome than was previously possible.

These Charts study the key parameters shown to be the important ones affecting dynamic responses. Below they are ranked from 1st to 4th according to their parameter sensitivity and they can be used independently of one another or together and cover the important design areas of:

1. Steering geometry (head tube angle, rake and trail)
2. Wheel properties (wheel diameter and moment of inertia)
3. Frame geometry (vertical and longitudinal position of the mass and wheelbase)
4. Mass and roil inertia (mass and moment of inertia of B)

The main advantages of these design charts are:

- they are scientifically based and justified
- they are relatively easy to use with the minimum of calculations required
- they enable a wider audience the ability to understand the design process and its outcomes
- they allow several parameters can be concurrently considered, so interactions can be studied

While their main disadvantages are:

- assumptions have to be clearly known and adhered to
- design boundaries may be hard to define and so unsafe designs may be produced (they are not necessarily conservative)

The next Chapter will consider how modern road bicycles fit onto the Charts, as represented by bicycles from historical approaches and by the 2013 Tour de France race. This will validate the Charts and illustrate their application and value.

Now that these Charts have been developed it is intended to seek comments from the bicycle fraternity including manufacturers to see how useful these design charts will in practice be to industry. Of course it is hoped they will prove of value and be easy to use and interpret.

7. DESIGN CHART VALIDATION

7.1. INTRODUCTION

This Chapter examines the validity of the four Design Charts proposed in Chapter Six. It was felt that the best way to do this was to apply the Charts to actual bicycle designs, first considering historical design practice and secondly by examining the bicycles that competed in the 2013 Tour de France (TdF) bicycle race.

Historical design practice is of particular interest for the following reasons:

- does the accepted “design lore of bicycles” say the same sorts of things about bicycles that the Charts indicate?
- and is there evidence of the sort of design evolution occurring over time that is predicted by the Charts?

And examining the 2013 Tour de France bicycles means that:

- the predictions of the Design Charts can be compared to the decisions made by designers of the latest top level bicycles
- the variations between different elite bicycle manufacturers can be examined with the Charts and any performance differences quantified
- it should be possible to see how close individual designs get to the various Chart limits

The specifications of the bicycles examined (both the historical and TdF bicycles) were obtained from cycling literature such as magazines, books, textbooks and websites. The sort of information required included details of wheelbase, wheel diameter, head tube angle, fork rake, frame size and seat tube angles. Information about two secondary parameters, frame size and seat tube angle were included, because even though they are not part of the Simulink mathematical model, they are commonly used within the industry.

7.2. HISTORICAL DESIGN PRACTICE

This section summarises the historical practices of manufacturers and designers regarding their bicycle design practice. By comparing their practices with the Design Charts, judgements can be made as to the validity of the Charts. How have bicycles changed over recent years and what have been the trends in design? Do the Charts and in particular their iso-handling lines make sense in terms of what the historical commentary says about bicycle performance?

Most manufacturers rely heavily on past practises, for example when referring to some recent work done by Schwab to improve bicycle geometry the Dutch manufacturer Batavus was reported as saying *“we had been using a trial and error system, this is the first chance we have had to do it a scientific way* (9).”

To find out about historical practice, the available literature was reviewed, focussing on the comments from elite riders and manufacturers. After reviewing their ideas and recommendations the following general observations were noted:

- while there was reasonable agreement on the head tubes angles (ranging between 71.5 and 76 degrees) there were wider variations suggested for the rake and trail values (40 to 67 mm and 33 to 60 mm respectively)
- reasonable agreement existed as a suitable seat tube angle range (between 71.5 to 76 degrees)
- but it is interesting that there was little acknowledgement of the UCI 5 cm or toe overlap limits by many sources
- most sources were silent on a wheelbase recommendation, which is interesting given that the sensitivity study rates wheelbase as a moderately significant parameter

Covering their views in more detail with regards to steering geometry, it is commonly believed that:

- the head tube angle is an important angle that defines the steering geometry and most suggested it should be between 72 and 74.5 degrees (10, 83)
- steeper head tube angles give faster handling (74, 75)
- also different types of bicycles require different steering geometries:
    - racing bicycles (such as those used in the Tour de France) require steep head tube angles (74, 83, 90)
    - and racing bicycles dedicated for climbing steep roads can use even steeper head tube angles with less rake (74, 75)
    - criterium bicycles (used for specialised road racing on tight street circuits) require quick handling around tight road circuits and have very steep head tube angles of up to 75 degrees with small fork rakes of 38 mm or less, resulting in trails of less than 50 mm (74)
    - time trial bicycles (used by individual riders racing against the clock) can make use of shallower head tube angles for more stability (74)
    - track bicycles (racing on banked, oval velodrome tracks) need slightly steeper head tube angles (98)
    - touring road bicycles (used for travelling over long distances on multiday camping trips) have the greatest need for stability and comfort and use shallower head tube angles (99)
- An argument was made by some for neutral handling where the bicycle would be neither twitchy nor sluggish; rather it would handle in a stable way. It was claimed that this occurs with a combination of rake and head tube angle that yield a 60 mm trail (91, 98).

With regards to frame geometry (and the associated wheelbase and seat tube angle parameters) it is commonly believed that:

- longer wheelbases and shallower seat tube angles are more comfortable (83, 90)
- regards the desired weight distribution (which is affected by both the wheelbase and the seat tube angle) two sources recommend a 45/55 front to rear weight distribution for the best handling, but no justification for this was provided (75, 100).
- but it is believed from: experimental work, Simulink model and Design Charts that this 45/55 ratio is not physically possible for conventional road bicycles, for example the benchmark bicycle has a 33/67 distribution and to achieve a 45/55 distribution the centre of mass would need to move forward by 120 mm, a distance which would be impossible to achieve on the BM bicycle
- steeper angles, shorter wheelbases and shorter fork rakes all make frames more rigid, stiffer and improve the ride and power transmission (75)
- also steeper seat tubes tend to shorten the wheelbase and make the bicycle more responsive (69)
- smaller frames need steeper seat tube angles to keep the wheelbase short (83)
- it was claimed that shorter riders have a proportionally shorter upper bodies and so need to be placed further forward over their pedals by using steeper seat tube angles (69).
- but the real reason may be that the almost universal use of stock 700C wheels which forces designers to squeeze everything together on a small bicycle in order to achieve an acceptably short wheelbase and top tube (101).
- different types of bicycles have different frame geometry requirements:
    - track bicycles need steeper seat tube angles and shorter wheelbases (69, 74, 90)
    - racing bicycles require moderately short wheelbases and steep seat tube angles (74, 83, 90)
    - touring road bicycles with a need for stability and comfort use shallower seat tube angles and longer wheelbases (74)

Pedalling efficiency is said by some to be affected by the seat tube angle:

- according to LeMond, seat tube angles of 74 degrees or less are required for efficient pedalling (69)
- but Ballantine says seat tube angle is partly determined by the length of the rider's thigh, so smaller bicycles have steeper seat tube angles (74)

- the Association of British Cycling Coaches (ABCC) gives the following formula to find the correct seat tube angle, to the nearest 0.5 degree (102)

$$Seat\ Tube\ Angle = \cos^{-1}\frac{(0.264 \times thigh\ length)}{lower\ leg\ length} \quad (50)$$

  For a benchmark rider (with a 184 cm height) with a thigh length of 62.5 cm and a lower leg length of 55.6 cm this becomes:

$$Seat\ Tube\ Angle = \cos^{-1}\frac{(0.264 \times 62.5)}{55.6} = 72.75\ or\ 73\ degrees$$

  Note that the benchmark bicycle has a seat tube angle of 74 degrees. This ABCC method is clearly anatomically based and is related to pedalling efficiency and not to any handling requirements. Pedalling efficiency is an interesting issue in its own right with many factors coming into play. To the author's best knowledge no agreement exists as to how best to measure this efficiency. The best available guides are those of Hinault and LeMond but these are over 25 years old, it seems that coaching advice on this issue remains a closely guarded secret (68, 69).

- Ricard et al compared the effect of different seat tube angles on triathletes' performances and concluded that increasing the seat tube angle from 72 to 82 degrees did not improve cycling power output but did improve running times on the next leg of the race. They recommended a seat tube angle for triathlon bicycles of at least 76 degrees (103).
- other researchers have claimed that triathletes using higher seat tube angles up to 80 degrees outperformed those with lower angles during the cycling leg of the race (104)
- and this is supported by the design of Boardman's Lotus 108 bicycle which had an effective seat tube angle of 80 degrees when used to break the One Hour Record in 1996 by covering 56.375 km in 60 minutes (83)

There is close agreement between these sources on the head tube angles and seat tube angles, but it surprising to see such a variation in the rake and trail values which have been shown to be so critical to the performance of the bicycle. The main recommendations for parameter values for road bicycles from these various sources are summarised in Table 38. By plotting these recommendations on the Steering Geometry and Frame Geometry Design Charts (see Figure 96 and Figure 97) it is possible to see what agreement exists between these sources and also to identify on these Charts what regions are regarded historically as desirable design envelopes.

From the plotted regions on the Design Charts in Figure 96 and Figure 97 it is clear that the recommendations are varied and have an arbitrary appearance, but perhaps this is to be expected given their empirical origin. People will have had different experiences and opinions as designers and riders and will also have different subjective responses to the same bicycles.

Table 38 Historical design practice [1]

Head tube angle degrees	Seat tube angle degrees	Rake mm	Trail mm	Wheelbase mm	Iso-handling line from Chart %	Source
72 to 74.5					N/A	(68)
72.5 to 74.5	71.5 to 74				N/A	(69)
73 to 76	72 to 76	40 to 45	43 to 54	980	65% to 100%	(74)
73 to 74		50 to 67	33 to 51		55% to 85%	(52)
72 to 74	72	47 to 50	45 to 60	1015 to 1065	70% to 110%	(75)
71.5 to 72.5	74 to 74.5				N/A	(105)
73.2		40	60		110%	(98)
71.5 to 76	71.5 to 76	40 to 67	33 to 60	980 to 1065	55% to 110%	**range of values**

Note 1 includes road, criterium, track, time trail and triathlon racing and touring bicycles

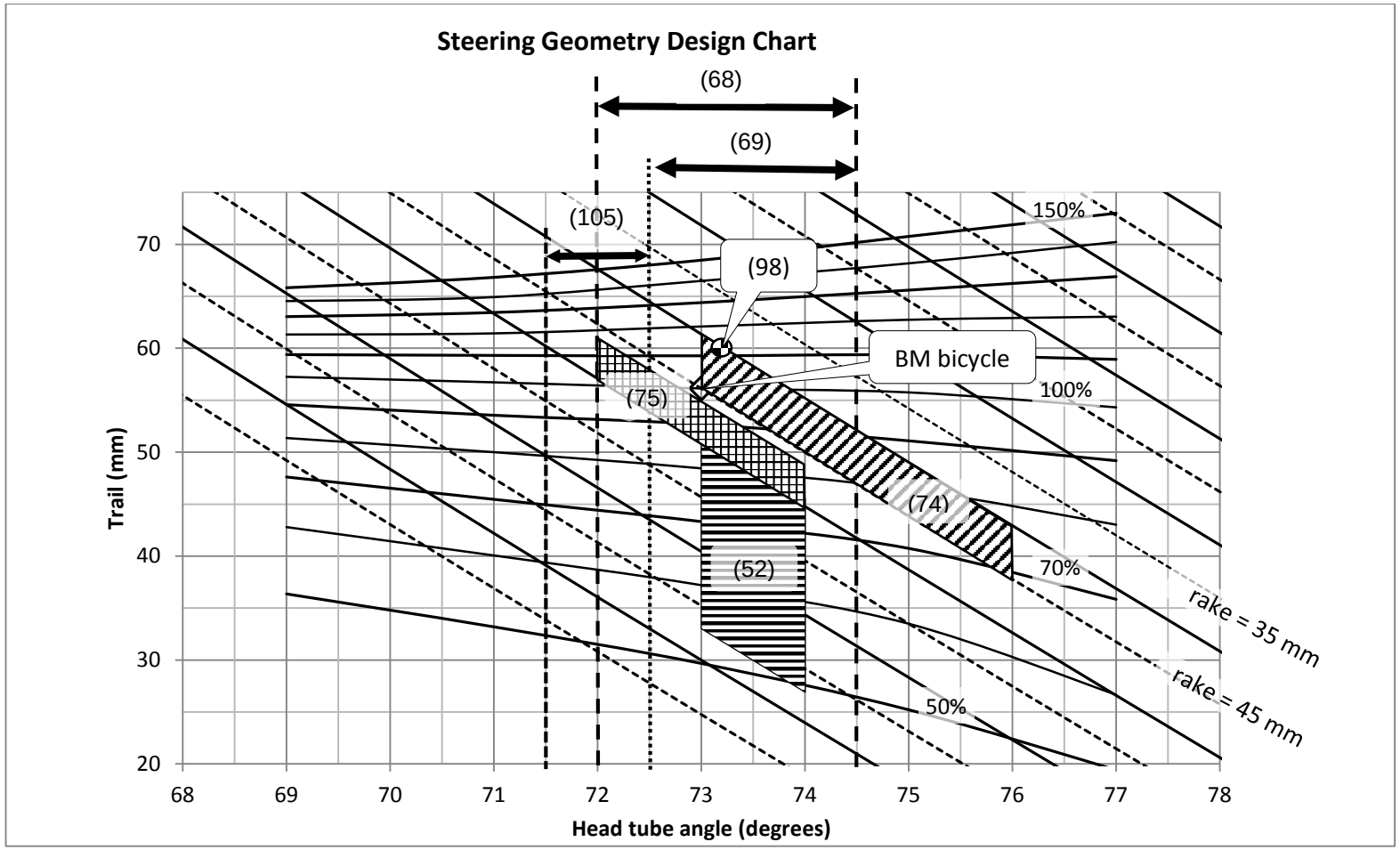

Figure 96 Steering Geometry Design Chart, indicating Table 38 recommendations, reference numbers are in brackets, see bibliography

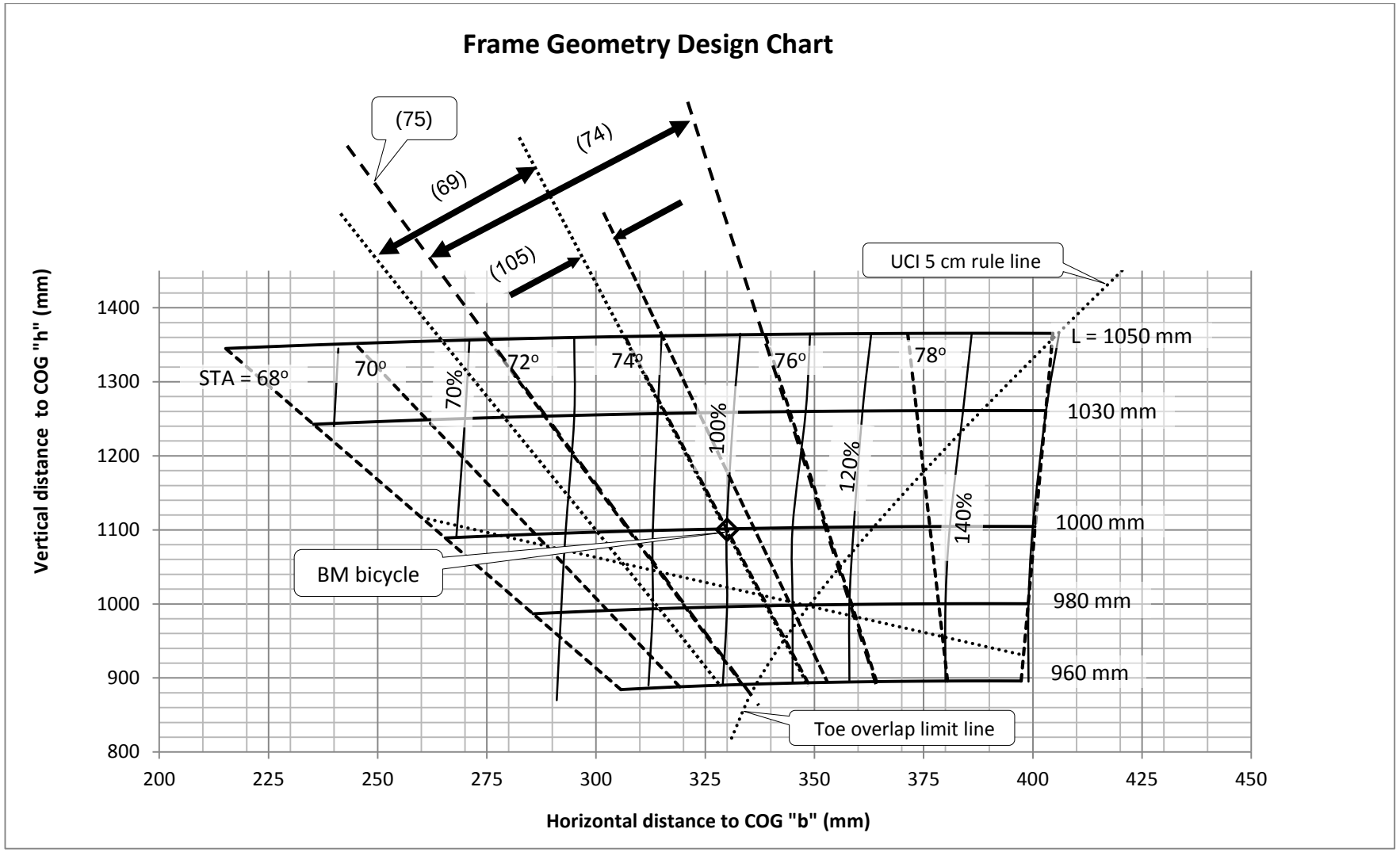

Figure 97 Frame Geometry Design Chart, indicating Table 38 recommendations, reference numbers are in brackets, see bibliography

Finally by comparing three bicycles from different eras (1930, 1950 and 2013) it was interesting to see how frame geometry has changed over eighty years, see Table 39. Steeper angles are now used along with shorter wheelbases and a reduction in trail has also occurred. We can see that seat tube angles over this time have gone from 68 degrees to 73.5 degrees, a 5.5 degree increase. Trail dropped from 70 mm to 47.15 mm and then rose to 59 23 mm (overall a 10.77 mm decrease). While the wheelbase has changed dramatically going from 1170 mm to 984 mm, a 186 mm reduction.

According to the Design Charts this would mean a significant reduction on settling time (and an increase in responsiveness). Comparing the 1930 English custom racing bicycle to the 2013 Bianchi Oltre and just allowing for the steering geometry changes the Oltre has 39% less settling time (180% vs. 110%). But when looking at the frame geometry the Oltre has 100% more settling time (100% vs. 50%) according to the Charts. So the change in steering geometry is compensated somewhat by changes in frame geometry showing the effect of interaction.

Kossack comments that what was once considered acceptable only for track bicycles has over time become acceptable for road bicycles and this is due to the big improvements in road surfaces. This has made the handling more responsive (75).

Table 39 Comparison of bicycles from 1930 to 2013 (75, 106, 107)

Bike	**Head tube angle degrees**	**Seat tube angle degrees**	**Rake mm**	**Trail Mm**	**Wheelbase mm**
1930 English custom racing bike	68.0	68.0	64.0	70.0	1120 to 1170[3]
1950 Bianchi 54.5 cm frame [1]	72.0	72.5	52.5	47.15	1020 to 1050 [3]
2013 Bianchi Oltre 55 cm frame [2]	72.5	73.5	45.0	59.23	984
Note 1 used by Coppi to win the 1950 Paris-Roubaix race					
Note 2 used in the 2013 TdF					
Note 3 different wheelbases were necessary as adjustments were used to tighten up the chain					

7.3. TOUR DE FRANCE 2013 BICYCLES

This next section considers the elite group of high performance road bicycles and riders that participated in the 2013 edition of the Tour de France (TdF) bicycle race which were chosen because:

- they participated in the world's most prestigious bicycle race and so they will have been designed with only the best performance in mind
- the different bicycle manufacturers represented at the TdF supplied their best bicycle design from their product ranges, the designs which best showcased all their knowledge and experience at this influential event

Validation of the Charts requires the parameter values of these elite bicycles to be compared using the Design Charts and this section asks the following questions:

- how do the latest designs measure up with regard to the handling predictions of the Design Charts?
- what are the differences in performance between the different manufacturers' designs?
- how close to the Design Chart limits do these bicycles get?

The Tour de France (TdF) is the pre-eminent international cycle race and is one of the three grand tours of road racing, the others being the Giro d'Italia (Tour of Italy) and the Vuelta a Espana (Tour of Spain) (108). These three races represent the pinnacle of international road cycle racing with the elite of professional cyclists competing. The 100th anniversary edition of the Tour de France road cycling race began on 29 July 2013, when 219 riders from 22 professional teams started from Porto-Vecchio in Corsica and it finished 23 days and 3400 km later in Paris with169 finishers.

The Tour is legendary for its gruelling, unforgiving nature and the toll it takes on the cyclists. *"I had always heard the Tour de France was hard, but that's when I realised it required an unimaginable level of strength, toughness and suffering"* a quote from Tyler Hamilton (multiple TdF rider) referring to a typical hard day in a recent Tour (109).

The 2013 TdF race was won by Chris Froome riding for the Sky Procycling Team and he averaged 40.6 km/hr over 21 days of racing (110). The group of TdF bicycles examined includes nearly all 30 models ridden by all 22 participating TdF teams. The bicycles and their respective teams are listed in Table 40. By examining these bicycles it should be possible to see what range of parameter values are considered desirable by the world's best manufacturers and riders. In order to do this it was first necessary to obtain a complete list of specifications for each model. Most of this information was obtained directly from manufacturers' official websites or specialist sector sources and where specifications were missing, it was possible by using other known dimensions to determine them either by calculation or by completing full size drawings.

It is variously estimated that there are about 1 billion bicycles in use in the world and about 20% of these could be classified as road bicycles. So the total market is large at about 200 million road bicycles, the balance being mainly mountain bicycles and hybrid bicycles.

Table 40 Tour de France 2013 teams and bicycles

No	Bicycle manufacturer	Bicycle model [1]	TdF Team 2013
1	BH	G6 Ultegra D12	Sojasun
2	BH	Ultralight Ultegra D12	Sojasun
3	Bianchi	Oltre	Vacansoleil-DCM
4	BMC	Teammachine SLR01	BMC Racing Team
5	BMC	Timemachine TMR01	BMC Racing Team
6	Cannondale	Supersix Evo	Cannondale
7	Canyon	Aeroad CF 9.0	Katusha Team
8	Canyon	Ultimate CF SLX	Katusha Team
9	Cervelo	R5	Garmin Sharp
10	Cervelo	RCA	Garmin Sharp
11	Cervelo	S5	Garmin Sharp
12	Colnago	C59	Team Europcar
13	Felt	F2 [2]	Team Argos-Shimano
14	Focus Bikes	Izalco Team SL Carbon	AG2r La Mondiale
15	Giant	Propel	Belkin Pro Cycling
16	Giant	TCR Advanced	Belkin Pro Cycling
17	Lapierre	Ultimate di2	FDJ.FR
18	Lapierre	Xelius Efi 800	FDJ.FR
19	Look	695 Aerolight	Cofidis Solutions Credits
20	Merida	Sculptura SL 909	Lampre-Merida
21	Orbea	Orca	Euskatel-Euskadi
22	Pinarello	Dogma 65.1 Think 2	Sky Procycling, Movistar
23	Ridley	Helium SL	Lotto-Belisol
24	Ridley	Noah FAST	Lotto-Belisol
25	Scott	Addict SL	Orica-Greenedge
26	Scott	Foil 40	Orica-Greenedge
27	Specialized	Tarmac SL 4	Astana Pro team, Team Saxo-Tinkoff [3] & Omega Pharm-Quick Step
28	Specialized	Venge	Team Saxo-Tinkoff & Omega Pharm-Quick Step
29	Trek	Domane 6.9	Radioshack-Leopard
30	Trek	Madone 7.9	Radioshack-Leopard
Note 1 includes all 30 models ridden by all 22 TdF teams, excepting Note 2			
Note 2 the Felt F1 model used is not available commercially and the only information available was for the Felt F2 model, which was said to be very similar to the F1			
Note 3 Saxo Tinkoff changed their name to Tinkoff Saxo in 2014			
Sources (108, 110)			

It seems that manufacturers are releasing less information about their bicycles' geometry than was common in the past. From a review of internet discussion forums this is frustrating to many riders (who wish to compare bicycles in detail before making their purchases) and it is hard to know why manufacturers are doing this.

In many cases manufacturers supplied two different models of their top bicycles for each TdF team.

- a very lightweight bicycle for the mountain stages, which makes it easier to climb as mass dominates
- and another more aerodynamic model for the individual time trial stages (where lone riders race against the clock) were aerodynamic drag dominates
- each rider had at least three individual machines allocated to them and the TdF "road train" included over 650 bicycles (costing close to 10 million NZD) as well as team cars and buses

7.3.1. MEDIUM SIZED BICYCLES

This first part of the analysis considers only the medium size TdF bicycles from each manufacturer, where medium size is defined as being the bicycle from each manufacturer as close as possible to a traditionally measured 550 mm frame. These medium sized bicycles were looked at first because they avoid the extreme parameter values of the large or small frames.

As there is no universal sizing system for bicycles and also because not all manufacturers supply the same sizes across their range, it was necessary to use a variety of ways to select a suitable medium sized bicycle from each manufacturer. Where conventional frame size information is provided by manufacturers it is used directly in this section. Where it was unavailable, best endeavours have been made to use other information (such as stack and reach dimensions) to choose equivalent sized bicycles from the manufacturers' ranges to allow a fair comparison to be made. The process used for selection is as follows:

- where a manufacturer defined their frame sizes (FS) in the traditional manner, a 550 mm bicycle was chosen or the next closest size (either a 540 or 560 mm)
- where stack dimensions only were given (Figure 13) a stack dimension as close as possible to 565 mm was chosen
- in a few remaining cases a best judgement decision was made after comparing a number of dimensions, to choose the frame closest to the medium size

After selection of this medium sized group, consideration was given was to how well they aligned with the Design Charts. First each bicycle was plotted onto the Steering Geometry Design Chart and this is shown in Figure 98. The plotted crosses indicate the 30 medium sized Tour de France 2013 bicycles (from Table 72 of Appendix F) with the diamond marker indicating the benchmark bicycle.

It can be seen that these bicycles lie closely along a line centred along the 45 mm rake line and it is noted that:

- they are spread plus/minus 5 mm each side of the 45 mm rake line
- the minimum trail of 44.7 mm (with a HTA 73.5 degrees) is for the Orbea Orca model
- the maximum trail of 63.4 mm (with a HTA 72.5 degrees) is for the BMC Teammachine
- the iso-handling lines range from 75% for the Orbea Orca to 125% for the BMC Teammachine
- meaning a 67% increase in the settling time of the front wheel after a sudden disturbance for the BMC bicycle compared to the Orbea
- this variation would make these two bicycles handle quite differently but obviously a 67% difference has been found to be acceptable even at this elite level.

Consideration of this information helps to further define the approximate design envelope that was sketched earlier in Figure 54 and it is concluded that it is acceptable to have variations of settling time plus/minus 25% compared to the benchmark bicycle (or between 75% and 125%) a 67% difference overall between the slowest and fastest settling time. Interestingly this design envelope overlaps major parts of three separate envelopes proposed independently by Wilson, Ballantine and Kossack (and previously shown in Figure 96) which is strong additional evidence that this region of the Chart produces successful designs (52, 74, 75). It should be noted that the boundaries of this design envelope are not precise at all and further work is required to really understand what happens to handling when the boundaries are exceeded. For example, it may be possible to identify which regions contain specific modes of instability, but at the moment this is not known.

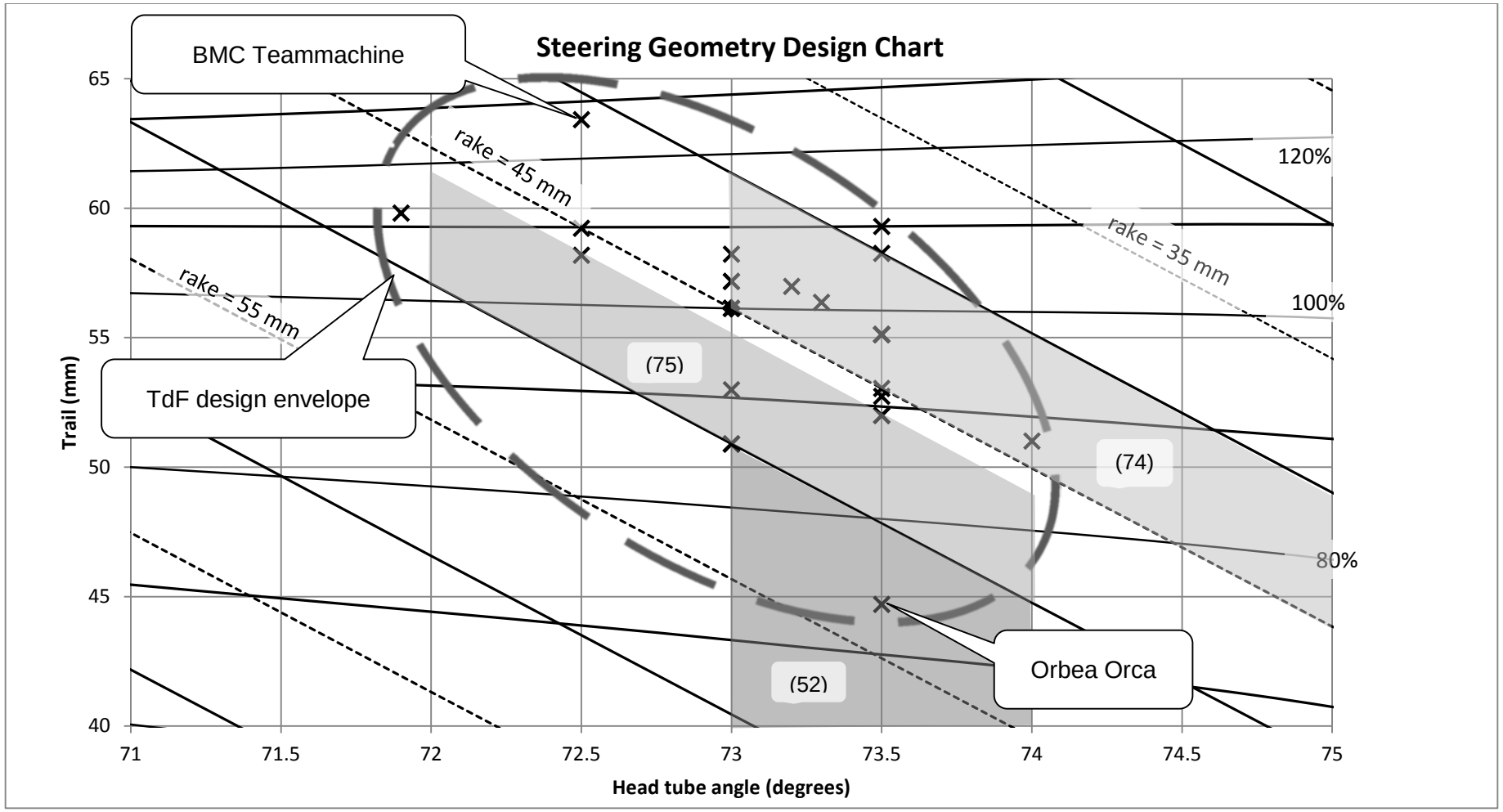

Figure 98 Steering Geometry Design Chart, indicating the 30 medium size bicycles models from the 2013 TdF (675 mm wheel dia), reference numbers are in brackets, see bibliography

7.3.2.THE FULL BICYCLE SIZE RANGE

The second part of this section considers how TdF bicycle geometries change across the entire size range. How do manufacturers treat the geometries of their smallest bicycles compared to their largest and are there any common trends evident amongst the manufacturers?

Eight 2013 TdF manufacturers provided enough information for this type of analysis to be done and their information is listed in Appendix F and this includes ten model ranges and 69 individual bicycle products. The remaining eleven TdF manufacturers were not included as their published specifications lacked the necessary details.

We will first consider the following three manufacturers in detail before considering all the models together.

1. Pinarello (a past and current winner of the TdF) is of interest because of some unique geometry
2. next Orbea is examined, also possessing an alternative and unique geometry
3. and finally Cannondale is considered as being representative of the majority of manufacturers

Pinarello is one of the most prestigious names in bicycle manufacturing and racing and was founded in 1952 and is based at Treviso in northern Italy. Famous for its success in racing, it has had the winning bicycle in 11 TdF races since 1988, including the 2013 Tdf where in addition to 1st place, Pinarello secured the 2nd and 8th places.

Pinarello has 13 sizes in its top of the line Dogma TdF model, with sizes ranging from 420 mm to 620 mm. Compare this to other manufacturers, most of whom only have 6 to 9 sizes in their ranges. Pinarello obviously places great importance in getting as perfect fit as possible for each rider by providing the greatest possible choice in sizes. They are also the only manufacturer who increases the front wheel trail value as frame sizes get larger while decreasing the head tube angle. All others do the opposite, that is they decrease trail for their larger frames, see Figure 99 and Table 41. The reason why Pinarello does this is not known and this means that the Pinarello larger sizes will have longer settling times. This is interesting because larger frames inherently have longer settling times due to their larger b and M values.

The second manufacturer Orbea is based in Mallabia in the Basque part of Spain and was founded in 1840, originally as a rifle and gun producer. Orbea began manufacturing bicycles in the 1930s and is part of the famous Mondragón Corporation, a workers' co-operative run on unusual ownership lines. Orbea bicycles have had great success in road, mountain bicycle and triathlon racing and have won world championships and Olympic medals. Orbea has a similar geometry to the other manufacturers, in that as the frames get larger, the head tube angles get larger, the seat tube angles smaller and the trail gets smaller. But Orbea is unusual because their rake gets larger with larger frames unlike all other manufacturers in this group, see Figure 99 and Table 41.

The third manufacturer Cannondale is the American division of Canadian Dorel Industries and was founded in 1971. Its bicycles are manufactured in China and Taiwan but its headquarters are in

Connecticut USA. Cannondale was a pioneer in introducing aluminium bicycle frames to the market but now makes many carbon fibre bicycles as well. They have been participating at the top level of road racing for many years and have been very successful. Their approach to frame geometry is representative of the majority of manufacturers at the top level. As Cannondale frames get larger, head tube angles get larger, seat tube angles get smaller and trail decreases, also Cannondale uses one rake dimension across its size range (which is not uncommon amongst manufacturers) see Figure 99 and Table 41.

The Steering Geometry Design Chart in Figure 100 plots individual bicycle types from all eight 2013 TdF manufacturers (covering ten model ranges) to clearly show overall how geometries vary with frame size as shown in Table 41. Note that because Specialized's "Tarmac" and "Venge" models have nearly identical geometry they were only plotted once per frame size (not twice).

The large range of TdF parameter and iso-handling values shown in Table 42 that quite a difference exists as to what sort of handling is considered desirable and different strategies employed amongst these manufacturers. The settling times vary from 75% to 160% compared to the benchmark bicycle and quite a range in the critical trail parameter is apparent (from 44.696 mm to 70.733mm).

It is interesting to compare this TdF group with the historical practise (discussed earlier in this Chapter) as they have many similarities and this is shown in Table 43. Considering two critical measures (trail and settling times) the TdF have a slightly wider range, which is interesting. Perhaps it would be expected that for such elite bicycles a tighter range would have occurred and there would be more agreement amongst the manufacturers than is actually evident.

The strategies of these TdF manufacturers are summarised in Table 41 and it can be seen that six manufacturers (Cannondale, Focus, Look, Specialised, Trek and Trek) have the same broad strategy, as their frames get larger the following changes occur:

- head tube angles get steeper
- seat tube angles get shallower
- trails decrease
- and rakes either don't change or get smaller
- most manufacturers use one rake size though Specialized and Orbea use two and Trek and Felt use four rake sizes
- where rake does change it remains the same across several frame sizes and then jumps to the next value rather than increasing progressively
- perhaps manufacturers prefer to keep only a few standard fork rakes and choose to vary the geometry by adjusting the head tube angle to achieve the desire outcome

The main exceptions to this strategy are Orbea and Pinarello

- for Orbea the rake gets larger (not smaller) as frames sizes increase
- Pinarello's larger frames have larger trails, a significant difference
- also Pinarello head tube angles get smaller and seat tube angles get larger the opposite of all the seven others

Table 41 Manufacturers' trends as frame sizes increase

Manufacturer	Head tube angle	Seat tube angle	Rake	Trail
1. Pinarello	gets smaller	gets larger	no change in size	gets larger
2. Orbea	larger	smaller	larger, 2 sizes	smaller
3. Cannondale	larger	smaller	no change	Gets smaller
4. Focus Bikes	larger	smaller	no change	smaller
5. Look	larger	smaller	no change	smaller
6. Specialized	larger	smaller	smaller, 2 sizes	smaller
7. Trek	larger	smaller or same	smaller, 4 sizes	smaller
8. Felt	larger	smaller	smaller, 4 sizes	smaller
exceptions to the general trends are underlined				

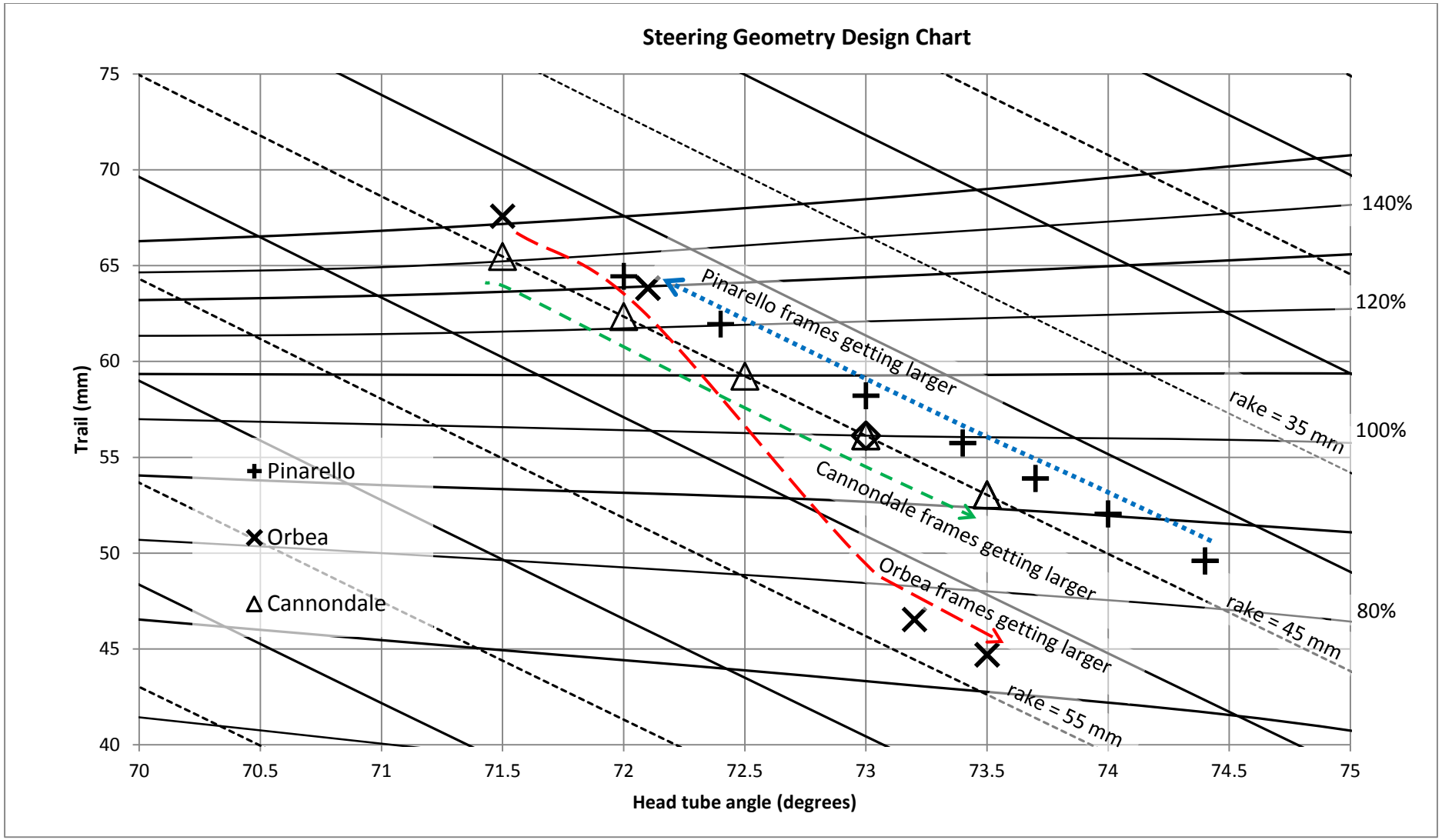

Figure 99 TdF Pinarello, Orbea & Cannondale steering geometries for different sized bicycle frames, wheel dia. 675 mm

Table 42 Summary of values for the smallest and largest frames from all manufacturers

Parameter	Smallest frames		Largest frames	
	Min value	Max value	Min value	Max value
Conventional Frame Size cm	42.00	49.00	58.00	62.00
Head Tube Angle degrees	70.30	74.40	72.00	74.00
Seat Tube Angle degrees	69.15	75.5	73.50	74.0
Rake mm	43.0	53.0	40.0	53.0
Trail mm	49.587	70.733	44.696	64.448
Settling times %	85	160	75	135

Table 43 Comparison of the TdF 2013 bicycles to historical practice

Parameter	TdF bicycles 2013	Historical Practice (Table 38)	Comments
Head tube angle degree	70.3 to 74.4	71.5 to 76	Tdf have lower min & max values
Seat Tube Angle degree	69.15 to 75.5	71.5 to 76	Tdf have a lower min value
Rake mm	40 to 53	40 to 67	Tdf have a lower max value
Trail mm	44.7 to 70.7	33 to 60	Tdf have higher min & max values
Settling times %	75% to 160%	50% to 110%	Tdf have higher min & max values

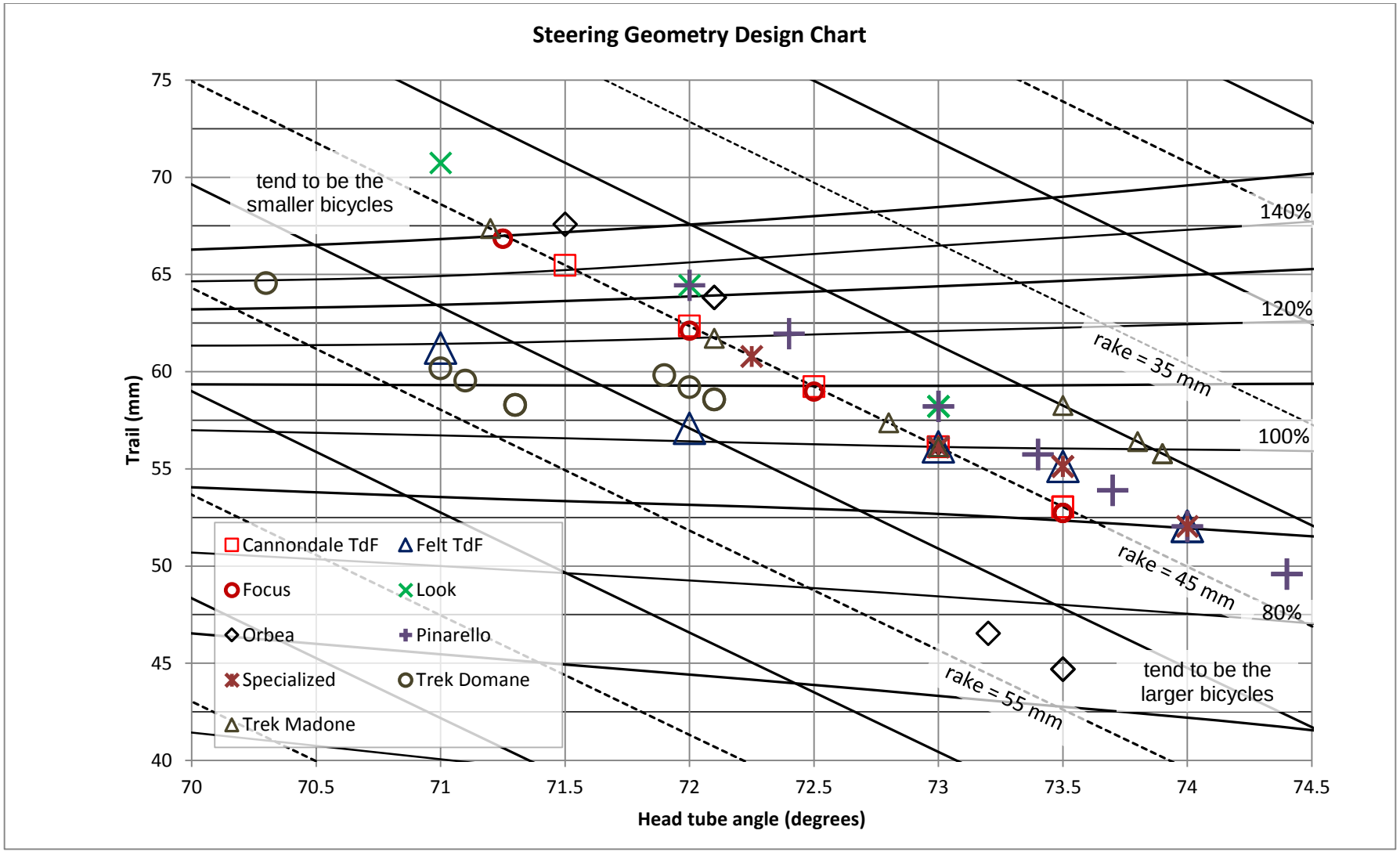

Figure 100 Steering Geometry Design Chart TdF bicycles, all sizes from selected manufacturers (675 mm wheel dia.)

Table 44 Parameters values for smallest and largest frames

Company & Model	Parameters									
	Frame Size cm		Head Tube Angle degrees		Seat Tube Angle degrees		Rake mm		Trail mm	
	smallest	largest	smallest	largest	smallest	largest	smallest	largest	smallest	largest
Pinarello Dogma 65.1 Think 2	42.0	62.0	74.40	72.00	69.15	73.40	43.0	43.0	49.587	64.448
Orbea Orca	48.0	60.0	71.50	73.50	74.75	73.20	43.0	53.0	67.583	44.696
Cannondale Supersix Evo	48.0	62.0	71.50	73.50	74.50	72.00	45.0	45.0	65.474	53.039
Focus Bikes Izalco Team SL Carbon	48.0	60.0	71.25	73.50	74.80	73.50	46.0	46.0	66.836	52.737
Look 695 Aerolight [1]	47.0	58.0	71.00	73.00	74.80	73.00	43.0	43.0	70.733	58.219
Specialized Tarmac SL 4 & Venge	49.0	60.0	72.25	74.00	75.50	72.50	45.0	43.0	60.785	52.044
Trek Domane 6.9	44.0	62.0	70.30	72.10	73.30	73.30	53.0	48.0	64.548	58.568
Trek Madone 7.9	47.0	62.0	71.20	73.90	74.60	72.50	45.0	40.0	67.358	55.781
Felt F2	48.0	60.0	71.00	74.00	74.50	73.00	52.0	43.0	61.214	52.044
Sources see Appendix F										
Note 1 Look specifies FS using a letter system (XS to XXL) a dimension in cm is estimated from other information										

7.4. WHEEL PROPERTIES DESIGN CHART

Unfortunately it wasn't possible to see how the TdF bicycles conform to this Chart which considers the effect of the wheel diameter and polar moment of inertia on handling. This is because the necessary information (exact wheel diameters and moments of inertia for individual bicycles) was not available. Therefore it was not possible to define a TdF design envelope on this Chart and this thesis is left with the experimental work outlined in Chapter Six and Appendix C. This considered a small number of experimentally measured wheels and used them to outline an approximate design envelope. More detailed work in this area needs to be done.

7.5. FRAME GEOMETRY DESIGN CHART

Next for consideration is the Frame Geometry Design Chart and because this Chart includes the rider influenced parameters of b and h it was necessary to look at individual riders as well as specific bicycles. It was decided to focus only on the top ten finishers from the 2013 TdF and to use their publically available physical characteristics and bicycle choices to define a design/rider envelope (their details are shown in Table 45 and Appendix F). Using this information it was possible to calculate the additional parameters required for plotting onto the Chart. These calculated results are shown in Table 46 and are based on the following assumptions:

1. inseam = height x 0.461 (based on the average anthropomorphic relationship for males (48))
2. saddle height = inseam x 0.885 (based on competitive coaching advice (68))
3. bicycle frame size = inseam x 0.65 (based on competitive coaching advice (68))
4. the wheelbase and seat tube angle are taken from each manufacturer's specifications after the frame size is found as per step 3
5. mass height h is calculated as per Appendix B
6. mass distance from the rear wheel b is calculated as per Appendix B

From the Design Chart in Figure 101 it can be seen that these ten TdF riders are strongly clustered towards the bottom of the Chart and are bunched near the toe overlap limit line, with one rider (Joaquin Rodriguez Oliver) right on this boundary. This implies that riders and designers are choosing to use bicycles that have as short a wheelbase and as shallow a seat tube angle as it is physically possible for them to ride without encroaching across the toe overlap limit. These bicycles will tend to be lively in their handling as they are between the 90% and 105% iso-handling lines.

The limits for this group of riders and their bicycles are:

- seat tube angles are between 72.5 to 74 degrees (which are similar to Hinault and Ballantine's recommendations in Table 38 (68, 74))
- wheelbases range from 980 to 1000 mm (similar to Ballantine's recommendation in Table 38 (74))
- and the iso-handling lines are 97% plus/minus 7.5% (90% to 105%)

This tight clustering is at least partly due to the similar physical characteristics of these riders who are all of average height or below and have very low male body masses, (the average height and mass is 177 cm and 63 kg respectively, see Table 45).

7.6. MASS AND ROLL INERTIA DESIGN CHART

The final part of this section looks at the Mass and Roll Inertia Design Chart and once again by considering the top ten individual riders from the 2013 TdF it was possible to define a design/rider envelope. These ten riders were plotted using the assumptions and equations from Appendices B and F plus these two following assumptions.

1. the moment of inertia of assembly B about the roll axis X (I_{XB}) is given by:

$$I_{XB} = (M_{rider} + M_{bike})h^{2} \quad (51)$$

   note that h is the calculated value from Table 46 *and this method of calculating the I_{XB} (as Mh^2) has been shown in Chapter Six to within 3.5 % of the actual value*

2. the bike has a mass of 6.8 kg which equals the minimum weight allowed by UCI regulations (3)

The completed Chart in Figure 102 shows a tight clustering of riders and bicycles

- centred about the line h = 1100mm plus/minus 50mm
- along this line's axis the rider and bike mass range from 64 to 76 kg (this includes the 6.8 kg mass of the bicycle)
- this also means the iso-handling lines range from 70 to 95% (80% plus15% minus 10%) which in comparison to some other results is a tight cluster
- this again highlights the fact that the riders are of slight weight and this combined with a low h value (1100 mm) and a low bicycle weight (6.8 kg) gives an acceptable handling performance, which tends to be on the responsive side

Table 45 Tour de France 2013 top ten individual finishers (published details)

TdF 2013 position	Rider surname	First name	Team	Bicycle manufacturer	Rider height mm	Rider mass kg
1	Froome	Chris	Sky Procycling	Pinarello	1860	69.0
2	Quintana Rojas	Nairo	Movistar Team	Pinarello	1660	57.3
3	Rodriguez Oliver	Joaquin	Katusha Team	Canyon	1690	57.0
4	Contador	Alberto	Team Saxo-Tinkoff	Specialized	1760	62.0
5	Kreuziger	Roman	Team Saxo-Tinkoff	Specialized	1830	65.0
6	Mollema	Bauke	Belkin Pro Cycling	Giant	1810	64.0
7	Fuglsang	Jakob	Astana Pro team	Specialized	1820	70.0
8	Valverde	Alejandro	Movistar Team	Pinarello	1780	61.0
9	Navarro	Daniel	Cofidos Solutions Credits	Look	1750	61.0
10	Talansky	Andrew	Garmin Sharp	Cervelo	1750	63.0
				average	1771	62.93
				standard deviation	59.41	4.09

Source (108)

Table 46 Tour de France 2013 top ten individual finishers (calculated details)

TdF 2013 position	Surname	Calculated Inseam mm	Calculated saddle height mm	Calculated frame size cm	Wheelbase mm	STA degrees	Calculated "h" mm	Calculated "b" mm	Calculated I_{YB} kgm^2
1	Froome	857.5	758.9	55.7	988.2	73.00	1109.0	318.0	93.225
2	Quintana Rojas	765.3	677.3	49.7	970.0	74.00	1020.0	337.0	66.690
3	Rodriguez Oliver	779.1	689.5	50.6	971.0	73.50	1019.0	332.0	66.247
4	Contador	811.4	718.1	52.7	970.0	74.00	1064.0	333.0	77.888
5	Kreuziger	843.6	746.6	54.8	978.0	73.50	1096.0	324.0	86.247
6	Mollema	834.4	738.5	54.2	986.0	72.50	1086.0	315.0	83.501
7	Fuglsang	839.0	742.5	54.5	978.0	73.50	1092.0	325.0	91.581
8	Valverde	820.6	726.2	53.3	978.1	73.70	1084.0	328.0	79.669
9	Navarro	806.8	714.0	52.4	979.5	74.00	1060.0	334.0	76.180
10	Talansky	806.8	714.0	52.4	972.0	73.00	1059.0	323.0	78.279
	average	816.43	722.54	53.1	977.1	73.47	1068.90	326.90	79.95
	standard deviation	27.39	24.24	1.78	6.12	0.48	29.12	6.82	8.65
Sources (108, 111-116)									

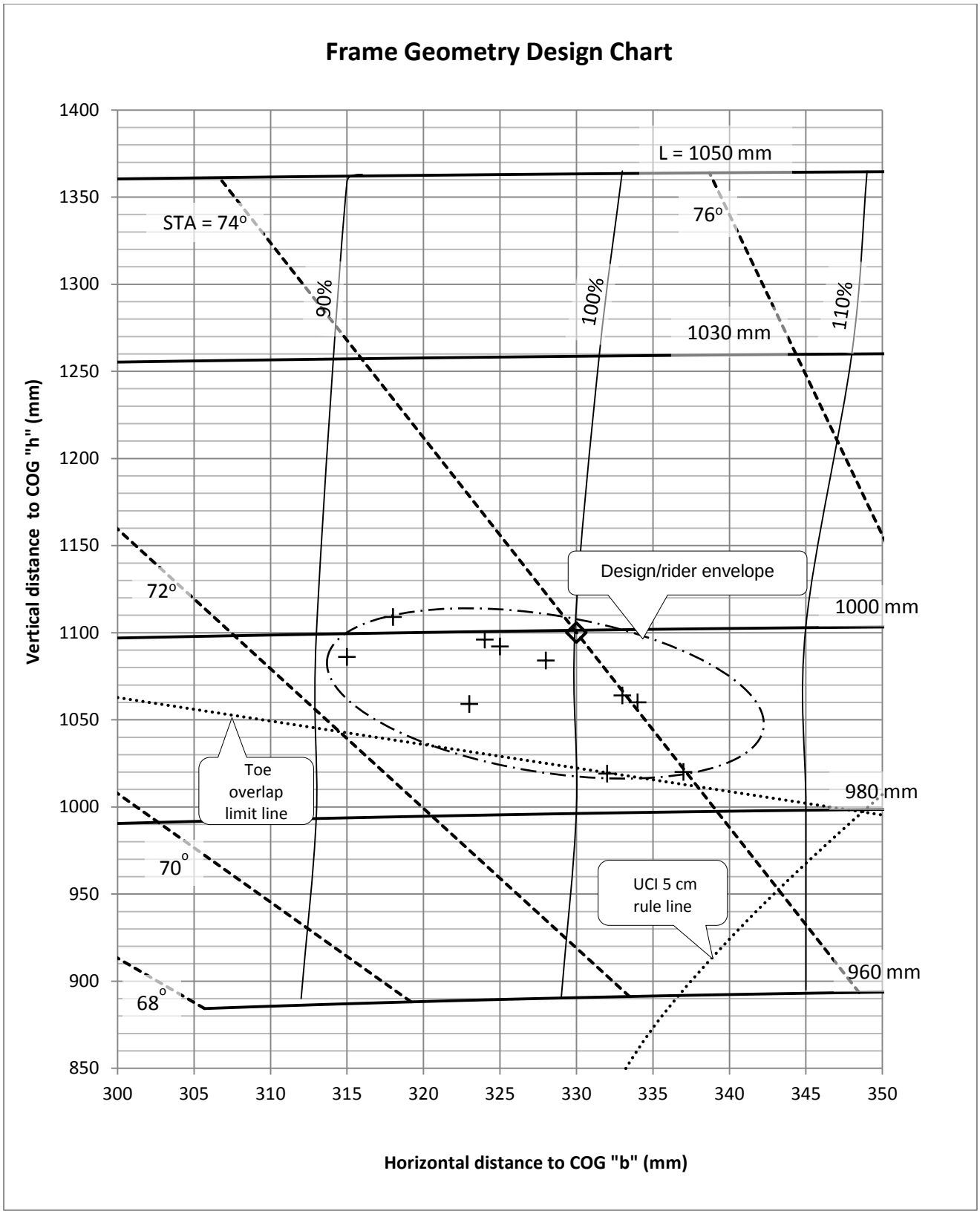

Figure 101 Frame Geometry Design Chart, indicating the 2013 TdF top ten individual finishers

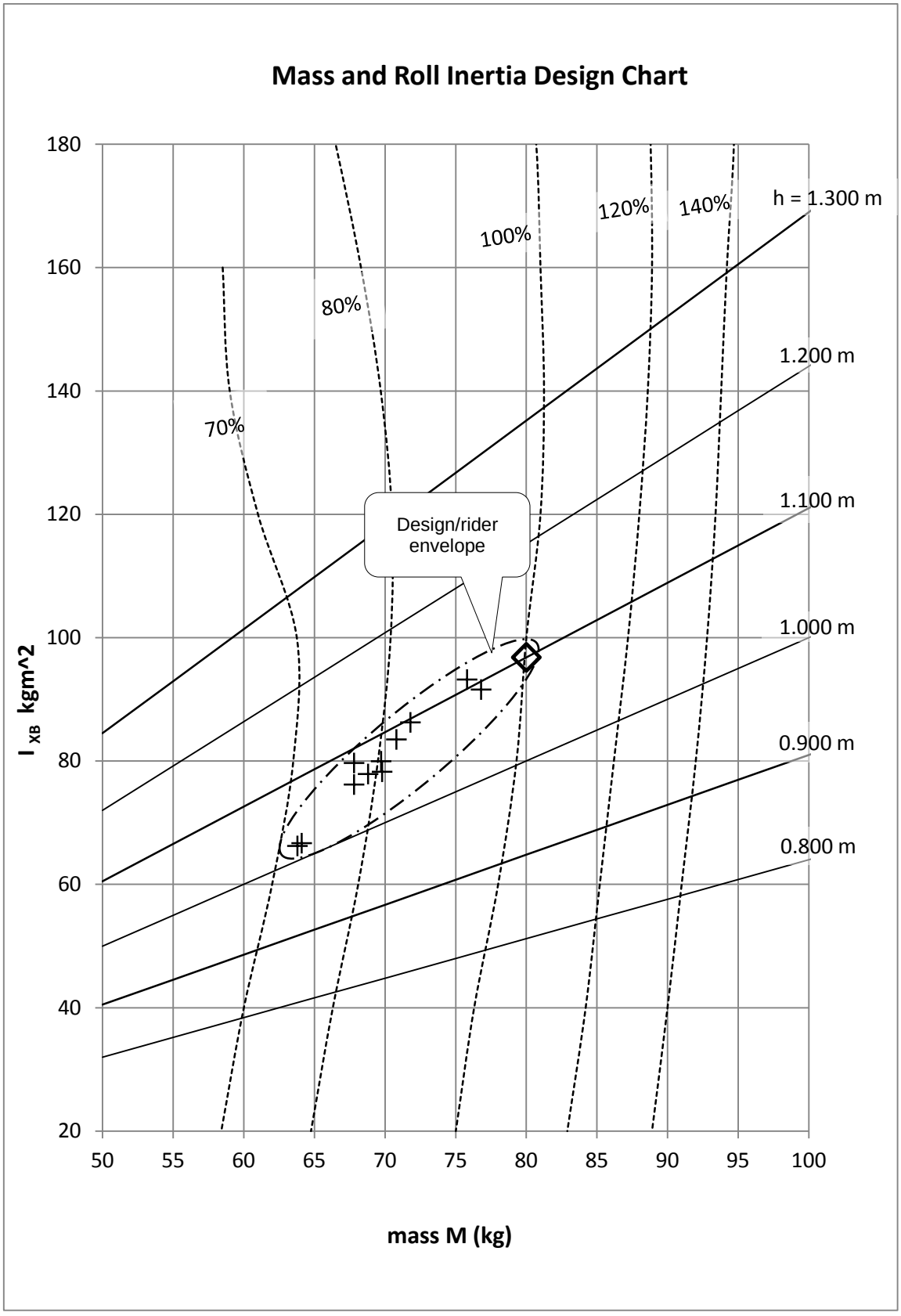

Figure 102 Mass and Roll Inertia Design Chart, indicating the 2013 TdF top ten individual finishers

7.7. REMARKS

The use of these Design Charts with their iso-handling lines takes the high level mathematical approach of the Simulink model and presents it in a way that is very easy to interpret. These Charts allow designers to explore the implications of different design choices with more confidence about the outcome than previously possible. All 11 parameters are important and can't be considered in isolation and these Charts are a way of combining up to 4 parameters so they can be considered together and displaying them in graphical way that is easy to follow.

This Chapter has shown that the bicycle manufacturers, as evidenced by historical practices and by elite TDF riders and bicycles, conform to the Charts and this indicates their relevance and usefulness. The results indicate appropriate design envelopes for designers to consider. The next Chapter will conclude this investigation and make overall comments about important findings.

8. CONCLUSIONS AND RECOMMENDATIONS

8.1. INTRODUCTION

This Chapter concludes the investigation into determining to what extent mathematical modelling can influence the dynamics of bicycle design and improve handling. Comments will be made about the development of a dynamic bicycle model and the implications for design. A new design methodology has been developed and that includes four new Design Charts with design envelopes that can guide bicycle designers.

8.2. COMMENTS ON OBJECTIVES

The main hypothesis of this investigation was to determine if mathematical modelling could influence bicycle design characteristics and improve handling performance. A key objective was to develop effective and valid design tools that bicycle designers could use to optimise their designs. In summary the objectives outlined in Chapter One have been met and this will now be discussed.

8.2.1. REVIEW OF LITERATURE

One early objective was to review the literature to see what was known and what remained to be done. The literature survey in Chapter Two examined the extensive research on bicycle dynamics and stability and that includes the development of equations of motion to describe bicycle motion. But the literature lacked information about how this research could be used to develop proper design methodologies. Designers lacked clear guidelines on how to optimise their designs and still relied on empirical observations and trial and error. Some of the studies on instability and the sensitivity of bicycles to design parameter changes were contradictory and needed resolving. Most of the evaluations of bicycle handling performance were subjective and were not quantified. So one objective was to develop a methodology that would define bicycle handling performance.

From the literature survey the following main points were noted:

- the literature included many examples of dynamic equations for bicycles but these were not well correlated to design parameters
- the equations are complicated with some parameters being important while others much less so
- to develop a suitable design methodology it is essential that only the critical parameters be considered
- the dynamic analysis of motion had not been looked at in relation to bicycle design

8.2.2.DYNAMIC BICYCLE MODEL

Chapter Three explained a dynamic bicycle model and described how it was developed and formulated and it justified the simplifications used to produce an appropriate model that could be solved but was still realistic enough to be relevant. The governing equations of motion and the resulting mathematical model of bicycle dynamics were described in more detail in Chapter Four and was solved using Simulink in a Matlab environment. This Simulink model included realistic steering geometry and could take the rider's steering input and after applying appropriate physical parameters (such as head tube angle, mass, wheelbase, etc.) it could find the dynamic response in terms of yaw and roll. Therefore it is capable of simulating bicycle motion, particularly counter-steering manoeuvres accurately predicting the dynamic response of different bicycles for a range of manoeuvres. It is adaptable and capable of analysing a wide range of designs. The model was validated by comparison with existing theory and then with an experimental investigation.

This Simulink bicycle model was used specifically to:

- look at the dynamic responses of the bicycle and see how they related to the rider
- investigate which design parameters in the equations were critical and which others less so
- determine the effectiveness of the model in examining bicycle performance
- determine the importance and significance of each torque term in the equations of motion
- examine the model's stability from its characteristic equation

8.2.3.SENSITIVITY STUDY

In Chapter Five a sensitivity study was undertaken to determine the Simulink model's sensitivity to changes in the key design parameters. This study was used to determine the effect each parameter had on the dynamic response in order to:

- to correlate the design parameters to the dynamic equations for the bicycle
- and to determine which parameters must be considered and which ones can be ignored so that the dynamic equations can be simplified while still maintaining a model that can accurately simulate bicycle behaviour
- develop a useful and valid design methodology to guide designers
- and to see if the bicycle could be optimised in terms of specific performance criteria

Before this study commenced it was necessary to obtain realistic, accurate benchmark values for each design parameters and this was done using experimental and theoretical methods. It was interesting to note that much of the literature used unsuitable values for these parameters which typically were derived from low performance bicycles.

From this study it was found that the most significant parameters were (in order of importance):

1. Head tube angle
2. Wheel diameter
3. Horizontal position of mass
4. Moment of inertia of wheels (about the X, Y and Z axes)
5. Mass
6. Wheelbase
7. Rake

The following four parameters that were found to be much less significant (in order of significance):

8. Height of mass
9. Moment of inertia of rear assembly B about roll axis
10. Moment of inertia of front assembly A about yaw axis
11. Moment of inertia of front assembly A about roll axis

8.2.4.DESIGN METHODOLOGY

One major aim of this investigation was to develop suitable design tools that manufacturers and designers could use to guide their bicycle design decisions. Designers need design methodologies based on scientific theories as opposed to the current empirical methods. Chapter Six developed a suitable design methodology based on the mathematical analysis of Chapters Three to Five.

The results of the model simulations have shown the importance of geometry on stability (particularly the head tube angles and rake dimensions). These results enabled practical design suggestions to be made that were eventually summarised in a series of bicycle design charts. But several design methodologies were first considered and evaluated to determine their suitability for practical use, and these included: criteria, tables, equations and charts. After consideration it was decided to recommend and develop the Design Chart methodology because of its clear advantages which include:

- it is scientifically based and justified
- it is easy to use and it allows a wide audience an understanding of the design process
- several parameters can be concurrently considered, so interactions can be studied and a wide range of design decisions can be contemplated at once
- its iso-handling lines quantify handling performance and are scientifically rigorous

The four Design Charts proposed in Chapter Six cover the design areas of:

1. Steering geometry (head tube angle, rake and trail)
2. Wheel properties (wheel diameter and moment of inertia)

3. Frame geometry (vertical and longitudinal position of the mass and wheelbase)
4. Mass and roil inertia (mass and moment of inertia of the rear assembly)

These four Design Charts can be used together in any order or separately. The results from the simulation study was analysed in order to see what combinations of key parameter values gave optimum performance in terms of handling. Handling performance was quantified by using an impulse response test and the 2% settling time for each design combination was recorded and compared to a benchmark bicycle. From these tests it was possible to plot non dimensional iso-handling line on the Charts.

8.2.5.DESIGN METHODOLOGY VALIDATION

Chapter Seven considered the validity the proposed Design Charts from Chapter Six. This was done by first considering historical design practice and secondly the elite group of riders and bicycles that competed in the 2013 Tour de France bicycle race. This Chapter showed that successful bicycle designs conformed well to the Charts and this confirms the Charts' relevance and usefulness. Individual bicycle designs can be plotted onto the Charts to determine their acceptability. These results helped to define appropriate design envelopes in the Charts for use as guidelines.

8.3. RECOMMENDATIONS FOR FUTURE STUDY

While this thesis has been successful in analysing bicycle motion in relation to design, a number of future developments could be considered.

- More simulation trials could be made using different combinations of geometry to add more detail to the Bicycle Design Charts.
- A steering feedback control loop could be added to the computer simulation model to check for the influence of rider feedback on instability.
- To date, little experimental work has been performed in the field of bicycle dynamics and this is a rich field to investigate.
    - experimental self-stability trials could further validate the model and the Design Charts.
    - dynamic examination of experimental bicycles close to the extremes of the charts (e.g. close to the edges of the design envelopes) could give more insights as to dynamic behaviour
    - experimental measurement of design parameters would provide more precision to the charts and the design envelopes
- It would be interesting to obtain more detailed information about elite riders and bicycles. For example exact mass positions, wheel diameters and moments of inertia. This would make it possible to further define the rider/design envelopes on these Charts.

8.4. CONCLUSIONS

This investigation has successfully developed a computer model for bicycle motion which can be used to study bicycle performance and stability. Performance was examined in terms of handling and the settling time after a disturbance. A main contribution of this research is the inclusion of realistic steering geometry and other parameters into the computer simulation model. Previous research used simplified bicycle models and inappropriate parameter values that yielded little insight into parameter selection and design. This has enabled important conclusions and recommendations to be made resulting in a new and original bicycle design methodology. The conclusions about bicycle performance have been summarised into four bicycle Design Charts which can be used to help design bicycles of good handling performance.

APPENDICES

APPENDIX A – SIMULINK MODEL

In this Appendix more complete details of the Simulink model are given than was provided in Chapter Four.

Table 47 Details of Simulink figures

Purpose	Figure
Standard Simulink model without added elements	Figure 103
The Fajans Simulink model	Figure 104
Simplified Simulink model to reproduce Fajans results	Figure 105
Complex Simulink model, all elements added	Figure 106
Steering torque subassembly, easily adjustable for different amplitude and time lag values	Figure 107

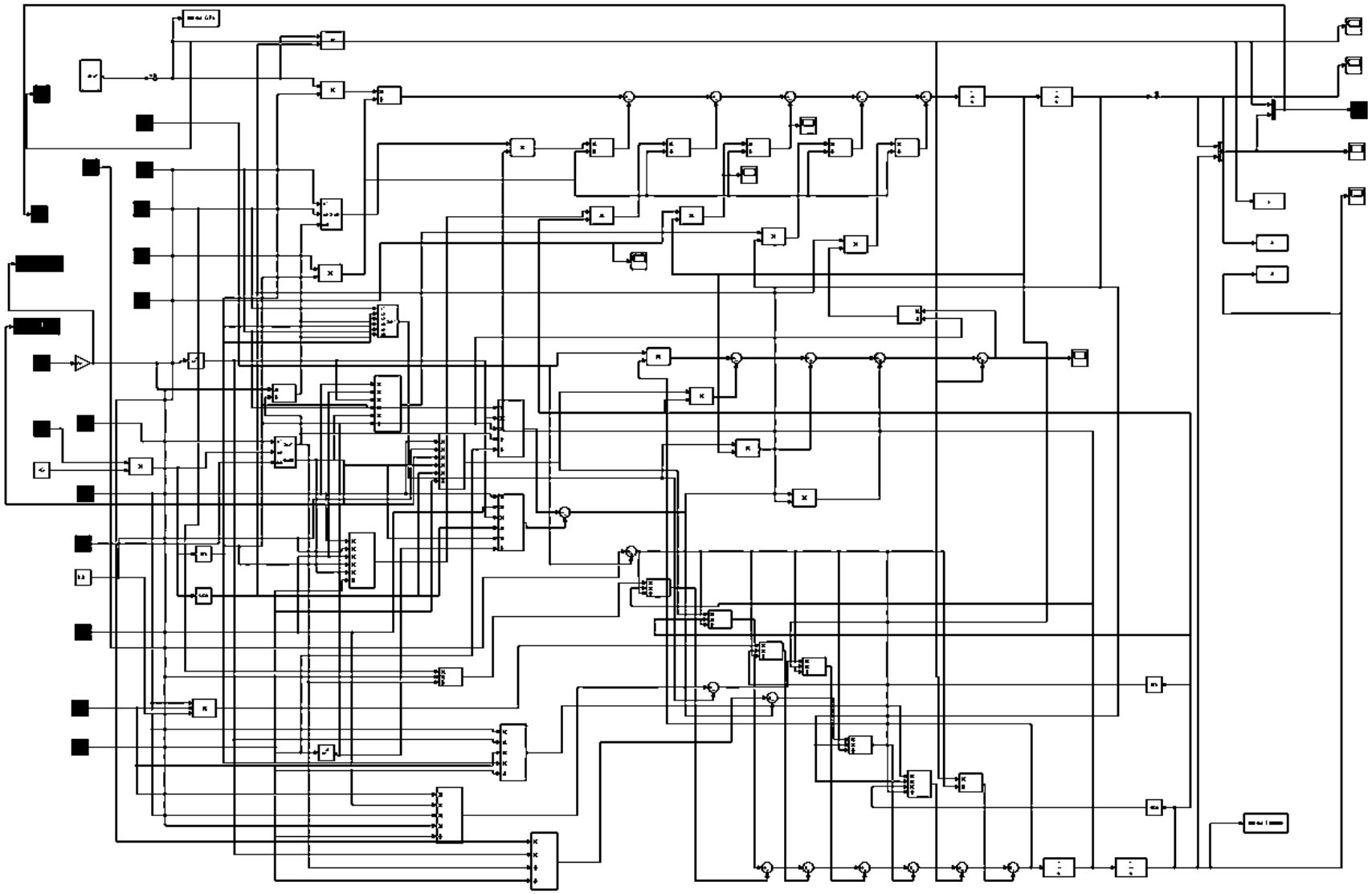

Figure 103 The standard Simulink model, without added elements for detailed analysis

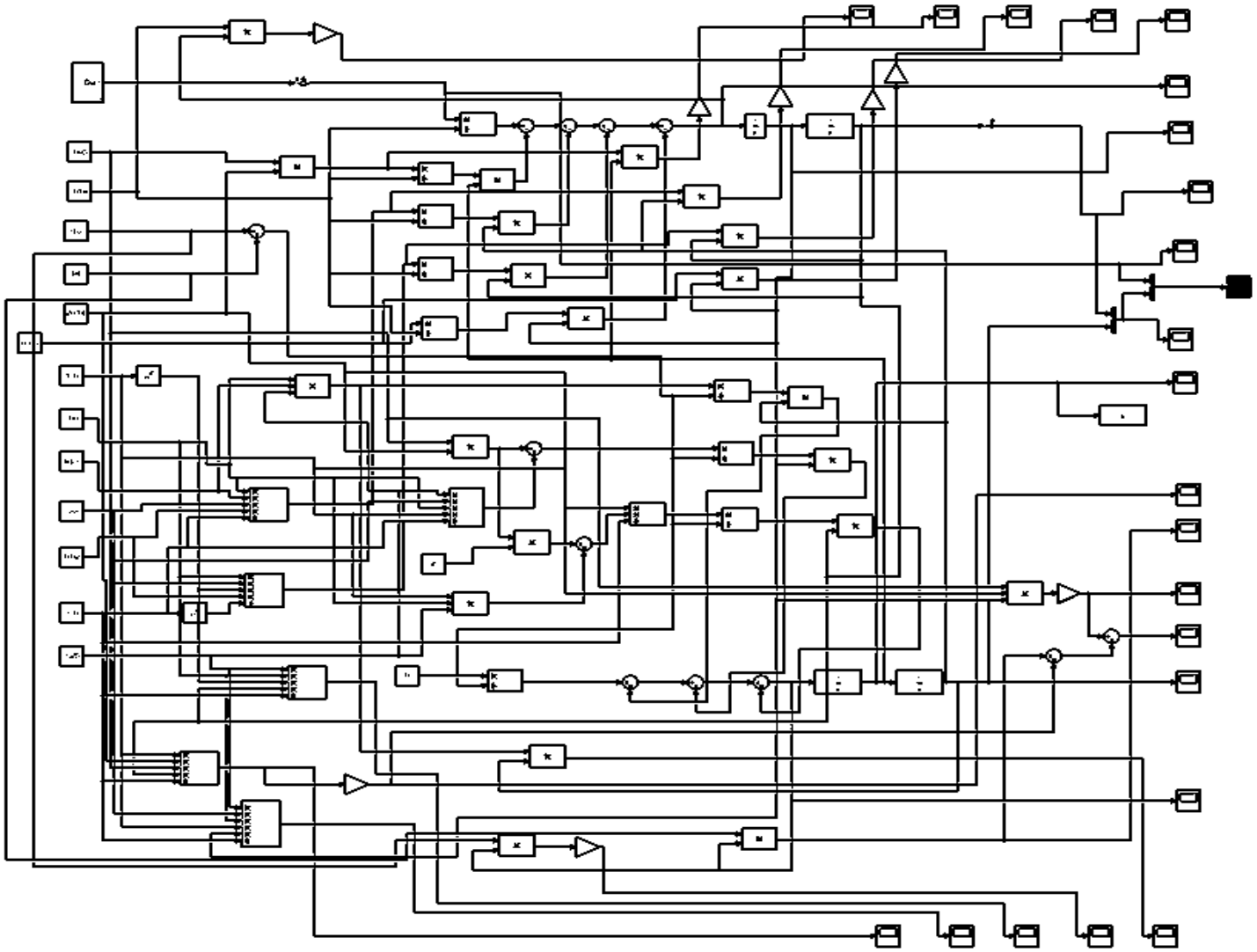

Figure 104 The Fajans Simulink model, capable of basic dynamic modelling of a simple bicycle

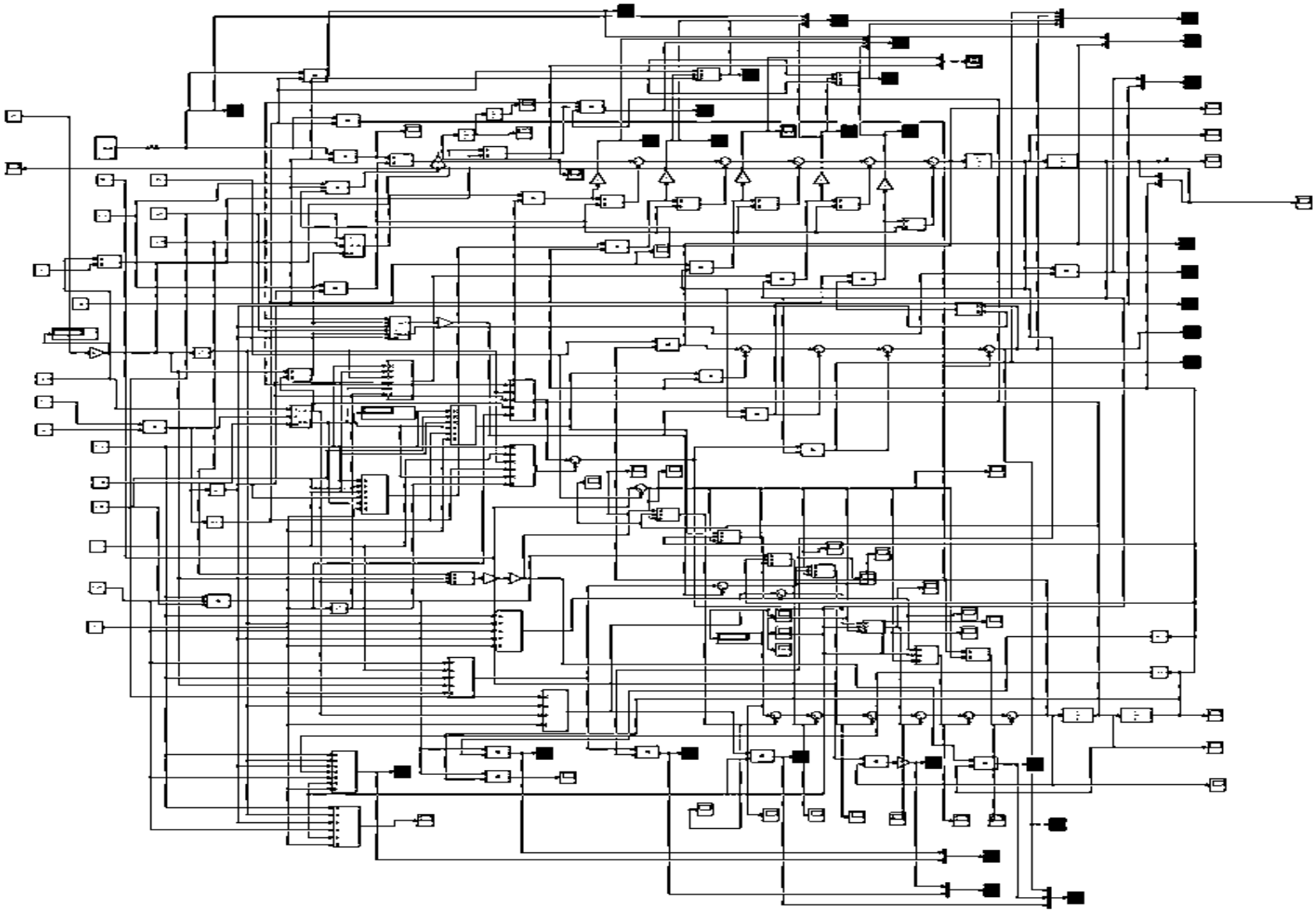

Figure 105 A simplified Simulink model able to reproduce Fajans' results

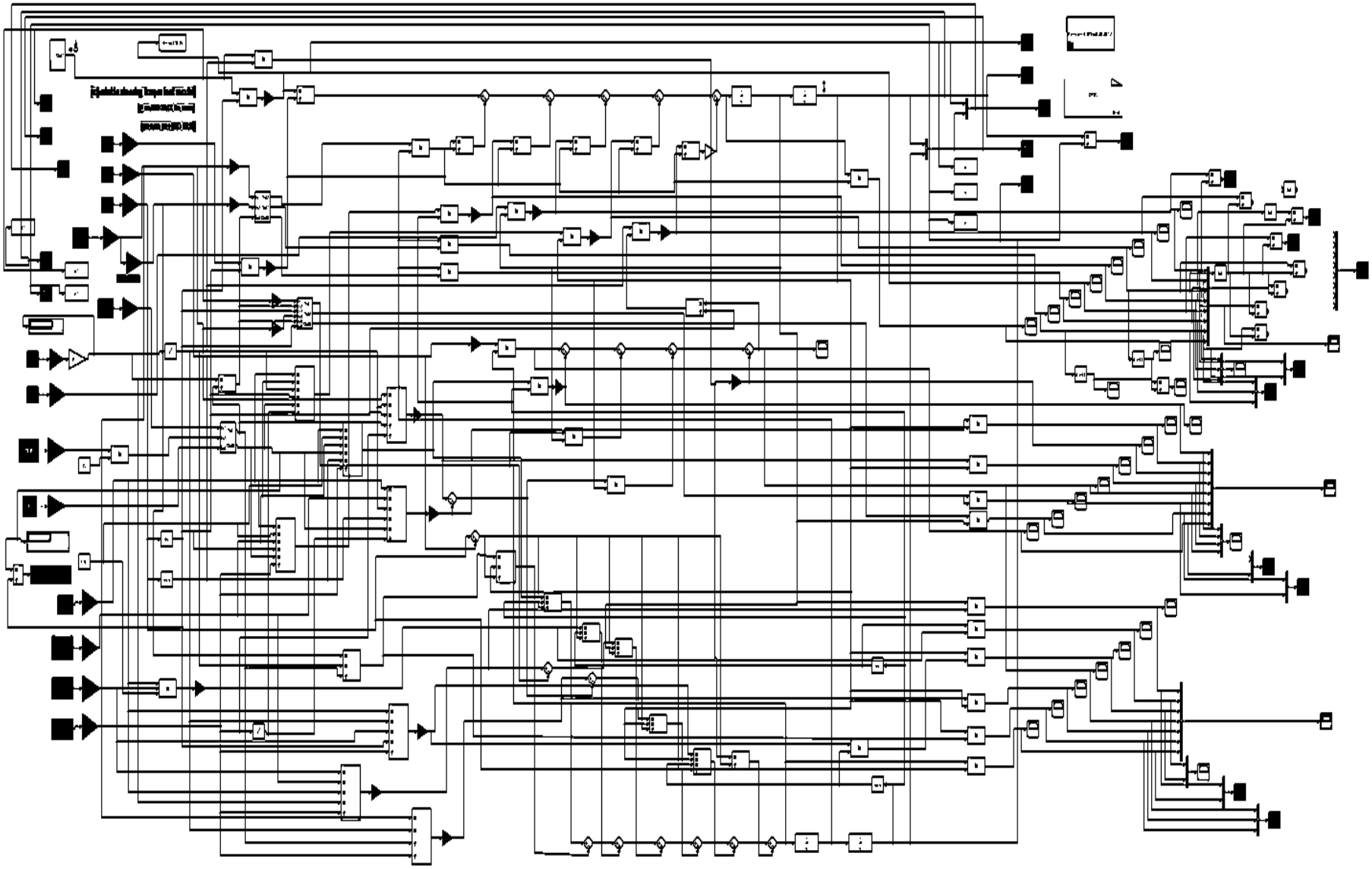

Figure 106 A more complex Simulink model, with all elements added for analysis of torque terms and sensitivity of parameters

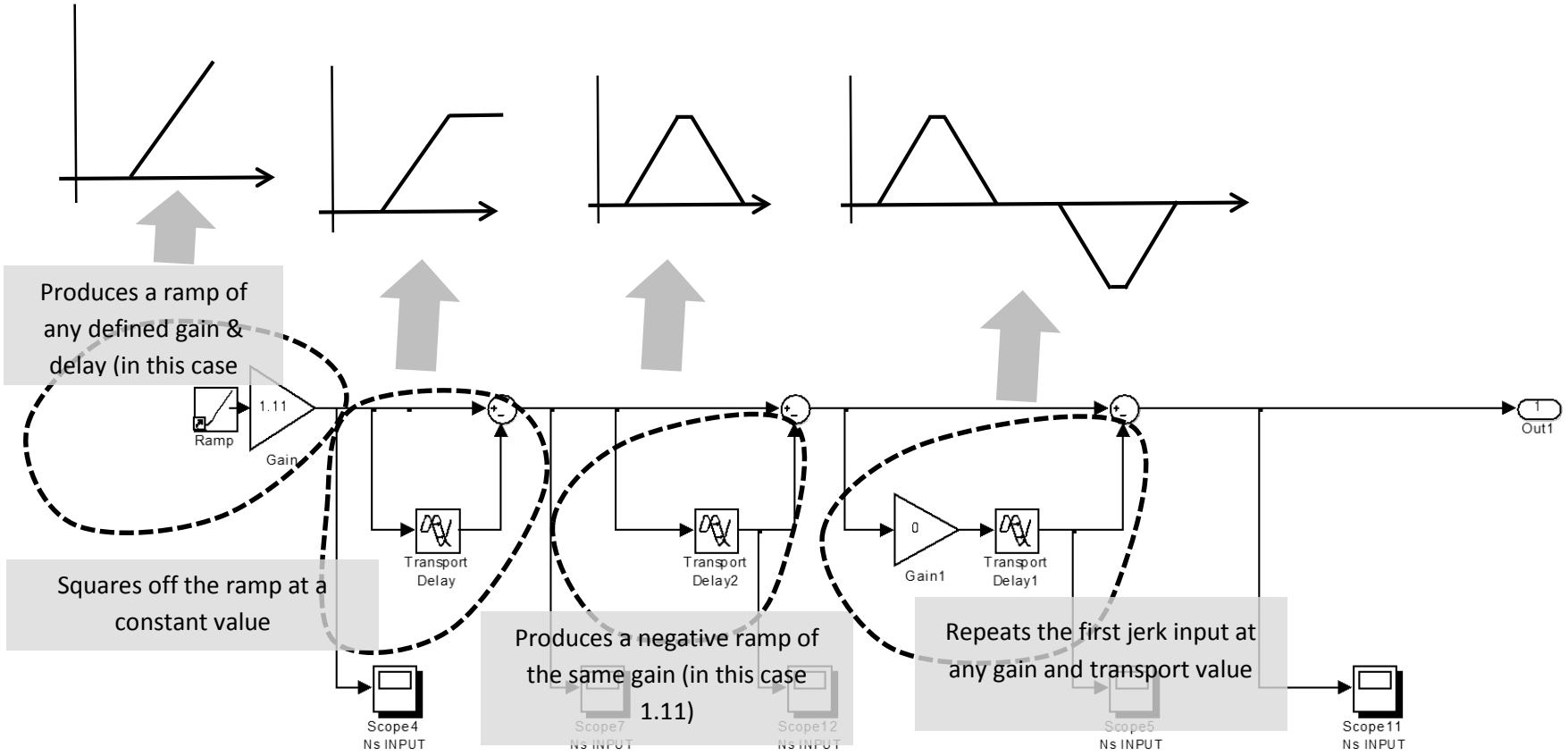

Figure 107 Simulink steering torque subassembly, capable of being adjusted for different amplitude and time lag values

APPENDIX B – FRAME GEOMETRY RELATIONSHIPS

This Appendix defines the relationships between the wheelbase, mass position (as defined by h and b), seat tube angle and saddle height parameters and these relationships were extensively used in Chapters Six and Seven to describe the development and validation of the Frame Geometry Design Chart (see relevant details in Table 48 and Figure 108 through to Figure 113).

B-1 FRAME GEOMETRY GENERAL EQUATIONS

The frame geometry general equations and basic procedure are now described (see Figure 108 and Table 48).

First find distance "h_1"which is from the rear wheel centre to point *B*

$$h_1 = {}^{r_1}/_{\cos\gamma} \tag{52}$$

Then distance "L_1"which is from the rear wheel centre to point *A*

$$L_1 = {}^{h_1 + r}/_{\tan\gamma} \tag{53}$$

Next find the height of the bottom bracket "h_3"

$$h_3 = r - h_4 \tag{54}$$

Find distance "O" from point *A* to the bottom bracket

$$O = {}^{h_3}/_{\sin\gamma} \tag{55}$$

Find distance "Q" from point *A* to point K

$$Q = O + P + j \tag{56}$$

Now we can find the angle "σ" Sigma

$$\tan\Sigma = {}^{k}/_{Q} \tag{57}$$

This allows distance “i” to be found (from the bottom bracket to centre of mass or COM)

$$i = Q\cos\Sigma$$

(58)

Find intermediate horizontal distance “L_2”

$$L_2 = i\cos(\Sigma + \gamma)$$

(59)

This allows the important dimension “b” to be found (the horizontal distance from the centre of the rear wheel to the centre of mass)

$$b = L_1 - L_2$$

(60)

Also equation (60) can be expanded out to:

$$b = \left[\frac{(r_1/\cos\gamma) + r}{\tan\gamma}\right] - \left[\frac{\left(\frac{h_3}{\sin\gamma}\right) + P + j}{\tan\gamma}\right]\cos(\Sigma + \gamma)$$

(61)

Finally distance “h” can be found (the vertical distance from the ground to the centre of mass)

$$h = i\sin(\Sigma + \gamma)$$

(62)

And equation (62) can be expanded out to

$$h = \left[\frac{\left(\frac{h_3}{\sin\gamma}\right) + P + j}{\cos\Sigma}\right]\sin(\Sigma + \gamma)$$

(63)

The frame size, wheelbase and saddle height relationships used in Chapter Six are summarised as follows:

Saddle height “P” equals:

$$P = 0.885 \times IS$$

(41)

Frame size “FS” equals:

$$FS = 0.65 \times IS$$

(42)

Therefore:

$$IS = {}^{P}/_{0.885}$$

(43)

Substitution gives:

$$FS = \left({}^{0.65}/_{0.885}\right) \times P$$

(44)

$$FS = 0.735 \times P$$

(45)

From 2013 Tour de France road bicycles (Appendix F) the empirical relationship between frame size and wheelbase was found and giving the following line of best fit, see Figure 124

$$L = 0.3077 \times FS + 822.5 \ \pm 20$$

(39)

For the benchmark bicycle which has a frame size of 550 mm this equation gives a wheelbase of 991.74 mm (-/+ 20 or between 971.74 and 1011.74 mm) which is close to the actual benchmark value used of 1000 mm

$$L = 0.3077 \times 550\ mm + 822.5\ mm \ \pm 20\ mm$$

$$L = 991.74\ mm \ \pm 20\ mm$$

By substituting “P” from equation (45) the wheelbase equation becomes:

$$L = 0.3077 \times (0.735 \times P) + 822.5 \ \pm 20$$

(46)

Which becomes the final equation necessary to find the toe overlap boundary:

$$L = 0.226 \times P + 822.5 \ \pm 20$$

(47)

B-2 TOE LIMIT LINE RELATIONSHIPS

This section of the Appendix uses the relationships between the wheelbase, mass position (as defined by h and b), seat tube angle and saddle height (P) parameters and to plot the toe limit line onto the Frame Geometry Design Chart, where the following assumptions were used:

1. Wheel diameter is 675 mm (2r)
2. Bottom bracket drop is 67.5 mm (h_4)
3. Clearance between seat tube centreline and rear wheel is 32.5 mm
4. Centreline of shoe is 130 mm from centreline of bicycle in a transverse direction "d_2" (this was measured experimentally)
5. Crank length is 165 mm "d_2" (measured experimentally)
6. Shoe extension from pedal spindle centreline is 120 mm"d_3" (measured experimentally)
7. Maximum permitted overlap between wheel and shoe is an allowance of 10 mm, an assumption based on rider preference (96)

The process using these equations to find the toe overlap limit line on the Frame Geometry Design Chart was:

First find vertical distance "h_1" which is from the rear wheel centre to point *B*

$$h_1 = {}^{r_1}/_{\cos\gamma}$$

(52)

Then find intermediate horizontal distance "L_3" from the rear wheel centre to the bottom bracket

$$L_3 = (h_1 + h_4)\tan\gamma$$

(64)

Now we can find the angle "α" alpha

$$\alpha = \sin^{-1}{}^{h_2}/_{r}$$

(65)

Find intermediate radius "r_2", which allows for the vertical drop of the shoe below the centre of the front wheel

$$r_2 = r\cos\alpha$$

(66)

Now we can find the angle "σ" sigma, which is the maximum amount of turn of the front wheel before contact with the shoe

$$\sigma = \sin^{-1}\ d_1/r_2$$

(67)

Find the second intermediate radius "r_3" which corrects the front wheel radius for turning through angle sigma

$$r_3 = d_1/\tan\sigma$$

(68)

Next find the intermediate horizontal distance "L_4" (the distance from the bottom bracket centre to the tip of the shoe) this is the space required for the shoe

$$L_4 = d_2 + d_3 + L_3$$

(69)

Finally find final horizontal distance "L_5" (from the centre of the rear wheel to the edge of the front wheel when turned and allowing for the drop of the bottom bracket) this is the clearance gap available

$$L_5 = L - r_3$$

(70)

Comments on the toe overlap

- if L_4 (the space required) equals L_5 (the gap available) then the tip of the shoe just touches the front wheel when it is turned through angle sigma
- if $L_4 < L_5$ then there is a gap between the wheel and the shoe
- if $L_4 < L_5$ then a toe overlap occurs
- some sources say an overlap of up to 10 mm (the allowance) is tolerable (96)
- and the Frame Geometry Design Chart of Chapter Six assumes the allowance is 10 mm,
- so the toe overlap limit line in the Frame Geometry Design Chart in Chapter Six is when:

$$L_4 = L_5 + allowance$$

(71)

$$and\ the\ allowance = 10\ mm$$

Table 48 Definitions of the terms required to calculate the seat tube angle and saddle height

Symbol	Parameter	Units
A	Intersection of seat tube centreline with ground	
b	Distance horizontally from rear wheel hub to centre of mass	mm
B	Intersection of seat tube centreline with vertical line passing through rear wheel hub centreline	
c	Clearance distance between seat tube centreline and outside of rear wheel	mm
C	Point on the ground directly below the rear wheel hub's centre	
COM	Centre of mass	
d_1	Crank sideways offset	mm
d_2	Crank length	mm
d_3	Shoe extension, from the centreline of the pedal spindle	mm
D	Intersection of ground and a vertical line tangential to rear of front wheel	
h	Distance vertically from ground to centre of mass	mm
h_1	Distance vertically from rear wheel hub to B	mm
h_2	Distance vertically from ground to B	mm
h_3	Distance vertically from ground to bottom bracket spindle centreline	mm
h_4	Distance vertically from wheel hub to bottom bracket spindle centreline (bottom bracket drop)	mm
i	Distance from A to COM	mm
j	Distance from J to K measured parallel to seat tube	mm
k	Distance from K to COM measured perpendicular to seat tube	mm
L	Wheelbase	mm
L_1	Distance horizontally from rear wheel hub to A	mm
L_2	Horizontal distance from A to COM	mm
L_3	Distance horizontally from rear wheel hub to centre of bottom bracket	mm
L_4	Distance horizontally from C to D	mm

L_5	Wheel base less r_3	mm
O	Distance from A to bottom bracket spindle centreline measured parallel to seat tube	mm
P	Saddle height (from bottom bracket spindle centreline to the top of the seat)	mm
r	Actual radius of rear wheel	mm
r_1	Clearance radius of rear wheel	mm
r_2	Adjusted radius of front wheel allowing for bottom bracket drop (h_4)	mm
r_3	Reduced radius of front wheel allowing for crank sideways offset (d_1) and rotation of the wheel	mm
STA	Seat tube angle also (also called γ gamma)	degrees
Σ	Angle between seat tube centreline and line A to COM (SIGMA)	degrees

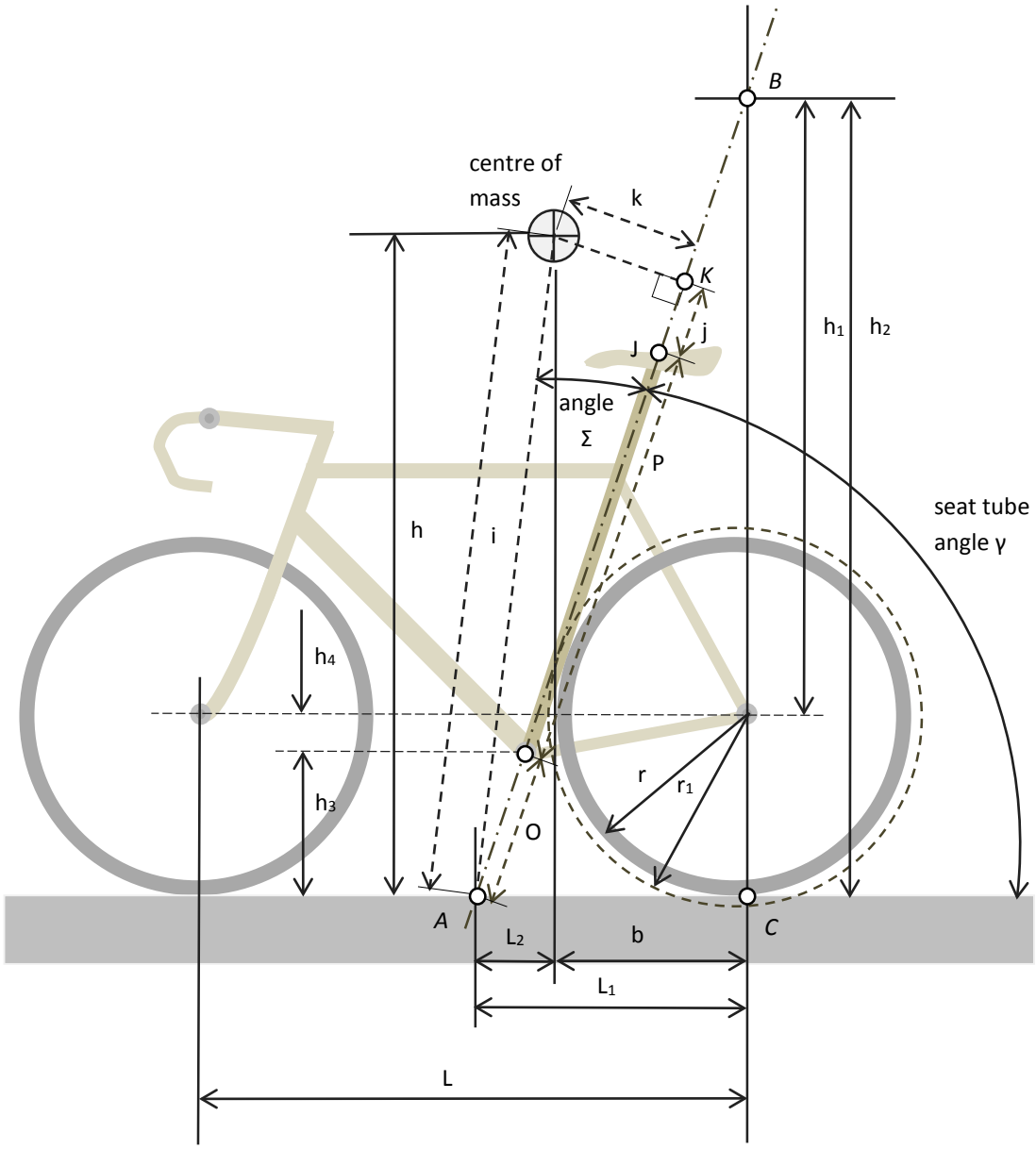

Figure 108 Defining the terms required to calculate the seat tube angle and saddle height from basic dimensions

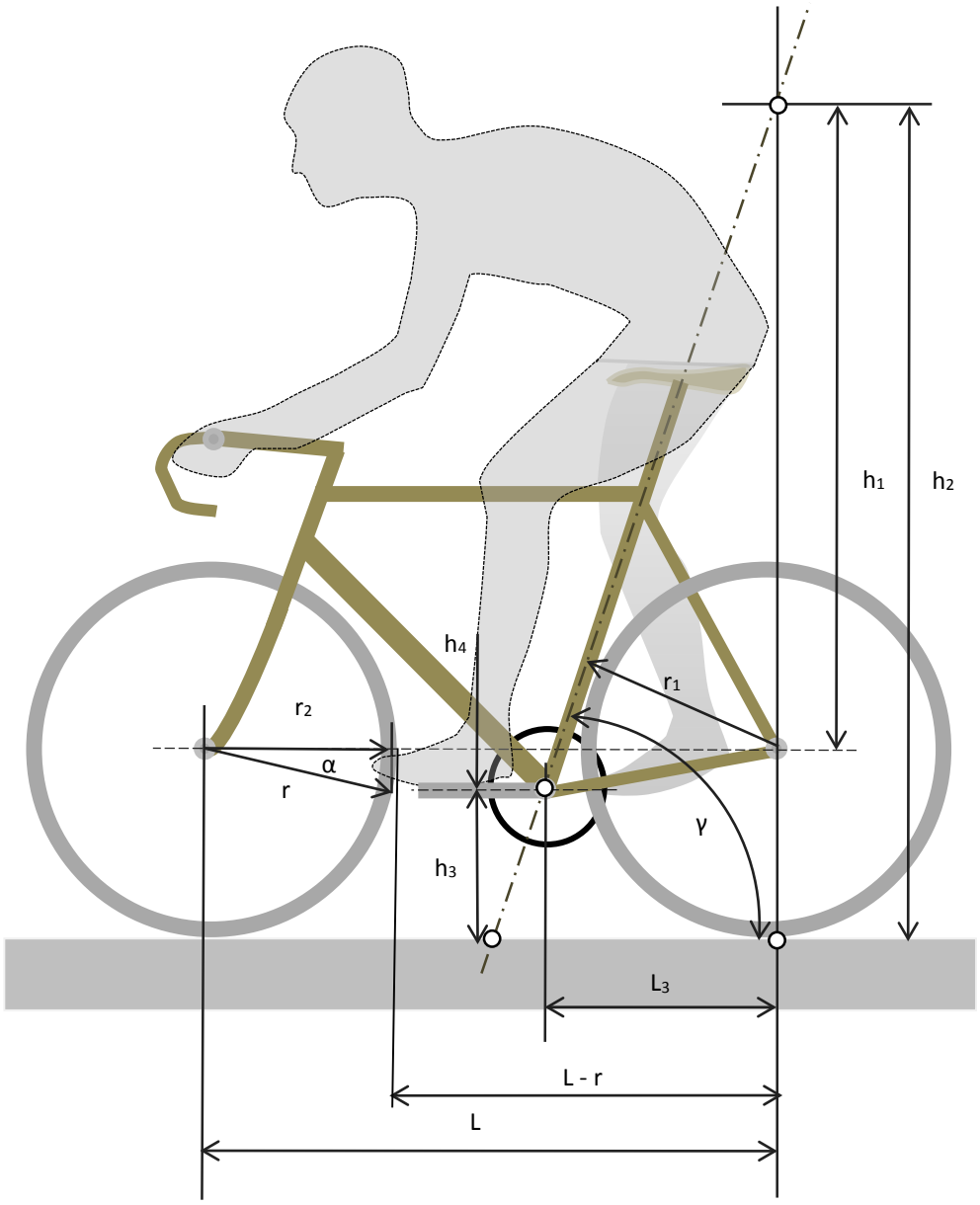

Figure 109 Toe overlap definitions and terms, used to define the toe overlap limit on the Frame Geometry Chart

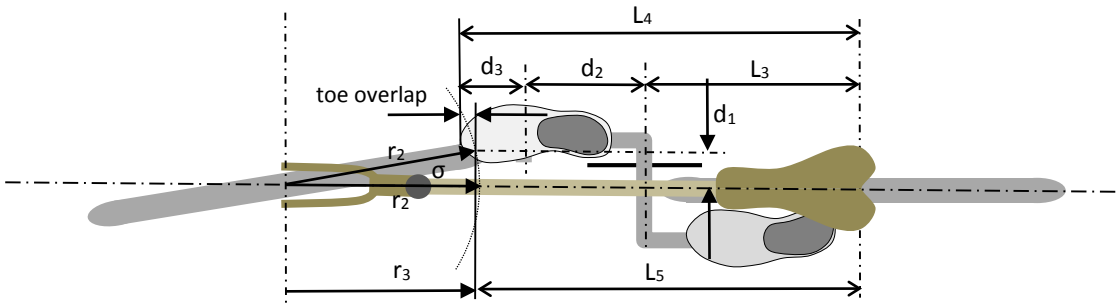

Figure 110 Top view of bicycle showing toe overlap and associated dimensions

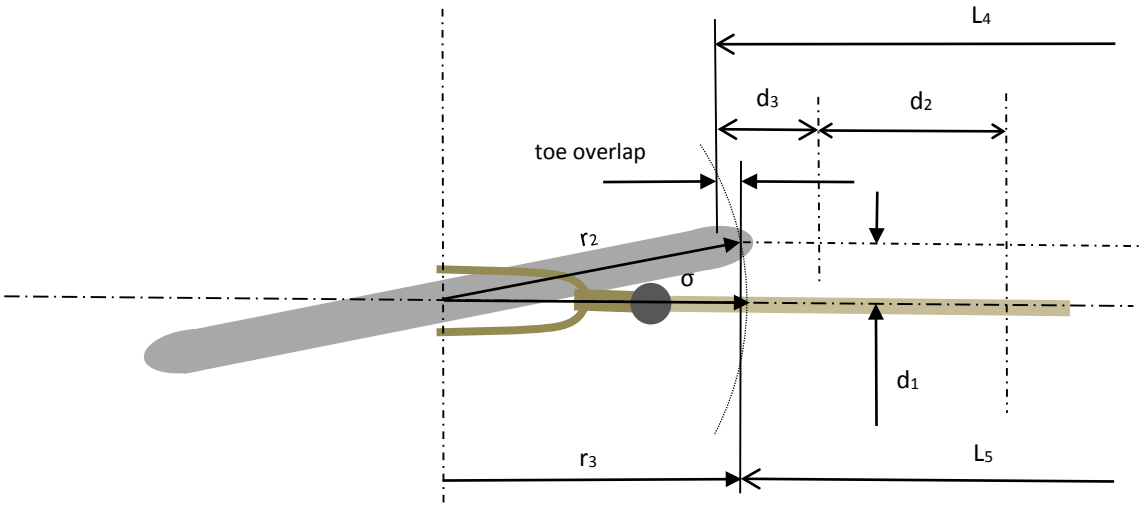

Figure 111 Closeup of toe overlap in figure above

Other useful terms are shown in Figure 112 and Figure 113

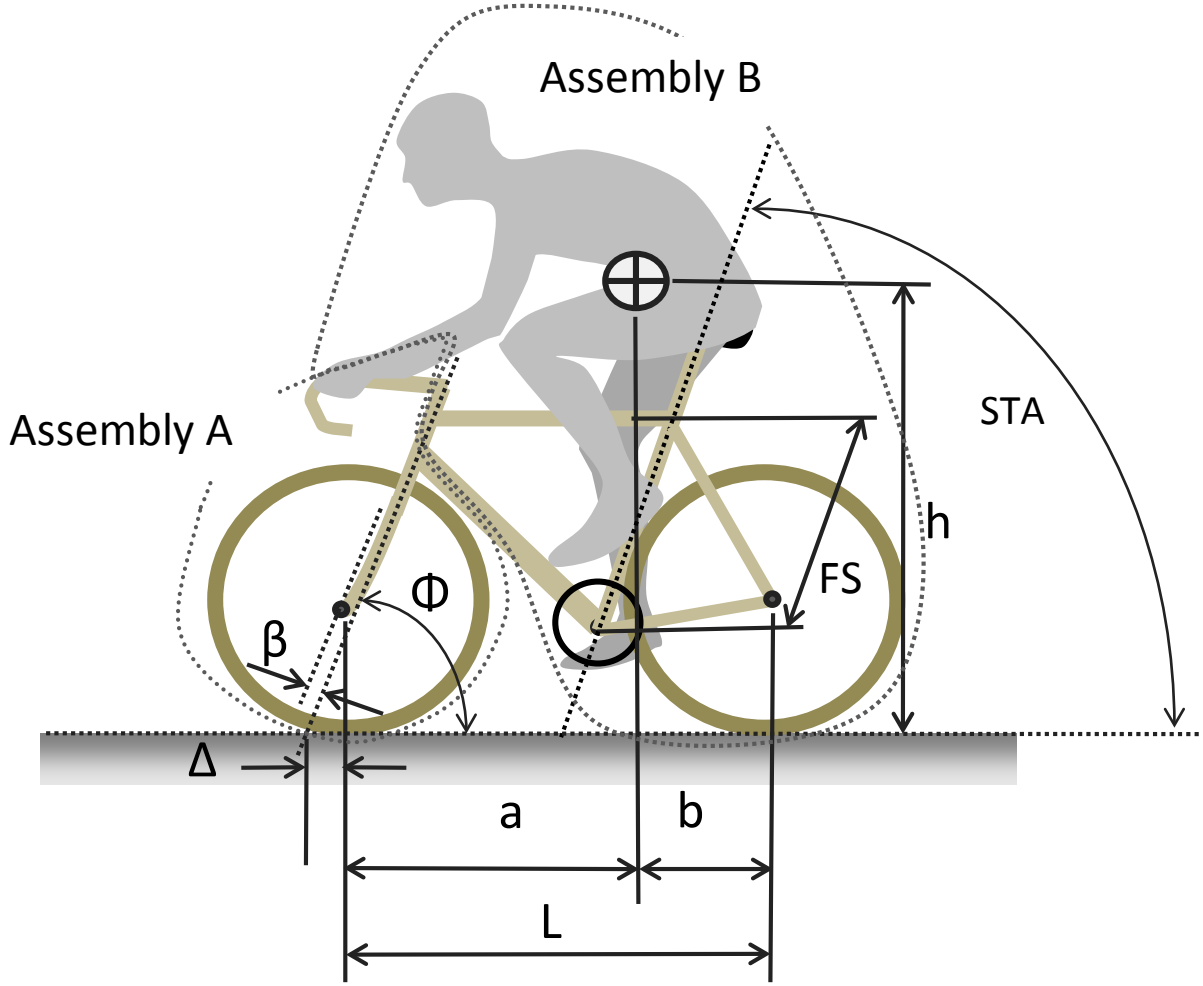

Figure 112 Bicycle term definitions and assemblies A and B

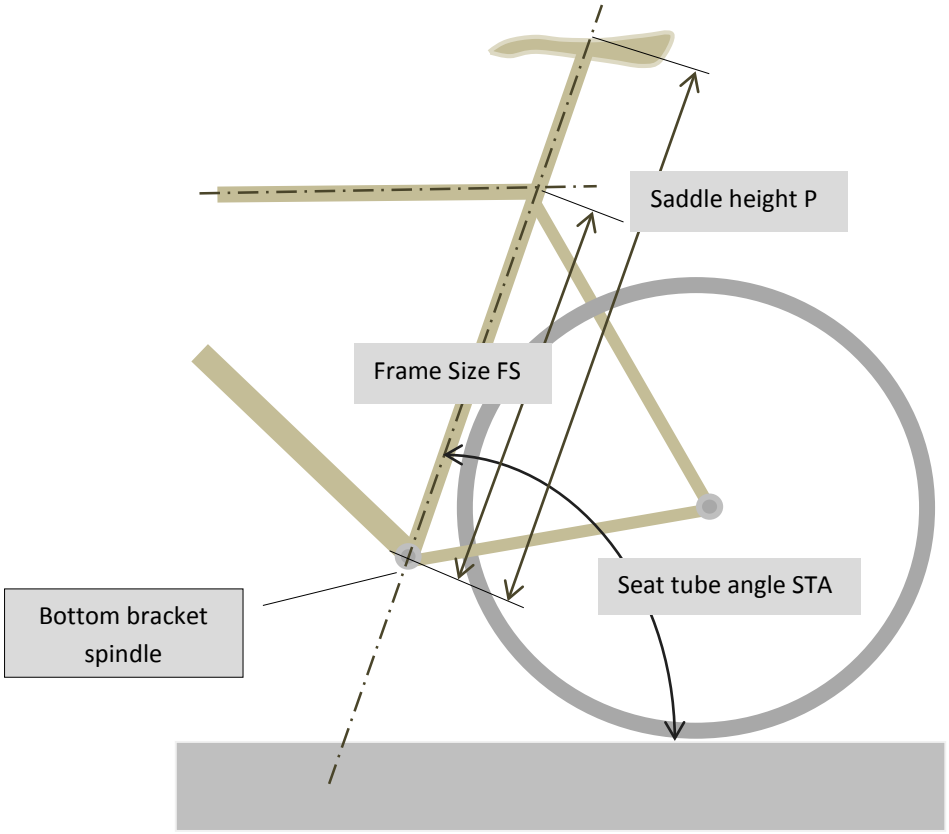

Figure 113 Defining the bicycle frame size, saddle height and seat tube angle

APPENDIX C – EXPERIMENTAL DETERMINATION OF PARAMETERS

The bicycle model needs appropriate parameter values to be determined in order for realistic dynamic simulations to occur and also in order for the sensitivity study to be undertaken. This Appendix discusses how these bicycle parameters were determined from: experiments, calculations and the literature. All the parameters, their definitions and values (as used in the Simulink model) are listed in Table 11 and Table 12.

The literature publishes a range of parameter values for actual bicycles but it is clear that many of the bicycles studied were not representative of modern high performance road bicycles. Typically the values are overly heavy and in the case of dimensions such as wheel diameters and wheelbases often inaccurate. Therefore it was necessary to apply more rigour to parameter determination in order to obtain the values necessary for this study.

It was convenient in this Appendix to group the parameters into three categories:

1. those associated with the rider (the human parameters)
2. the wheel parameters
3. and the parameters associated with rest of the bicycle, that is the bicycle main frame and the front forks

A combination of suitable methodologies was used to determine suitable parameter values and they enabled the determination to be achieved with some confidence. The following three methods were used:

1. experimental methods
2. engineering calculations
3. and evaluation of the literature

The following Table 49 lists which methods were used for each individual parameter, while Table 50 provides more details on the techniques and typical accuracy.

Table 49 Methodologies employed to find each bicycle parameter

Symbol	Parameter definition	Units	Methodologies used
human parameters			
M	mass of rider	kg	• experimental method using scales • reference to literature
b	horizontal distance from the rear wheel hub to the centre of rider mass	m	• experimental method using suspension technique • calculations • reference to literature
h	height of centre of rider mass	m	• experimental method using suspension technique • calculations • reference to literature
-	Rider height, inseam length, torso length, leg and arm lengths	m	• experimental method using rule and tape
I_X	moment of inertia of rider about X axis (roll)	kgm^2	• calculations • reference to literature
I_Z	moment of inertia of rider about Z axis (yaw)	kgm^2	• calculations • reference to literature
wheel parameters			
I_w	moment of inertia of wheels about X, Y and Z axes	kgm^2	• experimental method using compound pendulum • calculations • reference to literature
D	diameter of the bicycle wheel	m	• experimental method using rule • reference to literature
parameters associated with rest of the bicycle			
I_{XA}	moment of inertia of assembly A (excluding rider) about X axis (roll)	kgm^2	• experimental method using compound & bifilar pendulum • reference to literature
I_{XB}	moment of inertia of assembly B (excluding rider) about X axis (roll)	kgm^2	• experimental method using compound & bifilar pendulum • calculations • reference to literature
I_{ZA}	moment of inertia of assembly A (excluding rider) about Z axis (yaw)	kgm^2	• experimental method using compound & bifilar pendulum • reference to literature
L	bicycle wheelbase	m	• experimental method using tape • reference to literature
b	horizontal distance from the rear wheel hub to the centre of mass of bicycle	m	• experimental method using suspension technique • calculations • reference to literature
h	height of centre of mass of bicycle	m	• experimental method using suspension technique • calculations • reference to literature
M	mass of bicycle	kg	• experimental method using scales • reference to literature
Φ	head tube angle	degrees	• experimental method using angle protractor • reference to literature
β	fork rake (or offset)	m	• experimental method using rule and straight edge • reference to literature

Table 50 Details of techniques and accuracy

Symbol	Parameter definition	Units	Methodologies used and comments	Reading accuracy [1]
human parameters				
M	rider mass	kg	experimental scales	+/-100 g
-	distances	m	experimental rule and tape	+/-2.5 mm
I	moment of inertia of rider	kgm^2	not attempted	not known [2]
wheel parameters				
I	moment of inertia of wheel	kgm^2	digital stopwatch and engineering tape and rule	estimated as +/- 0.05 kgm^2 [3]
D	diameter of the bicycle wheel	m	experimental rule	+/-0.5 mm
parameters associated with rest of the bicycle				
I	moment of inertia of bicycle and forks	kgm^2	digital stopwatch and engineering tape and rule	estimated as +/- 0.05 kgm^2 [3]
L	bicycle wheelbase	m	engineering tape	+/-0.5 mm
b	hor. dist. from rear wheel hub to COM	m	engineering tape	+/-0.5 mm
h	vert. dist. from road hub to COM	m	engineering tape	+/-0.5 mm
M	mass	kg	experimental scales	+/-100 g
Φ	head tube angle	degrees	experimental angle protractor	+/-0.5^O
β	fork rake (or offset)	m	experimental rule and straight edge	+/-0.5 mm
FS	frame size	m	experimental rule	+/-0.5 mm
STA	seat tube angle	degrees	experimental angle protractor	+/-0.5^O
Note 1 engineering shop quality equipment was used but none of it was calibrated or certified, therefore the reading accuracy figures quoted are typical engineering shop values (117)				
Note 2 Hanavan estimated his results as generally within 10% of anthropomorphic studies (48)				
Note 3 based on measuring the dimensions, mass and time is within 1% of the true value				

C-1 HUMAN PARAMETERS

The model requires values for various human body parameters namely: mass, mass position and moments of inertia and though human subjects are simple to measure in terms of mass and dimensions such as height, they are more problematic with regards to measuring moments of inertia, particularly when a subject is in a cycling posture.

Some unsuccessful attempts were made to experimentally measure human moments of inertia using the bifiliar pendulum method. But it was found to be surprisingly difficult to obtain even approximate results due to the practical difficulties encountered and no useful results were obtained. It proved to be physically difficult to effectively suspend a person in the available workshop space due to a lack of headroom. In addition the slight changes in posture of a non-rigid human subject meant a wide variation in the recorded period was observed. Trying to sit still in a position that approximates the position of a seated rider on a bicycle was not easy.

Rather than spend more time trying to solve these problems it was decided after reviewing the available literature to rely on the exhaustive and authoritative work of Hanavan and others (48, 79). These studies have examined a large group of subjects with a wide range of body shapes and weights (covering the 5^{th}, 25^{th}, 50^{th}, 75^{th} and 95^{th} percentile groups) and have collated detailed tables for body heights, other dimensions, masses, COM positions and moments of inertia for many standard human postures, including several closely approximating a rider on a bicycle. One limitation of this study was that the subject population was exclusively male, so more work needs to be done to obtain accurate parameter values for female riders. We note one simple method found in the literature was claimed to be reasonably accurate for a standing subject. This was the Brenière method for calculating moments of inertia and uses the following two equations, where m is the subject's mass and H is the subject's height (118):

$$I_X = 0.0572mH^2 \tag{72}$$

$$I_Y = 0.0533mH^2 \tag{73}$$

Unfortunately this is no help for determining the moment of inertia for a rider on a bicycle because these formulas apply to only a standing person.

From this evaluation of the literature the human body parameter values used in this study are outlined in Table 51 and the values of particular interest for the benchmark bicycle are:

- It is assumed to be for Hanavan position no 18 (approximating a sitting rider, see Figure 14)
- The rider is a 95% male
- Height when standing = 1.857 m
- Total Mass = 91.05 kg
- Vertical position of COM measured from top of head = 0.686 m (or 1.171 m from ground)
- I_X lateral axis= 9.84 kgm^2
- I_Y transverse axis= 11.34 kgm^2
- I_Z longitudinal axis= 3.84 kgm^2

Table 51 Physical properties of the human body

Description	Height when standing m	Total Mass kg	Vertical position of COG measured from top of head	I_Z Longitudi-nal kgm^2	I_Y transverse kgm2	I_X lateral kgm^2	Comments
Standing upright arms by side	1.8	80	0.900	1.8	20	20	from simple measurements and calculations
Standing upright arms by side	1.8	80	0.900	n/a	13.82	14.83	from the Brenière equations (118)
Standing upright arms by side	n/a	n/a	n/a	1 – 1.75	10 - 15	10 - 15	from a range of values listed (78)
Standing upright arms by side	1.755	73.59	0.801	0.91	11.62	12.23	50% of males, Hanavan position no 1 (48)
Standing upright arms by side	1.796	80.27	0.815	1.09	13.23	13.95	75% of males, Hanavan position no 1 (48)
Standing upright arms by side	1.857	91.05	0.838	1.41	16.19	17.11	95% of males, Hanavan position no 1 (48)
Sitting in riding position	1.755	73.59	0.660	2.66	8.19	7.05	50% of males, Hanavan position no 18 (48)
Sitting in riding position	1.796	80.27	0.671	3.08	9.30	8.04	75% of males, Hanavan position no 18 (48)
Sitting in riding position	1.857	91.05	0.686	3.84	11.34	9.84	95% of males, Hanavan position no 18 (48)
range	1.755–1.857	73.59-91.05	N/A	0.91-3.84	9.3-20	7.05-20	
for details of Hanavan positions no 1 & 18, see Figure 10 and Figure 14							

C-2 WHEEL PARAMETERS

Pendulum experimental methods can be used to find the centres of gravity, radii of gyration and moments of inertia of complex bodies such as wheels and bicycle frames and two methods were used in this Appendix: the compound and the bifilar pendulum methods.

Using the compound pendulum method, the component (whether it was a wheel or tyre or bicycle frame) was freely suspended from a low friction fulcrum. The distance from the fulcrum suspension point to the component's centre of mass was accurately measured. Next the component was gently displaced from its equilibrium position about a horizontal axis. Care was taken to keep this displacement in plane and below a 6 degree half angle (in order to ensure at least three significant figures of accuracy). After release the component swung back and forth with a periodic motion, see Figure 114. The time taken for a fixed number of oscillations was accurately measured and this procedure was repeated at least three times. The times were averaged and the period was simply calculated. As the distance from the suspension point to the component's centre of mass and its mass was known, the radius of gyration and moment of inertia were easily calculated using equation (74) through to equation (76) (see also Table 52).

The results of all experiments, calculations and literature reviews regarding wheel properties are shown in Table 53 through to Table 55. From these tables the following comments and conclusions are made:

Experimental front wheel results

- average mass = 1.27 kg
- average I_Y = 0.0912 kgm^2
- average $I_{X/Z}$ = 0.0449 kgm^2

Experimental rear wheel results

- average mass = 1.635 kg
- average I_Y = 0.1017 kgm^2
- average $I_{X/Z}$ = 0.0500 kgm^2

Experimental tyre and tube results

- average mass = 0.407 kg
- average I_Y = 0.0515 kgm^2
- average $I_{X/Z}$ = 0.02575 kgm

Literature values

- range of mass = 1.5 – 3.92 kg
- range of I_Y = 0.120 – 0.408 kgm^2
- range of $I_{X/Z}$ = 0.060 – 0.204 kgm^2

Overall comments:

1. The experimental results show that the rear wheels are slightly heavier than the front wheels with slightly higher moment of inertia, but a reasonable approximation of values for both front and rear wheels is:
    a. mass = 1.4 kg
    b. I_Y = 0.100 kgm^2
    c. $I_{X/Z}$ = 0.050 kgm^2
2. The experimental values of tyres/tubes show that they contribution between 45 to 55% of the total moment of inertia of the complete wheel system (rim, spokes, hub, tyre and tube)
3. The values from the literature are without exception not appropriate for modern high performance road bicycles with the values being far too high for masses and moments of inertia (from 20 to 400% too high)

Compound pendulum equations

$$t = 2\pi\sqrt{\left({k_Y + h^2}/{gh}\right)} \tag{74}$$

$$k_Y = \sqrt{\left({ght^2}/{4\pi^2}\right) - h^2} \tag{75}$$

$$I_Y = Mk_Y^2 \tag{76}$$

Table 52 terms used in compound pendulum equations

Symbol	Term definition	Units
t	period of oscillation	sec/cycle
k_Y	radius of gyration about Y axis	m
h	distance from suspension point to centre of mass	m
M	mass of body (wheel)	kg
I wheels	moment of inertia of body (wheel) about Y axis	kgm^2

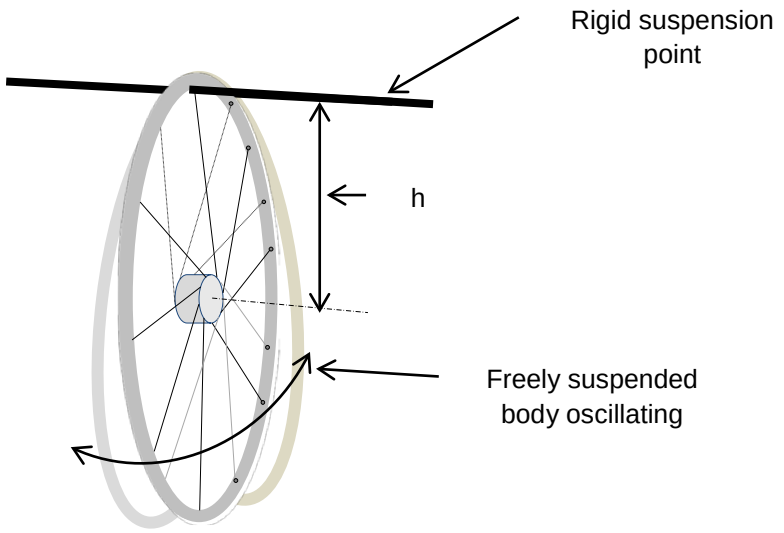

Figure 114 A compound pendulum setup to determine the bicycle wheel's moment of inertia

Table 53 Front wheel experimental results for mass and moments of inertia

Wheel type	Tyre type	Mass kg	I_Y Pitch/rotational kgm^2	I_X/I_Z yaw/roll kgm^2	Comments
700C x 23 wheel	700Cx23	1.220	0.0918	0.0473	I values from a simple engineering calculation
Mavic SUP Open Pro Suntour hub	Hutchinson 700Cx23	1.424	0.0871	0.0492	from compound pendulum experiments
Mavic MA3 Campagnola Chorus hub	Hutchinson 700Cx23	1.440	0.1077	0.0520	from compound pendulum experiments
Mavic MA3 Campagnola Chorus hub	none	0.958	0.0571	0.0286 [1]	from compound pendulum experiments
Shimano 105 rim & hub	Hutchinson 700Cx23	1.397	0.1095	0.0506	from compound pendulum experiments
ALTX 2800 A class Hub	Michelin Dynamic 700Cx23	1.162	0.0845	0.0421	from compound pendulum experiments
Airline Vuelta Shimano Ultegra hub	Clement Ultra performance 700Cx23	1.292	0.1006	0.0445	from compound pendulum experiments
	average	1.2704	0.0912	0.0449	
Note 1 this value was not found experimentally but was calculated from $I_X = ½ I_Y$					
All wheels are 700C					

Table 54 Rear wheel experimental results for mass and moments of inertia

Wheel type	Gear cluster	Tyre type	Mass kg	I_Y kgm^2 pitch/rotational	I_X/I_Z kgm^2 yaw/roll	Comments
Mavic Aksium Race rim & hub	No gears	Hutchinson 700Cx23	1.494	0.1020	0.0489	from compound pendulum experiments
Mavic SUP Campagnola Chorus hub	10 speed Campagnola Chorus cluster	Hutchinson 700Cx23	1.766	0.1017	0.0499	from compound pendulum experiments
Mavic SUP Shimano Ultegra hub	No gears	Clement Ultra performance 700Cx23	1.536	0.1014	0.0507 [1]	from compound pendulum experiments
Shimano 105 rim & hub	9 speed Shimano cluster	Hutchinson 700Cx23	1.894	0.1054	0.0527	from compound pendulum experiments
ALTX 2800 A class Hub	No gears or skewer	Hutchinson 700Cx23	1.487	0.0979	0.0477	from compound pendulum experiments
		average	1.635	0.1017	0.0500	
Note 1 this value was not found experimentally but was calculated from $I_X = ½ I_Y$						
All wheels are 700C						

Table 55 Tyre and tube only experimental results for mass and moments of inertia

Tyre type	Tyre condition	Tube type	Total Mass kg	I_Y kgm^2 pitch/rotational	Comments
700Cx23	n/a	700Cx23	0.359	0.0459	I values from a simple calculation
Hutchinson 700Cx23	new	Continental Race 700Cx18/25	0.496	0.0522	from compound pendulum experiments
WTB Carmino 700Cx23	worn	Continental Race 700Cx18/25	0.406	0.0421	from compound pendulum experiments
Maxxis Detonator 700Cx23	worn	Continental Race 700Cx18/25	0.377	0.0401	from compound pendulum experiments
Maxxis Detonator 700Cx23	worn	Continental Race 700Cx18/25	0.379	0.0427	from compound pendulum experiments
Michelin Select 700Cx28	worn	Continental Race 700Cx18/25	0.601	0.0642	from compound pendulum experiments
Michelin World Tour 700Cx32	new	Continental Race 700Cx18/25	0.674	0.0733	from compound pendulum experiments
		average	0.4703	0.0515	
these results are for the tyres and tubes only and all are 700C, it excludes the wheel rim, hub and spokes					

Table 56 Literature results for wheel mass and moments of inertia

Wheel type	Radius m	Total Mass kg	I_Y pitch/rotational kgm^2	I_X/I_Z yaw/roll kgm^2	Comments	Source
front wheel	0.350	3.00	0.280	0.140	Front wheel carrying measuring apparatus which increases weight	(14)
front wheel	0.342	2.02	0.162	0.081	heavy and small diameter	(44)
front wheel	0.325	2.09	0.218	0.109	heavy and very small diameter	(60)
front & rear wheels	0.350	1.50	0.140	0.070	small diameter	(13)
front & rear wheels	n/a	2.15	0.134	0.046	heavy	(28)
front & rear wheels	n/a	n/a	0.095	n/a		(12)
rear wheel	0.300	2.00	0.120	0.060	very small diameter	(14)
rear wheel	0.342	3.12	0.156	0.078	heavy and small diameter	(44)
rear wheel	0.325	3.92	0.408	0.204	very heavy and very small diameter	(60)

C-3 BICYCLE (FRAME AND FORK) PARAMETERS

The last group of parameters to be found were those associated with the bicycle frame and front forks. The suspension method was used to find the centre of mass of a bicycle (with and without wheels). Using this method the bicycle to be examined was freely suspended so that it could hang below a suspension point and find a stable equilibrium position. A plumb bob was hung from the suspension point and was allowed to settle beside the bicycle and the line of the plumb bob was marked. The bicycle was then suspended from a different suspension point and the procedure repeated. The intersection of the two marked lines indicated the centre of mass position of the bicycle on a two dimensional plane, see Figure 115 through to Figure 117. Additional suspension points can be used to improve accuracy or provide COM positions in other planes.

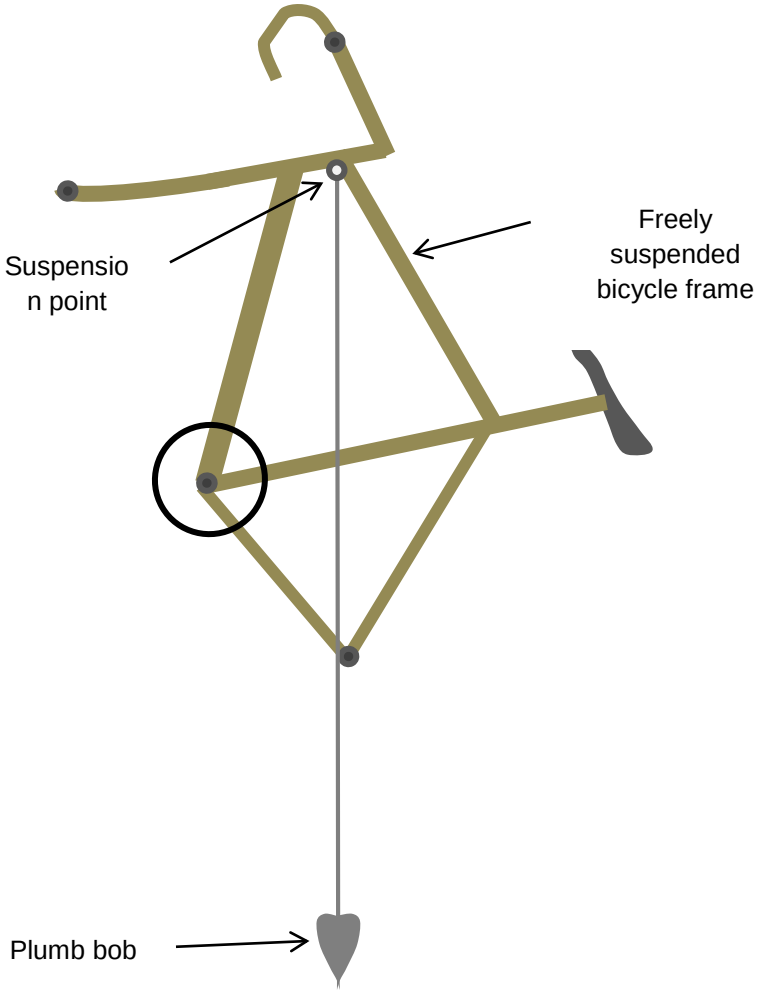

Figure 115 Bicycle frame suspended in the first position

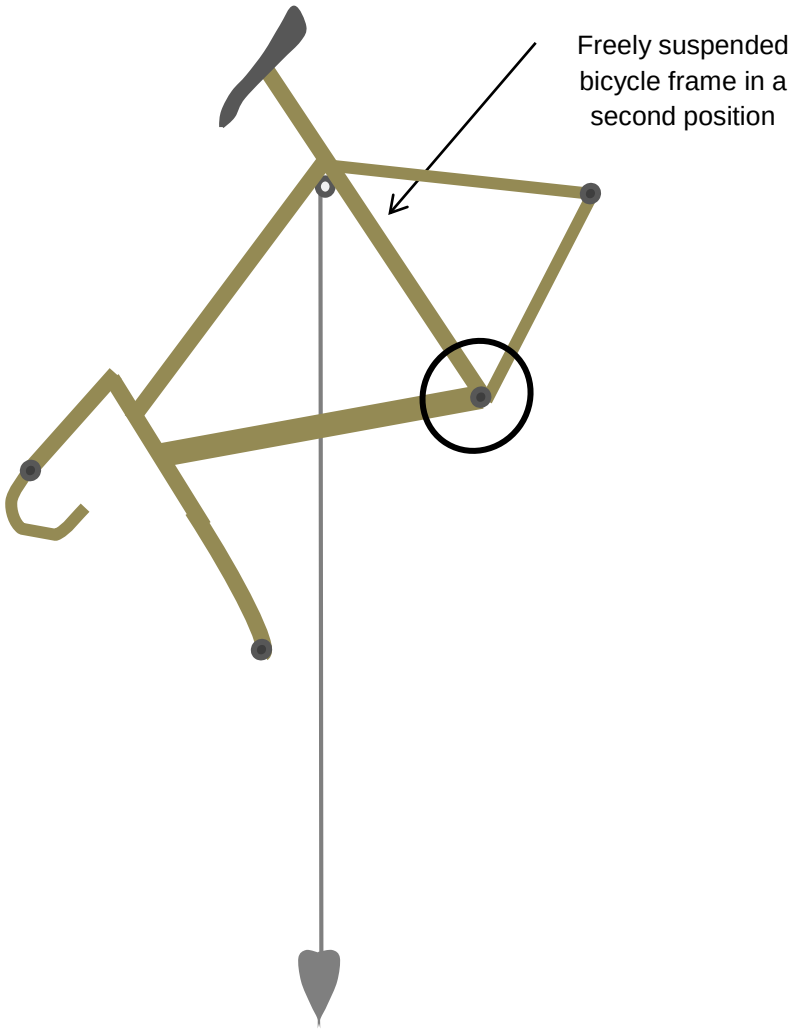

Figure 116 Bicycle frame suspended in the second position

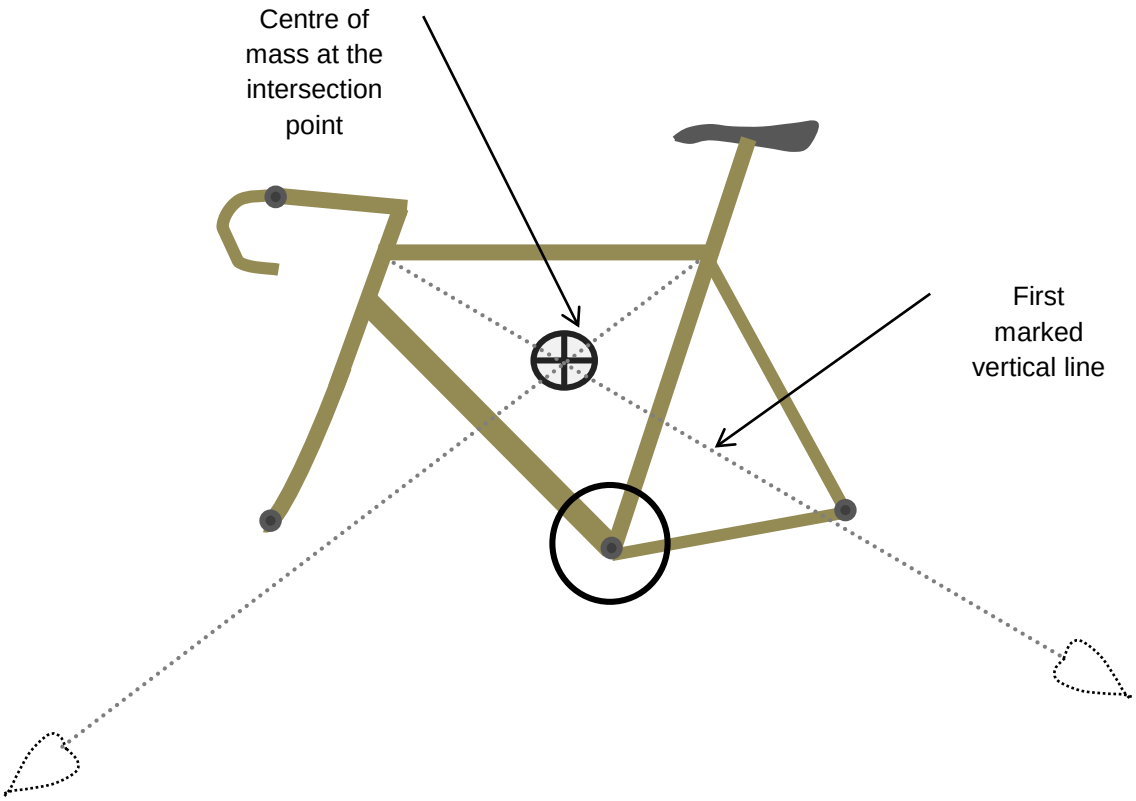

Figure 117 The location of the centre of mass is indicated by the intersection point

The bifilar pendulum method was used to find the moment of inertia of the bicycle and uses a similar procedure to the compound pendulum method. This time though the component (the bicycle frame) was freely suspended from two light and equal length cables. The length of each cable and the horizontal position of the bicycle frame's centre of gravity (previously found) relative to each cable was measured. The bicycle frame was gently displaced from its equilibrium position, this time about a vertical axis and again the displacement is in plane and below a 6 degree half angle. After release the bicycle frame swung backwards and forwards in a periodic motion and the time taken for a number of oscillations was accurately measured (again this was repeated at least three times and the results averaged and the period calculated). Having measured the length of each cable, the distance from each cable to the component's centre of gravity and the mass, the radius of gyration and moment of inertia are calculated using equation (77) through to equation (79).

$$t = 2\pi\sqrt{IL/Mgab} \tag{77}$$

$$I = \left(\frac{t}{2\pi}\right)^2 \frac{Mgab}{L} \tag{78}$$

$$I = Mk^2 \tag{79}$$

Table 57 Bifilar pendulum terms

Symbol	Term definition	Units
t	Period of oscillation	sec/cycle
k	Radius of gyration about a vertical axis (Z)	m
L	Distance from suspension points to centre of mass (length of each cord)	m
a	Horizontal distance from left hand cord to the body's centre of mass	m
b	Horizontal distance from right hand cord to the body's centre of mass	m
M	Mass of body	kg
I	Moment of inertia of body about a vertical (Z) axis	kgm^2
note it is often possible to arrange values a and b so they are equal and this simplifies the experiment		

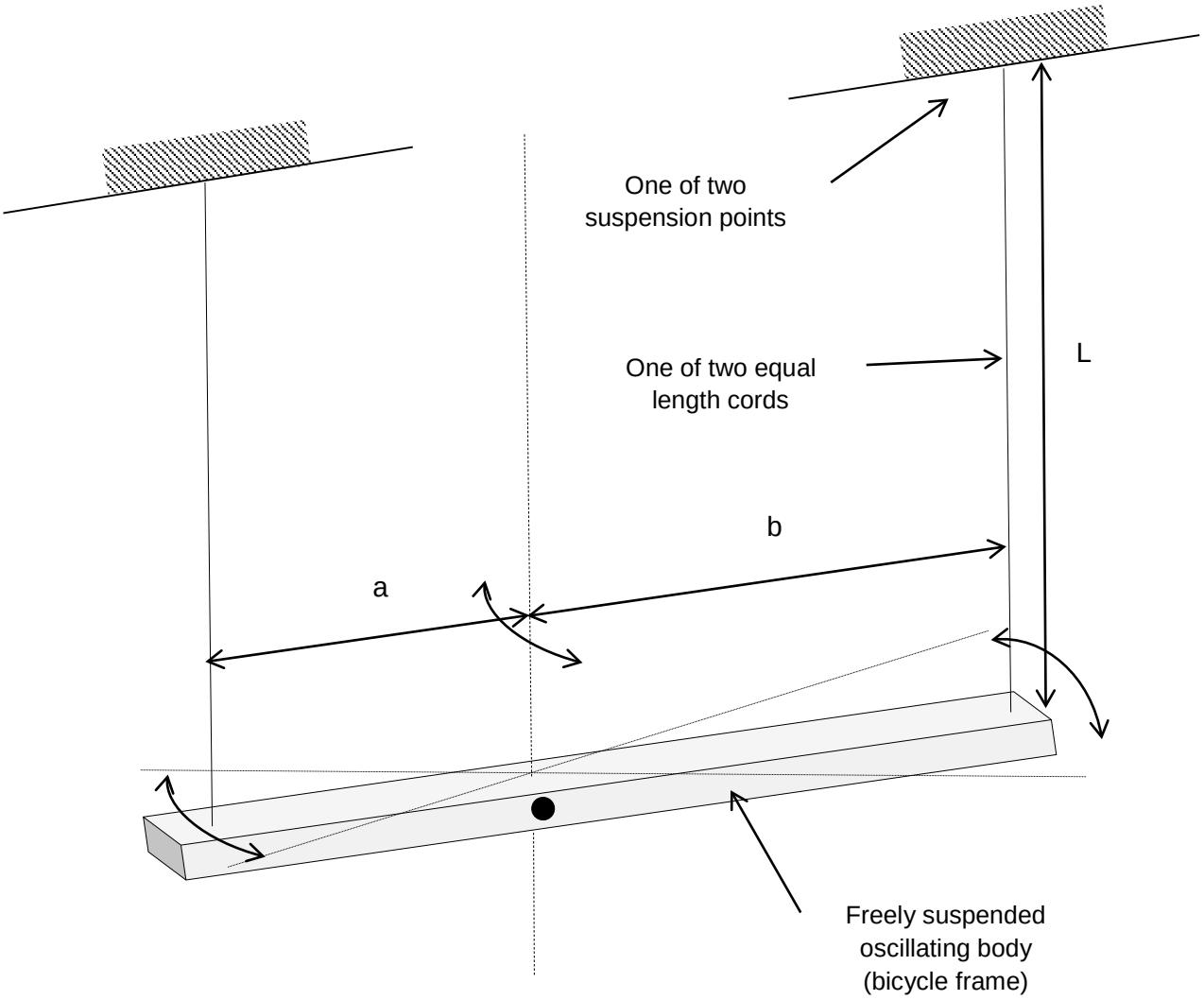

Figure 118 The bifilar pendulum experimental apparatus

It can be seen from these tables (Table 58 and Table 59) that more work needs to be done to obtain a greater range of experimental and calculated results, but they are better values than those of the literature (Table 60). The values in this table are incomplete and as is common in the literature, the wheel values are based on non-competitive bicycles that have less relevance to this study.

Table 58 Bike and frame experimental results for mass and moments of inertia

Bike type		Total Mass kg	Horizontal position of COM from road m	Vertical position of COM from centre of rear wheel m	I_Y pitch kgm^2	I_X roll kgm^2	I_Z yaw kgm^2	Comments
De Rosa Endurance	57cm 1999	9.0	0.500	0.482	1.9741	0.521	1.2928	Complete bike with wheels
Trek 1500	57cm 2004	8.5	0.475	0.489	2.4387	1.9566	1.5146	Complete bike with wheels
Trek 1500 (frame/fork only)	57cm 2004	6.0	0.513	0.505	1.3501	0.5324	0.8898	Frame with fork, groupset, handlebars etc. but without both wheels
average		7.83	0.496	0.492	1.9210	1.0033	1.2324	

Table 59 Front fork engineering calculations results for mass and moments of inertia

Bike type for fork, stem, Handlebars & wheel (assembly A)	Total Mass kg	Horizontal position of COM from road m	Vertical position of COM from centre of front wheel m	I_Y pitch kgm^2	I_X roll kgm^2	I_Z yaw kgm^2	Comments
Generic type	2.200	0.444	0.106	n/a	0.2250	0.0758	values from a simple calculation
De Rosa Endurance 57cm 1999 year	1.693	0.4495	0.053	n/a	0.6554	0.3851	calculated using experimentally measure values for wheels and forks (but not the handlebar and stem)
average	1.9465	0.44675	0.0795	n/a	0.4402	0.2305	

Table 60 Literature results for bicycles, frames & subassemblies for mass and moments of inertia

Assembly	Total Mass kg	I_Y pitch kgm^2	I_X roll kgm^2	I_Z yaw kgm^2	Comments	Source
Front fork assembly	n/a	n/a	0.84	0.079		(12)
Front fork assembly	4.0	0.06	0.0546	0.0114	excessively heavy	(14)
Front fork assembly	2.0	3.88	3.28	0.566		(13)
Front fork assembly	4.3	n/a	0.345	0.065	excessively heavy	(44)
Front fork assembly	4.04	0.384	0.421	0.041	excessively heavy	(60)
Rear assembly only (no wheel or rider)	11.05	1.934	0.407	1.558	excessively heavy	(60)
Rear assembly & rider	n/a	n/a	163.0	n/a	about roll axis at road level not about axis through COM	(12)
Rear assembly & rider	87.0	n/a	n/a	n/a	moderately heavy	(13)
Rear assembly & rider	85.0	11.0	9.20	2.80	moderately heavy	(14)
Rear assembly & rider	116	n/a	16.784	6.035	excessively heavy	(44)

C-4 EXPERIMENTAL BICYCLE APPARATUS DETAILS

The test bicycle was equipped with in-house custom designed and built measurement devices. These transducer devices measured the values of the front wheel yaw angle (σ) relative to a longitudinal axis and the roll angle (λ) of the bicycle relative to a vertical axis, see Figure 31 to Figure 33. A detailed list of the equipment used to conduct the experimental investigation is listed in Table 61.

Table 61 Experimental equipment list

Description	Purpose	Identification Details
Healing road bicycle	to mount the recording equipment on and to perform the required manoeuvres	Serial Number 31320838
Infra Red Distance Sensor	measures the roll angle	Sharp Corporation model GP2D12
Rotary electrical Potentiometer	measures the yaw angle	model Alpha 2C A25K
Data logger	records and stores the data	Custom made at AUT
Personal Computer (PC)	processes the recorded data	AUT Serial Number 34268
CodeVision AVR™ software	a C Language programming software package that receives data and saves it as a CSV file	Version 1.23.8
MATLAB™ software	converts the CSV file into a suitable format for detailed mathematical analysis	Version 6.5.0 Release 13

Roll angle sensor

The roll angle was measured using an infra-red (IR) distance measuring sensor mounted on a short bracket at the rear of the bicycle, see Figure 34 and Figure 35. As the bicycle rolls the IR sensor detects a change in its distance from the ground and this is used to calculate the actual roll angle.

The IR sensor is manufactured by the Elecom Group of the Sharp Corporation of Japan and is a GP2D12 model. This IR sensor generates a voltage output inversely proportional to the distance measured (or to the distance of a detected object). The GP2D12 sensor is tolerant of interference

from ambient light and differences in the color of objects being detected. For example it is possible to detect a black wall in full sunlight.

The output voltage signal from the CCD array will vary depending upon the amount of surface exposed to the IR beam. This voltage signal is used to determine the angle of reflection and therefore the distance to the surface. The angle of reflection can be found using the tan relationship and this indicates a non-linear relationship.

The graph shown in Figure 119 is of the output voltage vs. distance for the IR distance sensor and clearly shows that the output within the manufacturer's stated range of 10 cm - 80 cm, is not linear but is approximately logarithmic. It is necessary to calibrate and linearise the sensor's output using either a lookup table or a parametric function.

The graph also shows that once the sensor moves inside a certain distance range (i.e. below 10 cm); the output drops rapidly and starts to repeat values matching long range readings. The solution to this problem is to attach the sensor to the bicycle so that it will always be at least 10 cm above the ground even when the bicycle rolls to the maximum angle of 10^{o}. From Figure 119 it is clear that the best resolution for this sensor is when the distance measured ranges between 10 to 20 mm. This is because within this range the slope of the graph is steepest and is approximately linear.

Roll Angle Calculations

The IR distance sensor is located on a cantilevered bracket in a fixed position, making it possible to calculate the roll angle. The transverse position of the sensor (distance N) is fixed at 150 mm from the bicycle's centreline while the vertical position (distance K) is fixed at 140 mm above the ground. These positions have been calculated to give the best performance in terms of the IR sensor's performance. As the bicycle rolls, the IR sensor measures the change in distance to the ground (distance M), see Figure 34 and Figure 35. The roll angle λ is calculated from the following formula:

$$\lambda = \tan^{-1}\left(\frac{K-M}{N}\right) \tag{80}$$

From the values in Table 62, the worst IR sensor resolution is calculated as 0.357 degree per digital output value, [5 degrees ÷ (158-144) = 0.357]. The graph shown in Figure 120 represents the relation between the roll angle and the digital output and shows an approximately linear relation between them. Note that the maximum roll angle required to be measured was set at +/- 10° due to the limitations of the IR sensor.

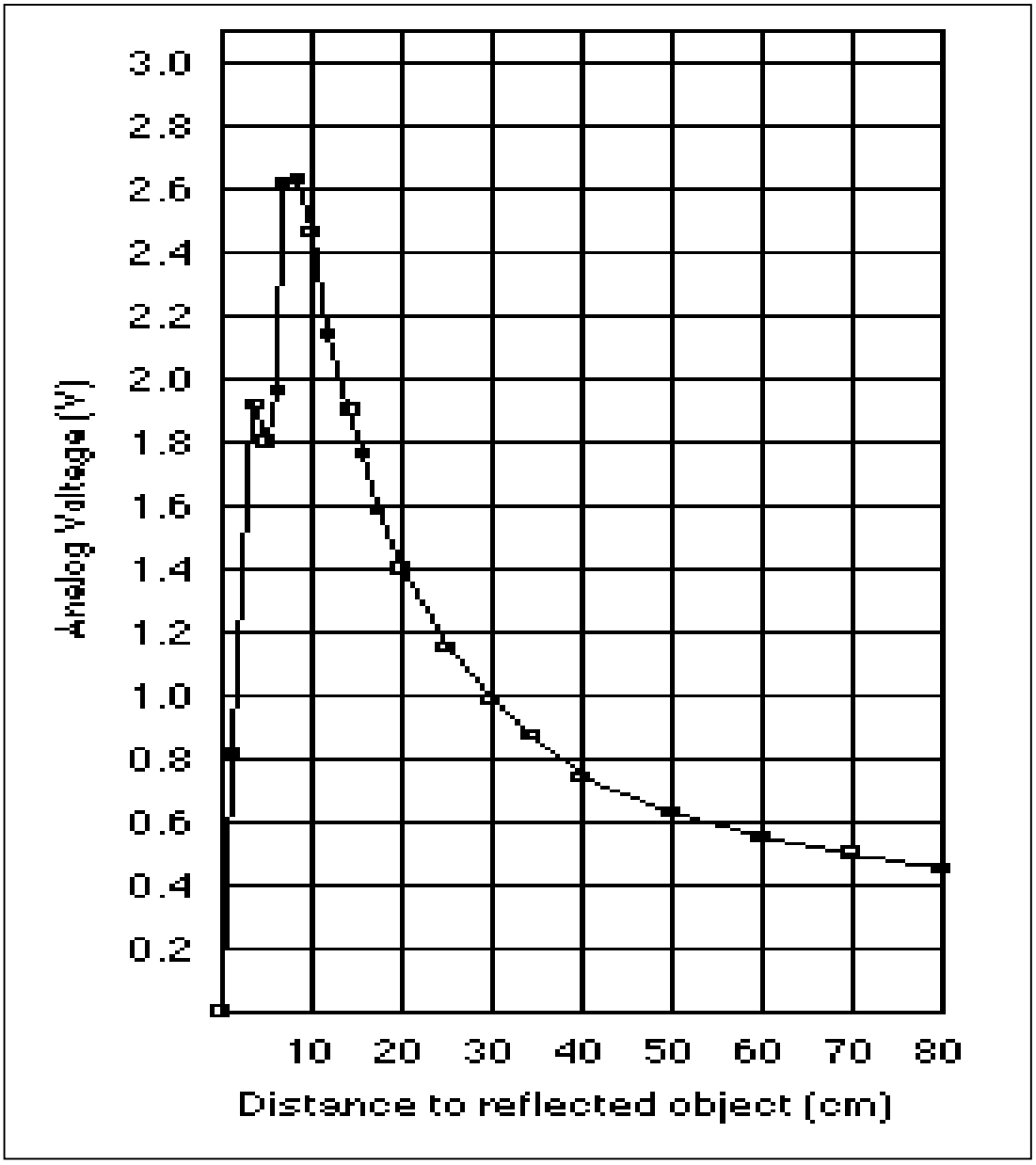

Figure 119 Output voltage vs. distance for the IR distance sensor (model GP2D12)

Table 62 IR sensor roll output values vs. roll angle

Roll angle of the bicycle (degrees)	Sensor distance M (mm)	Analogue output voltage (V)	Digital output [1]
-10º	113.55	2.1577	158
-5º	127.00	1.9662	144
0º	140.00	1.8140	133
5º	153.12	1.6900	124
10º	166.45	1.5830	116
Note 1 using 8 bit resolution and converted from the analogue voltage			

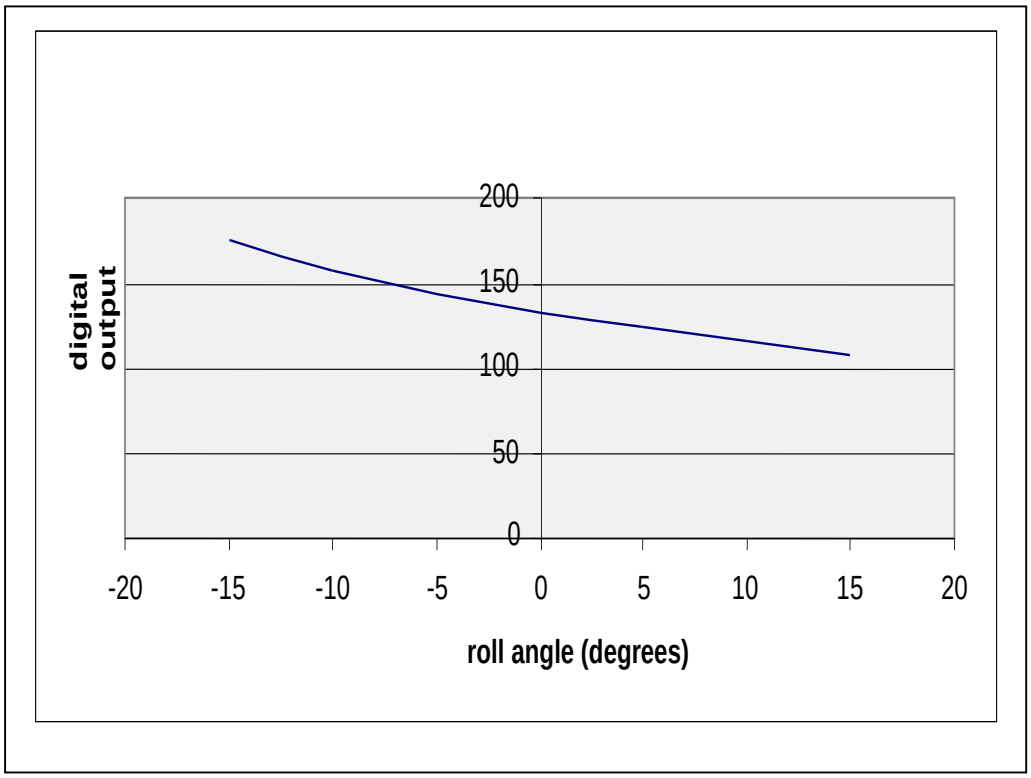

Figure 120 IR sensor roll angle vs. digital output

Memory Capacity Calculations

The sensor outputs are converted into a digital format by the microcontroller and stored in an external SRAM (static random access memory) ready for further processing. Since the memory used in this project is a 32K x 8 bits SRAM, it contains 32768 (32 x 1024) memory positions or spaces to store information. Both the roll and yaw angle values come in an 8-bit format and are stored in two different memory positions, therefore two memory positions are required every time a sample is made. So the maximum possible number of samples will be, 32768 ÷ 2 = 16384 samples.

The sampling rate is set at once per 10 ms and therefore 100 samples are made every second. This means that the maximum memory capacity is: 16384 samples ÷ 100 samples/sec = 163.84 seconds and this means the data logger can record a maximum of 2.73 minutes of experimental run time.

Yaw angle sensor

The yaw angle was measured using a rotary electrical potentiometer, of model type Alpha 2C A25K. The measurement principle employed by a potentiometer is that a change in resistance occurs as the steering stem is rotated making it possible to get an output proportional to the yaw angle of the front wheel. The potentiometer was directly attached to the steering stem using a simple rubber coupling, see Figure 33. The potentiometer (with a range of 0-20 MΩ, MegaOhms) was arranged so that a 10 MΩ output equals the zero degrees yaw angle. This places the straight ahead position of the handlebars exactly halfway within the operating range. Therefore an output signal of between 0-10 MΩ indicates left hand turns while a 10-20 MΩ signal indicates right hand turns.

Sensor calibration

When describing the performance of any measurement sensor, three main terms are frequently used:

- accuracy i.e. how close the recorded value is to the true value
- sensitivity i.e. the smallest input to which the sensor can respond
- precision i.e. the agreement amongst a set of readings

In order to define a particular sensor in relation to these terms it is necessary to calibrate the sensor. Calibration will measure each particular type of error for the sensors and allow corrective adjustments to be made. The standard procedure to calibrate a sensor is to adjust linearity at 50 % of the full scale range. Next, the span is adjusted at 90 % of the full scale range and finally any zero error is corrected at 10 % of the scale. The span and zero errors continue to be corrected until no further adjustment is needed. See the glossary for a definition of these calibration terms.

Calibration Procedure

A calibration record plotting the sensor's reading against the true value should be prepared for the sensor over its working range. The roll angle and yaw angle sensors were calibrated to give error free results and the calibration apparatus that was used included:

1. engineer's level
2. steel rule
3. plumb bob
4. assorted engineering clamps
5. flexible tape measure, twenty metres long

Both sensors were first checked to make sure their sign values (plus or minus) were correct. These can be easily changed by changing sign terms in the Matlab programme that converts the CSV file into a series of angular readings in degrees.

The IR sensor for measuring roll was checked for zero error. The bicycle was held firmly upright in a level position that was checked by both a level and plumb bob. The data logger was switched on and a recording was made of the roll angle. This was downloaded to a PC and processed by Matlab to give a sensor roll angle reading in degrees. If the sensor did not read zero the position of the roll angle transducer was moved to correct the signal. For example if the reading was greater than zero the sensor was moved down, if it was less then zero it was moved up. As a final check a rider was placed on the bicycle to compress the tyres to their operating condition and the zero test repeated. The pressure in the tyres drops slowly over time and so the sensor's height drops which means the zero calibration should be repeated frequently.

When checking the zero error of the yaw angle sensor, the bicycle was wheeled along a marked straight line with the handlebars locked in a fixed position. The handlebar position was adjusted until the bicycle would follow the straight marked line for at least twenty metres. This indicated that the steering handlebar was locked in the zero degrees position. Once this was done the data logger was switched on and a recording made of the yaw angle. Again this was downloaded to a PC and processed by Matlab to give yaw angle sensor reading in degrees. If the reading was not equal to zero the position of the yaw angle transducer was rotated to correct the signal. For a positive yaw angle error the potentiometer was rotated clockwise (when viewed from above), for a negative reading it was rotated anticlockwise.

Due to the difficulty experienced in adjusting both sensors, the zero error was not able to be eliminated. This experience suggests that a priority for any future investigations would be to improve the ability of this equipment to be easily and accurately calibrated.

Records of both sensor's calibration results were made, these tables compare recorded values to actual values and are shown in Table 63 and Table 64.

Table 63 Record of the calibration data for the Roll Angle Sensor

Actual angle (degrees)	**Sensor recorded angle (degrees)**
-10	-9
-5	-4
0	+1
+5	+6
+10	+11
The roll angle sensor zero error = +1	

Table 64 Record of the calibration data for the Yaw Angle Sensor

Actual angle (degrees)	**Sensor recorded angle (degrees)**
-30	-25
-20	-15
-10	-5
0	+5
+10	+15
+20	+25
+30	+35
The yaw angle sensor zero error = $+5^0$	

C-5 REMARKS

The easiest components to experimentally check are the wheels and the tyres by using the compound and bifilar pendulum methods which were successfully used to find values of radii of gyration and moments of inertia. Overall the experimental values agreed closely with most of the literature and with basic engineering calculations. The experiments were also very repeatable with period time readings often agreeing to within 0.05 seconds.

However the experiments are moderately sensitive to measurement error of the period or mass or dimensions. For example a 1% error in measuring the period of a bifilar pendulum leads to about a 2% error in the value of the moment of inertia.

It was also found that different manufacturers' wheels, rims, spoke arrangements and tyres can make a considerable change to the moments of inertia of up to +/- 15%. This is significant because as mentioned in Chapter 6 the wheel's moment of inertia about the rotational axis (I_{ZF}) was found to have some importance, a 1% increase decreases the settling time by a moderately significant 2% as noted in Chapter Five. Interestingly tyre contributes about 50% a wheel's overall moments of inertia. Also it was observed that even for the small selection considered in Table 55, different manufacturers' tyres can be over 100 grams lighter than others tyres and this will make a subsequent 20% reduction in the moment of inertia. This was for 700 x 23 tyres and 700C X 18/25 tubes only.

Engineering calculations were possible on some components, namely wheel moments of inertia, front forks, bicycle frame and these calculations had close agreement to the experimental values which allows some confidence in advancing the selected values for the benchmark bicycle.

Using the methods outlined in this Appendix it was possible to select realistic parameter values for the model including the moments of inertia for the main subassemblies of the bicycle model. These values are now presented in the benchmark bicycle in Table 13. In addition a more complete picture of the normal range of values has been obtained so that decisions about future variations to the model can be made with knowledge and confidence.

APPENDIX D –STABILITY ANALYSIS

This Appendix details the characteristic equation, applies the Routh Stability Criterion and performs a frequency analysis of the bicycle system.

D-1 CHARACTERISTIC EQUATION

For completeness in this Chapter the characteristic equation of the bicycle system was found as its roots determine the character of the time response of the system and they can be used to understand the natural transient response of the system. By equating the denominator of the system's transfer function equation to zero the characteristic equation is obtained. The characteristic equation's roots (poles) along with the roots of the numerator polynomial (zeros) are the critical frequencies of the system.

A necessary requirement for stability is for all of the roots of the characteristic equation to have negative real parts. So once the characteristic equation has been found the Routh Stability Criterion can be used to find out if it has any unstable roots without actually solving them and this is shown in this Appendix.

To find the characteristic equation from the current three equations of motion ((14, (19 and (24) it is helpful to ignore any terms which are very small.

The first equation considers yawing moments about the vertical Z axis for the front assembly A, equation (14) and has 8 terms, but which ones can be ignored? It was previously decided when evaluating the significance of each torque term in section 5.3 to consider excluding any term which has a maximum value of 10% or less of the maximum value of the largest term, unless there is a good reason to include it. The subsequent torque term analysis concluded that two terms could be ignored in (14: the Coriolis torque and the frame torque. This gave a simplified version of equation (14) with only 6 terms, see below:

$$T_{inertia} + T_{gyro/roll} = T_{steer} - T_{Jones} - T_{castor} - T_{damping} \tag{81}$$

Using coefficients E_1, E_2…E_n this becomes (see Table 62 for the E_n definitions)

$$(E_1 D^2 + E_5 D + \mathrm{E}_4)\sigma + (E_2 D + \mathrm{E}_3)\lambda = T_S \tag{82}$$

The second equation considers rolling moments about the horizontal X axis for the front assembly A ((19) and has 8 terms, The torque term analysis concluded that two terms could be ignored: the Coriolis torque and the steer torque. The simplified equation (19) with 6 terms, becomes:

$$T_{inertia} - T_{gyro/yaw} = T_{frame} + T_{gyro/cornering} + T_{castor} + T_{Jones} \tag{83}$$

Using coefficients F_1, F_2…F_n it becomes (see Table 62 for the F_n definitions)

$$T_f sin\phi = \mathrm{F}_1 D^2\lambda - F_5\lambda - F_2 D\sigma - \mathrm{F}_6\sigma$$

(84)

Finally the third equation deals with rolling moments about the horizontal X axis for the rear assembly B, equation (24) and this third equation had 7 terms. The torque term analysis concluded that one term could be ignored, the Coriolis torque, resulting in a simplified equation (24) with 6 terms, see:

$$T_{inertia} - T_{gyro/cornering} = -T_{frame} + T_{centrifugal} + T_{gravity} + T_{kink}$$

(85)

Using coefficients G_1, G_2…G_n it becomes (see Table 62 for the Gn definitions)

$$T_f\, sin\phi = -G_1 D^2\lambda + G_2 D\sigma + G_3\sigma + G_4\lambda$$

(86)

A total of 5 torque terms have been removed, resulting in reducing the original 23 terms down to 18 in these simplified equations. These simplified equations will now be used to find the characteristic equation of the bicycle.

Equating equations (84) and (86) we get:

$$\mathrm{F}_1 D^2\lambda - F_5\lambda - F_2 D\sigma - \mathrm{F}_6\sigma = -G_1 D^2\lambda + G_2 D\sigma + G_3\sigma + G_4\lambda$$

(87)

Using coefficients M_1, M_2…M_n(see also Table 66) this becomes:

$$\mathrm{M}_1 D^2\lambda - M_2\lambda = M_3 D + M_4\sigma$$

(88)

Which is rearranged to:

$$(\mathrm{M}_1 D^2 - M_2)\lambda = (M_3 D + M_4)\sigma$$

(89)

And

$$(M_3 D + M_4)\sigma - (\mathrm{M}_1 D^2 - M_2)\lambda = 0$$

(90)

Or

$$(M_3D + M_4)\sigma + (-\mathrm{M}_1 D^2 + M_2)\lambda = 0$$

(91)

Considering equations (82) and (91) these can be rewritten as:

$$U_1\sigma + U_2\lambda = T_S$$

(92)

$$V_1\sigma + V_2\lambda = 0$$

(93)

Converting this to a matrix form using coefficients U_n and V_n (see Table 66) we get:

$$\sigma + U_2\lambda = T_S$$

(94)

$$V_1\sigma + V_2\lambda = 0$$

(95)

$$\begin{bmatrix} U_1 & U_2 \\ V_1 & V_2 \end{bmatrix}\begin{bmatrix}\sigma \\ \lambda\end{bmatrix} = \begin{bmatrix} T_S \\ 0 \end{bmatrix}$$

(96)

$$\begin{bmatrix} (E_1D^2 - E_5D + E_4) & (E_2D + E_3) \\ (M_3D + M_4) & (M_2 - M_1D^2) \end{bmatrix}\begin{bmatrix}\sigma \\ \lambda\end{bmatrix} = \begin{bmatrix} T_S \\ 0 \end{bmatrix}$$

(97)

$$\sigma = \frac{\begin{bmatrix} T_S & U_2 \\ 0 & V_2 \end{bmatrix}}{\Delta} = \frac{V_2T_S}{U_1V_2 - V_1U_2}$$

(98)

$$\lambda = \frac{\begin{bmatrix} U_1 & T_S \\ V_1 & 0 \end{bmatrix}}{\Delta} = \frac{V_1T_S}{U_1V_2 - V_1U_2}$$

(99)

The determinant of $\begin{bmatrix} U_1 & U_2 \\ V_1 & V_2 \end{bmatrix}$ is equal to:

$$\Delta = U_1 V_2 - V_1 U_2 \tag{100}$$

And is the characteristic equation of the system

$$\Delta = (E_1 D^2 + E_5 D + E_4)(M_2 - M_1 D^2) - (M_3 D + M_4)(E_2 D + E_3) \tag{101}$$

The values for E_n and M_n are given in Table 65.

Also

$$\Delta = -E_1 M_1 D^4 - E_5 M_1 D^3 + [(E_1 M_2) - (E_4 M_1) - (E_2 M_3)]D^2 + [(E_5 M_2) - (E_3 M_3) - (E_2 M_4)]D + E_4 M_2 - E_3 M_4 \tag{102}$$

And

$$\Delta = \left(I_{ZA} D^2 + \frac{\Gamma}{\sin\phi} D + M \frac{\mathrm{bv}^2}{\mathrm{L}^2} \Delta_e\right)\left(\left(Mg \frac{b}{L} \cos \emptyset \Delta_e + Mgh\right) - (I_{XA} + I_{XB}) D^2\right) - \left(\left(I_{YF} \frac{v}{r} \sin \emptyset + \frac{Mhbv}{L}\right) D + \left[\left(I_{YF} \frac{v^2}{rL} \sin \emptyset + \frac{Mbv^2}{L^2} \cos \emptyset \Delta_e\right) + \left(\frac{Mhv^2}{L} \sin \emptyset + I_{YR} \frac{v^2}{rL} \sin \emptyset\right)\right]\right)\left(I_{YA} \frac{v}{r \sin \phi} D + Mg \frac{b}{L} \Delta_e\right) \tag{103}$$

Table 65 Coefficients for E_n, F_n and G_n

Coefficient	Equal to
E_1	I_{ZA}
E_2	$I_{YA}\frac{v}{r\sin\phi}$
E_3	$Mg\frac{b}{L}\Delta_e$
E_4	$M\frac{\mathrm{bv}^2}{\mathrm{L}^2}\Delta_e$
E_5	$\frac{\Gamma}{\sin\phi}$
F_1	I_{XA}
F_2	$I_{YF}\frac{v}{r}sin\,\phi$
F_3	$I_{YF}\frac{v^2}{rL}\sin\phi$
F_4	$\frac{\mathrm{Mbv}^2}{\mathrm{L}^2}\cos\phi\,\Delta_e$
F_5	$\frac{\mathrm{Mgb}}{\mathrm{L}}\cos\phi\,\Delta_e$
F_6	$F_3+F_4=I_{YF}\frac{v^2}{rL}\sin\phi+\frac{\mathrm{Mbv}^2}{\mathrm{L}^2}\cos\phi\,\Delta_e$
G_1	I_{XB}
G_2	$\frac{Mhbv}{L}$
G_3	$\frac{Mhv^2}{L}\sin\emptyset+I_{YR}\frac{v^2}{rL}\sin\emptyset$
G_4	Mgh

Table 66 Coefficients for Mn, Un and Vn

Coefficient	Equal to
M_1	$= F_1 + G_1 = I_{XA} + I_{XB}$
M_2	$= F_5 + G_4 = Mg\frac{b}{L}\cos\emptyset\Delta_e + Mgh$
M_3	$= F_2 + G_2 = I_{YF}\frac{v}{r}\sin\emptyset + \frac{Mhbv}{L}$
M_4	$= F_6 + G_3 = \left(I_{YF}\frac{v^2}{rL}\sin\emptyset + \frac{Mbv^2}{L^2}\cos\emptyset\Delta_e\right) + \left(\frac{Mhv^2}{L}\sin\emptyset + I_{YR}\frac{v^2}{rL}\sin\emptyset\right)$
U_1	$= (E_1D^2 + E_5D + E_4)$
U_1	$= \left(I_{ZA}D^2 + \frac{\Gamma}{\sin\phi}D + M\frac{\mathrm{bv}^2}{\mathrm{L}^2}\Delta_e\right)$
U_2	$= (E_2D + E_3)$
U_2	$= \left(I_{YA}\frac{v}{r\sin\phi}D + Mg\frac{b}{L}\Delta_e\right)$
V_1	$= (M_3D + M_4)$
V_1	$= \left(\left(I_{YF}\frac{v}{r}\sin\phi + \frac{Mhbv}{L}\right)D + \left(I_{YF}\frac{v^2}{rL}\sin\emptyset + \frac{Mbv^2}{L^2}\cos\emptyset\Delta_e\right) + \left(\frac{Mhv^2}{L}\sin\emptyset + I_{YR}\frac{v^2}{rL}\sin\emptyset\right)\right)$
V_2	$= (-M_1D^2 + M_2) = (M_2 - M_1D^2)$
V_2	$= \left(Mg\frac{b}{L}\cos\emptyset\Delta_e + Mgh - (I_{XA} + I_{XB})D^2\right)$

D-2 ROUTH STABILITY CRITERION

Once the characteristic equation was obtained the Routh Stability Criterion was used to find out if any unstable roots exist without actually solving them. For stability the coefficients in the first column of the Routh array must all be positive. If any coefficients are negative or zero then the system is not stable. The Routh Stability Criterion is now applied to this characteristic equation by using the parameters values from our benchmark bicycle (see Table 13).

It is interesting to see that results from the Routh Stability Criterion confirms many of the results of the sensitivity study in Section 5.4. For example it shows that the bicycle stability is most sensitive to changes in the parameters of head tube angle and damping, less sensitive to wheel diameter and velocity changes and not sensitive to changes of mass, mass position (both vertical and horizontal) and wheelbase.

Routh Stability Criterion Notation

The notation used is taken from Ogata and is now described (88). The characteristic equation is currently in the form:

$$\Delta = -E_1M_1D^4 - E_5M_1D^3 + [(E_1M_2) - (E_4M_1) - (E_2M_3)]D^2 + [(E_5M_2) - (E_3M_3) - (E_2M_4)]D + E_4M_2 - E_3M_4 \quad (102)$$

This is rearranged into the following format.

$$0 = a_0s^n + a_1s^{n-1} + a_2s^{n-2} + \cdots a_n$$

The coefficients of this polynomial are arranged in rows and columns in the following pattern conforming to Ogata's notation.

s^n	a_0	a_2	a_4	a_6
s^{n-1}	a_1	a_3	a_5	a_7
s^{n-2}	b_1	b_2	b_3	b_4
s^{n-3}	c_1	c_2	c_3	c_4
s^{n-4}	d_1	d_2	d_3	d_4

The coefficients b_1, b_2, b_3...b_n can be found as follows:

$$b_1 = \frac{a_1 a_2 - a_0 a_3}{a_1}$$

$$b_2 = \frac{a_1 a_4 - a_0 a_5}{a_1}$$

$$b_3 = \frac{a_1 a_6 - a_0 a_7}{a_1}$$

Coefficients c_1, c_2, c_3...c_n are:

$$c_1 = \frac{b_1 a_3 - a_1 b_2}{b_1}$$

$$c_2 = \frac{b_1 a_5 - a_1 b_3}{b_1}$$

$$c_3 = \frac{b_1 a_2 - a_1 b_4}{b_1}$$

And:

$$d_1 = \frac{c_1 b_2 - b_1 c_2}{c_1}$$

$$d_2 = \frac{c_1 b_3 - b_1 c_3}{c_1}$$

And so on as required until all necessary coefficients have been found.

Using the benchmark parameter values for the bicycle as given in Table 13 the Routh Stability Criterion gives the array of coefficients in Table 67.

Table 67 Routh array of coefficients

	a_o	a_2	a_4	a_6
s_4	-8.0	-7215.2	-55200.3	0.0
	a_1	a_3	a_5	a_7
s_3	-68.1	-11073.3	0.0	0.0
	b_1	b_2	b_3	
s_2	-5911.9	-55200.3	0.0	
	c_1	c_2	c_3	
s_1	-10437.4	0.0		
	d_1	d_2		
s_0	-55200.3	0.0		

From the first column it can be seen that there are no sign changes so the bicycle is stable (self-stable) under these benchmark conditions.

But if the velocity falls from the benchmark value of 6.944 m/s (about 25 km/hr) to 2.2 m/s (7.92 km/hr) the array changes to Table 68, there are two sign changes in the left-hand column indicating that the bicycle has become unstable.

What about the effect of other key parameters such as: head tube angle, wheel diameter and wheel moment of inertia? By changing each one of these parameters (one at a time) until a sign change occurs we can see how sensitive the bicycle is to these parameters. It is interesting to compare this to the sensitivity study completed in Chapter Six and note the obvious similarities.

The Routh Stability Criterion shows that the bicycle is sensitive to changes in head tube angle and rake, somewhat sensitive to wheel diameter and not sensitive to the other parameters. A full summary of the parameter changes required to make the bicycle unstable (according to Routh) are shown in Table 69.

Table 68 Routh array of coefficients, showing effect of a reduction in speed from 6.944 m/s (about 25 km/hr) to 2.2 m/s (7.92 km/hr)

	a_o	a_2	a_4	a_6
s_4	-8.0	-661.8	-5136.8	0.0
	a_1	a_3	a_5	a_7
s_3	-68.1	-588.1	0.0	0.0
	b_1	b_2	b_3	
s_2	-592.6	-5136.8	0.0	
	c_1	c_2	c_3	
s_1	2.3	0.0		
	d_1	d_2		
s_0	-5136.8	0.0		

Table 69 Summary of parameter changes required to cause instability, as indicated by the Routh Stability Criterion

Parameter	BM value	Value when sign changes	comments
Head tube angle	73.0 ^{O}	81.5 ^{o}	possible to be achieved
Wheel diameter	0.675 m	0.37 m	very small but possible
Wheel moment of inertia Y	0.10 kgm^2	1.04 kgm^2	not possible
Mass	80.0 kg	1495.0 kg	not possible
Wheelbase	1.000 m	12.000 m	not possible
Rake	0.045 m	0.0938 m	possible [1]
Height of mass	1.100 m	8.150 m	not possible
MOI XB	100 kgm^2	13.5 kgm^2	very small
MOI ZA	0,08 kgm^2	0.425 kgm^2	large but possible
MOI XA	0.2 kgm^2	-	no value caused instability
Note 1 this rake produces a trail of 0.512 mm when HTA is 73 degrees			

D-3 FREQUENCY ANALYSIS

The computer model can also be evaluated using Simulink to determine the system characteristics using a detailed frequency analysis. The enabled the response of the output yaw angle to a steering torque input across a range of frequencies to be plotted on Bode diagrams of magnitude and phase and this is shown in Figure 122.

The Bode diagram shows the typical -20dB/decade and -40dB/decade slopes of a 2^{nd} order transfer function. A resonance peak of about 5 Hz is observed which is similar to the empirical observations of this researcher in the field where on two occasions very strong resonant oscillations of the front wheel occurred at speeds of 45 km/hr with a frequency in the order of 5 cycles per second. Note that when the wheel circumference for a 675 mm diameter is divided by a speed of 12.5 m/s (45 km/hr) this gives a frequency of 5.894 Hz. So any excitation of the rotating front wheel at a speed of 45 km/hr would be close to the right frequency to cause a resonance condition.

At lower frequencies (below 5 Hz) the 1^{st} order part of the transfer equation dominates, while above the resonant frequency the 2^{nd} order portion dominates. The time constant from the 1^{st} order part of the transfer function is at approximately 66.67 seconds/cycle ($1/T = 1.5 \times 10^{-2}$ Hz). Finally the phase change diagram shows the expected phase shifts as the frequency changes.

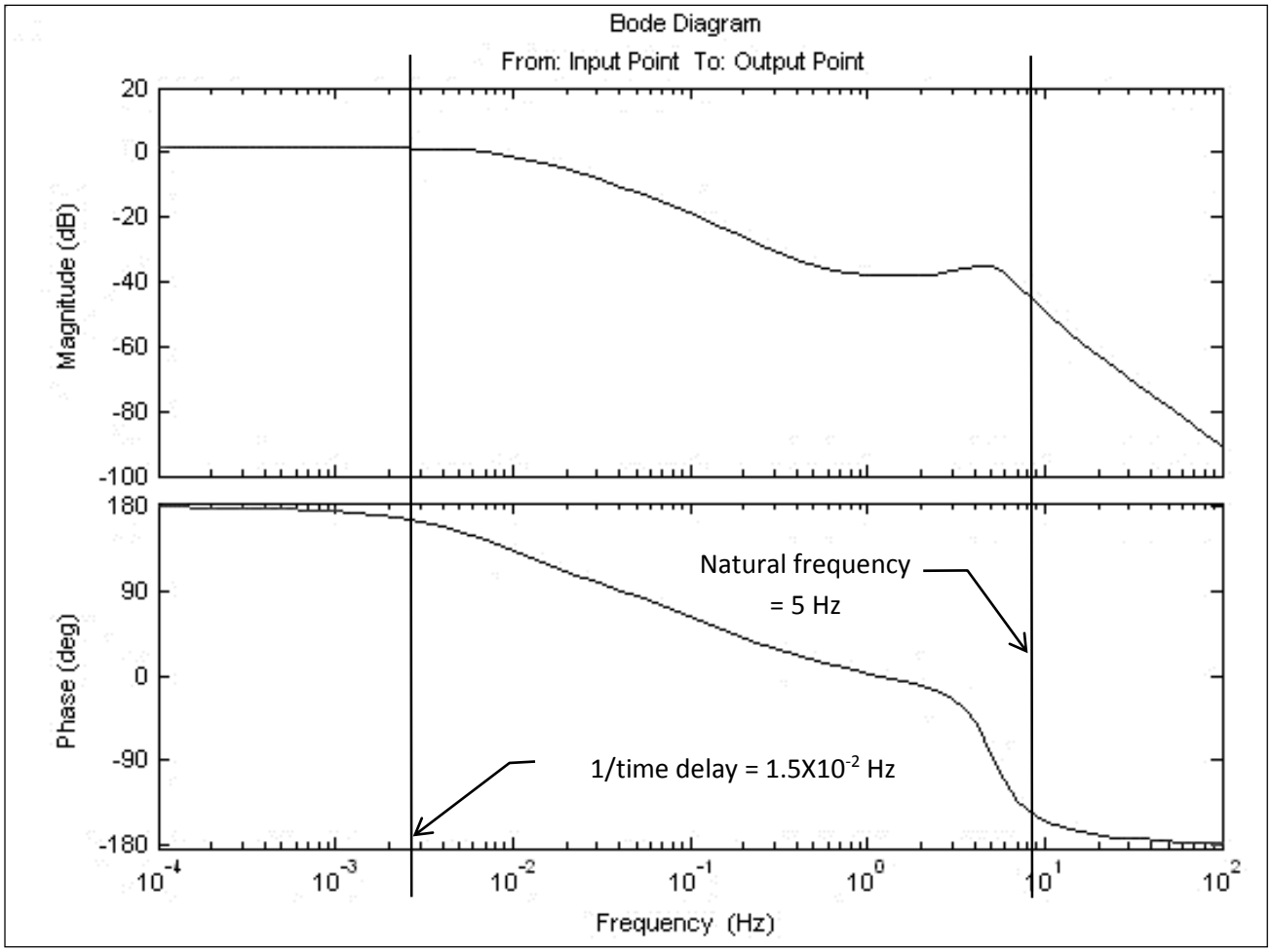

Figure 122 Bode diagrams of magnitude and phase for the benchmark bicycle Simulink model

APPENDIX E – WHEEL AND TYRE MANUFACTURER SPECIFICATIONS

This Appendix summarises manufacturers' specifications for road bicycle tyres based on the 700C standard wheel size. The specifications are used to establish relationships between the tyre width and actual outside wheel diameter (as opposed to the nominal diameter).

Table 70 Typical road bicycle tyre properties

ISO/ETRTO Code [1]	Tyre width mm	D [2] actual wheel diameter mm	D_N/D_{BM} [3]
700 X 18C	18	658.90	0.976
700 X 19C	19	662.09	0.981
700 X 20C	20	666.22	0.987
700 X 23C	23	671.79	0.995
700 X 25C	25	674.82	1.000
700 X 28C	28	682.14	1.011
700 X 30C	30	685.32	1.015
700 X 32C	32	688.35	1.020
700 X 35C	35	692.80	1.026
700 X 37C	37	700.28	1.037
700 X 38C	38	693.92	1.028
700 X 40C	40	703.47	1.042
Note 1 ETRTO (European Tyre and Rim Technical Organisation) code = tyre size			
Note 2 actual diameter varies from the nominal 700mm value and actual BM wheel diameter			
Note 3 is the variation from the 675 mm benchmark wheel where D_N = actual wheel diameter for indicated ETRTO code size and D_{BM} = actual diameter for benchmark wheel			
These are the averaged results from two manufacturers (64, 81)			

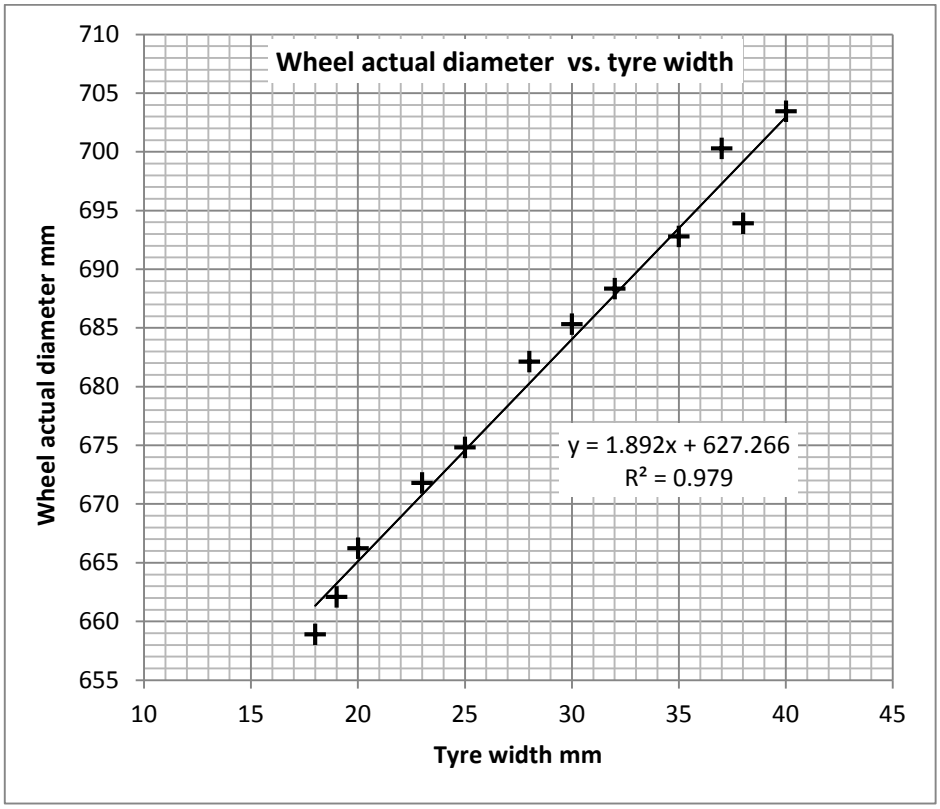

Figure 123 Relationship of tyre width and actual wheel diameter for 700C wheels, from Table 70

APPENDIX F – TOUR DE FRANCE 2013 BICYCLE SPECIFICATIONS

This Appendix lists all the information from the 2013 Tour de France used in this Thesis including: the teams, the top 10 finishers and their bicycle models including their specifications. This information was made use of in Chapter Seven which validated the Design Charts described in Chapter Six.

The Tour de France (TdF) is the pre-eminent international cycle race and is one of the three grand tours of road racing, the others being the Giro d'Italia (Tour of Italy) and the Vuelta a Espana (Tour of Spain) (108). These three races represent the pinnacle of international road cycle racing with the elite of professional cyclists competing. The 100th anniversary edition of the Tour de France road cycling race began on 29 July 2013, when 219 riders from 22 professional teams started from Porto-Vecchio in Corsica and it finished 23 days and 3400 km later in Paris with169 finishers.

The 2013 TdF race was won by Chris Froome riding for the Sky Procycling Team and he averaged 40.6 km/hr over 21 days of racing (110). The group of TdF bicycles examined includes nearly all 30 models ridden by all 22 participating TdF teams. The bicycles and their respective teams are listed in Table 71. By examining these bicycles it should be possible to see what range of parameter values are considered desirable by the world's best manufacturers and riders. In order to do this it was first necessary to obtain a complete list of specifications for each model. Most of this information was obtained directly from manufacturers' official websites or specialist sector sources and where specifications were missing, it was possible by using other known dimensions to determine them either by calculation or by completing full size drawings.

Table 71 Tour de France 2013 Teams and bicycles

No	Manufacturer	Type	TdF Team
1	BH	G6 Ultegra D12	Sojasun
2	BH	Ultralight Ultegra D12	Sojasun
3	Bianchi	Oltre	Vacansoleil-DCM
4	BMC	Teammachine SLR01	BMC Racing Team
5	BMC	Timemachine TMR01	BMC Racing Team
6	Cannondale	Supersix Evo	Cannondale
7	Canyon	Aeroad CF 9.0	Katusha Team
8	Canyon	Ultimate CF SLX	Katusha Team
9	Cervelo	R5	Garmin Sharp
10	Cervelo	RCA	Garmin Sharp
11	Cervelo	S5	Garmin Sharp
12	Colnago	C59	Team Europcar
13	Felt	F2 [1]	Team Argos-Shimano
14	Focus Bikes	Izalco Team SL Carbon	AG2r La Mondiale
15	Giant	Propel	Belkin Pro Cycling
16	Giant	TCR Advanced	Belkin Pro Cycling
17	Lapierre	Ultimate di2	FDJ.FR
18	Lapierre	Xelius Efi 800	FDJ.FR
19	Look	695 Aerolight	Cofidis Solutions Credits
20	Merida	Sculptura SL 909	Lampre-Merida
21	Orbea	Orca	Euskatel-Euskadi
22	Pinarello	Dogma 65.1 Think 2	Sky Procycling, Movistar
23	Ridley	Helium SL	Lotto-Belisol
24	Ridley	Noah FAST	Lotto-Belisol
25	Scott	Addict SL	Orica-Greenedge
26	Scott	Foil 40	Orica-Greenedge
27	Specialized	Tarmac SL 4	Astana Pro team, Team Saxo-Tinkoff & Omega Pharm-Quick Step
28	Specialized	Venge	Team Saxo-Tinkoff & Omega Pharm-Quick Step
29	Trek	Domane 6.9	Radioshack-Leopard
30	Trek	Madone 7.9	Radioshack-Leopard
Note 1 the Felt F1 model used in the Tour is not available commercially and the only information available was for the Felt F2 model, said to be very similar to the F1			
includes all 31 models ridden by all 22 TdF teams, excepting for Note 1			
Sources (108, 110)			

Table 72 Tour de France bicycles of 2013 medium sized frames only (nominal FS 55 cm)

No of models	Company	Type	Wheelbase mm	Rake mm	Head Tube Angle degrees	Seat Tube Angle degrees	Wheel size mm	Conventional Frame Size cm (if specified)	Stack height mm	calculated effective trail mm for 675 mm wheel	Manuf. FS
1	BH	G6 Ultegra D12	990	48	73	72.5	675		549	52.99	MD size
2	BH	Ultralight Ultegra D12	985	50	73	72.5	675		549	50.90	MD size
3	Bianchi	Oltre	984	45	72.5	73.5	675	55		59.23	55 FS
4	BMC	Teammachine SLR01	1014	41	72.5	73.5	675		565	63.42	55 FS
5	BMC	Timemachine TMR01	1005	46	72.5	74	675		560	58.18	54 FS
6	Cannondale	Supersix Evo	991	45	73	73.5	675	56	558	56.13	56 FS
7	Canyon	Aeroad CF 9.0	985	44	74	73	675		556	51.00	
8	Canyon	Ultimate CF SLX	980.4	39	73.5	73.5	675	56	560	59.30	M (56)
9	Cervelo	R5	982	43	73.5	73	675	56	580	55.13	56 FS
10	Cervelo	RCA	982	43	73.5	73	675	56	580	55.13	56 FS
11	Cervelo	S5	982	43	73.5	73	675	56	580	55.13	56 FS
12	Colnago	C59	1008	43	73.3	72.75	675	56		56.36	56 FS
13	Felt	F2	983	43	73.5	73.5	675	56	548	55.13	56 FS
14	Focus Bikes	Izalco Team SL Carbon	978	46	73.5	73.5	680	56		52.74	56 FS

15	Giant	Propel	1001	50	73	72.5	675	55.5		50.90	L/55.5
16	Giant	TCR Advanced	1001	50	73	72.5	675	55.5	569	50.90	L/55.6
17	Lapierre	Ultimate di2	990	45	73	73	675	55	570	56.13	L
18	Lapierre	Xelius Efi 800	990	45	73	73	675	55	570	56.13	L
19	Look	695 Aerolight	979.5	43	73	74	676	56	559.5	58.22	M
20	Merida	Sculptura SL 909	985	45	73.5	73.5	675		565	53.04	54
21	Orbea	Orca	988	53	73.5	73.2	675		572	44.70	55
22	Pinarello	Dogma 65.1 Think 2	988	43	73.2	73	675	56		56.98	560
23	Ridley	Helium SL	990	46	73.5	73.5	675		575	52.00	M
24	Ridley	Noah FAST	990	46	73.5	73.5	675		575	52.00	M
25	Scott	Addict SL	994	44	73	73.3	675	56	568	57.17	L/56
26	Scott	Foil 40	994	44	73	73.3	675		569	57.17	L/56
27	Specialized	Tarmac SL 4	986	43	73.5	73.25	675	56	564	55.13	560
28	Specialized	Venge	986	43	73.5	73.25	675	56	566	55.13	561
29	Trek	Domane 6.9	1008	48	71.9	73.3	675	56	591	59.81	56
30	Trek	Madone 7.9	980	40	73.5	73.3	675	56	577	58.25	56
		max	1014.0	53.0	74.0	74.0	680.0	56.0	591.0	63.42	
		min	978.0	39.0	71.9	72.5	675.0	55.0	548.0	44.70	
		average	990.0	44.9	73.2	73.2	675.2	55.8	567.0	55.15	
		standard deviation	9.40	3.09	0.43	0.40	0.92	0.38	10.70	3.64	
Sources (77, 106, 111-116, 119-130)											

Table 73 Details of the entire size range for 8 selected manufacturers' 2013 TdF bicycles

No of models	Company	Type	Manufacturer FS	Wheelbase mm	Rake mm	Head Tube Angle degrees	Seat Tube Angle degrees	Wheel size mm	Conventional Frame Size cm (if specified)	Stack height mm	calculated trail mm for 675 mm wheel
1	Cannondale	Supersix Evo	48	961	45	71.50	74.50	675	48	513	65.474
2	Cannondale	Supersix Evo	50	967	45	72.00	74.50	675	50	519	62.345
3	Cannondale	Supersix Evo	52	973	45	72.50	74.00	675	52	526	59.230
4	Cannondale	Supersix Evo	54	975	45	73.00	73.50	675	54	544	56.128
5	Cannondale	Supersix Evo	56	991	45	73.00	73.50	675	56	558	56.128
6	Cannondale	Supersix Evo	58	996	45	73.50	73.00	675	58	577	53.039
7	Cannondale	Supersix Evo	60	1008	45	73.50	72.50	675	60	596	53.039
8	Cannondale	Supersix Evo	62	1012	45	73.50	72.00	675	62	620	53.039
1	Felt	F2 [1]	48	969	52	71.00	74.50	675		500	61.214
2	Felt	F2	51	971	50	72.00	74.00	675		514	57.087

3	Felt	F2	54	974	45	73.00	73.00	675		526	56.128
4	Felt	F2	56	983	43	73.50	73.50	675	56	548	55.125
5	Felt	F2	58	1000	43	74.00	73.50	675		569	52.044
6	Felt	F2	60	1022	43	74.00	73.00	675		607	52.044
1	Focus Bikes	Izalco Team SL Carbon	48	975	46	71.25	74.80	680	48		66.836
2	Focus Bikes	Izalco Team SL Carbon	50	975	46	71.25	74.30	680	50		66.836
3	Focus Bikes	Izalco Team SL Carbon	52	978	46	72.00	74.00	680	52		62.105
4	Focus Bikes	Izalco Team SL Carbon	54	980	46	72.50	74.00	680	54		58.969
5	Focus Bikes	Izalco Team SL Carbon	56	978	46	73.50	73.50	680	56		52.737
6	Focus Bikes	Izalco Team SL Carbon	58	993	46	73.50	73.50	680	58		52.737
7	Focus Bikes	Izalco Team SL Carbon	60	1005	46	73.50	73.50	680	60		52.737
1	Look	695 Aerolight	XS	971.8	43	71.00	74.80	676			70.733
2	Look	696 Aerolight	S	977.2	43	72.00	74.50	676			64.448
3	Look	697 Aerolight	M	979.5	43	73.00	74.00	676	56	559.5	58.219
4	Look	698 Aerolight	L	992.4	43	73.00	73.80	676			58.219
5	Look	699 Aerolight	XL	1005.1	43	73.00	73.50	676			58.219
6	Look	700 Aerolight	XXL	1009.8	43	73.00	73.00	676			58.219

1	Orbea	Orca	48	970	43	71.50	74.75	675		500	67.583
2	Orbea	Orca	51	970	43	72.10	73.50	675		530	63.822
3	Orbea	Orca	53	980	43	72.10	73.50	675		552	63.822
4	Orbea	Orca	55	988	53	73.50	73.20	675		572	44.696
5	Orbea	Orca	57	998	53	73.20	73.20	675		590	46.534
6	Orbea	Orca	60	1013	53	73.50	73.20	675		621	44.696
1	Pinarello	Dogma 65.1 Think 2	420	960.4	43	74.40	69.15	675	42		49.587
2	Pinarello	Dogma 65.1 Think 2	440	960.4	43	74.40	70.00	675	44		49.587
3	Pinarello	Dogma 65.1 Think 2	465	969.5	43	74.40	70.50	675	46		49.587
4	Pinarello	Dogma 65.1 Think 2	470	971.5	43	74.00	71.40	675	47		52.044
5	Pinarello	Dogma 65.1 Think 2	500	971.5	43	74.00	71.40	675	50		52.044
6	Pinarello	Dogma 65.1 Think 2	515	973.5	43	73.70	72.00	675	52		53.891
7	Pinarello	Dogma 65.1 Think 2	530	979.6	43	73.70	72.50	675	53		53.891
8	Pinarello	Dogma 65.1 Think 2	540	979.6	43	73.40	72.80	675	54		55.743
9	Pinarello	Dogma 65.1 Think 2	550	988.6	43	73.40	72.80	675	55		55.743
10	Pinarello	Dogma 65.1 Think 2	560	989.7	43	73.00	73.20	675	56		58.219
11	Pinarello	Dogma 65.1 Think 2	575	994.7	43	73.00	73.70	675	58		58.219

12	Pinarello	Dogma 65.1 Think 2	595	1003.7	43	72.40	73.40	675	60		61.950
13	Pinarello	Dogma 65.1 Think 2	620	1031.9	43	72.00	73.40	675	62		64.448
1	Specialized	Tarmac SL 4 & Venge	490	970	45	72.25	75.50	675	49	504	60.785
2	Specialized	Tarmac SL 4 & Venge	520	970	45	73.00	74.00	675	52	526	56.128
3	Specialized	Tarmac SL 4 & Venge	540	978	45	73.00	73.50	675	54	543	56.128
4	Specialized	Tarmac SL 4 & Venge	560	986	43	73.50	73.25	675	56	564	55.125
5	Specialized	Tarmac SL 4 & Venge	580	1003	43	73.50	73.00	675	58	591	55.125
6	Specialized	Tarmac SL 4 & Venge	600	1013	43	74.00	72.50	675	60	612	52.044
1	Trek	Domane 6.9	44	983	53	70.30		675	44	510	64.548
2	Trek	Domane 6.9	47	986	53	71.00		675	47	527	60.157
3	Trek	Domane 6.9	50	996	53	71.10		675	50	546	59.532
4	Trek	Domane 6.9	52	1003	53	71.30		675	52	561	58.284
5	Trek	Domane 6.9	54	1010	53	71.30		675	54	575	58.284
6	Trek	Domane 6.9	56	1008	48	71.90	73.30	675	56	591	59.813
7	Trek	Domane 6.9	58	1022	48	72.00		675	58	611	59.190
8	Trek	Domane 6.9	60	1032	48	72.10		675	60	632	58.568
9	Trek	Domane 6.9	62	1042	48	72.10		675	62	656	58.568

1	Trek	Madone 7.9	47	971	45	71.20	74.60	675	47	522	67.358
2	Trek	Madone 7.9	50	971	45	72.10	74.60	675	50	535	61.720
3	Trek	Madone 7.9	52	973	45	72.80	74.20	675	52	547	57.367
4	Trek	Madone 7.9	54	978	45	73.00	73.70	675	54	555	56.128
5	Trek	Madone 7.9	56	980	40	73.50	73.30	675	56	577	58.254
6	Trek	Madone 7.9	58	987	40	73.80	73.00	675	58	598	56.399
7	Trek	Madone 7.9	60	1000	40	73.90	72.80	675	60	615	55.781
8	Trek	Madone 7.9	62	1008	40	73.90	72.50	675	62	634	55.781
		Maximum		**1042.0**	**53.0**	**74.40**	**75.50**				
		Minimum		**960.4**	**40.0**	**70.30**	**69.15**				
		Average		**988.2**	**45.3**	**72.76**	**73.30**				
		Standard deviation		**18.66**	**3.51**	**1.01**	**1.13**				
Note 1 the Felt F1 model used in the Tour is not available commercially and the only information available was for the Felt F2 model, said to be very similar to the F1											
Sources: (77, 111, 113, 115, 121, 123, 124, 128)											

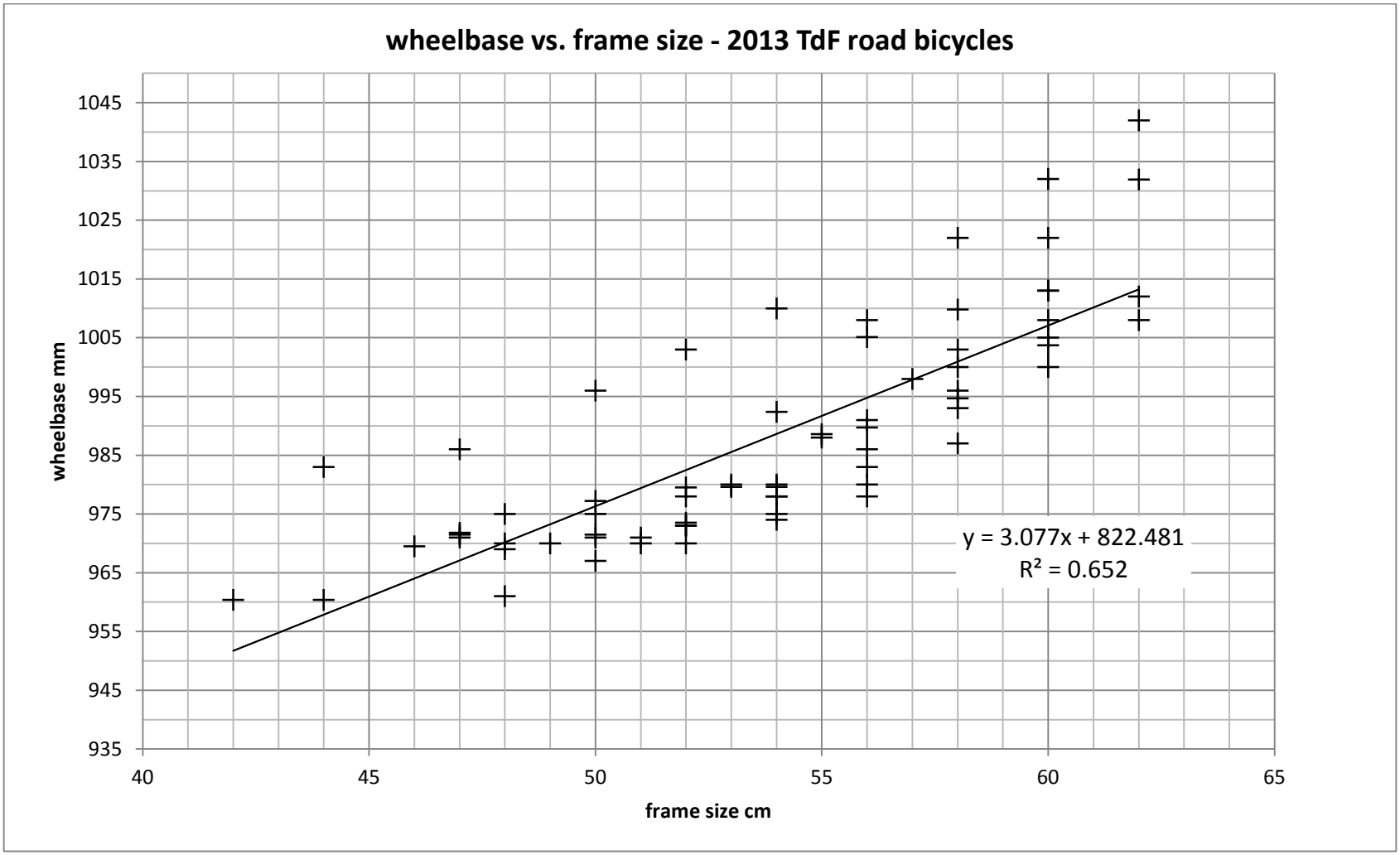

Figure 124 Relationship between wheelbase and frame size for thirty 2013 TdF bicycle models in Table 73

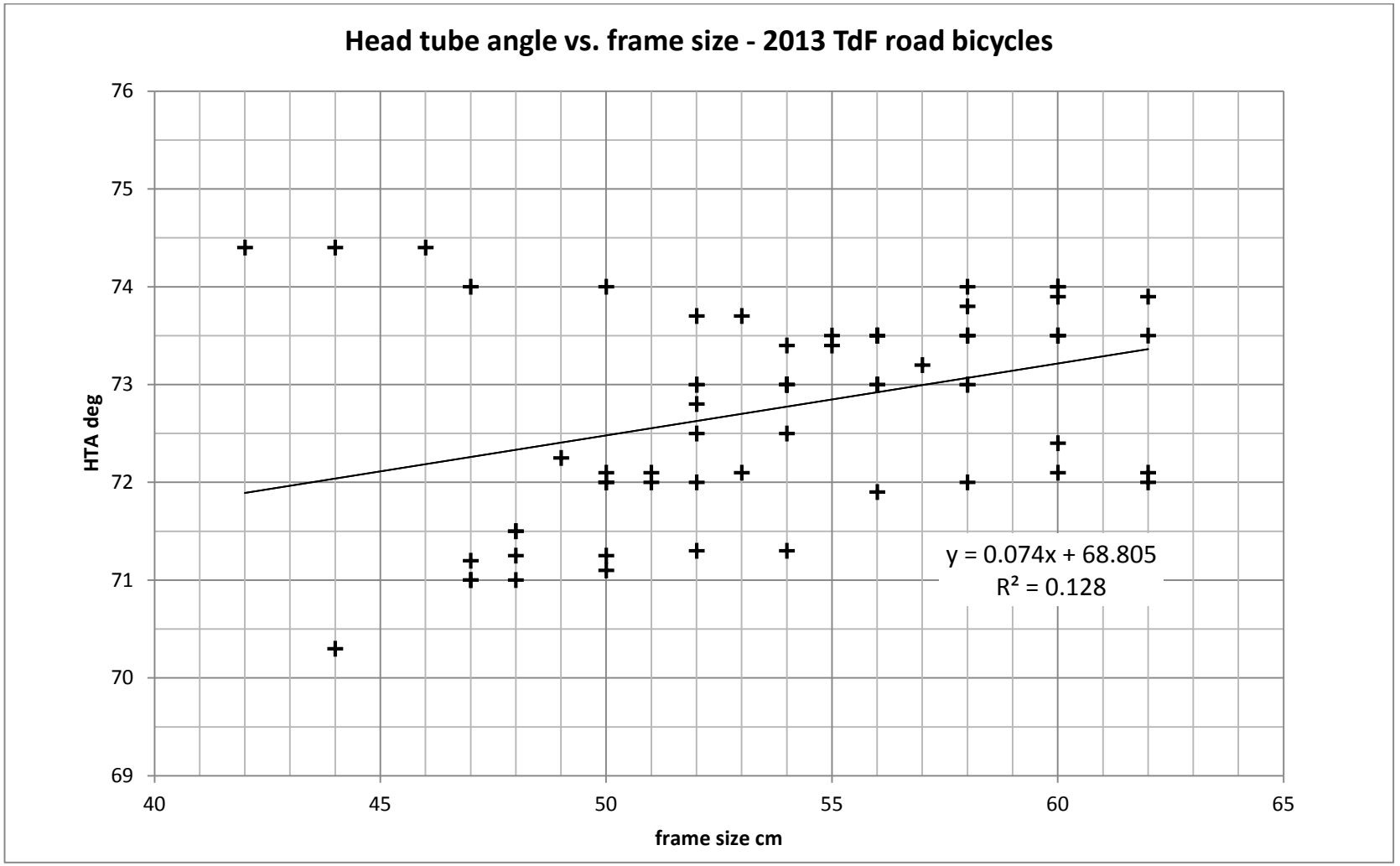

Figure 125 Relationship between head tube angle and frame size for thirty 2013 TdF bicycle models in Table 73

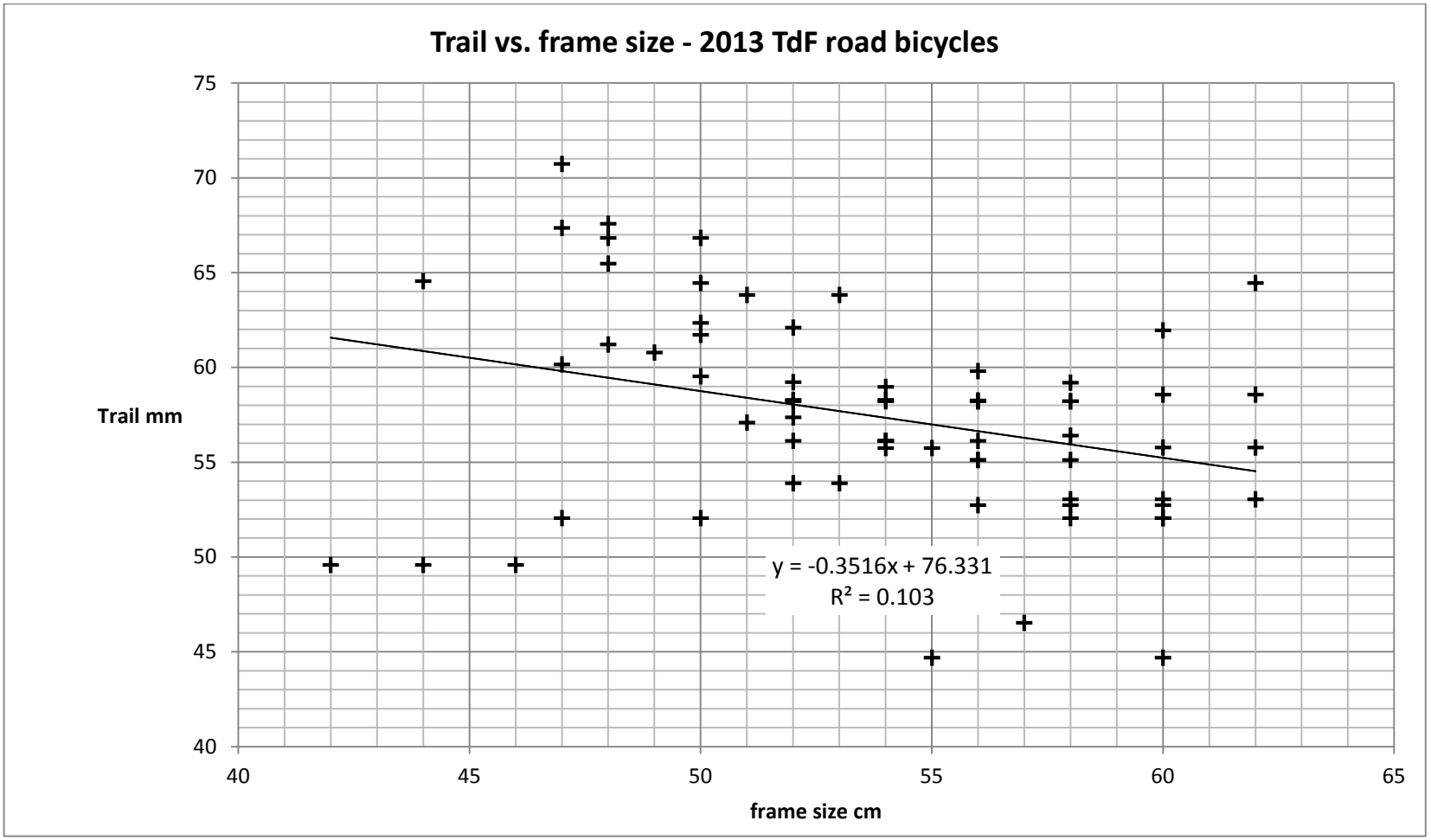

Figure 126 Relationship between trail and frame size for thirty 2013 TdF bicycle models in Table 73

Table 74 Tour de France 2013 top ten individual finishers and their recorded details

Surname	First name	Team	Bike type	TdF 2013 position	Height mm	Weight kg
Froome	Chris	Sky Procycling	Pinarello	1	1860	69.0
Quintana Rojas	Nairo	Movistar Team	Pinarello	2	1660	57.3
Rodriguez Oliver	Joaquin	Katusha Team	Canyon	3	1690	57.0
Contador	Alberto	Team Tinkoff-Saxo	Specialized	4	1760	62.0
Kreuziger	Roman	Team Tinkoff-Saxo	Specialized	5	1830	65.0
Mollema	Bauke	Belkin Pro Cycling	Giant	6	1810	64.0
Fuglsang	Jakob	Astana Pro team	Specialized	7	1820	70.0
Valverde	Alejandro	Movistar Team	Pinarello	8	1780	61.0
Navarro	Daniel	Cofidos Solutions Credits	Look	9	1750	61.0
Talansky	Andrew	Garmin Sharp	Cervelo	10	1750	63.0
				average	**1771**	**62.93**
				standard deviation	**59.41**	**4.09**

Source (108)

Table 75 Tour de France 2013 top ten individual finishers and their calculated details

Surname	TdF 2013 position	Calc. Inseam mm	Calc. saddle height mm	Calculated frame size cm	Wheelbase mm	STA degrees	Calculated "h" mm	Calculated "b" mm	Calculated MOI_{YB} kgm^2
Froome	1	857.5	758.9	55.7	988.2	73.00	1109.0	318.0	93.225
Quintana Rojas	2	765.3	677.3	49.7	970.0	74.00	1020.0	337.0	66.690
Rodriguez Oliver	3	779.1	689.5	50.6	971.0	73.50	1019.0	332.0	66.247
Contador	4	811.4	718.1	52.7	970.0	74.00	1064.0	333.0	77.888
Kreuziger	5	843.6	746.6	54.8	978.0	73.50	1096.0	324.0	86.247
Mollema	6	834.4	738.5	54.2	986.0	72.50	1086.0	315.0	83.501
Fuglsang	7	839.0	742.5	54.5	978.0	73.50	1092.0	325.0	91.581
Valverde	8	820.6	726.2	53.3	978.1	73.70	1084.0	328.0	79.669
Navarro	9	806.8	714.0	52.4	979.5	74.00	1060.0	334.0	76.180
Talansky	10	806.8	714.0	52.4	972.0	73.00	1059.0	323.0	78.279
average		**816.43**	**722.54**	**53.1**	**977.1**	**73.47**	**1068.90**	**326.90**	**79.95**
standard deviation		**27.39**	**24.24**	**1.78**	**6.12**	**0.48**	**29.12**	**6.82**	**8.65**
Sources (108, 111-116)									

The calculations in Table 75 are based on the following assumptions:

1. Inseam = height X 0.461 (48)
2. Saddle height = inseam X 0.885 (68)
3. Bicycle frame size = inseam X 0.65 (68)
4. Wheelbase is taken from manufacturers' specifications after the frame size is calculated
5. Seat Tube Angle is taken from manufacturers' specifications
6. h calculated as per Appendix B
7. b calculated as per Appendix B
8. I_{XB} = (mass of rider + mass of bike) x h^2
9. mass of bike = 6.8 kg- (equals the UCI limit)

APPENDIX G – DESIGN TABLE SERIES & DESIGN EQUATION

This Appendix details two additional design methodologies one based on the use of design tables and second on a design equation.

G-1 DESIGN TABLE SERIES

This Design Table Series summarises recommendations about bicycle design in a tabular format.

1. this Road Bicycle Design Table Series consists of five tables prepared for frame sizes (FS) between 490 to 610 mm
2. the recommendations are set out in a codified way for the designer to use
3. the design criteria they are based on uses empirical knowledge and experience
4. these five Tables are based on the same guidelines already detailed in Design Criteria Table 30 from Chapter Six.
5. the correct Design Table is found by using the inseam (IS) measurement (see Figure 127) to calculate the preferred frame size, see Table 76 and Figure 128

Once the correct frame size has been found, choose its corresponding Design Table to make decisions about the following parameters, wheelbase, fork rake, head tube angle and seat tube angle, see Table 76 to Table 81.

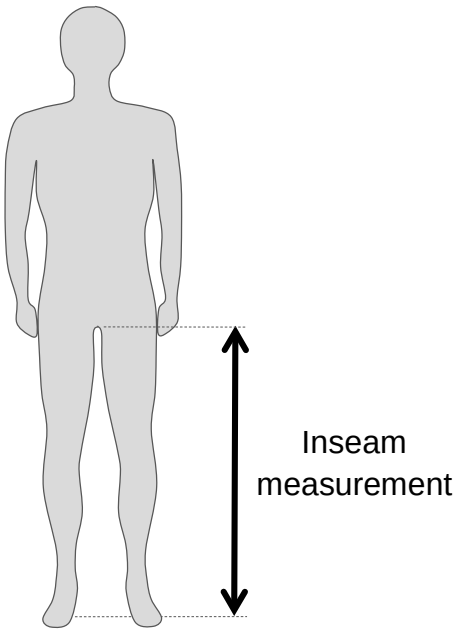

Figure 127 Cyclist inseam dimension measured along the inside of the leg

Table 76 Frame size table – indicates the correct frame size for range of inseam measurements

Ideal inseam (mm)	Min to max inseam ranges (mm)	Recommended Frame Size (mm)
754	730 to 777	490
800	778 to 822	520
846	823 to 869	550
892	870 to 914	580
938	915 to 960	610

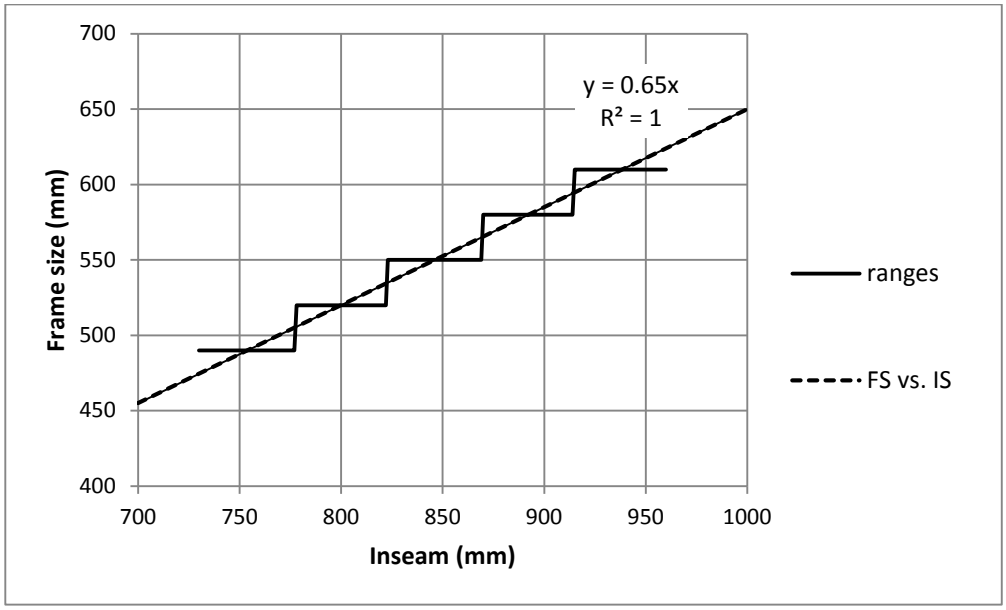

Figure 128 Frame size (FS) vs. inseam (IS) with bands of inseam ranges, from Table 76

The selection of the correct frame size is based on a factor of 0.65 as per the formula below:

$$FS = 0.65 \times IS \tag{60}$$

Table 77 Design Table - for 490 mm frame size road bicycles

Variable	Definition	Target value	Min value	Max value
IS	Rider inseam measurement	754	730	777
Δ	Trail (critical)	59 mm	49 mm	69 mm
L	wheelbase	973 mm	953 mm	993 mm
beta	Fork rake (or offset)	46 mm	43 mm	53 mm
phi	Head tube angle	72.5º	71.0º	74.0º
STA	Seat tube angle	74.3º	71.0º	75.5º

Table assumptions

- for performance road bicycles only
- for 490 mm frame size only
- based on 700c wheels

Table 78 Design Table - for 520 mm frame size road bicycles

Variable	Definition	Target value	Min value	Max value
IS	Rider inseam measurement	800	778	822
Δ	Trail (critical)	58 mm	48 mm	68 mm
L	wheelbase	983 mm	963 mm	1003 mm
beta	Fork rake (or offset)	46 mm	42 mm	53 mm
phi	Head tube angle	72.5º	71.0º	74.0º
STA	Seat tube angle	74º	71.2º	75.2º

Table assumptions

- for performance road bicycles only
- for 520 mm frame size only
- based on 700c wheels

Table 79 Design Table - for 550 mm frame size road bicycles

Variable	Definition	Target value	Min value	Max value
IS	Rider inseam measurement	846	823	869
Δ	Trail (critical)	57 mm	47 mm	67 mm
L	wheelbase	992 mm	972 mm	1012 mm
beta	Fork rake (or offset)	45.5 mm	42.5 mm	53 mm
phi	Head tube angle	73.0°	71.5°	74.5°
STA	Seat tube angle	73.6°	71.5°	74.8°

Table assumptions

- for performance road bicycles only
- for 550 mm frame size only
- based on 700c wheels

Table 80 Design Table - for 580 mm frame size road bicycles

Variable	Definition	Target value	Min value	Max value
IS	Rider inseam measurement	892	870	914
Δ	Trail (critical)	56 mm	46 mm	66 mm
L	wheelbase	1001 mm	981 mm	1021 mm
beta	Fork rake (or offset)	45 mm	41 mm	53 mm
phi	Head tube angle	73.0°	71.5°	74.5°
STA	Seat tube angle	73.2°	74.4°	71.8°

Table assumptions

- for performance road bicycles only
- for 580 mm frame size only
- based on 700c wheels

Table 81 Design Table - for 610 mm frame size road bicycles

Variable	Definition	Target value	Min value	Max value
IS	Rider inseam measurement	938	915	960
L	wheelbase	1010 mm	990 mm	1030 mm
Δ	Trail (critical)	55 mm	45 mm	65 mm
beta	Fork rake (or offset)	45 mm	40 mm	53 mm
phi	Head tube angle	73.5°	72.0°	75.0°
STA	Seat tube angle	72.8°	72.0°	74.0°

Table assumptions

- for performance road bicycles only
- for 610 mm frame size only
- based on 700c wheels

G-2 DESIGN EQUATION

Consideration was given as to whether an overall design equation could be developed. After evaluation it was decided that this approach was unsuitable but a brief description is included in this Appendix for completeness.

Mathematical equations such as those used to develop the Simulink model used in this investigation would of course provide the most accurate analysis. But a Simulink model is not considered to be a suitable design technique, rather it is a modelling method which requires experience on the part of the user and access to Matlab and Simulink. A major problem with Simulink models is they are hard to use, not easily interpreted and require training and experience.

However once the sensitivity study in Chapter Five was completed it seemed worth considering if its results could be used to formulate a simple equation to predict the handling performance of any specific bicycle design. Such a design equation if successful, could potentially allow a designer to quickly evaluate the effect of changing one or more parameters. It was hoped that this could be better method than using Design Criteria or Design Tables as the interaction of several parameters could be examined. In addition it would not be based on equations and rules taken from past experience rather it would be based on dynamic responses.

The design equation formulated from the sensitivity study is:

$$Handling\ Index = C_D \frac{\Delta D_N}{D_O} + C_b \frac{\Delta b_N}{b_O} + C_M \frac{\Delta M_N}{M_O} + C_h \frac{\Delta h_N}{h_O} + C_{Iza} \frac{\Delta Iza_N}{Iza_O} + C_{Ixa} \frac{\Delta Ixa_N}{Ixa_O} + C_{Ixb} \frac{\Delta Ixb_N}{Ixb_O} + C_\beta \frac{\Delta \beta_N}{\beta_O} + C_L \frac{\Delta L_N}{L_O} + C_{Izf} \frac{\Delta Izf_N}{Izf_O} + C_\phi \frac{\Delta \phi_N}{\phi_O} \quad (104)$$

- where C_D, C_b, C_M etc. are coefficients taken from the sensitivity study of the Chapter Five, note that they are linear terms and therefore are only valid across a short range (Table 28)
- parameters D, b, M etc. are defined in Table 82
- subscript N refers to the parameter value of the new bicycle design that is to be examined
- and subscript O refers to the "old" parameter value of the benchmark bicycle (see Table 82)

Using the coefficients given in Table 28 this equation becomes:

$$Handling\ Index = 0.05753 \frac{\Delta D_N}{D_O} + 0.02072 \frac{\Delta b_N}{b_O} + 0.01976 \frac{\Delta M_N}{M_O} + 0.002698 \frac{\Delta h_N}{h_O} + 0.001038 \frac{\Delta Iza_N}{Iza_O} + 0.00063 \frac{\Delta Ixa_N}{Ixa_O} + (-0.001067) \frac{\Delta Ixb_N}{Ixb_O} + (-0.01412) \frac{\Delta \beta_N}{\beta_O} + (-0.01565) \frac{\Delta L_N}{L_O} + (-0.02021) \frac{\Delta Izf_N}{Izf_O} + (-0.05925) \frac{\Delta \phi_N}{\phi_O} \quad (105)$$

The equation's output, the handling index, is a non-dimensionalised number (which is expressed as a ratio or percentage of the benchmark settling time) and this gives an overall handling score.

Unfortunately after using this equation several times it was found to be a poor predictor of the Simulink results, even for very small parameter changes. But perhaps this should not be a surprise given the nonlinear dynamic behaviour of a bicycle.

The results of four calculations using the equation are summarised in Table 79 , in which all three new designs (A, B and C) showed significant variances when compared to the results of Simulink simulations. The design equation's calculation of the 2% settling time had an error of between 6 to 40% over that of the value given by Simulink, unacceptable errors and therefore this approach was discontinued.

Table 82 Handling equation results for three new designs A, B & C

	Parameter	Units	Benchmark bicycle values	Design A	Design B	Design C
D	Diameter of the bicycle wheel	m	0.675	0.670	0.674	0.670
b	Hori dist. C of rear wheel to COM	m	0.330	0.320	0.329	0.330
M	Mass	kg	80.00	78.00	79.00	80.00
h	Height of centre of mass (COM)	m	1.100	1.050	1.110	1.100
I_{ZA}	MOI of A about Z axis (yaw)	kgm^2	0.080	0.081	0.081	0.080
I_{XA}	MOI of A about X axis (roll)	kgm^2	0.200	0.210	0.210	0.200
I_{XB}	MOI of B about X axis (roll)	kgm^2	100.00	95.00	99.00	100.00
β	fork rake	m	0.045	0.043	0.044	0.045
L	bicycle wheelbase	m	1.000	0.990	0.995	1.000
I_{ZW}	MOI of wheels	kgm^2	0.100	0.098	0.099	0.100
Φ	head tube angle	degrees	73.00	73.50	73.75	76.00
Handling Equation Score			0.000	-0.00079	-0.00033	-0.05426
Predicted 2% Settling time		sec	10.1	10.092	10.0967	9.5520
Actual 2% Settling time from the Simulink simulation		sec	10.1	8.95	9.47	6.81
Variance between prediction and Simulink		**%**	**0% [1]**	**+12.76%**	**+6.62%**	**+40.26%**
Note 1 this is a trivial result						

BIBLIOGRAPHY

1. ISO 8855:2011 Road vehicles vehicle dynamics & road-holding ability Vocabulary (2011).
2. Jones DEH. The Stability of the Bicycle. Physics Today. 1970;23(4):34 - 40.
3. Union Cycliste Internationale UCI 2013. Available from: http://www.uci.ch/templates/UCI/UCI8/layout.asp?MenuId=MTYzMDQ&LangId=1.
4. Klein RE. Using Bicycles to teach System Dynamics. IEEE Control Systems Magazine. 1989;9(3):4-9.
5. Klein RE, editor Novel systems and dynamics teaching techniques using bicycles. Proceedings of the American Control Conference; 1988.
6. Whitt FR, Wilson DG. Bicycling Science: Ergonomics and Mechanics: MIT Press (MA); 1974.
7. Sharp A, editor. Bicycles and Tricycles, An Elementary Treatise On Their Design And Construction: London: Longmans, Green; 1896.
8. Sharp RS. The Lateral Dynamics of Motorcycles and Bicycles. Vehicle System Dynamics. 1985;14(4):265-83.
9. Brooks M. Easy Rider. New Scientist. 2011;No 2814 (28 May 2011):4.
10. Whitt FR, Wilson DG. Bicycling Science 2nd Ed. 2nd ed. Cambridge, USA: MIT Press (MA); 1982.
11. Brand S. Freeman Dyson's Brain [Online interview]. Feb 1998 [updated 22 Aug 2013]. Available from: http://www.wired.com/wired/archive/6.02/dyson_pr.html.
12. Fajans J. Steering in Bicycles and Motorcycles. American Journal of Physics. 2000;68(7):654 - 9.
13. Astrom KJ, Klein, R. E., Lennartsson, A. Bicycle Dynamics and Control. IEEE Control Systems Magazine. 2005 (Aug 2005):26-47.
14. Meijaard JP, Papadopoulos JM, Ruina A, Schwab AL. Linearized Dynamics Equations for the Balance and Steer of a Bicycle: A Benchmark and Review. Proceedings of the Royal Society of London-A. 2007;463(2084):1955-82.
15. Whipple FJW. The stability of the motion of a bicycle. The Quarterly Journal of Pure and Applied Mathematics. 1899;30(120):312–48.
16. Meijaard JP, Papadopoulos J, Ruina A, Schwab AL. Historical Review of Thoughts of Bicycle Self-Stability. Cornell University, 2011.
17. Cox AJ. Angular Momentum and Motorcycle Counter Steering,: A Discussion and Demonstration. American Journal of Physics. 1998;66:1018 - 21.
18. Brooks. Easy Rider. New Scientist. 2011 28 May 2011;2814(28 May 2011):4.
19. Moon FC. Applied Dynamics: With Applications to Multibody and Mechatronic Systems: John Wiley & Sons, USA; 1998.
20. Timoshenko S, Young DH, editors. Advanced Dynamics. USA: McGraw-Hill; 1948.
21. Lowell J, McKell HD. The Stability of Bicycles. American Journal of Physics. 1982;50(12):1106–12.
22. Rankine WJM. On the Dynamic Principles of the Motion of Velocipedes. The Engineer. 1869 6 Aug 1869;28(79):5.
23. Bourlet C. Traité des bicycles et bicyclettes, suivi d'une application à la construction des vélodromes: Gauthier-Villars et fils; 1895.
24. Bourlet C. Étude Théoretique sur la Bicyclette. Bulletin de la Societe Mathematique de France. 1899;27:47 - 67 & 76 - 96.
25. Psiaki ML. Bicycle Stability, A Mathematical and Numerical Analsis [Bachelor of Arts in Physics]. Princeton NJ: Princeton University; 1979.
26. Hand RS. Comparisons and Stability Analysis of Linearized Equations of Motion for a Basic Bicycle Model [Master of Science]: Cornell University NY; 1988.
27. Franke G, Suhr W, Rieß F. An advanced model of bicycle dynamics. European Journal of Physics. 1990;11:116-21.
28. Seffen KA, Parks GT, Clarkson PJ. Observations on the Controllability of Motion of Two-wheelers. Proceedings of the Institution of Mechanical Engineers, Part I: Journal of Systems and Control Engineering. 2001;215(2):143-56.
29. Den Hartog JP. Mechanical Vibrations. New York: Dover Publishers; 1985.
30. Jackson AW, Dragovan M. An Experimental Investigation of Bicycle Dynamics. 1998.

31. Prince J. An Investigation into Bicycle Steering and Roll Responses [Master of Engineering]. Auckland: Auckland University of Technology; 2004.
32. Prince PJ, Al-Jumaily AM. Bicycle Steering and Roll Responses. Journal Title: Journal of Multi-body Dynamics, Proceedings of the Institution of Mechanical Engineers Part K [PIK]. 2012 June 2012;226(2):95-107. Epub June 2012.
33. Sharp RS. The Stability and Control of Motorcycles. Journal of Mechanical Engineering Science. 1971;13(5):316–29.
34. Kooijman JDG, Schwab AL, Meijaard JP. Experimental Validation of a Model of an Uncontrolled Bicycle. Multibody System Dynamics. 2008;19(1):115-32.
35. Higbie J. The Motorcycle as a Gyroscope. American Journal of Physics. 1974;42:701 - 2.
36. Hunt H. A Bike with a Reverse-spinning Wheel 2006. Available from: http://www2.eng.cam.ac.uk/~hemh/gyrobike.htm.
37. Astrom KJ, Klein RE, Lennartsson A. Bicycle Dynamics and Control: Adapted Bicycles for Education and Research. IEEE Control Systems Magazine. 2005;25(4):26-47.
38. Klein RE, editor The University of Illinois bicycle project1992: Pergamon.
39. Kirshner D. Some Nonexplanations of Bicycle Stability. American Journal of Physics. 1980;48:36 - 8.
40. Le Henaff Y. Dynamical Stability of the Bicycle. European Journal of Physics. 1987;8:207-10.
41. Foale T, Willoughby V. Motorcycle Chassis Design: The Theory and the Practice: Osprey, UK; 1988.
42. Lignoski B. Bicycle Stability, Is the Steering Angle Proportional to the Lean? Physics Department, The College of Wooster, Wooster, Ohio. 2002;44691.
43. Sharma HD, Umashankar N, editors. A Fuzzy Controller Design for an Autonomous Bicycle System. Proceedings of IEEE International Conference on Engineering of Intelligent Systems; 2006; Islamabad.
44. Kooijman JDG, Schwab AL, Moore JK, editors. Some observations on human control of a bicycle2009.
45. Moore JK, Kooijman JDG, Schwab AL. Rider Motion Identification during normal Bicycling by means of Principal Component Analysis Multibody Dynamics 2009, Eccomas Thematic Conference; Warsaw, Poland2009.
46. Moore J, Hubbard M. Parametric Study of Bicycle Stability (P207). The Engineering of Sport 7. 2008:311-8.
47. Moore JK, Hubbard M, Kooijman JDG, Schwab AL, editors. A Method for Estimating the Physical Properties of a Combined Bicycle and Rider. Proceedings of the ASME 2009 International Design Engineering Technical Conferences & Computers and Information in Engineering Conference, DETC2009 2009; San Diego CA.
48. Hanavan EP. A Mathematical Model of the Human Body. Ohio: Aerospace Medical Division, USAF, 1964 October 1964. Report No.: AMRL-TR-64-102.
49. Lynch JP, Roland RD. Computer animation of a bicycle simulation. ACM, 1972.
50. Bourlet C. La bicyclettes, sa construction et sa forme: Gauthier-Villars et fils; 1899.
51. Davison RCR, A C. Upright Frames and Steering. Cycling. 1935;03 July:5.
52. Wilson DG, Papadopoulos J. Bicycling Science 3rd Ed. 3rd ed. Cambridge, USA: The MIT Press; 2004 2004. 472 p.
53. Doebellin EO, editor. System Modelling and Response: Theoretical and Experimental Approaches: Ohio State University; 1980.
54. Cocco G. Motorcycle Design and Technology: How and Why. Milan: Giorga Nada Editore Publisher; 1999.
55. Cossalter V, Dora A, Lot R. Steady turning of two wheeled Vehicles. Vehicla Systems dynamics. 1999;31:157 -81.
56. Suryanarayanan S, Tomizuka M, Weaver M, editors. System Dynamics and Control of Bicycles at High Speeds. Proceedings of the American Control Conference; 2002; Anchorage Alaska.
57. Meijaard JP, Popov AA. Multi-body modelling and analysis into the non-linear behaviour of modern motorcycles. Proceedings of the Institution of Mechanical Engineers, Part K: Journal of Multi-body Dynamics. 2007;221(1):63-76.
58. Getz NH, Marsden JE, editors. Control for an Autonomous Bicycle. Proc of the IEEE International Conference on Robotics and Automation; 1995: Citeseer.
59. WHPVA. World Human Powered Vehicle Association 2013. Available from: http://www.whpva.org/land.html#300.

60. Chen CK, Dao TS, editors. Dynamics and Path-Tracking Control of an Unmanned Bicycle. Proceedings of ASME 2005 International Design Engineering Technical Conferences & Computers and Information in Engineering Conference; 2005; Long Beach, California USA.
61. Ringwood JV, Feng R, editors. Bicycle Wheel Wobble A Case Study in Dynamics. Proceedings of 4th International Conference on Informatics in Control, Automation and Robotics; 2007; Angers, France.
62. Donida F, Ferreti G, Savaresi SM, Tanelli M, Schiavo F, editors. Motorcycle dynamics library in modelica. Proceedings of 5th International Modelica Conference; 2006; Vienna.
63. Meijaard JP, Papadopoulos JM, Ruina A, Schwab AL. Supplementary Appendices. Proceedings of the Royal Society Series A. 2007.
64. Dressel A, Rahman A. Measuring sideslip and camber charactersitics of bicycle tyres. Vehicle System Dynamics. 2011 2011;2011(1-14).
65. Gillespie TD. Fundamentals of Vehicle Dynamics. 1st ed. Warrendale PA: Society of Automotive Engineers Inc; 1992 1992.
66. Meriam JL, Kraige LG. Engineering Mechanics - Dynamics. 3rd ed: John Wiley & Sons; 1998 1993.
67. TALU. Introduction: Bicycle Design & the Recumbent Bicycle 2010. Available from: http://talu.com/introduction.php.
68. Hinault B, Genzling C. Road Racing: Techniques and Training: Springfield Books; 1988.
69. LeMond G. GK. Greg LeMond's Complete Book of Bicycling: Penguin Group USA; 1987.
70. Glaskin M. Cycling Science. 1st ed. Lewes: Frances Lincoln Ltd; 2012 2012.
71. Pruitt AL, Matheny F. Andy Pruitt's Medical Guide For Cyclists: RbR Publishing Co. Available from: http://www,RoadBikeRider.com.
72. Taylor R. Taylor's Bike Shop. Available from: http://taylorsbikeshop.com/about/competition-road-pg521.htm.
73. Clark J, Joss W. Cyclosportives - A Competitor's Guide. Ramsbury: The Crowood Press Ltd; 2011.
74. Ballantine R, Grant R. Richard's Ultimate Bicycle Book: DK Publishing; 1992.
75. Kossack J. Bicycle Frame: World Publications, California, USA; 1975.
76. Guru R. Original Giant Once Edition updated 2012. Available from: http://www.retrobike.co.uk/forum/viewtopic.php?t=182820.
77. Trek Bikes 2013. Available from: http://www.trekbikes.com/nz/en/.
78. Damavandi M, Allard P, Barbier F, Leboucher J, Rivard CH, Farahpour N. Estimation of Whole Body Momement of Inertia Using Self-imposed Oscillations.
79. Dempster WT. Space Requirements of the Seated Operator. Ohio: Wright Air Development Center, USAF, 1955 July 1955. Report No.: 55-159 Contract No.: 55-159.
80. ISO 5725-1 Accuracy (trueness and precison) measurement methods and results, ISO 5725-1(1994).
81. Cateye. Tire Size Chart 2012. Available from: http://www.cateye.com/en/support/manual/.
82. Mercier J, http://visual.ly/tour-de-france-2013-cyclists-profiles. What are the cyclists profiles in the Tour de France 2013? Available from: http://visual.ly/tour-de-france-2013-cyclists-profiles.
83. Burke ER. High Tech Cycling. 2nd ed. Burke ER, editor: Human Kinetics Publishing; 2003.
84. Peng C, Cowell, P. A., Chisholm, C. J., Lines, J. A. Lateral Tyre Dynamic Characteristics. Journal of Terramechanics. 1994 1994;31(6):20.
85. Minorsky N. Directional Stability of Automatically Steered Bodies. Journal of American Society of Naval Engineers. 1922 1922;34 (2).
86. Doebellin EO. Measurement Systems Application and Design. 5th Ed ed. New York: McGraw-Hill; 2004 2004. 1078 p.
87. Dorsey J. Continuous and Discrete Control Systems. 1st ed: McGraw Hill; 2002.
88. Ogata K. Modern Control Engineering. 4th ed: Prentice Hall; 2002.
89. Curry B. BikeCAD 2013. Available from: http://www.bikecad.ca/jones_stability.
90. van der Plas R. Bicycling Technology: Bicycle Books Inc; 1991 1991.
91. Moulton D. The Ideal handling Bicycle 2010 [updated 03 June 2010]. Available from: http://davesbikeblog.squarespace.com/blog/category/bicycle-design?currentPage=2.
92. Wilson DG. Bicycling Science. 3rd ed. Cambridge, USA: The MIT Press; 2004 2004. 472 p.

93. IHPVA. International Human Powered Vehicle Association 2013. Available from: http://www.ihpva.org/home/.
94. ITU. International Triathlon Union 2013. Available from: http://www.triathlon.org/.
95. 01.02.2013 UR. UCI Cycling Regulations Version 01.02.2013 2013. Available from: http://www.uci.ch/Modules/BUILTIN/getObject.asp?MenuId=MTY2NjU&ObjTypeCode=FILE&type=FILE&id=34033&LangId=1.
96. Moulton D. Toe overlap: no problem 2006. Available from: http://davesbikeblog.squarespace.com/blog/2006/11/5/toe-overlap-no-problem.html.
97. Hogg S. Sensitive Issues. Available from: http://www.stevehoggbikefitting.com/wp-content/uploads/2011/06/sensitive_issues.pdf.
98. Walker D. The Truth about Track Bike Frame Geometry by Don Walker 2013. Available from: http://www.urbanvelo.org/issue3/urbanvelo3_p44-45.html.
99. Ringer B. New Zealand by Bike: Reed; 1994.
100. Kolin MJ, de la Rosa DM. The Custom Bicycle. Press R, editor: Rodale Press; 1979 1979.
101. Rodriguez A, Erickson G. 650 versus 700C wheels 2010. Available from: http://www.rodbikes.com/articles/toeoverlap.html.
102. Asso of British Cycling Coaches, How to Set Up Your Road Bike 2013. Available from: http://www.abcc.co.uk/how-to-set-up-your-road-bike/.
103. Ricard MD, Hills-Meyer P, Miller MG, Michael TJ. The Effects of Bicycle Frame Geometry on Muscle Activation and Power during a Wingate Anaerobic Test. Journal of Sports Science and medicine. 2006;01 March 2006(5):25 - 32.
104. Price D, Donne B. Effect of variation in seat tube angle at different seat heights on submaximal cycling performance in man. Journal of Sports Science. 1997;15:395 - 402.
105. Woods D, Guinness R. The Dean Woods Manual of Cycling: Angus & Robertson; 1995.
106. Bianchi Bikes 2013. Available from: http://www.bianchi.com/nz/home/home.aspx.
107. Griffiths G. Now and Then. Bicycling Australia. 2003 May/June 2003.
108. Le Tour de France 100 official website. official website of the Tour de France]. Available from: http://www.letour.fr/le-tour/2013/us/overall-route.html.
109. Hamilton T, Coyle, D. The Secret Race. 1st ed. London: Transworld, Random House, London; 2012. 382 p.
110. Farrelly A. Tour de France Team Bike round-up: All the road bikes in this year's race 2013 [updated 5 July 2013]. Available from: http://road.cc/content/feature/85959-tour-de-france-team-bike-round-all-road-bikes-years-race.
111. Pinarello Bikes 2013. Available from: http://www.pinarello.com/it.
112. Canyon Bikes 2013. Available from: http://www.canyon.com/_en/shop/.
113. Bikes S. Specialized Bikes 2013. Available from: http://www.specialized.com/us/en/bikes/road.
114. Giant Bicycles 2013. Available from: http://www.giant-bicycles.com/en-nz/.
115. Look Cycle 2013. Available from: http://www.lookcycle.com/en/int.html.
116. Cervelo Bikes 2013. Available from: http://www.cervelo.com/en/.
117. Timings RL. Manufacturing Technology Vol 1 2nd ed. Harlow: Longman Scientific & Technical; 1992 1992. 412 p.
118. Brenière Y. Why we walk the way we do. Journal of Model Behaviour. 1996 1996;28(4).
119. BH Bikes 2013. Available from: http://bhbikes-us.com/.
120. BMC Bikes 2013. Available from: http://www.bmc-racing.com/int-en/home/.
121. Cannondale Bikes 2013. Available from: http://www.cannondale.com/nzl/.
122. Colnago Bikes. 2013.
123. Felt Bicycles 2013. Available from: http://www.feltbicycles.com/.
124. Focus Bikes 2013. Available from: http://www.focus-bikes.com/.
125. Lapierre Bicycles 2013. Available from: http://www.lapierrebicycles.com/road.
126. Ritchey Bikes 2013. Available from: http://ritcheylogic.com/.
127. Merida. Merida Bikes 2013. Available from: http://2014.merida-bikes.com/#country-selection.
128. Orbea Bikes 2013. Available from: http://www.orbea.com/.
129. Ridley Bikes 2013. Available from: http://www.ridley-bikes.com/be/nl/intro.
130. Scott Bikes 2013. Available from: http://www.scott-sports.com/de/en/category/bike/.